Synthesis and Characterization of Novel Photocrosslinkable Poly(2-Oxazoline)-Based Hydrogel Systems for the Application as Biosensor Matrix

DISSERTATION

Zur Erlangung des Grades

eines Doktors der Naturwissenschaften

im Promotionsfach Chemie

vorgelegt von

M.Sc. Christian Petri

geboren in Marburg

eingereicht bei der Naturwissenschaftlich-Technischen Fakultät

der Universität Siegen

Siegen 2018

Die vorliegende Arbeit wurde in der Zeit von September 2013 bis September 2017 in der Arbeitsgruppe Makromolekulare Chemie der Universität Siegen angefertigt.

Acknowledgements

Zusammenfassung

Gegenstand und Ziel dieser Arbeit war die Synthese und Charakterisierung eines photovernetzbaren und thermoresponsiven Hydrogelsystems für die spätere Verwendung als Biosensormatrix. Aufgrund ihrer unteren kritischen Lösungstemperatur (LCST) sind Poly(2-Oxazoline) für diese Art der Anwendung besonders gut geeignet. Zudem besteht die Möglichkeit, die LCST durch die gezielte Copolymerisation von verschiedenen Monomeren zu variieren, die sich aufgrund ihrer unterschiedlichen Seitenketten in ihrer Hydrophobizität unterscheiden.

Zu diesem Zweck wurde zunächst ein verbesserter Syntheseweg eines neuartigen Benzophenon-2-Oxazoline (BPOxa) basierenden Photovernetzers entwickelt und dieser mit verschiedenen 2-Alkyl-2-Oxazolinen (2-Ethyl-, 2-*n*-Propyl- und 2-isoPropyl-2-Oxazoline) copolymerisiert um zunächst den Einfluss auf den Trübungspunkt des jeweiligen BPOxa Copolymersystems zu untersuchen. Dabei wurde festgestellt, dass die Copolymerisation mit BPOxa eine starke Absenkung des Trübungspunktes im Vergleich zu den entsprechenden 2-Alkyl-2-Oxazolinen Homopolymeren zur Folge hat, welches aus der hohen Hydrophobizität der Benzophenonfunktionalität resultiert. Die anschließende Herstellung von Hydrogelschichten aus den entsprechenden Copolymeren erfolgte durch die Bestrahlung mit UV Licht mit einer Wellenlänge von 365 nm. Diese Schichten wurden dann unter der Verwendung von Oberflächenplasmonenresonanz- / Optische Wellenleitermoden-Spektroskopie (SPR/OWS) hinsichtlich ihres Quellverhaltens in Wasser untersucht. Dabei wurde festgestellt, dass höhere Bestrahlungsdosen zu niedrigeren Quellgraden führen, was aus der höheren Vernetzungsdichte innerhalb der entsprechenden Hydrogelschichten resultiert. Zusätzlich wurde noch die Phasenübergangstemperatur sowie das Quellverhalten in Abhängigkeit von der Zusammensetzung der Copolymere untersucht. Hier zeigte sich, dass sowohl die Phasenübergangstemperatur als auch das Quellverhalten mit dem jeweiligen Trübungspunkt der entsprechenden Copolymere korreliert.

Ein weiteres Ziel dieser Arbeit war die Entwicklung einer multifunktionellen Sensormatrix für die Verwendung als SPR Biosensor. Zu diesem Zweck wurde ein 2-Azid-2-Oxazoline (AzOxa) Derivat entwickelt, welches einerseits zur Anbindung von Analyt-spezifischen Liganden dienen kann oder aber zur Verbesserung der Antifouling-Eigenschaften der entsprechenden

Zusammenfassung

Hydrogelmatrix. Dazu wurde zunächst der Einfluss des 2-Azid-2-Oxazoline Comonomers auf den Trübungspunkt von Poly(2-Ethyl-2-Oxazoline) und Poly(2-isoPropyl-2-Oxazoline) untersucht. Dabei wurde festgestellt, dass es zu einer linear verlaufenden Absenkung des Trübungspunktes mit zunehmendem AzOxa-Gehalt kommt. Diese Beobachtung steht im Widerspruch zu den zu erwartenden Ergebnissen, da sich die Polarität der Copolymere im Vergleich zu den entsprechenden Homopolymeren mit einem zunehmenden AzOxa-Gehalt ebenfalls erhöht. Zusätzlich wurden verschiedene Antifouling-Derivate (z.B.. Sulfo- und Carboxybetaine, Oligoethylenglycol und Oligoethylenglycol-sulfobetain) unter Verwendung der Kupfer-katalysierten Azid-Alkin-Cycloaddition (CuAAC) in die jeweiligen Polymere eingebunden. Die anschließend hergestellten Hydrogelschichten wurde dann unter Zuhilfenahme von SPR/OWS bezüglich ihres Quellverhaltens sowie ihrer Phasenübergangstemperatur charakterisiert. Dabei wurde festgestellt, dass der Quellgrad (SR) sehr stark durch die entsprechenden Antifouling-Derivate beeinflusst wird, wobei der geringste SR für unmodifizierte Polymere und der höchste SR für zwitterionische Polymersysteme gefunden wurde. Diese Ergebnisse basieren auf dem stärker hydrophilen Charakter der modifizierten Polymere, welcher mit dem Trübungspunkt der Copolymere korreliert.

Zusätzlich beinhaltet diese Arbeit die Synthese und Charakterisierung photovernetzbarer und thermoresponsiver Poly(*N*-isopropylacrylamid)- sowie photovernetzbarer Dextran-Hydrogelsysteme, welche in Anlehnung an bereits bestehende Publikationen hergestellt wurden. Die daraus resultierenden Anwendungen sind in den Publikationen beschrieben, die sich aus der Zusammenarbeit mit Jakub Dostalek und Wolfgang Knoll vom Austrian Institute of Technology - AIT ergeben haben.

Summary

The main work of this thesis is focused on the synthesis and characterization of novel photocrosslinkable and thermoresponsive hydrogel systems for the application as biosensor matrix. Poly(2-oxazoline)s are very attractive polymers for this application, as they exhibit a lower critical solution temperature (LCST) in aqueous media, with the possibility of tuning this LCST by copolymerization of monomers with different hydrophobic side chains.

For this purpose, an optimized synthesis route of a novel benzophenone-2-oxazoline-based photocrosslinker (BPOxa) photocrosslinker was developed and this monomer was copolymerized with various 2-alkyl-2-oxazolines (2-ethyl-, 2-*n*-propyl- and 2-isopropyl-2-oxazoline), to study the impact on the cloud point of the resulting thermoresponsive BPOxa copolymer systems. Here it was found that the large hydrophobic benzophenone moieties cause a significant decrease of the cloud point temperature compared to the corresponding 2-alkyl-2-oxazoline homopolymers. Poly(2-oxazoline)-based hydrogel layers were fabricated from these polymers by photocrosslinking with UV light at wavelength of 365 nm. The fabricated layers were characterized by surface plasmon resonance and optical waveguide mode spectroscopy (SPR/OWS) with respect to their swelling properties in aqueous media, showing that an increasing irradiation dose leads to a decrease in swelling ratio as a direct consequence of the higher crosslinking density in the respective hydrogel network. In addition, phase transition temperature and swelling ratio were studied for polymer networks of varying monomer composition, which was found to correlate to their cloud point in aqueous media.

Another major application target of this thesis is the development of a multifunctional sensor matrix in SPR-based biosensors. For this purpose, an azido-2-oxazoline derivative (AzOxa) was developed, which can serve as a post-modification unit for the incorporation of analyte-specific ligands or as a conjugation site for antifouling motives to improve protein binding resistance of the polymer network. First, the impact of the novel azido-2-oxazoline comonomer on the cloud point of poly(2-ethyl-2-oxazoline) and poly(2-isopropyl-2-oxazoline) derivatives was studied. A linear decrease of the cloud point temperature for an increasing AzOxa content was found, which is contrary to the expected trend for increased polarity of polymers with higher amounts of the more polar azide group (compared to plain alkyl

Summary

substituents), but apparently, a higher tendency for chain aggregation is introduced with the N_3 groups. Additionally, different alkyne-modified antifouling motives (e.g. sulfo- and carboxybetains, oligoethylene glycol and oligoethylene glycol-sulfobetaine) were developed and incorporated into the AzOxa copolymer backbone by copper(I) catalyzed azide-alkyne cycloaddition reaction (CuAAC). The conjugated hydrogels were characterized by SPR/OWS, with respect to their swelling behavior in aqueous solution. It was found that the swelling ratio (SR) of the prepared hydrogel layers is strongly influenced by the nature of the alkyne conjugate, as the SR increases from the non-modified polymer to the oligoethylene glycol and the zwitterionic systems. The results are explained by the increasing hydrophilic character of the modified polymers in correlation to their cloud point in aqueous media.

In addition, this work includes the synthesis and characterization of photocrosslinkable and thermoresponsive poly(*N*-isopropylacrylamide)-based and photocrosslinkable dextran-based hydrogel systems (in analogy to previous publications). Resulting applications are highlighted by the joint publications that emerged from the collaboration with Jakub Dostalek and Wolfgang Knoll in the context of the Austrian Institute of Technology (AIT) partner group.

List of Abbreviations

AzOxa	2-(3-azidopropyl)-2-oxazoline
BP	Benzophenone
BPAAm	*N*-(4-benzoylphenyl)acrylamide (Benzophenone acrylamide)
BPOxa	2-[3-(4-benzoylphenoxy)propyl]-2-oxazoline
CB	Carboxybetaine
CROP	Cationic ring opening polymerization
CuAAC	Copper(I) catalyzed Azide-Alkyne cycloaddition reaction
COOH	Carboxylic acid
DCM	Dichloromethane
Đ	Dispersity
DMAc	Dimethylacetamide
4-DMAP	4-dimethylaminopyridine
DMSO	Dimethyl sulfoxide
EBP	Epoxybenzophenone
EBP-CMD	Epoxybenzophenone-carboxymethyl dextran
EDC x HCl	1-(3-Dimethylaminopropyl)-3-ethylcarbodiimid hydrochloride
EO-A	2-{2-[2-(prop-2-yn-1-yloxy)ethoxy]ethoxy}ethan-1-ol
EO-Tos	2-{2-[2-(prop-2-yn-1-yloxy)ethoxy]ethoxy}ethyl 4-methylbenzenesulfonate
EO-DMAm	*N,N*-dimethyl-2-{2-[2-(prop-2-yn-1-yloxy)ethoxy]ethoxy}ethan-1-amine
EO-SB	3-{dimethyl{2-[2-(prop-2-yn-1-yloxy)ethoxy]ethyl}ammonio}propane-1-sulfonate
EO-CB	3-{dimethyl{2-[2-(prop-2-yn-1-yloxy)ethoxy]ethyl}ammonio}propanoate
EtOAc	Ethyl acetate
EtOxa	2-ethyl-2-oxazoline
Et$_3$N	Triethylamine
h	Hour
isoPrOxa	2-isopropyl-2-oxazoline
MeCN	Acetonitrile

List of Abbreviations

|	
MeI	Methyl iodide
MeOH	Methanol
MeOTf	Methyl trifluoromethansulfonate (Methyltriflate)
MeOTs	Methyl p-toluenesulfonate (Methyl tosylate)
min	Minute
$\bar{M}_n$	Number average of the molar mass distribution
$\bar{M}_w$	Weight average of the molar mass distribution
MWAP	Microwave-assisted polymerization
NaH	Sodium hydride
NHS	*N*-hydroxysuccinimide
NIPPAm	*N*-isopropylacrylamide
NMP	*N*-methyl-2-pyrrolidone
NMR	Nuclear magnetic resonance
NaI	Sodium iodide
n-PrOxa	2-*n*-propyl-2-oxazoline
OEG	Oligo ethylene glycol
OWS	Optical waveguide mode spectroscopy
pNIPAAm	Poly(*N*-isopropylacrylamide)
r.t.	Room temperature
SB	Sulfobetaine
SEC	Size exclusion chromatography
SPR	Surface plasmon resonance
TCM	Trichloromethane/Chloroform
TFAA	Trifluoroacetic anhydride
TFA-NHS	2,5-dioxopyrrolidin-1-yl 2,2,2-trifluoroacetate
TLC	Thin layer chromatography
TMS	Tetramethylsilane

Contents

1. Introduction

1. Introduction

Over the last decades, biosensors have gained a key importance in many different fields, like food safety for monitoring quality and safety of the product, in biomedicine for the diagnosis of diabetes or as an environmental sensor for the detection of ozone, to name only a few prominent examples. Another interesting field were biosensors are applied is early cancer screening, which is based on the detection of biomarkers, peptides or proteins present in the blood system of the patient.[1-3] Especially optical biosensors based on surface plasmon resonance and optical waveguide mode spectroscopy (SPR/OWS) have experienced a growing interest, as they enable direct, real-time and label free detection of a large variety of different chemical and biological compounds. Thereby, the signal is generated by monitoring the change of refractive index caused by the immobilization of analyte molecules onto a sensor surface or matrix, respectively.[2, 4] For measurements in aqueous environments surface attached hydrogels as biosensor matrix may be an ideal choice for the application in such optical sensors. Their advantage lies in the much higher number of detection units available in the three-dimensional polymer network compared to binding sites that are directly attached to the sensor surface in a planar geometry. Furthermore, hydrogels based on thermoresponsive polymers can be used for an additional signal enhancement by thermally collapsing of the swollen hydrogel layer, which increases substantially the number of analyte molecules per volume directly at the sensor surface. The overall concept of such a biosensor is depicted in **Figure 1**.[5-6]
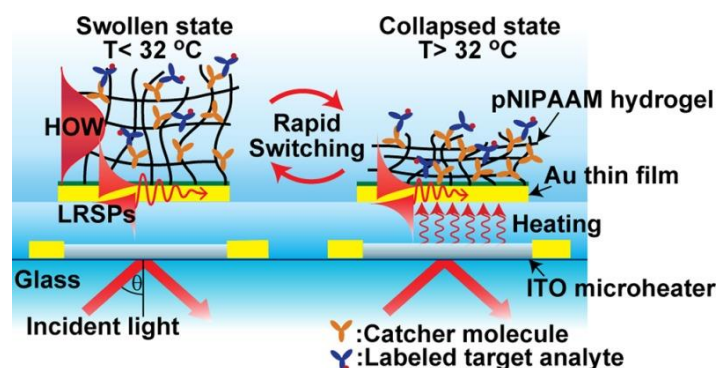
Figure 1: Schematic description of the hydrogel biosensor concept applied in this work.[5]

1. Introduction

1.1 Objectives and Aim of the Thesis

The aim of this thesis was the synthesis, characterization and functionalization of a novel thermoresponsive hydrogel binding matrix for the application in optical biosensing. This binding matrix should then be applied later for the detection of biomarkers in peripheral blood. Relevant requirements applicable to this material are effective antifouling characteristics to prevent unspecific adsorption of biomolecules present in the analyte solution and high swelling ratios for efficient accesses of analyte molecules to the binding sites embedded in the hydrogel matrix. In addition, the material should possess thermoresponsive properties to control its swelling ratio by changing the environmental temperature. In order to combine these requirements in one material, poly(2-oxazoline)s were chosen as basis, as they can show thermoresponsive behavior in aqueous media and have potential low fouling behavior.[7] Surface attachment and crosslinking of the respective material should be performed using the well-established benzophenone photochemistry, which allows crosslinking after deposition of the polymer material onto the respective substrate and thus provides a convenient way of processing. A second aspect of this thesis was the characterization of the deposited layers with respect to their temperature dependent swelling by SPR/OWS. Thereby hydrogel layers of varying phase transition temperatures should be prepared by copolymerization of different 2-alkyl-2-oxazolines. The experiment for the characterization of the hydrogel layers was designed in such a way that the polymer films supported at least two waveguide modes, which allows the determination of refractive index and layer thickness independently from each other.

Another aspect of this thesis was the synthesis and implementation of a post-modification unit by copolymerization with an azide-carrying 2-oxazoline derivative, which can either serve as a coupling site for alkyne modified proteins or for the integration of different functional groups (e.g. carboxylic acid, sulfobetaine, carboxybetaine, oligoethylene glycol). The chemical and optical properties of the deposited layers should then by determined by OWS with respect to their phase transition temperature and swelling ratio. Finally, the application as biosensor matrix was investigated by immobilizing alkyne-modified derivatives in the sensor matrix using a copper(I) catalyzed azide-alkyne cycloaddition reaction. In these post-modification experiments, the successful coupling should be monitored by OWS.

1. Introduction

Beside the synthesis of a novel poly(2-oxazoline)-based binding matrix, already existing platforms should be improved or their properties tuned for specific biosensor applications. For this purpose, mainly photocrosslinkable poly(*N*-isopropylacrylamide)-based polymers, but also dextran-based photocrosslinkable sensor matrices of different average molar mass should be adopted. In both cases, benzophenone photocrosslinking was chosen to perform crosslinking of the hydrogel material and a carboxylic acid functionality served as a potential binding site.

2. Theory

2.1 Oxazolines and Poly(2-oxazoline)s

2.1.1 Monomer Synthesis and Polymerization Mechanism

Oxazolines, also referred to as cyclic imino ethers or cyclic imidic esters, were reported for the first time in 1889.[8-9] The five membered heterocyclic compounds occur in three different isomeric structures, which can be differentiated by the location of the respective double bond (**Figure 2**).[9]
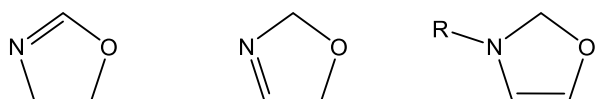
Figure 2: Isomeric structures of 2-, 3-, 4-Oxazolines.

2-Oxazolines have received a growing interest in research since the discovery of its cationic ring opening polymerization (CROP) in the 1960s.[10-14] Beside the use as protecting groups for carboxylic acids in organic synthesis as well as reagents for the synthesis of chiral compounds (e.g. carboxylic acids, lactones, alcohols)[15], the main focus of 2-oxazoline research lies on the synthesis and characterization of novel monomers and polymers. Several routes have been investigated for the preparation of 2-oxazoline monomers[16-17] carrying aliphatic or aromatic substituents or functional groups (e.g. alkene, alkyne, ester, carboxylic acid, amine, alcohol).[10] In 1974 Witte and Seeliger published the most common preparation method for the synthesis of 2-alkyl and 2-aryl-2-oxazolines.[18] For this purpose, mixtures of alkyl-/aryl-nitriles and ethanolamine were heated in the presence of catalytic amounts of metal salts (e.g. $ZnCl_2$, $Zn(OAc)_2$ or $Cd(OAc)_2$) and the respective products were isolated by fractional distillation (**Scheme 1**). This method was also applied for the synthesis of 2-isopropyl-2-oxazoline and 2-n-propyl-2-oxazoline, which were used in this thesis for the preparation of thermoresponsive hydrogel layers.
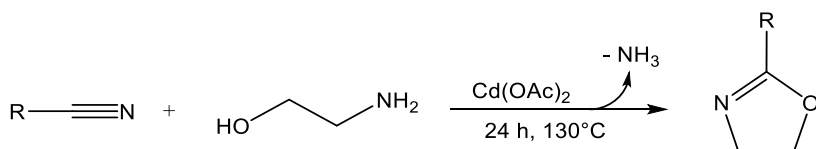
Scheme 1: Synthesis of 2-alkyl-2-oxazolines following Witte and Seeliger.

2. Theory

Another common way for the synthesis of 2-oxazoline monomers is based on the coupling of carboxylic acids with 2-chloroethylamine hydrochloride.[16, 19] By activation of the carboxylic acid functionality with thionylchloride[20-21] or active ester coupling[22-23] (e.g. EDC/NHS or TFA-NHS) the reaction proceeds at room temperature to the respective amide. In the final step, ring closure is achieved by either heating of the respective educt in the presence of anhydrous K_2CO_3[19-20] or by reaction with a base (e.g. KOH, NaOH, Et_3N)[24-27] at room temperature (**Scheme 2**). This method is mostly applied for the synthesis of more complex 2-oxazolines, carrying additional functional groups or having high boiling points, which prevents isolation via fractional distillation. In this thesis, 2-oxazoline monomers with benzophenone or azide functionality were prepared following this method.
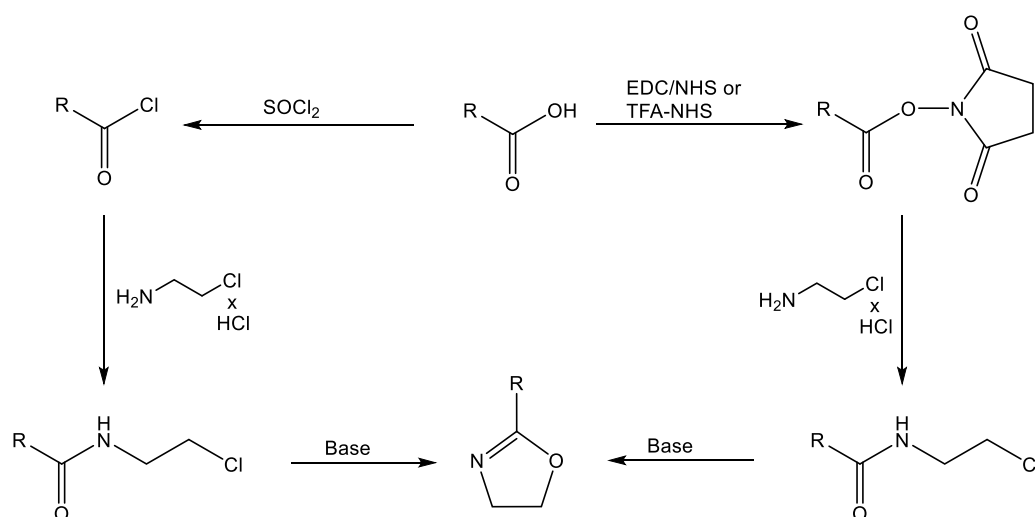
Scheme 2: Synthesis of 2-oxazolines by amidation of carboxylic acids followed by ring closure.

Various initiators have been used for the polymerization of 2-oxazolines, such as Lewis acids (e.g. BF_3, $AlCl_3$), salts of Lewis acids (e.g. $Et_3O^+BF_4^-$), strong protic acids (e.g. $HClO_4$, H_2SO_4, HBr), sulfonate esters (e.g. MeOTf, MeOTs), and alkyl halides (e.g. $PhCH_2Br$, MeI) to name only a few of each type.[28-29] In general, CROP of 2-oxazoline monomers is initiated by an electrophile and can proceed via two different types of propagating species, which can be either ionic or covalent, resulting in poly(N-acyl ethylene imine)s or poly(2-oxazoline)s with the general structure depicted below (**Scheme 3**).[8, 28]
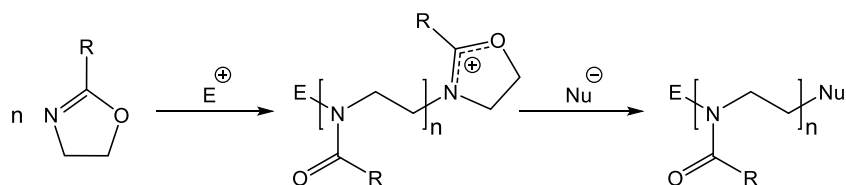
Scheme 3: General polymerization procedure of 2-substituted-2-oxazolines.

Whether the reaction proceeds via an ionic or a covalent type, is strongly determined by the nucleophilicity of the initiator counter ion, but also depends on the nucleophilicity of the respective monomers.[8, 28-29] To explain the difference between both types of reactions in more detail, their corresponding mechanisms are depicted in **Scheme 4** and **Scheme 5**.

Ionic Mechanism:

    1. Initiation
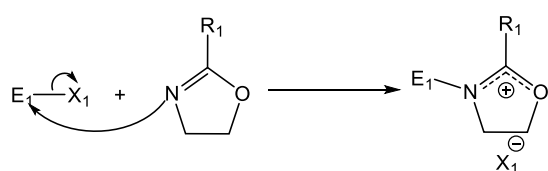
    2. Propagation and Termination
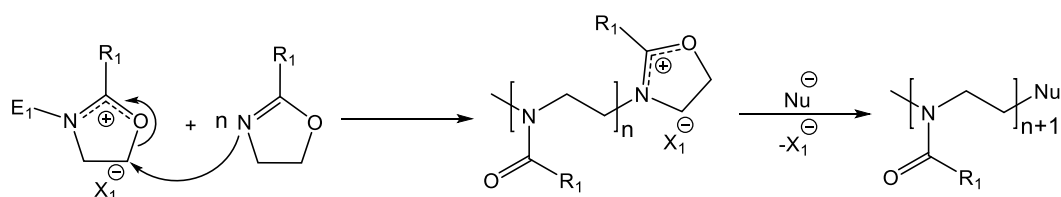
Scheme 4: Ionic mechanism for CROP of 2-oxazolines.

2. Theory

In the first step of the ionic polymerization type, a 2-oxazolinium salt is formed by the reaction of the electrophile E_1 with a respective monomer. In turn, this 2-oxazolinium salt undergoes ring-opening reaction by the nucleophilic attack of a nitrogen atom of another monomer in C(5) position, which results in bond cleavage between O(1)–C(5). This type of reaction is observed for initiators generating counter ions X_1^- less nucleophilic than the monomer.[8, 28]

Covalent Mechanism:

1. Initiation
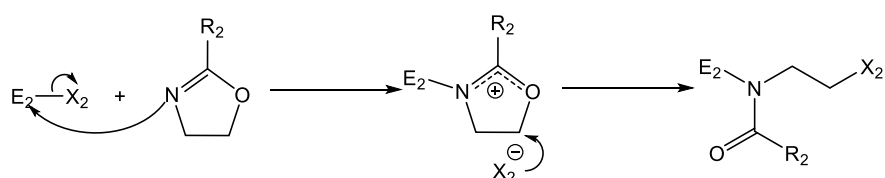
2. Propagation and Termination
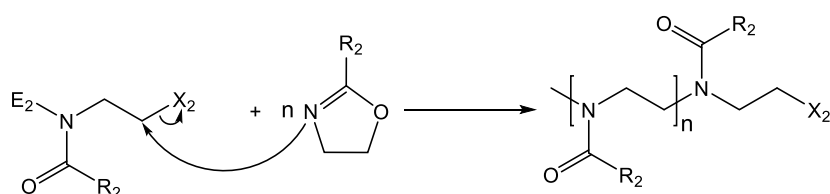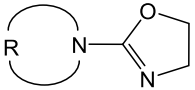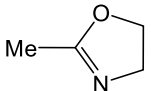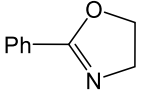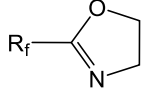
Scheme 5: Covalent mechanism for CROP of 2-oxazolines.

For initiators that generate counter ions X_2^- with higher nucleophilicity than the respective monomer, the 2-oxazolinium salt is attacked by the counter ion itself and the polymerization proceeds via a covalent linkage between C(5)-X_2. A short overview of the relation between the type of CROP and the nucleophilicity of initiator counter ion and monomer is shown in **Table 1**.

Table 1: Type of propagating species vs. monomer and counter ion nulcleophilicities.[28]

Monomer	Nucleophilic Counterions, $X^{\ominus}$				References
	Nucleophilicity ←				
	$Cl^{\ominus}$	$I^{\ominus}$	$OTs^{\ominus}$	$OTf^{\ominus}$	
R–N oxazoline (cyclic)	Ionic & Covalent	Ionic & Covalent	Ionic	Ionic	30-31
Me-oxazoline	Covalent	Ionic	Ionic	Ionic	32-33
oxazoline	Covalent	Covalent	Ionic	Ionic	34
Ph-oxazoline	-	Covalent	Ionic	Ionic	35
R_f-oxazoline	-	Covalent	Ionic	Ionic	36-37

(Left vertical axis label: Nucleophilicity ↑)

$R_f = C_2F_5, C_3F_7$

In general, the CROP can proceed via a quasi-living polymerization mechanism, where side reactions like chain transfer or termination reactions are highly reduced.[28] However, the living character of the reaction is only achieved under appropriate reaction conditions.[28] If living reaction conditions are achieved, a simple end group functionalization is possible by choosing terminating agents with a higher nucleophilicity than the respective monomer.[38] For this purpose water[39], alcohols[40], carboxylic acids[41] or secondary amines[42-44] have been used extensively. Another way for the introduction of an end group functionality is their direct incorporation into the respective initiator (e.g alkyne, azide or epoxide modified tosylate or triflate), which makes CROP a very versatile type of polymerization.[45-47] An overview of common functional initiators and terminating agents is depicted in **Scheme 6** and **Scheme 7**.
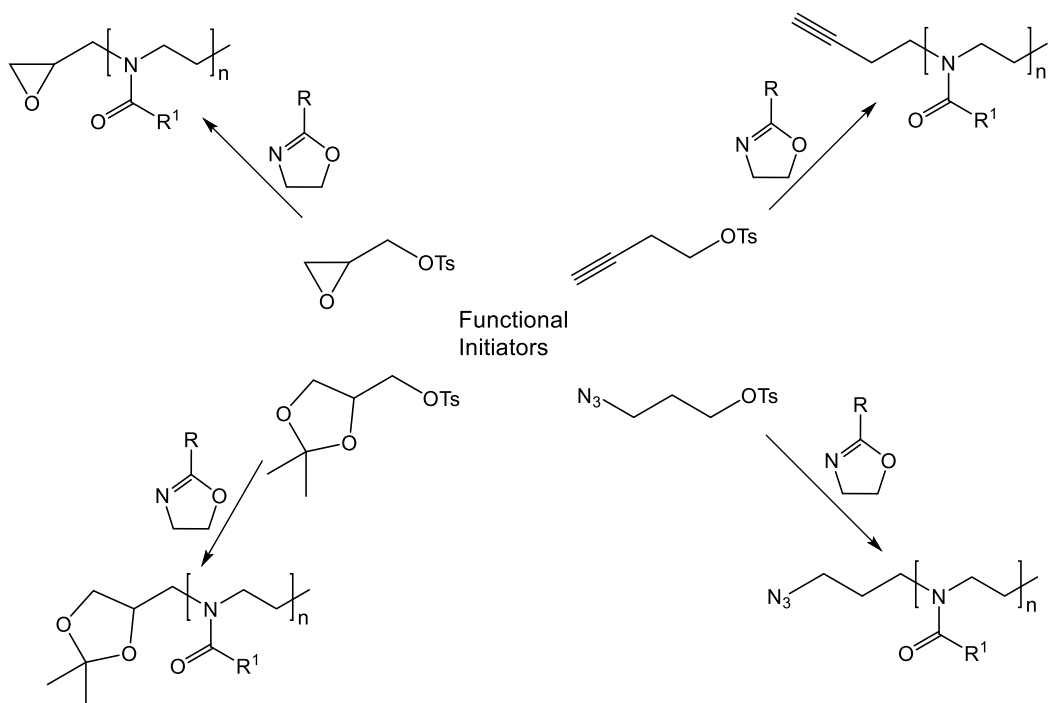
Scheme 6: Examples of end group functionalization via initiators.
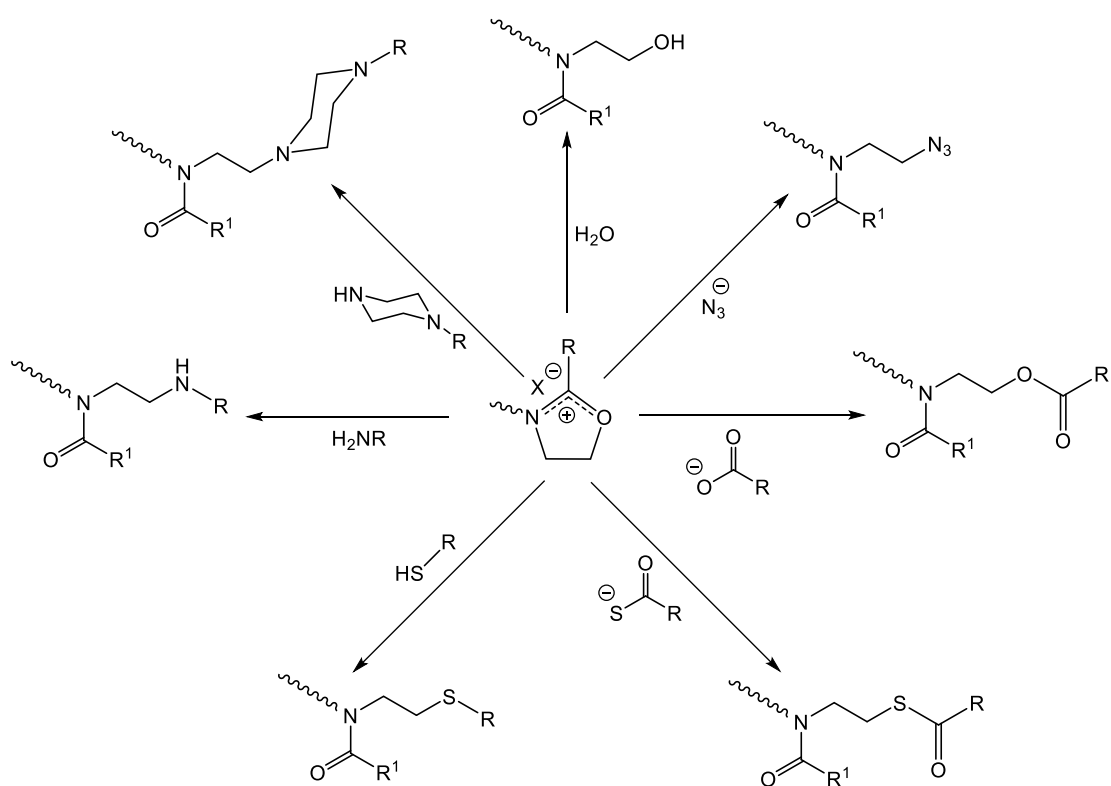
Scheme 7: Examples of end group functionalization via quenching agents.[38]

2.1.2 Side Reactions in CROP of 2-Oxazolines

The mechanism of chain transfer and reinitiation reactions in CROP of 2-oxazolines was discussed first by Litt et. al. in 1975.[48] They studied the reaction kinetics of different 2-alkyl- and 2-phenyl-2-oxazolines using different types of initiators and postulated a mechanism for the side reaction that can take place during the polymerization (**Scheme 8** and **Scheme 9**). First, a proton transfer from the carbon in α-position to the nitrogen atom of an unreacted monomer takes place. Consequently, the active polymer chain end is converted to a neutral species under formation of C=C double bond between α-C-C(2). The newly formed positively charged monomer can propagate further, acting as an initiator and is responsible for low molecular mass tailing in the SEC curves, which is quite often observed for the polymerization products of 2-oxazolines.[40]
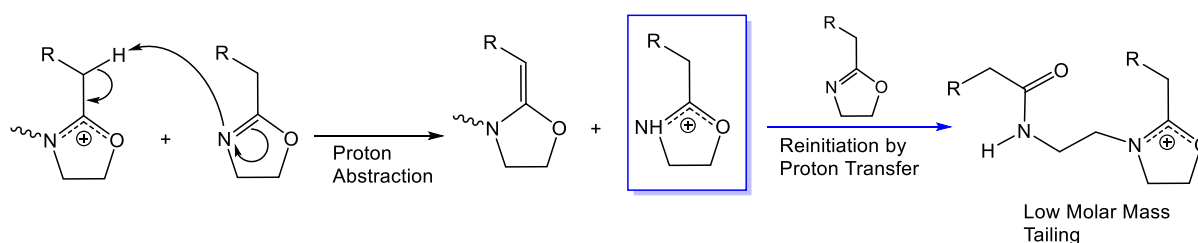
Scheme 8: Chain transfer mechanism to monomer in CROP of 2-oxazolines.

After the chain transfer reaction, the generated enamine species at the previously active chain end can act as a nucleophile and react with active polymer chain ends. This process is much slower than the actual propagation reaction and becomes significant primarily for extended polymerization times. These chain coupling reactions lead to an increased molar mass, which can be observed as a shoulder in the SEC diagram.[40, 48] In addition, after chain coupling took place still active polymer chain ends can undergo further propagation or chain transfer reactions, generating branched or star shaped polymer chain ends.[48]

2. Theory
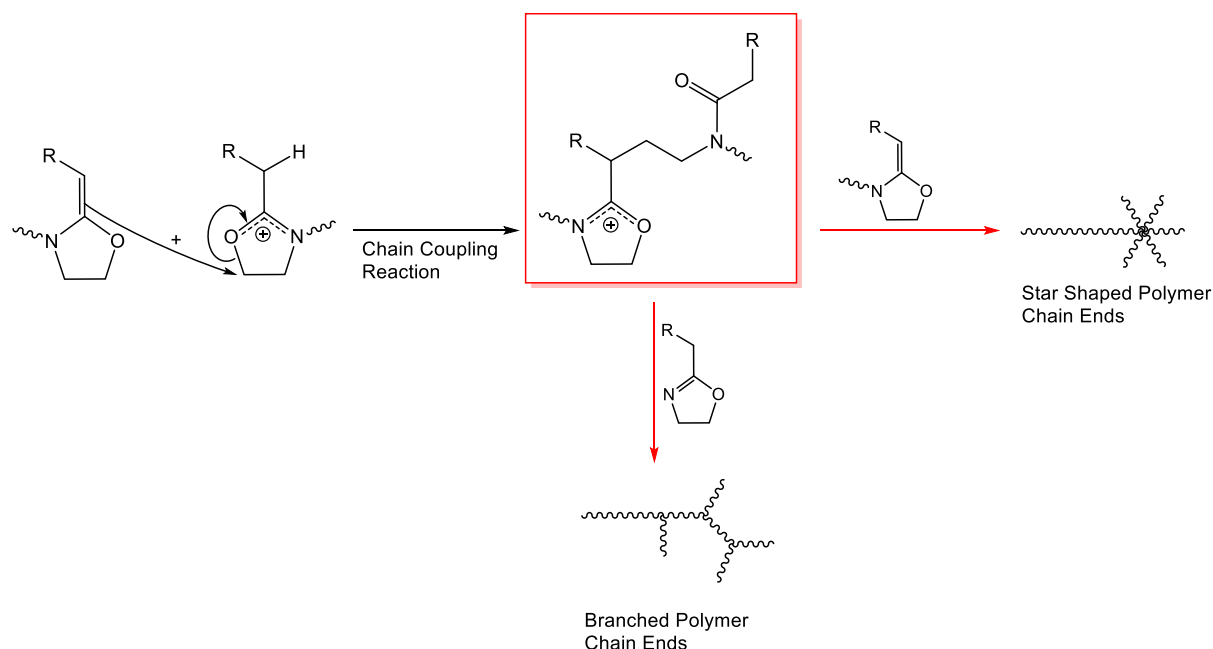
Scheme 9: Chain coupling mechanism in CROP of 2-oxazolines.[48]

In general, these unwanted side reactions occur more often under certain reaction conditions. As for example, higher reaction temperatures increase the probability for chain transfer and coupling reactions. Among others, this was studied by Hoogenboom et. al. for the polymerization of 2-ethyl-2-oxazoline initiated by benzyl bromide using DMAc as solvent. Above a reaction temperature of 100°C, tailing of the molar mass curves was observed by SEC analysis and additionally indicated by the orange appearance of the reaction mixtures.[49]

Besides the temperature, the nature of the initiator and the monomer-initiator ratio M/I have an impact on the probability of side reactions. Again, Hoogenboom et. al. investigated this correlation for the polymerization of 2-ethyl- and 2-methyl-2-oxazoline using MeOTf, MeOTs, MeI or benzyl bromide as initiators, respectively. They found that side reactions occur more frequently for lower M/I ratios, due to the increased number of active centers. Additionally it was found that an increasing nucleophilicity of the initiator counter ion tend to cause side reactions more often.[39]

At last, the influence of the respective monomers used for the polymerization was studied. Here, it was found that monomers with activated α-methylene groups (e.g. 2-benzyl-2-oxazoline) show higher tendencies for the occurrence of side reactions than non-activated monomers or monomers with sterically hindered α-methylene groups (e.g. 2-isobutyl-2-oxazoline).[48, 50-51] A SEC elution diagram of poly(2-isopropyl-2-oxazoline), which was

synthesized in this work, is depicted below (**Figure 3**). The diagram shows the typical bimodal distribution caused by intrinsic chain coupling, as well as the broadening of the SEC curve, which is related to reinitiation reaction. These data were also compared to literature results,[40] which showed a similar behavior.
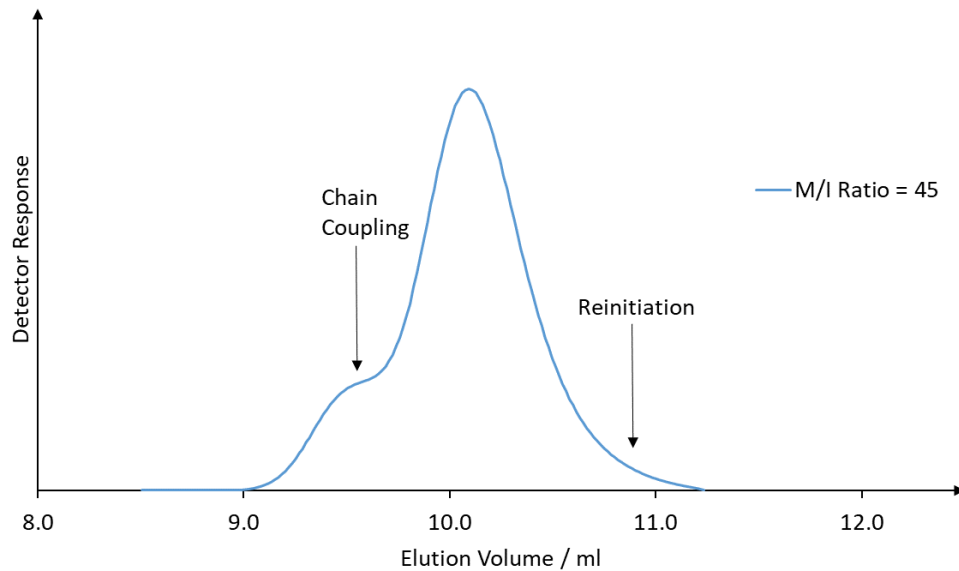
Figure 3: RI detector signal SEC elution diagram of poly(2-isopropyl-2-oxazoline) as synthesized with a M/I = 45 and a reaction temperature T = 140°C. Dispersity Đ = 1.14 as calculated by SEC analysis (higher elution volumes correspond to smaller hydrodynamic radii of the polymer chains, which is usually related to smaller polymer masses).

In an ideal case, molar mass distribution in living ionic polymerization is narrow (relating to a Poisson distribution) with dispersity values Đ close to 1.0, because all polymer chains are initiated at the same time and the reaction proceeds without termination or chain transfer reactions.[48] Side reactions in CROP cause a broadening of molar mass distribution, leading to dispersity values Đ of 1.5 and higher as shown in **Chapter 4.1** and **4.2**.

2.2 Thermoresponsive Polymers

Stimuli responsive polymers, also known as "smart" polymers, attract increasing interest with respect to biomedical applications, such as drug delivery,[52] tissue engineering[53] or diagnostics.[5] These materials are characterized by an abrupt change of their properties, such as solubility, or in the form of surface-attached gels[54] by their permeability,[55, 56] E-modulus[57] or optical density,[5, 58] due to small changes of the environmental conditions, like temperature, pH, solvent or ion concentration, to mention only a few.[59-62] One of the most frequently studied stimuli responsive materials are thermoresponsive polymers, which can be further subdivided into polymers showing lower critical solution temperature (LCST) or upper critical solution temperature (UCST).[59, 63-64]

In general, LCST and UCST can be defined as a specific temperature for which the components of a mixture show complete miscibility (see also **Figure 4**) for all concentration ratios, while heating above (LCST) or cooling below (UCST) this temperature limit leads to their demixing.[59, 65-66] Demixing of thermoresponsive polymer solutions is indicated by precipitation or at least clouding of an initially transparent solution.[59] While focusing on biomedical applications, all polymers discussed in this thesis show their thermoresponsive behavior in water or aqueous media, like buffer-solutions. A typical phase diagram of thermoresponsive polymers is depicted in **Figure 4**, which is obtained by plotting the phase transition temperature as a function of the polymer-volume fraction. There, the LCST and UCST specifically corresponds to a minimum and maximum, respectively, while points along the respective coexistence curves (spinodal) refer to so-called cloud points.[59, 63]
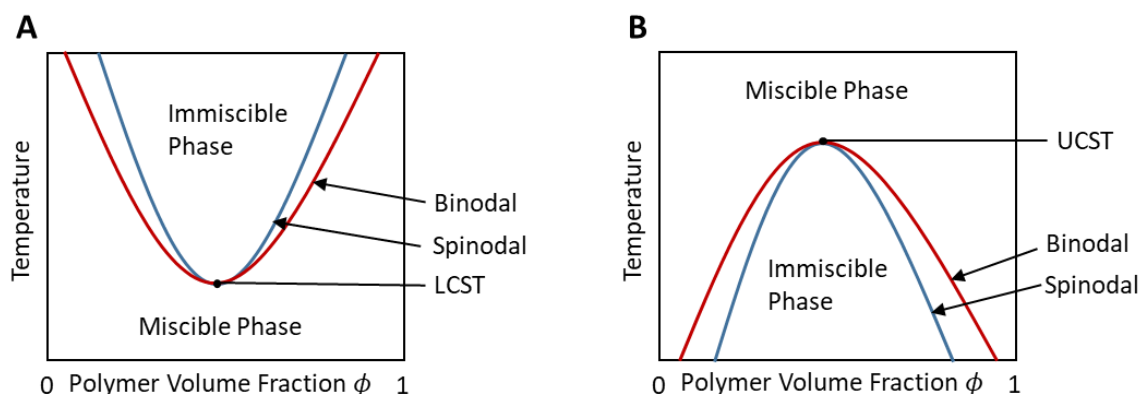
Figure 4: Typical diagram temperature vs. polymer–volume fraction for LCST (**A**) and UCST (**B**) polymers.

2. Theory

For a polymer–water system, the coexistence curve can be described either as a set of conditions at which mixing and demixing coexists or as a boundary between a polymer–water solution and a two-phase system. The process of phase separation can be described by the Gibbs free energy of mixing ΔG_M. While mixing is observed for negative values of ΔG_M, positive values indicate phase separation. Polymer–solvent systems exhibit the same behavior, since negative values of ΔG_M are observed for the respective polymer solutions and positive ones for phase separation.[59, 66-67] In general, the Gibbs free energy of mixing ΔG_M is expressed as follows:

$$\Delta G_M = \Delta H_M - T\Delta S_M \tag{1}$$

While the entropy of mixing ΔS_M exhibits always positive values during the solution process, because of the increasing number of available arrangements (corresponding to an increase in configurational entropy), ΔH_M can have a positive (endothermic) or negative (exothermic) contribution to the Gibbs free energy of mixing ΔG_M, which depends on the balance between polymer-polymer, solvent-solvent and polymer–solvent interactions. In an ideal case the solvent–solvent interactions are equal to solvent–polymer and polymer-polymer interactions and thereby $\Delta H_M = 0$, which is also defined as theta conditions.[65-66] Thermodynamics of polymer solutions are described in more detail by the Flory-Huggins theory, which includes solvent–solvent, polymer–polymer and polymer–solvent interactions, represented by the Flory-Huggins interaction parameter χ_{12}.[65-66] ΔG_M, ΔH_M, ΔS_M are then given by

$$\Delta H_M = n_1\phi_2\chi RT \tag{2}$$

$$\Delta S_M = -R[n_1 ln\phi_1 + n_2 ln\phi_2] \tag{3}$$

$$\Delta G_M = RT[n_1 ln\phi_1 + n_2 ln\phi_2 + n_1\phi_2\chi_{12}] \tag{4}$$

Where n_1 and n_2 represent the number of moles for each component in the system and ϕ_1 and ϕ_2 represent the volume fractions of solvent and polymer. For polymers showing an LCST behavior, the process of phase separation is based on an increase in entropy.[59, 68] At temperatures below the LCST, hydrophobic parts of the respective polymer chains are surrounded by water molecules, which is also known as hydrophobic hydration. The generated water shell is enthalpically favored, due to the formation of stronger hydrogen bonding compared to bulk water, which results in a negative contribution to the enthalpy of mixing ΔH_M. However, this ordered structure goes along with a decrease in entropy, because

the number of possible arrangements is reduced, resulting in a negative contribution to the entropy of mixing ΔS_M. Upon heating of the polymer solution, phase separation occurs above the LCST due to an overall gain in entropy. Water molecules that are released from the polymer surrounding water shell have a positive contribution to the entropy of mixing ΔS_M, which is much larger compared to the negative contribution of the aggregating polymer. As a result, the polymer shows an inverse dissolution behavior, which is mainly based on an overall gain in entropy.[68-70]

The most intensively studied thermoresponsive polymer is poly(N-isopropylacrylamide) with a LCST of 32°C, approximately. Other well studied polymers showing LCST behavior in aqueous solution are 2-oxazoline-based polymers, whereby three poly(2-alkyl-2-oxazoline) homopolymers are known for their thermoresponsive behavior in pure water.[71] Chemical structure and corresponding LCST of those homopolymers are depicted in **Figure 5**.
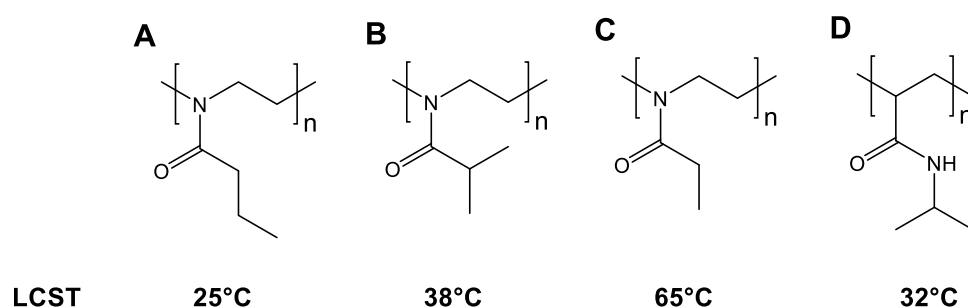
Figure 5: Chemical structure of some LCST polymers with their corresponding transition temperature. (**A**) poly(2-n-propyl-2-oxazoline), (**B**) poly(2-isopropyl-2-oxazoline), (**C**) poly(2-ethyl-2-oxazoline), (**D**) poly(N-isopropylacrylamide).

In general, the LCST of thermoresponsive polymers can be tuned by copolymerization with more hydrophilic or hydrophobic monomers, respectively. Additionally, the degree of polymerization and polarity of the respective end groups have an impact on the LCST.[71-73] It is worth noting, that for polymer solutions showing an upper critical solution temperature (UCST), the effect of phase separation is based on an enthalpically driven process. While raising the temperature above the UCST, the dissolving process occurs due to an increased formation of polymer-water hydrogen bonds, resulting in an overall gain in enthalpy of mixing ΔH_M.[59, 69]

2.3 Gels and Hydrogels

During the last decades, gels and as specially hydrogels show a growing interest with respect to biomedical applications, such as wound dressing, cell culture platforms or drug delivery, due to their biocompatibility and their stability in aqueous media.[74-76] The first notable application of hydrogels goes back to the year 1960 when Lim and Wichterle synthesized a biocompatible hydrogel based on poly(2-hydroxyethyl methacrylate), which was later used for the fabrication of contact lenses.[77-79]

In general, a gel can be defined as a dispersed system based on a porous three-dimensional, network-forming material, whereas the interstitial volume is occupied by a liquid (lyogel) or gas (xerogel).[80-82] In case of a polymer-based hydrogel, the three-dimensional polymeric network is specifically swollen by water. Its ability to absorb water arises from the presence of hydrophilic groups in the respective polymer chains.[82-83] The network structure of hydrogels is formed by interconnected (cross-linked) polymer chains, which prevent the network from dissolving. Such swollen gels possess properties that have both characteristics of liquids as well as of solids and hence lead to a material with viscoelastic behavior. Their highly porous structure allows the diffusion of liquid and dissolved compounds, such as nutrients, drugs and analytes.[74, 77, 82, 84] Crosslinks between single polymer chains can be either of chemical nature in the form of covalent bonds, resulting in so-called permanent hydrogels, or of physical nature. Hydrogels formed by physically bonded networks show often reversible crosslinking, with the possibility to redissolve the network by changing environmental conditions like pH, temperature or the ionic strength of the respective swelling liquid. In these physical networks, the interconnections between single polymer chains can be based on coordinative, electrostatic, hydrophobic or dipole-dipole interactions, as well as chain entanglements.[75, 81-82, 84]

Hydrogels can be derived either from natural occurring polymers or of synthetic origin (**Figure 6**). Hydrogels based on natural occurring polymers are mostly based on polypeptides, polysaccharides and polynucleotides, attracting particular attention with respect to biomedical applications due to their biocompatibility and biodegradability.[75, 82, 85] For the preparation of these gels, often post-modification reaction of the as-derived polymers are required to introduce the ability of network formation via crosslinking (e.g. photocrosslinkable

dextran)[6, 86]. Non-modified natural based hydrogels are also known, with intrinsic gel-forming properties. As an example, hydrogels from alginate are prepared by adding calcium ions to an aqueous alginate solution. In this particular case, the resulting network is based on the formation of physical crosslinks.[87-88] Additional functional groups (e.g. amino, carboxylic acid, hydroxy) can be incorporated by post-modification in order to tune the chemical properties of such hydrogels towards certain applications.[6, 82, 89-90]

Synthetically derived hydrogels are mostly based on macromolecular systems obtained by free radical polymerization, like for example poly(acrylate)s, poly(methacrylate)s, poly(vinylalcohol) or poly(vinylpyrrolidone).[77, 82, 85] Polymers formed by other reaction types include poly(ether)s, poly(urethane)s and poly(2-oxazoline)s, which have been used extensively for hydrogel fabrication.[77, 81, 91-92] The properties of synthetically derived hydrogels can be easily adjusted via copolymerization with monomers carrying functional groups, allowing post-modification of the respective polymers or hydrogel networks.[5, 93-95] In addition, polymer blends of natural occurring and synthetic polymers have been successfully employed to enable crosslinking or to improve the properties of the corresponding hydrogels.[90, 96]
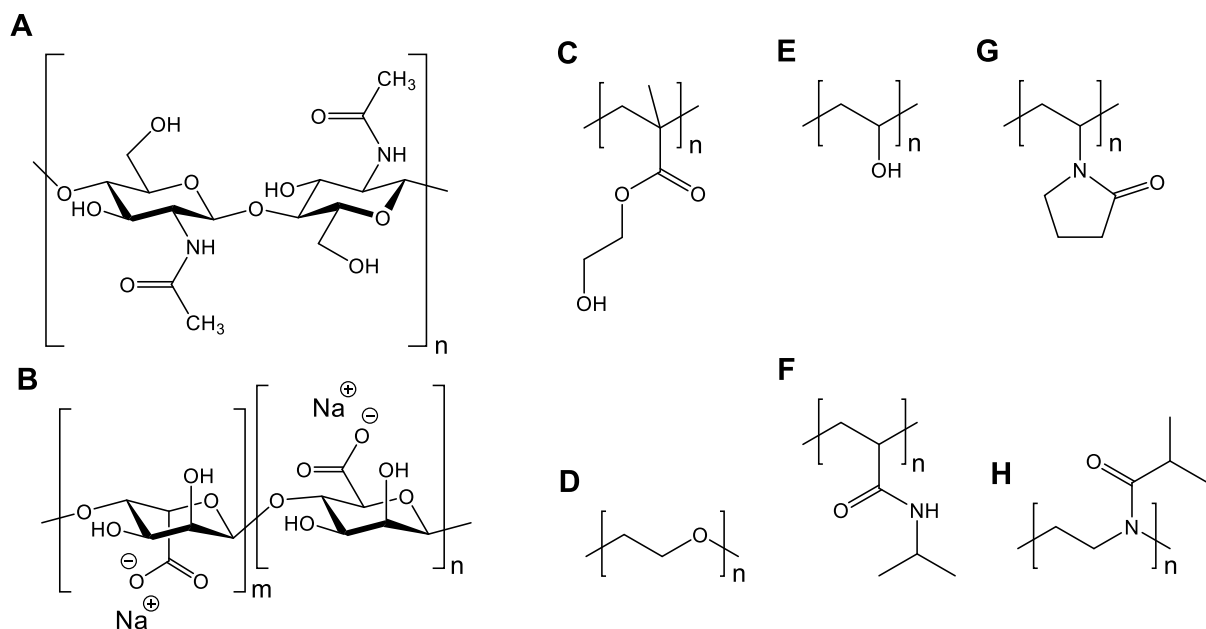
Figure 6: Common natural and synthetic polymers used for hydrogel fabrication. (**A**) Chitin, (**B**) sodium alginate, (**C**) poly(hydroxyethylmethacrylate), (**D**) poly(ethylene glycol), (**E**) poly(vinyl alcohol), (**F**) poly(*N*-isopropylacrylamide), (**G**) poly(*N*-vinyl pyrrolidone), (**H**) poly(2-isopropyl-2-oxazoline).

2.4 Swelling of Hydrogels

When the dry hydrogel network is brought into contact with water, these materials can swell by multiple times to their initial weight and volume, respectively. The swelling process is induced by hydration of the most polar groups inside the respective polymeric network, also referred to as primary bound water.[77, 97] In a second step, water molecules start to interact with the hydrophobic parts of the network, which is known as the secondary bound water.[77, 97] Both, primary and secondary bound water molecules contribute to the total amount of bound water. After complete hydration of the polymer chains, the network undergoes an additional swelling process, which is a result of the osmotic driving force towards (hypothetical) infinite dilution. Obviously, complete dilution of the network is opposed by the covalent or physical crosslinks, which sustain an elastic network retraction force resulting from the coiling chain segments between the crosslinks. The balance between osmotic swelling pressure and entropically driven chain retraction result in an equilibrium swelling state of the hydrogel. The additionally absorbed water is referred to as free or bulk water, that fills the space between the already hydrated polymer chains.[77, 97-98] The overall water content and thus the mechanical properties of swollen hydrogels is influenced by different factors, such as the environmental temperature, crosslinking density and polymer–water interactions. In general, higher crosslinking densities impart shorter chain segments, which increases the elastic retraction force and consequently decrease the amount of bulk water in the network and the associated swelling ratio. Inversely, lower crosslinking densities lead to polymer networks with higher swelling ratios. Also the presence of ionic moieties has an influence on the swelling ratio, as it can be observed that charged hydrogel networks show higher swelling ratios compared to neutral ones with otherwise identical architecture. The reasons are the very high polarity of the ionic groups in the polymer chain and the higher concentration of counter ions within the hydrogel structure. These free ions impart an additional osmotic pressure, which renders the hydrogel capable of absorbing larger amounts of water.[77, 83, 98-99] Beside the importance of the swelling ratio, the swelling kinetics (also called swelling response) of hydrogels is of high interest, as it directly relates to the efficiency of solute/mass transport of nutrients, gases or bioactive agents (e.g. growth factors) through network. These characteristics are of fundamental relevance for the application of such hydrogels in

regenerative medicine.[74] Tanaka and Fillmore[100] developed in 1979 a theory to describe the swelling kinetics of gels, which is based on the equation:

$$t = \frac{a^2}{D} \qquad (5)$$

Where D represents the diffusion coefficient of the liquid medium within the gel, a the dimension of the gel and t the characteristic time for swelling of the gel. This equation states, that the response time is strongly influence by the dimensions (and consequently the geometric shape) of the respective gels. It is obvious, that small-sized hydrogel materials, like mircogels, show a much quicker response time than larger 3D bulk gels. Furthermore, spherically shaped gels show a much faster response compared to surface attached ones for constant values of a, because of the much larger surface–volume ratio.[100-101]

Swelling of surface attached and free, non-restricted networks differs strongly from each other. Free hydrogels can swell isotropically in all three space dimensions and the amount of absorbed water, also referred to as equilibrium water content EWC can be conveniently determined by the mass of the respective hydrogel in dry and swollen state, as given by the equation:

$$EWC = \frac{W_t - W_{dry}}{W_t} \times 100\% = \frac{W_w}{W_t} \times 100\% \qquad (6)$$

The degree of swelling D_S can be expressed as:

$$D_S = \frac{W_t}{W_{dry}} \qquad (7)$$

Here, W_w represents the mass of the absorbed water, W_t the combined mass of absorbed water and the dry hydrogel and W_{dry} the mass of the hydrogel in the dry state.[77, 81]

In contrast, surface-attached networks swell in an anisotropic fashion, with a swelling gradient that increases away from the surface and a strong tendency for buckling of the respective hydrogel surface.[82, 102] In addition, the surface-attached networks experience a higher linear swelling ratio compared to unconstrained ones, which results from the fact that their attachment limits the expansion within the substrate plane, which gives rise to a higher osmotic pressure and thereby to additional swelling in the extension direction normal to the substrate surface.[102-103]

3. Characterization Methods

3.1 UV/VIS Spectroscopy

UV/VIS spectroscopy measures the wavelength dependent transmittance of a sample, which was exploited in this thesis to study the temperature dependent aggregation of the newly synthesized thermoresponsive polymers in aqueous solution. The interaction of electromagnetic radiation with molecules leads to several different processes, like transmittance, reflection, scattering and absorbance. Absorbance induces further processes like emission (fluorescence, phosphorescence) or photochemical reactions. In UV/VIS spectroscopy the absorbance and related to that, the excitation of electrons, is typically investigated for wavelength between 200–800 nm. For organic substances, excitation occurs predominantly for electrons with lowest binding energy, corresponding to π–electrons of double and triple bonds of unsaturated compounds and aromatic systems or for lone pair electrons excited into anti-bonding orbitals.[104-107] Characteristic bands of a UV/VIS spectrum can be used for qualitative analysis of unknown samples. For a known substance, quantification of concentration is achieved by comparing absorbance values of a fixed wavelength with a calibration curve. According to Lambert–Beer's–Law, the absorbance E depends linear on the concentration c of a certain substance, with the molar extinction coefficient ε_0 and d, representing the path length of the beam that passes the sample solution.[105, 107]

$$E = log_{10} \frac{I_0}{I} = \varepsilon_0 cd \qquad (8)$$

However, linearity of Lambert–Beer's–Law is only given for a certain concentration range, mostly less than 0.01 M, and deviations at higher concentrations are primarily due to interactions between analyte molecules in close proximity to each other (like aggregation effects).[108] Additionally, UV/VIS spectrometry can be used for turbidity measurements, especially for the investigation of cloud points of thermoresponsive polymers in solution. Therefore, the polymer solution is heated up while measuring the transmittance of the sample. The cloud point is then defined as the temperature at which a transmittance of T = 50% is reached.[109-111] The reduction of the transmittance is caused by absorption or scattering of the incidence light at aggregated polymer particles, which are present above the cloud point and grow with increasing temperature and time. The amount of absorbed or scattered light

scales with size and concentration of the respective particles as well as the wavelength of the incoming light. In this case, the transmittance is given by

$$T = {}^{I}/_{I_0} = kcd \qquad (9)$$

Here, I represents the transmitted light intensity, I_0 the incidence light intensity, k the molar turbidity coefficient, c the particle concentration and d the pathway through the polymer solution.

3.2 Thermal Analysis of Polymers (DSC/TGA)

DSC is a thermal analysis method for the investigation of temperature dependent phase transitions taking place, while a sample is heated up with a constant heating rate. It has been used frequently for studying the thermal properties of natural and synthetic polymers, with respect to their melting and crystallization behavior. Also, the determination of the glass transition temperature T_g of polymers and the investigation of endo- or exothermal reactions have been performed frequently by using DSC.[65, 112-113] In this thesis, DSC was applied for the determination of the glass transition temperature of different 2-alkyl-2-oxazoline-based homo- and copolymers, with respect to changes in their composition.

For the measurement a sample and a reference, normally an empty aluminum pan, are placed into a measuring cell and heated up with a constant temperature rate. During the measurement, both sample and reference are kept at the same temperature. Endo- or exothermal processes (e.g. melting or crystallization) as well as the glass transition result in a change of the specific heat capacity and the related differences in heat flow are compensated by adjusting the energy input to the system. As a consequence, the detected signal is derived from the different energies necessary for keeping sample and reference at the same temperature. The signal is often expressed as difference in heat flow between sample and reference with respect to time or temperature.[65, 113-115] During an exothermal process, energy is released from the system and the change in heat flow is expressed as negative peak, while an endothermal process shows the opposite behavior. For the glass transition temperature T_g a step like signal is observed.[65, 114-115]

Conventional DSC analysis has its limitations with respect to separation of overlapping processes, like molecular relaxation and glass transition or melting and crystallization taking place while a polymer sample is heated up.[115-116] In order to address this limitation, modulated DSC (M-DSC) was introduced by Reading in 1994,[117] which differs in the temperature ramp applied for the measurement. In a conventional DSC, the temperature is raised linear with time, whereas in M-DSC an oscillating heating profile is overlaid on a linear temperature ramp. In other words, in M-DSC the temperature is continuously increased by applying an oscillating heating rate (compare **Figure 7**).[115-117]

A

B
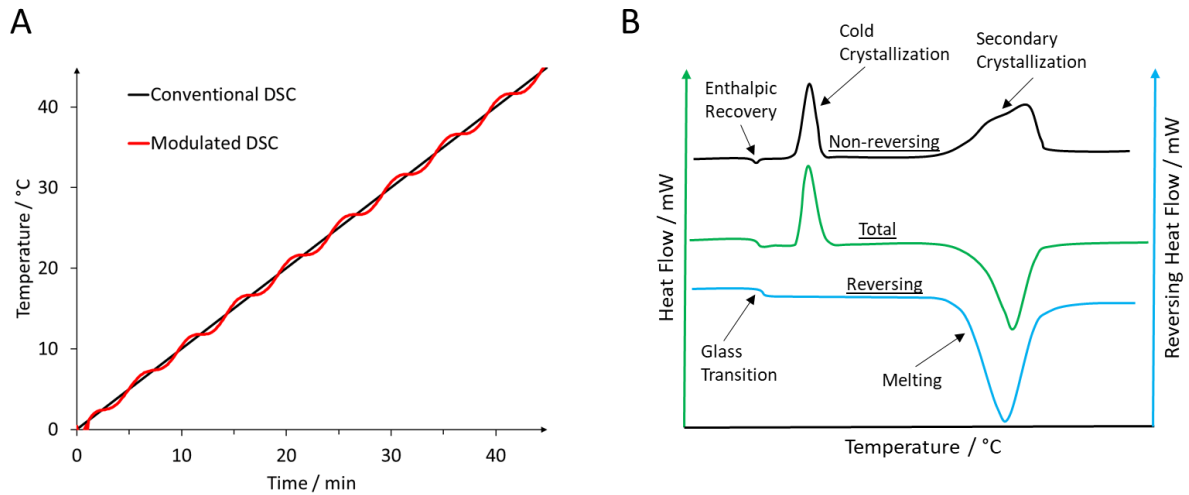
Figure 7: (**A**) Comparison between conventional DSC (**black**) and modulated DSC (**red**) temperature ramp. (**B**) Signal traces after deconvolution (reversing and non-reversing) and schematic representation of possible thermal transitions that can occur while heating a polymer sample.

By using this method, a reversing contribution can be extracted from the total heat flow signal, which allows determination of the non-reversing component by subtracting the reversing from the total heat flow.[114-115, 118] Events that contribute to the reversing part are thermodynamic equilibrium processes like glass transition and melting. Kinetically driven events like crystallization, curing or decomposition appear in the non-reversing part.[114-115] In many cases TGA (thermogravimetric analysis) experiments are performed prior to DSC in order to gain information about the decomposition behavior of the respective polymers. Furthermore, TGA is used to analyze polymers with respect to additives (e.g. inorganic fillers) or volatiles (e.g. moisture, softener, solvent residues), with the possibility to couple the TGA method to an IR- or mass spectrometer.[119-121]

3.3 Size Exclusion Chromatography

Size exclusion chromatography (SEC), also referred to as gel permeation chromatography (GPC), is a technique that is used for the characterization of soluble polymers (linear, branched or star-shaped) with respect to their average molar mass and molar mass distribution.[122] The technique of SEC was developed by Porath and Flodin[123] and first applied for the investigation of water soluble polymers using crosslinked dextran gels as column material.[123-124] The working principle of SEC is rather simple. A polymer sample is dissolved in a proper solvent (the mobile phase) and passed through a column packed with a granular, porous material, the stationary phase, with different pore sizes (approximately from 5-50 nm). The separation process is based on the hydrodynamic radii of the polymer chains. Smaller molecules remain longer in the column compared to larger ones, because they can access most of the available pore volume by diffusion, which increases their pathway through the column and thereby the elution time.[122, 124-125] As such, the ideal SEC mechanism is based solely on an entropic process. Depending on the application, different kinds of column materials are applied, like porous silica or highly crosslinked polymers like polystyrene-polydivinylbenzol networks.

For signal recording, many different detectors are available. Most common detectors are concentration sensitive detectors (e.g. UV-detector, refractive index (RI) detector). Here, the signal is proportional to the polymer concentration in the eluent. As these detectors measure only polymer concentration in relation to the elution volume, a calibration curve of polymer standards with defined molar masses is necessary for data evaluation in order to correlate the molar mass of an unknown sample with its corresponding elution volume. For this purpose, the elution time of polymer standards with different molar masses is measured and compared with the polymer sample. Ideally, these standards have narrow molar mass distributions and the same or at least a similar chemical structure and composition to minimize analysis errors resulting from polymer interactions with the column material (enthalpic contribution). In general, a concentration sensitive detector is indispensable, if the ratio between polymers of different molar masses needs to be quantified.[122, 124-125] The second class of detectors used in SEC are the molar mass sensitive detectors (e.g. viscosity detectors, light scattering detectors). In combination with a concentration sensitive detector, direct determination of molar masses of polymer fractions is possible.[122] In this case, the concentration has to be known for data

evaluation, due to the fact that scattering intensity R_θ and viscosity η are concentration dependent.

3.4 Atomic Force Microscopy

Atomic force microscopy (AFM) is a technique for the investigation of surfaces on the atomic scale, invented by Binnig, Quate and Gerber in 1985.[126] In polymer sciences, this technique has been used frequently for imaging of surface topographies, characterization of mechanical properties by nano-indentation, measuring of adhesion forces between tip and polymer sample and for the determination of swelling ratios of surface attached hydrogel layers.[57, 127] In this thesis AFM was applied for the investigation of the elastic modulus of surface-attached and water-swollen layers of thermoresponsive poly(2-oxazoline) hydrogels with different crosslinking densities at temperatures below and above their phase transition temperature.

The measurement principle of AFM is based on attractive and repulsive forces between the tip at a flexible cantilever and the sample surface, which cause deflection of the cantilever. An image of the surface topography is then generated by moving the tip across a certain area and simultaneous monitoring the cantilever deflection at each point.[128-129] For measuring of the deflection, a laser beam is directed onto the backside of the cantilever and the reflected beam is detected by a photodiode. During the measurement, the vertical and horizontal positioning of the cantilever with respect to the sample surface is controlled by piezoelectric actuators.[129-130].

AFM can be performed in several different operation modes. The most common ones are contact or static mode and tapping mode.[128-130] In contact mode, the cantilever is brought into direct contact with the sample surface and its deflection as a function of the surface profile results from repulsive tip–sample interactions.[131] While maintaining permanent contact with the surface, either the deflection of the cantilever or the distance between cantilever and average sample plane are kept constant (aka "constant height" mode). If a constant deflection of the cantilever is applied, also the force is constant while the distance between tip and sample varies. Operating the AFM in constant height mode, the applied force and thus the deflection of the cantilever changes with variations in surface asperities.[129-130] As the cantilever works like a flat spring, its mechanical properties are defined by its spring constant.[132]

In general, the contact mode is predominantly applied for stationary nano-indentation measurements of soft materials without moving the sample in the x-y-plane, because in such

a lateral scanning process the high surface friction could damage the tip and sample (besides notorious tip contamination problems).[130, 133-134] When using the nano-indentation method, a force–distance curve (**Figure 8**) is generated measuring tip deflection during sample approach and retraction, which can be analyzed for the characterization of the sample's mechanical properties, like E-modulus or adhesion forces present between tip and sample[132, 135].
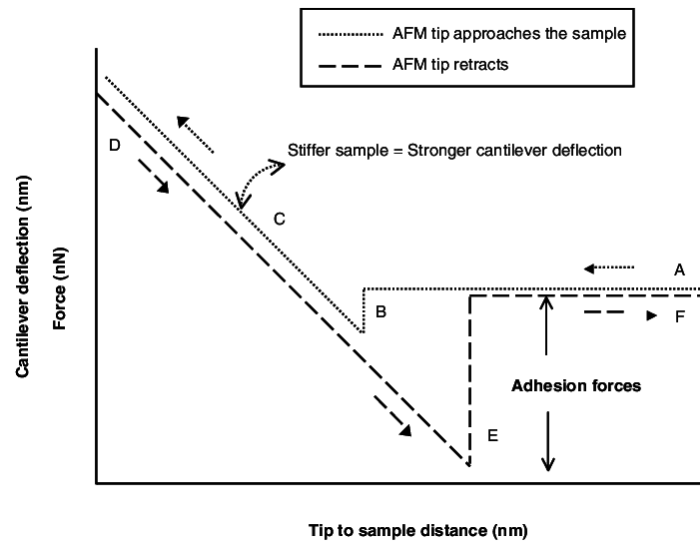
Figure 8: Schematic of an idealized AFM force–distance curve.[136]

While approaching the surface (trace (**A**) in **Figure 8**), the cantilever is bend downwards in response to attractive forces between the tip and the sample. This process, also called snap on (**B**), is either caused by capillary forces of condensed water or van der Waals interactions between tip and sample. Upon further approach, the subsequent repulsive contact (**C**) with the surface bends the cantilever in the opposite direction away from the surface, following Hooke's law. When the tip is retracted (**D**) from the surface, at first the cantilever bending slowly relaxes to the point of zero force (around the height of line (**A**)) and then the cantilever is again bend downwards, due to attractive interactions, like adhesion or capillary forces (**E**).[128-130] Depending on the nature and strength of these interactions, the resulting force–distance curve may vary strongly from the one depicted in **Figure 8**.

Surface topographies of soft samples, like swollen hydrogel layers or biological samples, are mostly measured using the tapping mode.[133-134] In this mode, the cantilever is driven to oscillate with a certain frequency and consequently the tip periodically touches the sample surface. The amplitude of the oscillating is influenced by the surface topography. While

scanning planar areas the amplitude stays constant, whereas bumps and holes cause a change in the amplitude of the oscillating cantilever. Bumps lead to a decrease of the amplitude, due to the reduced space between the surface and the tip, while holes have the opposite effect, resulting in an increased amplitude. Consequently, the amplitude changes according to the surface topography of the sample. An advantage of this method compare to the contact mode is the reduced surface friction between tip and sample, reducing also the propensity of tip and surface damage.[127-130]

3.5 Surface Plasmon Resonance and Optical Waveguide Mode Spectroscopy

3.5.1 Surface Plasmon Resonance Spectroscopy (SPR)

Surface plasmon resonance spectroscopy is an optical analysis technique of dielectric media in contact with an electrically conducting surface, which can be used for example, to investigate the interaction of molecules with a respective metal surface. In the context of biosensing, it has been frequently employed as a platform to study binding reactions of analytes, like proteins or drugs, with ligands attached to surfaces or immobilized in a sensor matrix.[5, 137-139] Furthermore, the swelling and collapsing behavior of thermoresponsive hydrogel layers could be characterized in great detail by SPR.[5, 82, 140]

The principle of SPR spectroscopy is based on the excitation of surface plasmons by light, which in general can be described as surface charge oscillations at the interface of a metal (e.g. Au or Ag) in contact with a dielectric (e.g. glass). [141-142] According to Snell's law, impinging light is refracted at the interface of two transparent materials with different refractive indices n_1 and n_2. Thereby the angle of incidence is larger than the angle of refraction when the incoming light passes the optically denser medium at last. If the incoming light passes the optically denser medium first, this process is vice versa. For the second phenomenon another process, the total internal reflection, can be observed when the angle of incidence reaches the so-called critical angle. At this point, light is propagating at the interface of both materials, whereas for larger angles total internal reflection occurs. The critical angle θ_c is derived from Snell's law and given by the following equation, with n_1 being the refractive index of the optical denser medium.[141-144]

$$\frac{sin\theta_1}{sin\theta_2} = \frac{n_2}{n_1} \qquad with \qquad \sin\theta_c = \frac{n_2}{n_1} \tag{10}$$

Total internal reflection causes an important side effect at the interface of both materials, called the evanescent field penetrating the optical less dense medium. The range l of the evanescent field standing perpendicular to the surface is given by:

$$l = \frac{\lambda}{2\pi\sqrt{(n\,\sin\theta)^2 - 1}} \qquad with \quad \theta > \theta_c \tag{11}$$

and decays exponentially with the distance to the interface.[142, 145]

3. Characterization Methods

Today's SPR are mostly designed according to Kretschmann (**Figure 9A**), who developed its setup in 1971.[146] Here, a gold layer of approximately 50 nm is placed at the interface. The evanescent field is able to penetrate the layer and induces the excitation of the surface plasmons.[142] A requirement for the excitation is that the wave vector of the evanescent field matches the wave vector of the surface plasmon, which is realized only when p-polarized light is used.[117, 141, 145, 147] The wave vectors of the evanescent field K_{ev} and the surface plasmon K_{SP} are given by the equations below, with wavelength λ and angle of incidence θ_{SPR} of the incoming light and the refractive index n_1 of the optically denser medium. The wave vector of the surface plasmon depends on the refractive index of the gold layer n_{Au} and on the refractive index of the optically less dense medium n_2 above the gold layer, which in most cases is water or air.[141-142, 146]

$$K_{ev} = \frac{2\pi}{\lambda} n_1 \sin \theta_{SPR} \qquad (12)$$

$$K_{SP} = \frac{2\pi}{\lambda} \sqrt{\frac{n_2^2 n_{Au}^2}{n_2^2 + n_{Au}^2}} \qquad (13)$$

The resonance angle θ_{SPR} can be determined by equating both vectors $K_{ev} = K_{SP}$ and by solving the equation for $\sin \theta_{SPR}$. At this point, resonant coupling between the evanescent field and the free electrons of the metal surface takes place, resulting in excitation of the surface plasmon and, associated therewith, an energy loss of the incoming light.[142] In practice, the intensity of the reflected light is recorded with respect to the angle of incidence of the incoming light. During resonant coupling the intensity of the reflected light decreases, whereby the resonance angle θ_{SPR} is equal to the minimum of the recorded curve.[145]

$$\sin \theta_{SPR} = \frac{1}{n_1} \sqrt{\frac{n_2^2 n_{Au}^2}{n_2^2 + n_{Au}^2}} \qquad (14)$$

By adsorption of molecules onto the gold layer or for a polymer layer coated on top, the refractive index n_2 is changed and consequently the resonance angle θ_{SPR} shifts (**Figure 9B**). The change of the refractive index is used for data analysis and gives information about absorption–desorption processes, like thiol monolayer formation on a gold substrate[141, 148-149], protein absorption onto thiol monolayers[149-151], or temperature dependent swelling–collapsing of thermoresponsive polymers.[5, 140] Also capturing of analytes like proteins by functionalized thiol monolayers or by a surface-attached polymer matrix can be monitored

using SPR, as all processes involve a change of the refractive index n_2.[5, 147] For this purpose biorecognition elements are needed, which can be attached either directly onto the gold as a monolayer or immobilized in a sensor matrix of a swollen polymer network, that is attached to the substrate.[5, 147, 152-153]
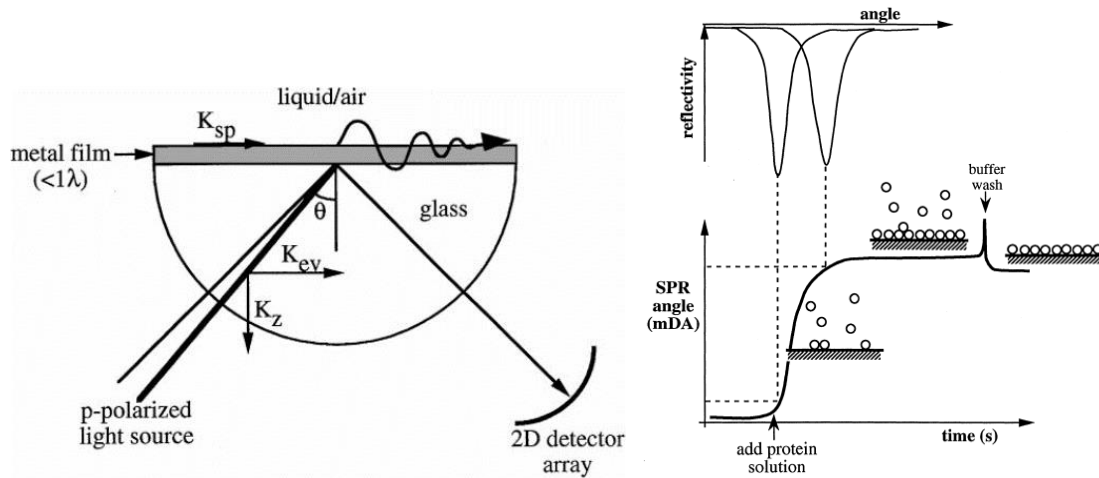
Figure 9: SPR setup according to Kretschmann (**A**) and angular shift during an absorption–desorption process (**B**).[141]

3.5.2 Optical Waveguide Mode Spectroscopy (OWS)

Like surface plasmon resonance spectroscopy, optical waveguide mode spectroscopy (OWS) is a technique that can be used for the investigation of biomolecule interactions with a binding matrix and for the characterization of dry *versus* swollen state polymer layers.[94-95] In general, the measuring principle corresponds to the setup used for surface plasmon resonance spectroscopy[145], described in **Figure 9A**, employing thicker surface layers (for the here described dry hydrogel films about >500 nm) that can sustain waveguide modes. If the analyzed surface films sustains waveguide modes, OWS in combination with SPR allows the independent determination of film thickness and refractive index, whereas both values are convoluted in the SPR signal (for thin films with a thickness below the extend of the evanescent field, while for thicker films only the refractive index can be determined).[145, 154-155] In this thesis, OWS was applied for the characterization of the temperature-dependent swelling behavior of surface-attached poly(2-alkyl-2-oxazoline)-based hydrogel layers in water, with respect to their refractive index and their layer thickness.

An optical waveguide can be defined as transparent material, which is confined in one or two dimensions, with a refractive index higher than the surrounding material. Light is coupled into and able to propagate along such a waveguide, if the conditions for total internal reflection are fulfilled at its interfaces as descript in chapter **3.5.1** and additionally, a momentum match of incidence light and waveguide mode occurs. As a result, incident and reflected light waves undergo constructive interference, with a phase shift of multiples of 2π.[145, 154, 156] In contrast to surface plasmons, guided modes can be excited using either s- or p–polarized light, whereas the propagating constant β represents the pathway of the propagating wave through the waveguide[145, 155], which is given as follows:

$$\beta = k_0 n_w \sin \theta \tag{15}$$

$$k_0 = \frac{2\pi}{\lambda} \tag{16}$$

In practice, OWS measurements can be performed in the same way as already described for SPR. During an angular scan the intensity of the reflected light is recorded. Sharp intensity dips that arise above the critical angle θ_c are related to an energy transfer of the incoming light into the waveguide and therewith the occurrence of a guided mode. The number of such

guided modes observed during an angular scan depends on thickness and refractive index of the respective waveguide material. For polymers, guided waves are normally observed starting from layer thicknesses of approximately 500 nm in the dry state, for which a refractive index of 1.5 is assumed.[145, 154] For p-polarized light, number and position of guided modes for a waveguide with a certain layer thickness d and the refractive index n_w can be estimated by using **equation 17**.

$$\tan(\kappa d + m\pi) = \frac{\kappa(\gamma_m + \gamma_t)}{\kappa^2 - \gamma_m\gamma_t} \tag{17}$$

With m representing the mode number and d the layer thickness of the respective waveguide. The expressions for κ, γ_m and γ_t denote the transverse propagating constants in the waveguide, bottom (e.g. metal layer) and top layer (e.g. air or water) for p-polarized light[95] and are given by the equations below:

$$\kappa = \sqrt{n_w^2 k_0^2 - \beta^2} \tag{18}$$

$$\gamma_m = \sqrt{\beta^2 - n_m^2 k_0^2} \tag{19}$$

$$\gamma_t = \sqrt{\beta^2 - n_t^2 k_0^2} \tag{20}$$

For the characterization of a dry or swollen polymer, n_w represents the layer refractive index, while n_m and n_t denote the refractive indices of the metal layer and air or water.[95] Changes in refractive index or thickness of the respective polymer layer influences the propagation constant β and thus the angular position of the waveguide modes. Therefore, this method can be used for the analysis of swelling–collapsing processes of hydrogels or the investigation of analyte binding within a sensor matrix made from such hydrogels.[95, 154-155] For simultaneously evaluation of thickness and refractive index only by OWS, at least two different guided modes are needed. Layers showing only one mode can be analyzed according their refractive index only. Therefore, the angular scan has to be performed using s- and p-polarized light each. As a result, the guided modes observed for both polarizations are shifted. By simultaneously evaluation of both measurements, the refractive index of the respective polymer layer can be determined.[145, 154]
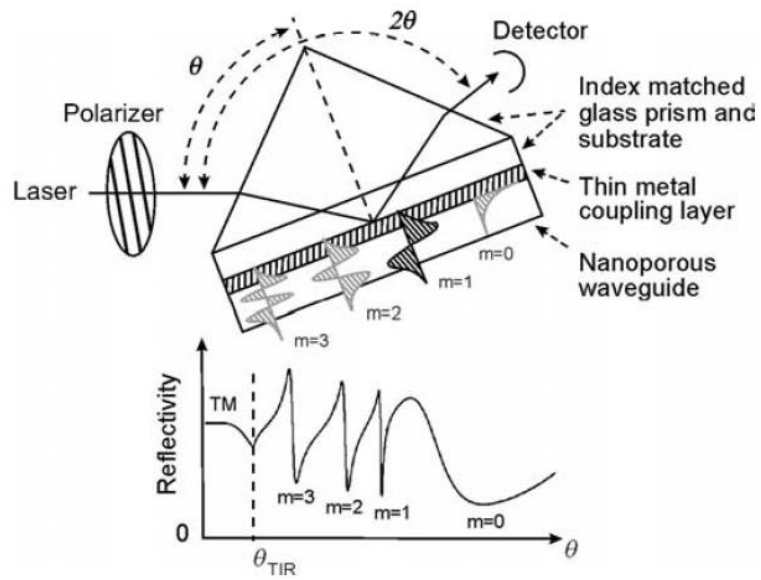
Figure 10: General setup for OWS according to Kretschmann.[154]

4. Results and Discussion

4.1 Polymerization Behavior of 2-Alkyl-2-Oxazolines

In this chapter, the influence of different reaction parameters for cationic ring opening polymerization (CROP) on the molar mass distribution of different poly(2-alkyl-2-oxazoline) homopolymers is studied. In addition, a novel method for the analysis of high molar mass chain coupling reaction product was applied, by amine end group functionalization and subsequent modification with phenyl isocyanate. As already discussed in **Chapter 2.1.2**, the polymerization of 2-oxazolines is often accompanied by side reactions and their occurrence depends strongly on factors like temperature, initiator concentration and the nucleophilicity of the monomer and initiator counter ion. To reduce these side reactions to a minimum, different reaction conditions were applied and their influence on the molar mass distribution was investigated by SEC. For this purpose, 2-ethyl-, 2-*n*-propyl-, and 2-isopropyl-2-oxazoline homopolymers were synthesized in acetonitrile using MeOTf as initiator and morpholine to quench the polymerization reaction (**Scheme 10**).
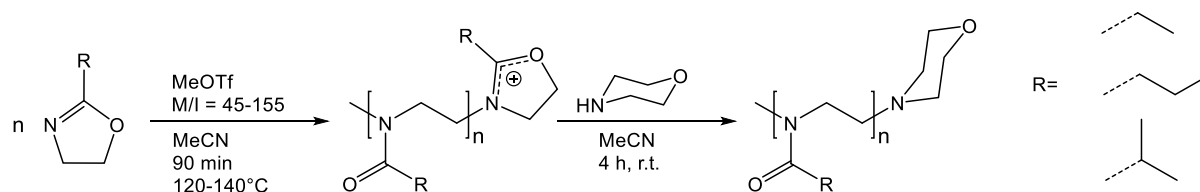

Scheme 10: CROP of different poly(2-alkyl-2-oxazoline) homopolymers with variation of the monomer-initiator concentration ratio (M/I), reaction temperature, and alkyl substituents in the monomers.

CROP of 2-oxazolines is primarily performed using microwave-assisted polymerization (MWAP), as it provides a significant acceleration of the reaction compared to conventional thermal heating.[157-158] The significant higher rates observed for MWAP are based on thermal effects, like overheating of the solvent or selective heating of highly absorbing species involved in the reaction step. Another advantage of this non-contact heating method is the more uniform temperature profile compared to conventional heating and concomitant elimination of wall effects.[157-159] In this thesis, all synthesized 2-oxazoline-based polymers were prepared by MWAP.

4. Results and Discussion

4.1.1 Dependence of Molar Mass Distribution on Nature of the Monomer

First, the influence of the alkyl substituent (2-ethyl-, 2-*n*-propyl-, and 2-isopropyl chains) in the respective monomer was investigated, while temperature and monomer-initiator ratio M/I were kept constant. For the polymerization in acetonitrile, a reaction temperature of 140°C was chosen as upper limit, as it is known that high reaction temperatures promote the occurrence of side reactions in CROP of 2-oxazolines (see **Chapter 2.1.2**). The resulting SEC diagrams of the MWAP products are depicted in **Figure 11** and the corresponding data summarized in **Table 2**.
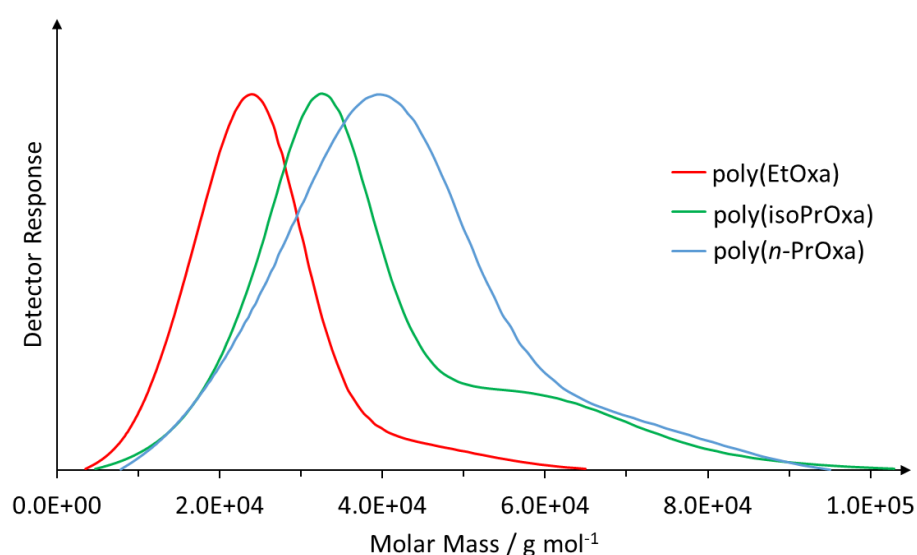
Figure 11: Dependence of molar mass distribution on monomer structure, as determined by SEC. M/I=155/1. Reaction time: 90 min, ΔT=140°C polymerized in acetonitrile.

Table 2: Experimental SEC data of poly(2-alkyl-2-oxazoline) homopolymers from MWAP CROP.

Exp.-Nr.	Monomer	Yield [%]	$\bar{M}_{w,\,SEC}$ [×10³ g mol⁻¹]	Dispersity Đ[a)]
PEC089a1	EtOxa	78	36.9	1.17
PEC089a2	*n*-PrOxa	61	33.3	1.18
PEC089a3	isoPrOxa	81	21.6	1.13

Monomer/initiator (M/I) ratio: 155/1, reaction time: 90 min, ΔT=140°C. [a)]$Đ = \bar{M}_w/\bar{M}_n$.

4. Results and Discussion

The SEC analysis of the polymerization products shows a relatively narrow molar mass distribution for all synthesized homopolymers, with a dispersity $Đ = \bar{M}_w/\bar{M}_n$ ranging from 1.13–1.18, which is typically for CROP. The low dispersity, particularly of the main polymer fraction, indicate the living character of the polymerization reaction. Furthermore, the SEC diagrams show a more or less pronounced bimodal distribution with a high molar mass shoulder, which increases in the order 2-ethyl- < 2-*n*-propyl- < 2-isopropyl-2-oxazoline. The high molar mass fraction results from chain coupling reactions between an active chain end and an enamine species, generated by proton abstraction, which was already described above in **Chapter 2.1.2** and depicted in **Scheme 9**. These observations are consistent with literature reports, as the α-carbon of the respective monomers becomes more reactive in the same order (2-ethyl- < 2-*n*-propyl- < 2-isopropyl-), caused by an increasing positive inductive effect with increasing number of carbon atoms on the alkyl substituent. The differences in weight-average molar mass $\bar{M}_w$ observed for the different homopolymer types (at constant M/I) are also caused by side reactions during CROP. As the α-carbon of 2-isopropyl-2-oxazoline is more reactive compared to 2-ethyl-2-oxazoline and 2-*n*-propyl-2-oxazoline, proton abstraction and subsequent reinitiation is more probable. The mechanism of this side reaction, which was explained above in **Chapter 2.1.2** and depicted in **Scheme 8**, leads to low molar mass tailing and generally to lower degrees of polymerization.

Another factor that has an impact on the average hydrodynamic radius of the polymer coil, from which the apparent molar mass $\bar{M}_w$ of polymers are derived in SEC, are solvent–polymer interactions. Homopolymers of 2-ethyl-, 2-*n*-propyl-, and 2-isopropyl-2-oxazoline differ strongly with respect to their polarity, indicated by their LCST in water ranging from 25–70°C in the order 2-*n*-propyl- < 2-isopropyl- < 2-ethyl-2-oxazoline. Consequently, this may lead to different solvent–polymer interactions and thus different polymer coil expansions.

4.1.2 Dependence of Molar Mass Distribution on Monomer-Initiator Ratio

In a second experimental series, 2-isopropyl-2-oxazoline homopolymers of varying molar masses were prepared by using different M/I ratios, while keeping reaction time and temperature constant. Selection of the monomer was based on the fact that 2-isopropyl-2-oxazoline showed the highest tendency for side reactions in the above described experiments. The corresponding SEC diagrams of the synthesized polymers are depicted in **Figure 12** and the associated data summarized in **Table 3**.
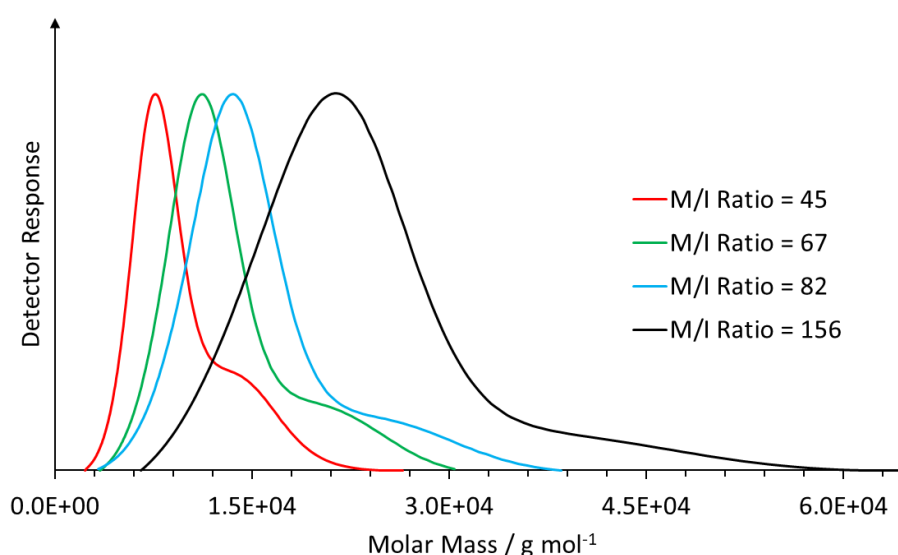
Figure 12: Dependence of molar mass distribution on M/I ratio for poly(2-isopropyl-2-oxazoline)s, as determined by SEC. Reaction time: 90 min; ΔT=140°C polymerized in acetonitrile.

Table 3: Experimental data for MWAP CROP of poly(2-isopropyl-2-oxazoline)s at varying M/I ratio, as determined by SEC.

| Exp.-Nr.	M/I Ratio	Yield [%]	$\bar{M}_{w,\,SEC}$ [×10^3 g mol^{-1}]	Dispersity Đ
PEC092a1	45	66	8.38	1.14
PEC092b2	67	71	11.7	1.14
PEC092b1	82	72	13.7	1.15
PEC092c1	156	61	20.8	1.12

Reaction time: 90 min, ΔT=140°C.

4. Results and Discussion

The data above show again a very narrow molar mass distribution (specifically of the main polymer fraction) for all synthesized polymers with a dispersity ranging from 1.12–1.15. By varying M/I, homopolymers of different molecular weights are accessible (here in the range of 8-20 × 10^3 g mol^{-1}). It is obvious that reduction of the initiator concentration by a factor of two, leads approximately to double the average molar mass (as expected for a living polymerization mechanism). The corresponding SEC diagrams show a higher tendency of chain coupling reaction for higher initiator concentrations, represented by the high molar mass shoulder, which is directly related to the increased concentration of active centers present in the respective reaction mixtures.

4.1.3 Dependence of Molar Mass Distribution on Reaction Temperature

In a third experimental series, the influence of the reaction temperature on the polymerization products was studied between 120-140°C, while keeping M/I constant. Again, all synthesized homopolymers were based on 2-isopropyl-2-oxazoline. Corresponding SEC diagrams are depicted in **Figure 13** and the data summarized in **Table 4**.
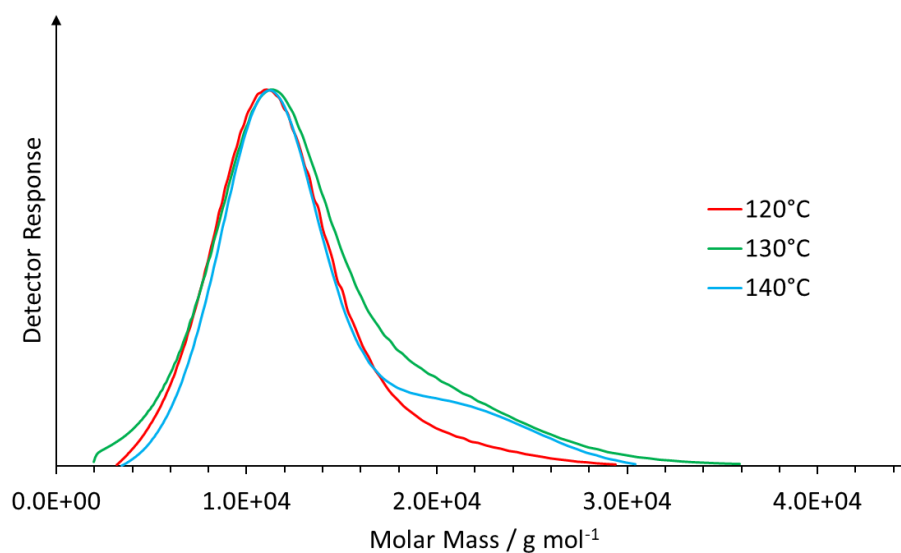
Figure 13: Dependence of molar mass distribution on varying reaction temperature for poly(2-isopropyl-2-oxazoline), as determined by SEC. M/I=72. Reaction time: 90 min, reaction medium: acetonitrile.

Table 4: Experimental data for poly(2-isopropyl-2-oxazoline)s prepared with varying reaction temperature.

Exp.-Nr.	Reaction Temp. / °C	Yield [%/mg]	$\bar{M}_{w,\,SEC}$[a] [$\times 10^3$ g mol^{-1}]	Dispersity Đ[b]
PEC093d2	120	67	10.9	1.11
PEC093d1	130	70	11.4	1.20
PEC093b2	140	65	11.7	1.14

Monomer/Initiator (M/I) Ratio: 72/1. Reaction time: 90 min, reaction medium: acetonitrile.

4. Results and Discussion

SEC analysis of the different poly(2-isopropyl-2-oxazoline)s shows the temperature dependence of side reaction in CROP for the polymerization of 2-isopropyl-2-oxazoline. It was found that higher reaction temperatures support the occurrence of chain coupling reactions in CROP of 2-alkyl-2-oxazolines, again visible as a high molar mass shoulder in the respective SEC diagram. This behavior can be explained by an Arrhenius-type activation of the coupling reaction with increasing temperature, so that the rate constant associated with the reaction barrier of the chain coupling reaction has a steeper T-dependence compared to the propagation rate constant. Additionally, the SEC data demonstrate that the average molecular weight $\overline{M}_w$ exhibit only a small dependence on the set reaction temperature, as all three polymerizations exhibit nearly equal values for $\overline{M}_w$, with a small tendency to higher $\overline{M}_w$ for higher reaction temperatures.

Finally, it can be concluded that a reaction temperature set to 120°C and a reaction time of 90 min appears optimal for microwave-assisted CROP of 2-alkyl-2-oxazoline-based polymers, showing the least proportion of side reaction products.

## 4.1.4 End group Modification of Poly(2-Alkyl-2-Oxazoline)s

In final set of experiments, the accessibility to functional end groups for poly(2-alkyl-2-oxazoline)s was investigated. For this purpose, an amine functionalized poly(2-isopropyl-2-oxazoline) was synthesized by quenching the polymerization reaction with ethylene diamine. Subsequently, the amine functionality was transformed into a urea species by reaction with phenyl isocyanate, resulting in a polymer carrying a UV active chain end, which allows the analysis by SEC using both the UV- and RI-detector. Corresponding reaction conditions and reactants are depicted in **Scheme 11**. When an excess of phenyl isocyanate is used for conversion of the amine groups, additional functionalization reactions may occur at the secondary amine positions.
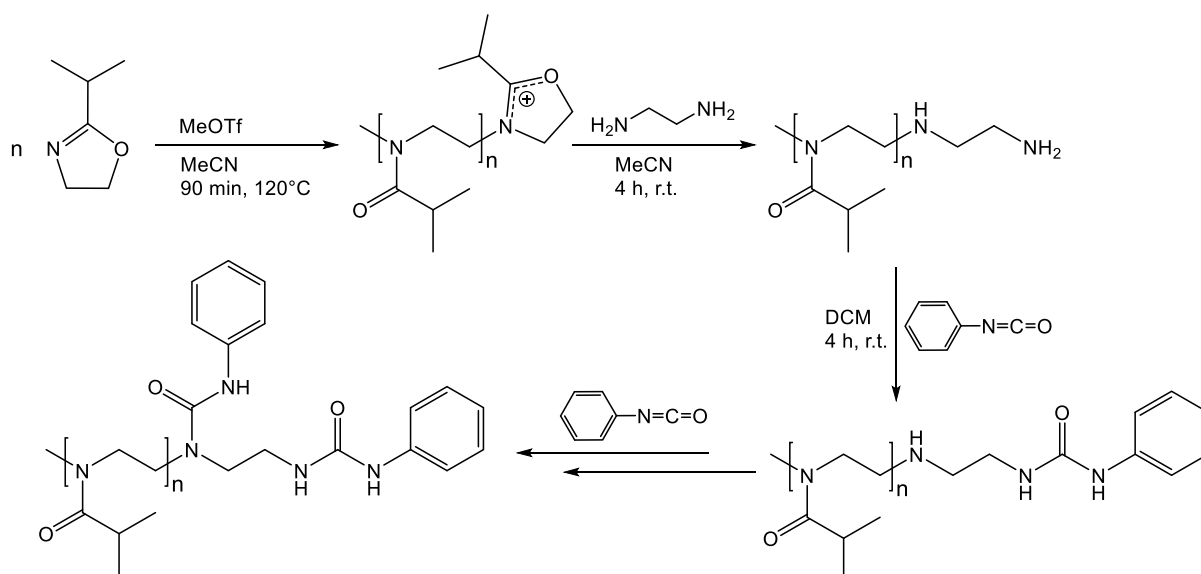
Scheme 11: Preparation of poly(2-isopropyl-2-oxazoline) with amine end groups and subsequent reaction with phenyl isocyanate.

The amino-terminated polymers and their corresponding phenyl isocyanate-modified products were investigated by SEC with respect to their average molar mass. Their cloud point in aqueous solution was determined by UV/VIS spectroscopy. Corresponding SEC diagrams are depicted in **Figure 14** and the associated data summarized in **Table 5**.

4. Results and Discussion
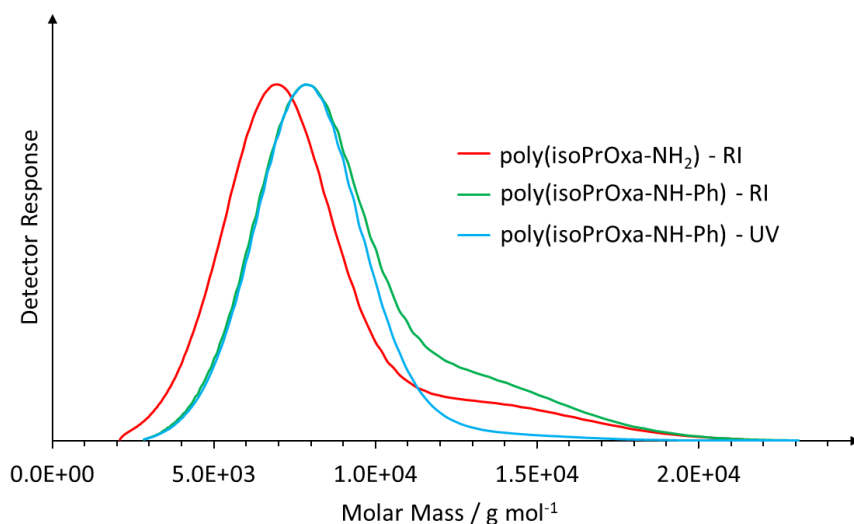
Figure 14: Molar mass distribution of amino-terminated poly(2-isopropyl-2-oxazoline) and the respective poly(2-isopropyl-2-oxazoline modified with phenyl isocyanate, as determined by SEC analysis. M/I ratio: 45/1, reaction temperature 120°C, reaction time: 90 min, polymerization medium: acetonitrile.

Table 5: Experimental SEC data of amino-terminated poly(2-isopropyl-2-oxazoline) before and after modification with phenyl isocyanate.

Exp.-Nr.	$\bar{M}_{w,\,SEC}$ $[\times 10^3 \text{ g mol}^{-1}]$	Dispersity Đ	LCST / °C
PEC094a1	6.98	1.12	32.1
PEC094a1m1	8.21	1.09	N/A[a)]

Monomer/initiator (M/I) ratio: 45/1, reaction time: 90 min. [a)]Polymer is not soluble in water.

The results from SEC analysis show a shift of the average molar mass $\bar{M}_w$, which indicates the successful modification of the amine end group with phenyl isocyanate. This assumption is further supported by the occurrence of an UV signal, which can only be detected for the phenyl isocyanate-modified polymer (the amino-terminated polymer is UV inactive). An additional and very interesting result from the observation of **Figure 14** is the absence of the high molar mass shoulder in the signal of the UV-detector. Apparently, the polymer chains in the high molar mass shoulder visible in the signal of the RI-detector, do not carry any phenyl groups. A probable explanation for this observation is the fact, that chain coupling reactions lead to polymers with star-shaped chain ends. The active centers associated with these crowded chain ends are sterically strongly hindered (see **Scheme 8** and **Scheme 9**), which prevents efficient reaction with diethyl amine and further modification with phenyl

isocyanate. UV/VIS spectroscopy showed a cloud point of 32.1°C for the amino-terminated polymer. In comparison, after reaction with phenyl isocyanate the polymer become insoluble in water, which corroborates successful modification of the amino-terminated poly(2-isopropyl-2-oxazoline).

4.1.5 Chapter Summary and Conclusion

In this chapter, the influence of several different reaction parameters on the molar mass distribution of 2-oxazolines was investigated by size exclusion chromatography. It was found that chain coupling reactions are enhanced by higher reaction temperatures and higher initiator concentrations. While higher reaction temperatures promote side reactions in general, high initiator concentrations on the other hand result in an increasing number of active centers, which can undergo proton abstraction and chain coupling reactions (**Scheme 8** and **Scheme 9**). Beside these reaction parameters, also the nature of the chemical structure of the monomer has an impact on the occurrence of side reactions during CROP of 2-oxazolines. Here it was found, that proton abstraction in α-position to the 2-oxazoline ring system becomes more pronounced in the order of 2-ethyl- < 2-*n*-propyl- < 2-isopropyl-2-oxazoline, which results from the increasing inductive effect of the respective side chains. These results are consistent to observations reported in the literature and allow optimization of the reaction conditions needed for the synthesis of poly(2-oxazoline)s with a narrow molar mass distribution and a minimum proportion of side reaction products.

Furthermore, end group accessibility was investigated by quenching the polymerization reaction with ethylene diamine and subsequent modification with phenyl isocyanate. Here it was found that the high molar mass shoulder observed by SEC analysis, showed no UV activity after the isocyanate-modification. This leads to the conclusion that these polymer chains do not carry any amine functionality. A potential explanation for this behavior is that chain coupling reactions cause sterically strongly hindered star-shaped chain ends, which reduces their probability to react with diethyl amine in the quenching step and prevents a further modification with phenyl isocyanate.

4.2 Preparation and Characterization of Thermoresponsive and Photocrosslinkable Poly(2-Alkyl-2-Oxazoline)-Based Hydrogel Films

In this chapter, the synthesis and fabrication of photocrosslinkable and thermoresponsive poly(2-alkyl-2-oxazoline)-based hydrogel layers is demonstrated. Crosslinking of the respective layers as well as their covalent attachment to the underlying substrate was realized by using benzophenone photochemistry. For this purpose, a novel benzophenone-2-oxazoline monomer (BPOxa) and a novel benzophenone-disulfide (BPdiS) derivative were developed. In order to fine-tune the phase transition temperature of the surface attached hydrogel layers, the monomer composition was varied in the copolymerization reaction of different 2-alkyl-2-oxazolines.
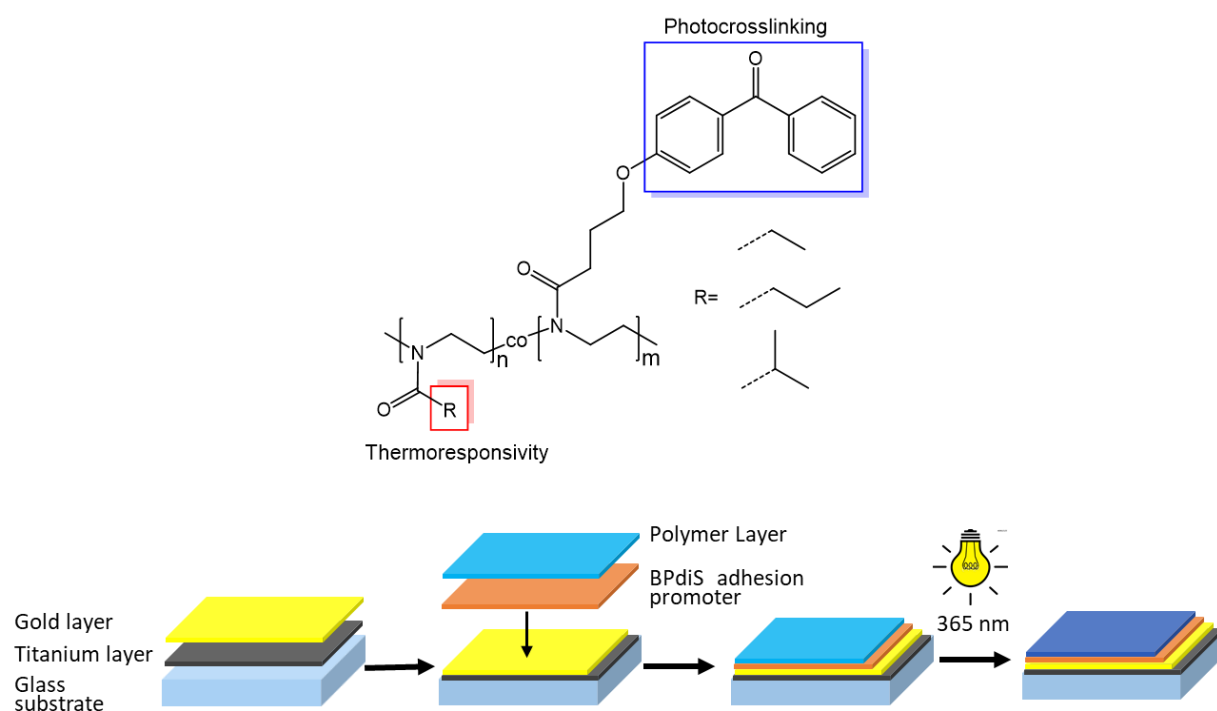
Figure 15: Poly(2-alkyl-2-oxazoline) layer fabrication exploiting benzophenone photochemistry.

Smart polymeric coatings attract a growing interest due to their responsiveness to variations in the surrounding medium, like temperature, pH, ion concentration, and magnetic or electric fields.[59-61] These characteristics render them useful for a broad range of biomedical technologies, such as separation systems, biosensor platforms, or drug carrier systems.[5, 52-53]

4. Results and Discussion

For such applications, water-soluble, temperature responsive polymers (e.g. poly(*N*-isopropylacrylamide) or poly(2-oxazoline)s) are of special interest, due to the possibility to reversibly control their aggregation behavior by changing temperature.[71, 94] Poly(2-oxazoline)s, synthesized by cationic ring opening polymerization, are one of these classes of polymers exhibiting lower critical solution temperature (LCST) in aqueous media and potential biocompatibility.[160-161] The possibility of tuning their LCST by copolymerization of monomers with different hydrophobic side chains provides access to thermoresponsive polymers with a broad range of transition temperatures. In addition, changes in molar mass or varying end groups also influence their LCST.[71] Photoreactive crosslinker units, incorporated into the respective polymer chains and additionally immobilized onto a solid substrate, provide a common way for the formation of stable crosslinked and surface bound polymer layers. Copolymerization of benzophenone-carrying monomers are therefore an ideal choice, as it allows exact control over the polymer composition and by this the benzophenone concentration along the polymer chain. The possibility to perform crosslinking after coating these polymers from solution onto the respective substrates via irradiation with UV light (245–365 nm) extends the radius of operation substantially, as it allows film preparation up to approximately 3 μm. This approach was already utilized for the surface attachment of several different types of polymers.[82, 94, 162] Two previous approaches using benzophenone photochemistry for the surface attachment of poly(2-alkyl-2-oxazoline)s are reported:

1.) They were either based on substrate modification with respective benzophenone silanes and immobilizing benzophenone-free poymer,[163] resulting in very thin polymer layers of a few nanometer.

2.) Or they involved modification of the preformed polymer with photoreactive groups, requiring several polymeranalogous reaction steps, like side chain hydrolysis and benzophenone coupling, with limited control over the polymer composition and LCST).[164-165]

Photocrosslinkable poly(2-alkyl-2-oxazoline)s were already successfully synthesized by using thiol-ene coupling chemistry[166-167] or by the incorporation of coumarin units[168] using UV light of λ=300 nm to induce photo-dimerization. Both methods have the disadvantage of needing two mutually reactive units in close proximity to facilitate efficient crosslinking. Furthermore, crosslinking based on thiol-ene coupling chemistry is susceptible to oxidation. Among others, this oxidation process can form covalent disulfide crosslinks between two thiol units, even

without UV irradiation, causing a limited storability. Compared to that, benzophenone units are stable in the absence of UV light and need C-H bonds for crosslinking, only.
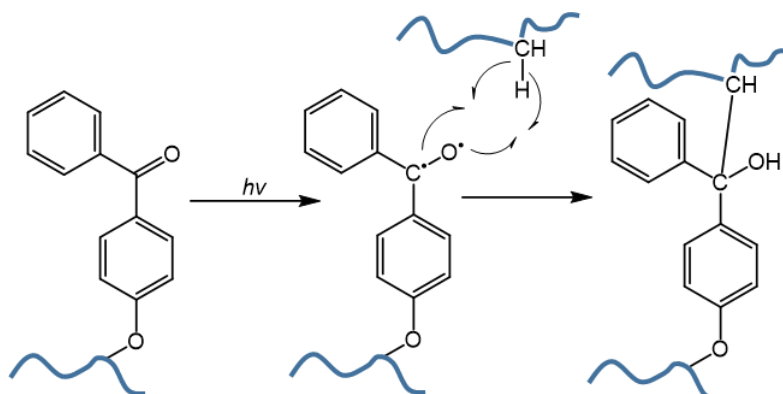

Scheme 12: Photocrosslinking reaction of benzophenone-modified polymers.

Benzophenone-based photocrosslinking represents a very robust and universally applicable method for the fabrication of polymeric networks. Via irradiation with UV light (254 to 365 nm) the lone electron pair of the carbonyl functionality undergoes an $n \rightarrow \pi^*$ transition under formation of a diradical. This diradical is able to react with any C-H bond of neighboring polymer chains, resulting in the formation of covalent chemical bonds. In the absence of appropriate C-H moieties, the activated species can relax back into its initial state without losing the ability of reactivation.[82, 163, 169]

4. Results and Discussion

4.2.1 Synthesis of a Benzophenone-Containing Gold and Silicon Adhesion Promoter

For the characterization of the swelling behavior of thermoresponsive hydrogel layers by SPR/OWS, it is crucial to prevent their detachment from the respective Au substrate. Based on to the affinity of sulfur-containing compounds to Au, a novel benzophenone-disulfide adhesion promoter was developed, which allows the covalent attachment of the respective hydrogel layer to the underlying substrate. The corresponding synthesis steps for the preparation of 3,3'-disulfanediylbis[*N*-(4-benzoylbenzyl)propanamide] (**2**) (BPdiS) are depicted in **Scheme 13**.
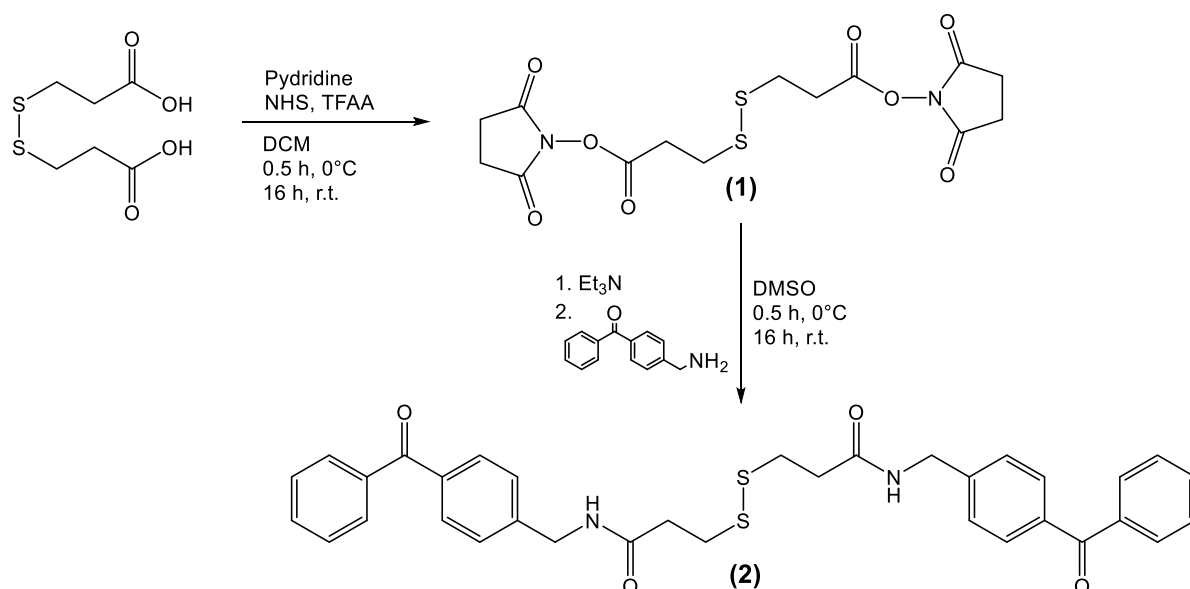
Scheme 13: Synthesis of benzophenone-disulfide adhesion promoter for Au substrates.

The synthesis of 3,3'-disulfanediylbis[*N*-(4-benzoylbenzyl)propanamide] (**2**) is performed by activating the carboxylic acid groups of 3,3'-dithiodipropionic acid with trifluoroacetic anhydride (TFAA) and *N*-hydroxysuccinimide (NHS) (the respective abbreviations in the reaction schemes are defined in the **List of Abbreviations** at the beginning of this thesis), followed by coupling of the obtained intermediate product bis(2,5-dioxopyrrolidin-1-yl) 3,3'-disulfanediyldipropanoate (**1**) with 4-aminomethyl benzophenone in the presence of Et$_3$N. Subsequently, the product is obtained by extraction with DCM with an overall yield of approximately 42 % of the theory. The product was characterized by ^{1}H and ^{13}C NMR spectroscopy.
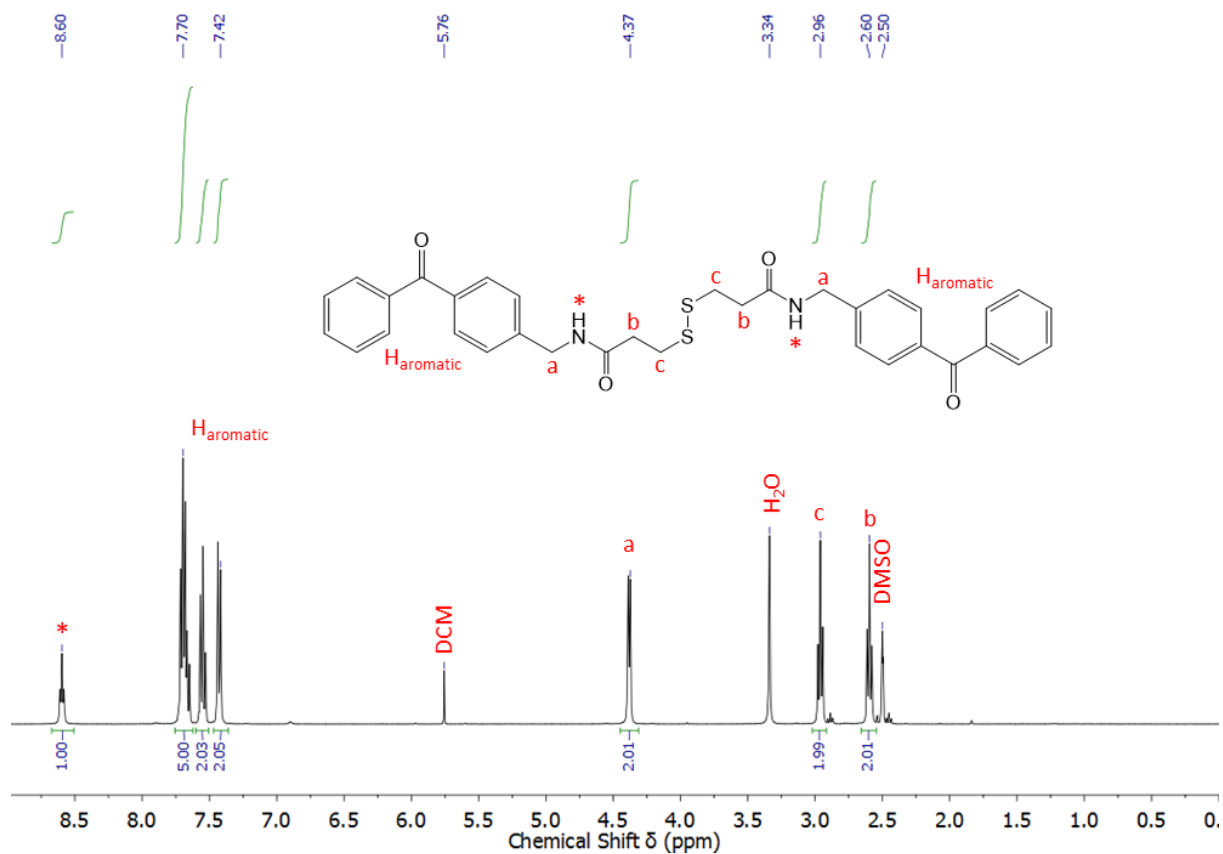
Figure 16: ^{1}H NMR spectrum of 3,3'-disulfanediylbis[*N*-(4-benzoylbenzyl)propanamide] recorded in DMSO-d$_6$.

The ^{1}H NMR spectrum depicted in **Figure 16** shows signals between 7.42–7.70 ppm, which can be assigned to the aromatic protons (H$_{aromatic}$) of both benzophenone groups. The methylene group, located between the amide functionality and the benzophenone moiety, can be assigned to the signal at 4.37 ppm (a) and the remaining ethylene group to the signals at 2.60 ppm and 2.96 ppm (b+c). Additionally, the single amide proton was found at 8.60 ppm. All integrals are in line with the theoretical values, which corroborates the structural assignment and demonstrates the purity of the product, whereas small traces of DCM (5.76 ppm) are still present, remaining from the isolation procedure of the final product.

4. Results and Discussion

For the immobilization of the respective hydrogel layers onto glass substrates, a benzophenone-based triethoxysilane (BPTES) adhesion promoter was synthesized, as previously reported.[162-163, 170]
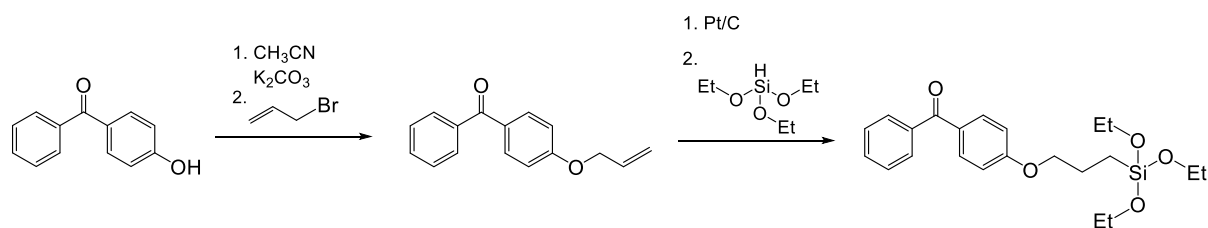
**Scheme 14:** Synthesis of phenyl{4-[3-(triethoxysilyl)propoxy]phenyl}methanone (BPTES).

4.2.2 Synthesis of a Benzophenone-2-Oxazoline Photocrosslinker and Copolymerization with Various 2-Alkyl-2-Oxazolines

For successful copolymerization of two or more different monomers with control over the polymer composition, it is particularly important to employ monomers with equal or at least similar copolymerization parameters. Functional moieties directly attached to the polymerizable group can strongly influence the copolymerization behavior and consequently the overall composition of the respective polymers. For example, the reported copolymerization of 2-phenyl-2-oxazoline with 2-ethyl-2-oxazoline proved the strong dependence of the build-in ratio onto the copolymerization parameters r_i and therewith the overall polymer composition.[171] Depending on the nucleophilicity of the respective initiator counter ion, the reactivity ratio for both monomers ranges form $r_{EtOxa} = 7.9 - 10.1$ and $r_{PhOxa} = 0.18 - 0.30$, which results in quasi-diblock copolymers. In contrast, for the copolymerization of 2-methyl-2-oxazoline with 2-ethyl-2-oxazoline a comonomer reactivity ratio of $r_{EtOxa} = 1.18$ and $r_{MeOxa} = 0.34$ was found.[172]

For the fabrication of photocrosslinkable and thermoresponsive poly(2-alkyl-2-oxazoline)-based coatings, an optimized synthesis route of a novel benzophenone-2-oxazoline-based photocrosslinker was developed (**Scheme 15**). To prevent the electronic influence of the aromatic unit on the 2-oxazoline reactivity and resulting build-in ratios, a propylene oxide spacer was inserted between the benzophenone moiety and the 2-oxazoline ring (see Compound **6** of **Scheme 15**). This precaution should result in nearly equal copolymerization parameters r_{BPOxa} and r_{alkyl} (2-ethyl-, 2-isopropyl-, 2-n-propyl-2-oxazoline) and furthermore a good correlation between monomer-feed and copolymer composition.

4. Results and Discussion
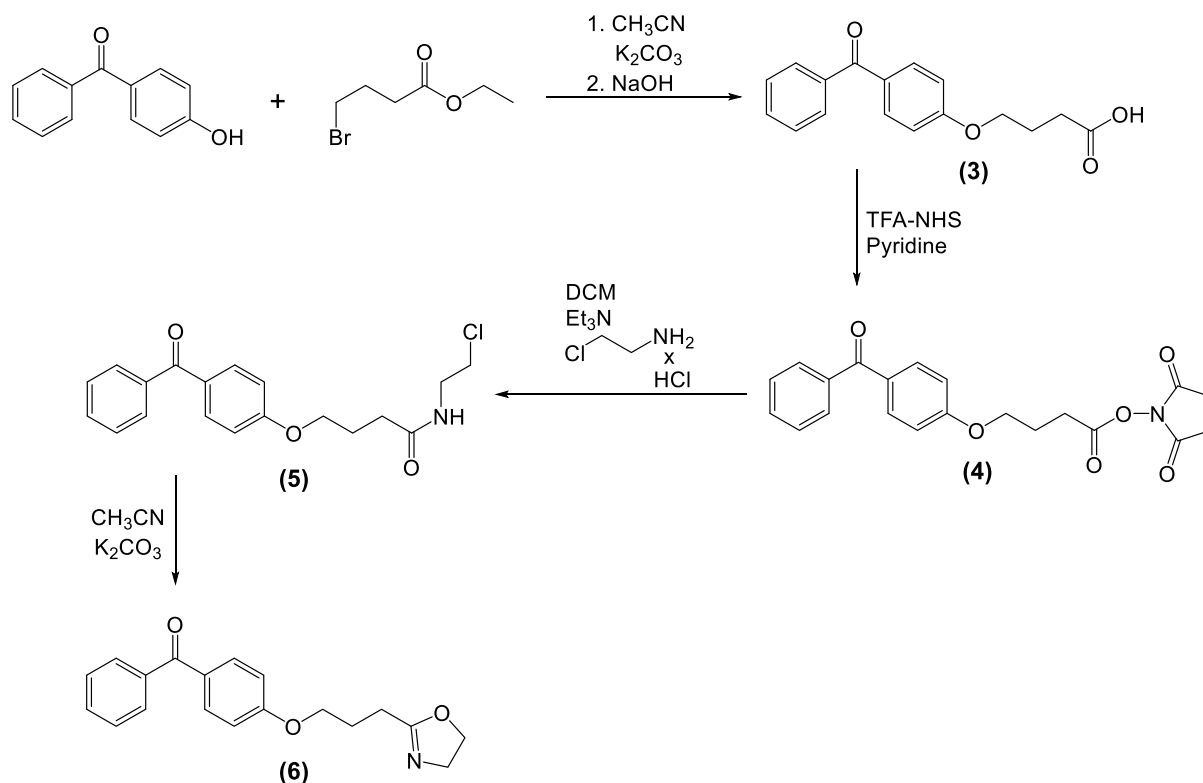
Scheme 15: Developed route for the synthesis of 2-[3-(4-benzoylphenoxy)propyl]-2-oxazoline

The synthesis of the benzophenone-2-oxazoline based photocrosslinker **(6)** was performed by coupling 4-hydroxybenzophenone to ethyl 4-bromobutyrate. For this purpose, the hydroxyl functionality of 4-hydroxybenzophenone is deprotonated with K_2CO_3, followed by a nucleophilic attack of the negative charged oxygen at the bromine-substituted carbon. Ethyl 4-(benzoylphenoxy)butanoic acid **(3)** is then obtained by alkaline hydrolysis of the corresponding ester, using NaOH dissolved in a mixture of water and methanol. To promote the subsequent reaction to 4-(4-benzoylphenoxy)-*N*-(2-chloroethyl)butanamide **(5)**, the acid functionality of **(3)** is transferred into an activated species by using trifluoroacetic anhydride and *N*-hydroxysuccinimide. The reaction of the resulting NHS ester **(4)** with 2-chloroethylamine hydrochloride to **(5)** is then performed at room temperature with a yield of nearly 90 %. Ring closure to the corresponding 2-[3-(4-benzoylphenoxy)propyl]-2-oxazoline **(6)** (BPOxa) is then accomplished by heating of 4-(4-benzoylphenoxy)-*N*-(2-cloroethyl)butanamide **(5)** in the presence of anhydrous K_2CO_3. With an overall yield of nearly 65 % of the theory, this synthesis route presents a straightforward method for the preparation of benzophenone-2-oxazoline-based photocrosslinker.
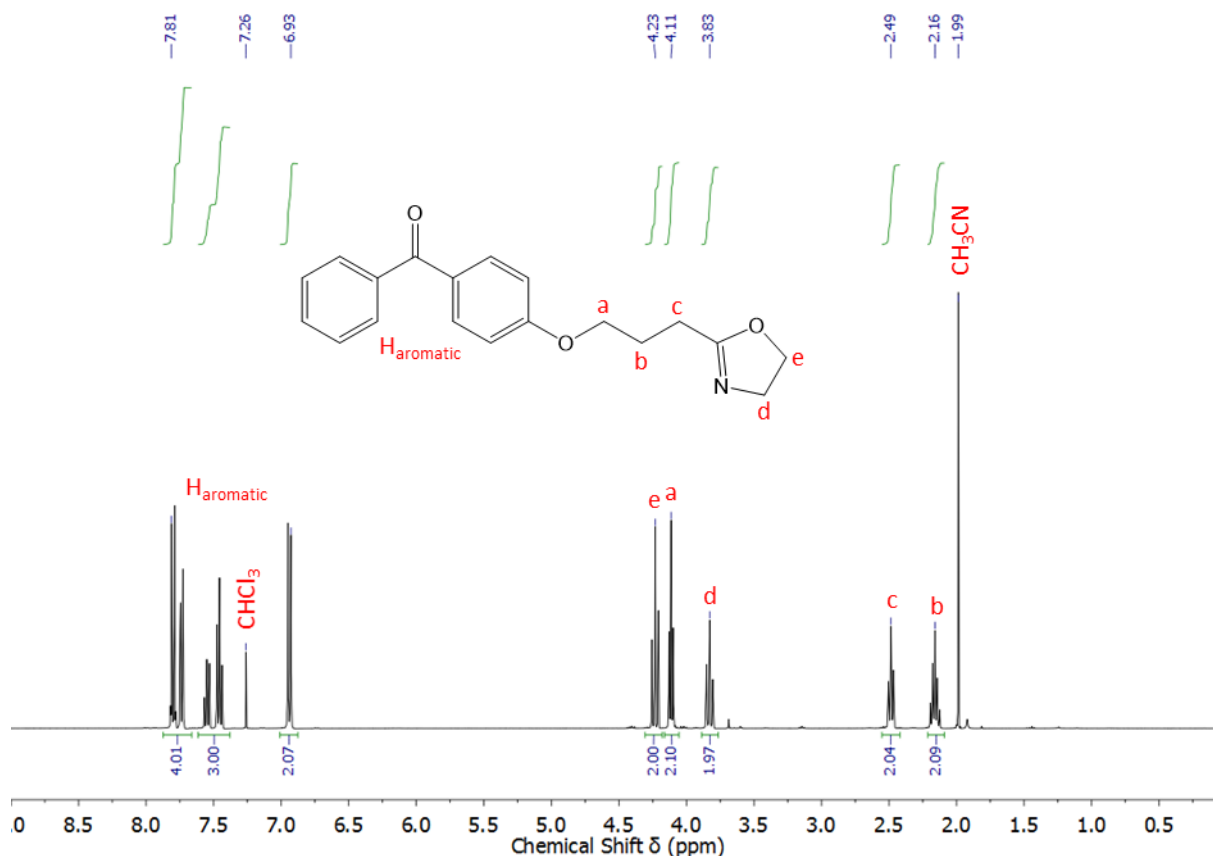
Figure 17: ^{1}H NMR spectrum of the benzophenone-based 2-oxazoline monomer recorded in CDCl3.

Figure 17 shows the corresponding ^{1}H NMR spectrum of the synthesized photocrosslinker. Signals between 6.93–7.81 ppm are associated to the aromatic protons (H$_{aromatic}$) of the benzophenone functionality, whereas the signal at 7.26 ppm can be assigned to the solvent peak (CDCl3). Signals at 4.11 (a) and 4.23 (e) ppm belong to the methylene groups of the 2-oxazoline ring system. The protons of the propylene spacer, located between the benzophenone and the 2-oxazoline ring, are observed at 2.16 (b), 2.49 (c) and 3.83 (d) ppm. All signals and integrals are in line with the theoretical values, which underpins the successful synthesis and purity of the product. Small traces of MeCN (1.99 ppm) are still present as a result from the isolation procedure of the final product.

The synthesized BPOxa photocrosslinker was then copolymerized with various 2-alkyl-2-oxazolines (2-ethyl-, 2-isopropyl-, 2-*n*-propyl-2-oxazoline), to study its polymerization behavior. All homo-, co- and terpolymers were prepared by microwave-assisted CROP in acetonitrile using MeOTf as initiator (M/I= 150/1 and 300/1) and morpholine or water for quenching of the polymerization reaction (**Scheme 16**). The synthesized polymers were

studied with respect to their composition by ^{1}H NMR analysis and with respect to their dispersity Đ and weight-average molar mass $\bar{M}_w$ by SEC analysis.
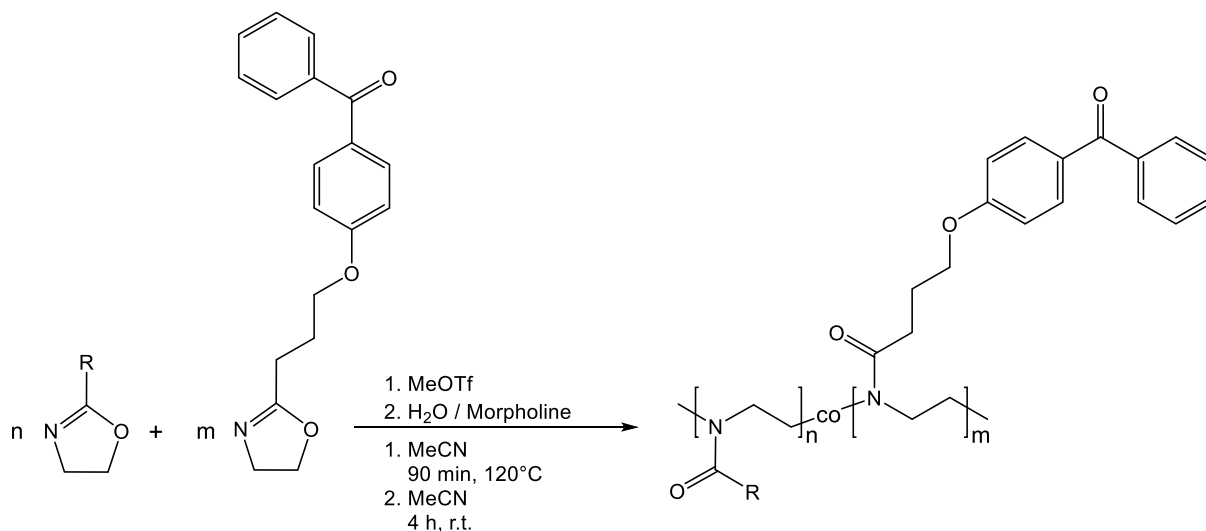
Scheme 16: Reaction conditions for the synthesis of benzophenone-containing poly(2-alkyl-2-oxazoline) homo-, co- and terpolymers.

Table 6: Summarized characterization data of benzophenone-containing homo-, co-, and terpolymers for a M/I ratio = 150/1.

Exp.–Nr.	Monomer feed ratio	Polymer composition[a]	$\bar{M}_{w,\,SEC}$[b] $[\times 10^3\,g\,mol^{-1}]$	Dispersity Đ[c]	Yield / %
PEC089a1	EtOxa$_{100}$	poly(EtOxa$_{100}$)	36.9	1.17	90
PEC100a1	EtOxa$_{99}$/BPOxa$_1$	poly(EtOxa$_{99}$-BPOxa$_1$)	23.0	1.29	94
PEC100a2	EtOxa$_{97}$/BPOxa$_3$	poly(EtOxa$_{98}$-BPOxa$_2$)	30.3	1.47	87
PEC100a3	EtOxa$_{95}$/BPOxa$_5$	poly(EtOxa$_{94}$-BPOxa$_6$)	27.6	1.54	93
PEC100a4	EtOxa$_{89}$/BPOxa$_{11}$	poly(EtOxa$_{90}$-PBOxa$_{10}$)	25.0	1.55	91
PEC116a	BPOxa$_{100}$	poly(BPOxa$_{100}$)	45.1	1.51	66
PEC089a3	isoPrOxa$_{100}$	poly(isoPrOxa$_{100}$)	23.9	1.13	81
PEC100a5	isoPrOxa$_{95}$/BPOxa$_5$	poly(isoPrOxa$_{94}$-BPOxa$_6$)	17.0	1.36	81
PEC089a2	*n*-PrOxa$_{100}$	poly(*n*-PrOxa$_{100}$)	33.0	1.18	61
PEC100a6	*n*-PrOxa$_{95}$/BPOxa$_5$	poly(*n*-PrOxa$_{94}$-BPOxa$_6$)	31.6	1.49	72
PEC100a7	*n*-PrOxa$_{47}$/isoPrOxa$_{47}$/BPOxa$_6$	poly(*n*-PrOxa$_{48}$-isoPrOxa$_{46}$-BPOxa$_6$)	18.2	1.35	83
PEC100a8	isoPrOxa$_{72}$/EtOxa$_{23}$/BPOxa$_5$	poly(isoPrOxa$_{72}$-EtOxa$_{23}$-BPOxa$_5$)	17.6	1.80	78

Monomer/initiator (M/I) ratio: 150/1 in acetonitile. [a]As calculated from ^{1}H NMR analysis. [b]As determined by SEC analysis. [c] Đ = $\bar{M}_w/\bar{M}_n$ determined from SEC analysis. All polymerization reactions were quenched with morpholine.

**Table 7:** Summarized characterization data of benzophenone-containing homo-, co-, and terpolymers for a M/I ratio = 300/1.

Exp.–Nr.	Monomer feed ratio	Polymer composition[a]	$\bar{M}_{w,\,SEC}$[b] $[\times 10^3\ \text{g mol}^{-1}]$	Dispersity $\text{\DJ}$[c]	Yield / %
PEC103a1	isoPrOxa$_{98}$/BPOxa$_2$	poly(isoPrOxa$_{98}$-BPOxa$_2$)	29.4	1.54	79
PEC103a4	isoPrOxa$_{65}$/n-PrOxa$_{33}$/ BPOxa$_2$	poly(isoPrOxa$_{63}$-n-PrOxa$_{35}$-BPOxa$_2$)	30.1	1.89	65
PEC103a5	isoPrOxa$_{79}$/EtOxa$_{19}$/ BPOxa$_2$)	poly(isoPrOxa$_{79}$-EtOxa$_{19}$-BPOxa$_2$)	32.2	2.10	86
PEC103a9	n-PrOxa$_{98}$/BPOxa$_2$	poly(n-PrOxa$_{97}$-BPOxa$_3$)	41.6	1.24	75
PEC103a11	EtOxa$_{98}$/BPOxa$_2$	poly(EtOxa$_{97}$-BPOxa$_3$)	31.3	1.67	76

Monomer/initiator ratio M/I: 300/1 in acetonitrile. [a]As calculated from ^{1}H NMR analysis. [b]As determined by SEC analysis. [c]$\text{\DJ} = \bar{M}_w / \bar{M}_n$ calculated by SEC analysis. All polymerization reactions were quenched with water.

The data summarized in **Table 6** (M/I ratio=150/1) and **Table 7** (M/I ratio=300/1) show a narrow molar mass distribution with a dispersity $\text{\DJ}$ of 1.55 or smaller for nearly all synthesized copolymers, which demonstrates the ionic (quasi-living) character of the CROP mechanism of these 2-oxazolines. Homopolymers based on 2-alkyl-2-oxazolines exhibit a narrower molecular weight distribution compared to copolymers including BPOxa. A general trend can be observed for the series poly(2-ethyl-2-oxazoline-*co*-2-benzophenone-2-oxazoline). Here, the dispersity $\text{\DJ}$ continuously increases with the BP content form 1.17 for poly(EtOxa) up to 1.55 for poly(EtOxa$_{90}$-BPOxa$_{10}$) copolymers. This observation was also made for the copolymer systems poly(isoPrOxa-BPOxa) and poly(n-PrOxa-BPOxa). Polymers composed of three different types of monomers showed the highest dispersity $\text{\DJ}$ values. A possible explanation for the broadening of the molar mass distribution is that chain transfer reactions are stronger supported by the BPOxa monomer, where the carbonyl functionality of the benzophenone group may act as a proton acceptor (**Figure 18**).
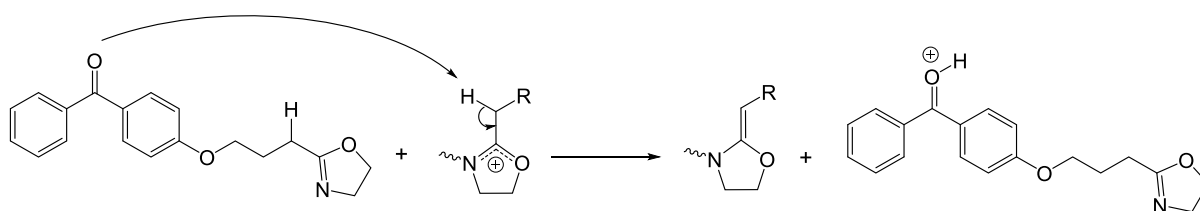
Figure 18: Possible side reactions for the copolymerization of BPOxa with various 2-alkyl-2-oxazolines.

4. Results and Discussion

The composition of the synthesized homo-, co- and terpolymers was determined by ^{1}H NMR, recorded in CDCl$_3$. First, the neat poly(BPOxa$_{100}$) homopolymer was investigated to identify the spectral positions of the proton signals, to ensure that the bands of the propylene oxide spacer and those of the polymer backbone do not overlap (**Figure 19**).
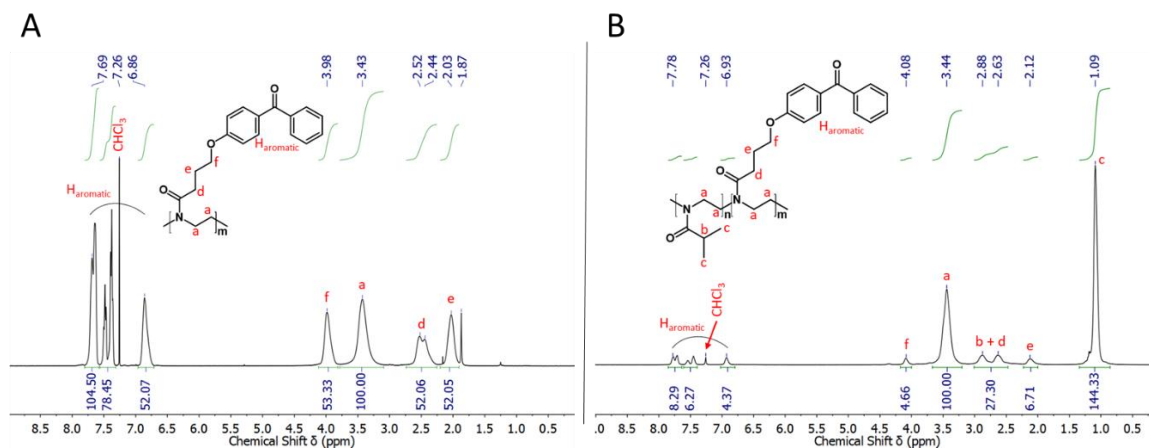
Figure 19: Comparison of the ^{1}H NMR spectrum of poly(BPOxa$_{100}$) (**A**) and poly(isoPrOxa$_{91}$-BPOxa$_9$) (**B**), both recorded in CDCl$_3$.

The signals between 6.86–7.69 ppm are associated to the aromatic protons (H$_{aromatic}$) of the benzophenone functionality. The signal of the polymer backbone is located at 3.43 ppm and the signals at 2.03, 2.44–2.52 and 3.98 ppm belong to the protons of the propylene spacer, located between the backbone and the benzophenone group. All observed bands are clearly separated from each other and hence unambiguous copolymer analysis by ^{1}H NMR can be conducted.

The composition of the synthesized co- and terpolymers was determined by comparing the peak integrals of the polymer backbone with the integral of the aromatic system of the benzophenone group. For this purpose, the integral of the polymer backbone was set to 100 and the integrals of the aromatic protons (H$_{aromatic}$) was multiplied by 4/9, which corresponds then directly to the benzophenone proportion in the respective co- and terpolymers. Results summarized in **Table 6** show a very good agreement between monomer feed ratio and polymer composition for all synthesized polymers, indicating that poly(2-oxazoline) with a defined benzophenone concentration are conveniently accessible by copolymerization of 2-alkyl-2-oxazolines (2-ethyl-, 2-isopropyl-, 2-n-propyl-2-oxazoline) with the developed BPOxa monomer.

4.2.3 Cloud Point Dependence on Benzophenone Content

As a next step, the cloud point dependence on the benzophenone concentration was investigated by UV/VIS spectroscopy. Prior to the cloud point measurements, a wavelength scan was performed to specify the absorption characteristics of the benzophenone photocrosslinker. These measurements were conducted in ethanolic solutions for the series of poly(2-ethyl-2-oxazoline-*co*-2-benzophenone-2-oxazoline)s with 0.01 wt% polymer concentration. Ethanol was chosen as solvent due to the insolubility of copolymers with benzophenone concentrations higher than 6 mol % (Poly(EtOxa$_{94}$-BPOxa$_6$) and Poly(EtOxa$_{90}$-BPOxa$_{10}$)) in pure water. To exclude a solvent dependent absorption shift, one additional spectrum of Poly(EtOxa$_{98}$-BPOxa$_2$) was recorded in aqueous solution.
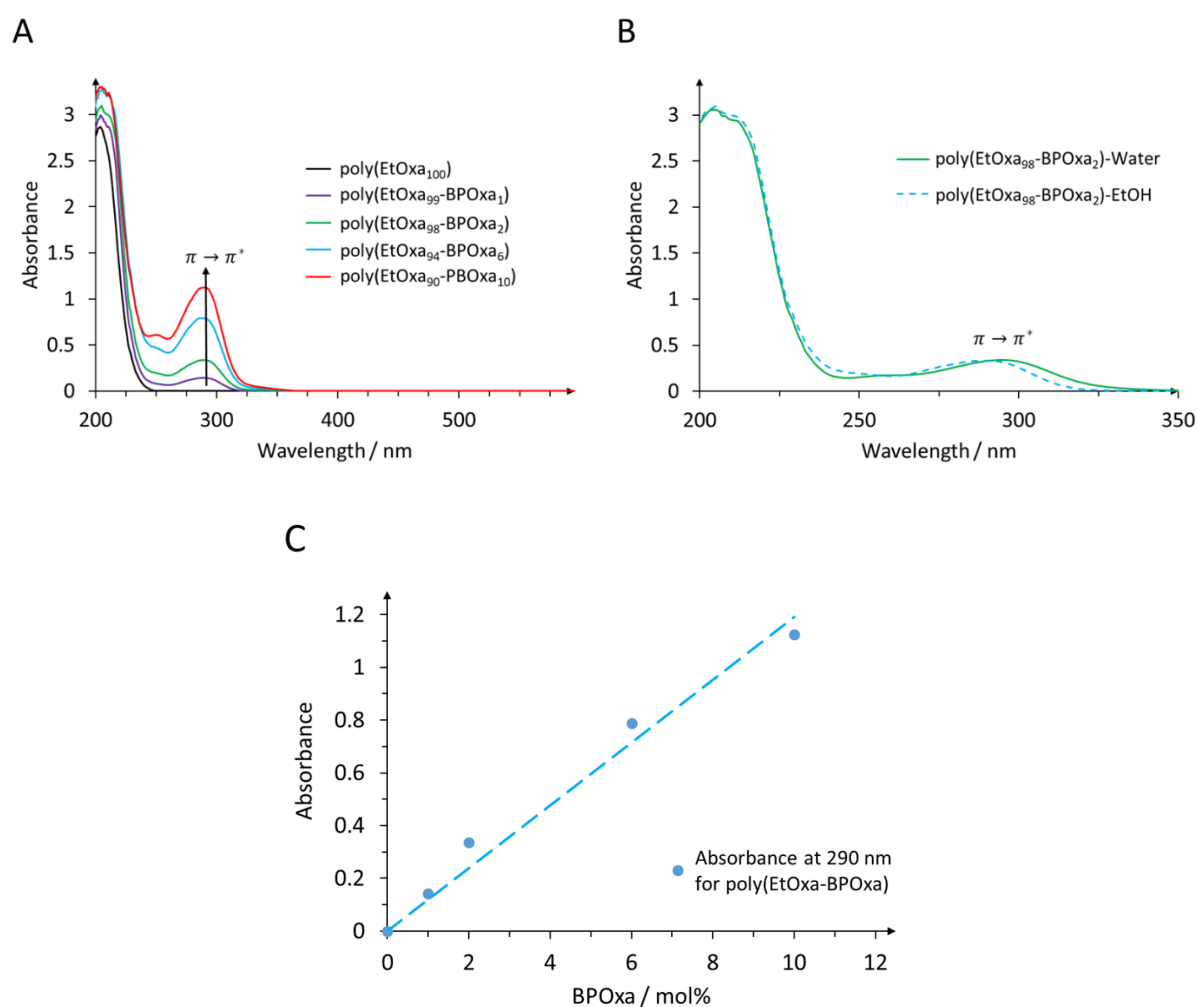
Figure 20: UV/VIS absorption spectra of poly(2-ethyl-2-oxazoline-co-2-benzophenone-2-oxazoline) in 0.01 wt% ethanolic solution (**A**) and as 0.01 wt% aqueous solution (**B**). Absorbance at 290 nm for poly(2-ethyl-2-oxazoline-co-2-benzophenone-2-oxazoline) with varying BPOxa content (**C**). Absorbance error ±5 %.

4. Results and Discussion

The spectra, recorded in ethanol, (**Figure 20A**) show the wavelength dependent UV/VIS absorption for the system poly(2-ethyl-2-oxazoline-*co*-2-benzophenone-2-oxazoline) with different benzophenone concentrations. A strong absorption band with a maximum at 290 nm is observed, which can be assigned to the $\pi \rightarrow \pi^*$ transition of the benzophenone moiety. The absorption at 290 nm increases with increasing benzophenone content in the respective copolymers. By plotting the absorption maximum as a function of the benzophenone concentration (**Figure 20C**) it emerges that the curve flattens towards higher absorbance values, which results from the non-linear relationship of Lamber-Beer's law for absorbance values higher than approximately 0.8. By changing the solvent from ethanol to water (**Figure 20B**), the $\pi \rightarrow \pi^*$ transition undergoes a red shift from 290 nm (ethanol) to 297 nm (water), which results from the stronger hydrogen bonding of the water molecules with the carbonyl functionality of the benzophenone group. For wavelengths higher than 365 nm the UV absorption drops to about zero. Consequently, temperature-dependent cloud point measurements were performed by recording the transmittance at a wavelength of 550 nm (far above 365 nm), where interference by absorption can be excluded, using 0.3 wt% aqueous polymer solutions with a heating and cooling rate of 1 K min^{-1}. The cloud point was defined as the temperature, at which a transmittance of 50 % was reached during the heating and cooling cycles.

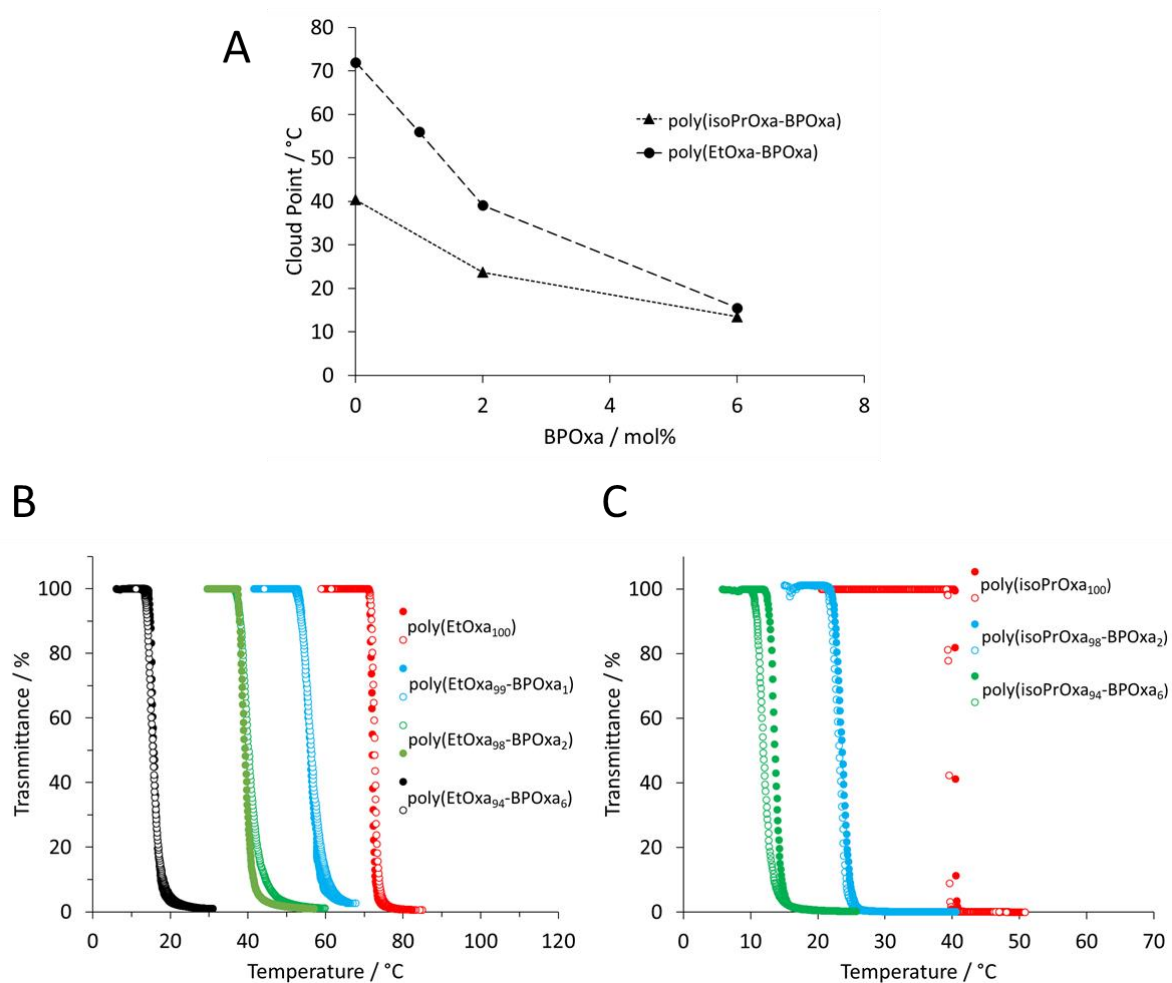**Table 8:** Cloud point dependence on benzophenone photocrosslinker content for various poly(2-oxazoline)s.

Exp.–Nr.	Polymer composition[a]	Cloud Point[a] Heating $C_{p,h}$ / °C	Cloud Point[a] Cooling $C_{p,c}$ / °C	Hysteresis[b] / °C
PEC089a1	poly(EtOxa$_{100}$)	72.5 ± 1	72.0 ± 1	0.5
PEC100a1	poly(EtOxa$_{99}$-BPOxa$_1$)	56.3 ± 1	56.0 ± 1	0.3
PEC100a2	poly(EtOxa$_{98}$-BPOxa$_2$)	40.2 ± 1	39.1 ± 1	1.1
PEC100a3	poly(EtOxa$_{94}$-BPOxa$_6$)	15.7 ± 1	15.5 ± 1	0.2
PEC100a4	poly(EtOxa$_{90}$-BPOxa$_{10}$)	N/A[c]	N/A[c]	N/A[c]
PEC116a	poly(BPOxa$_{100}$)	N/A[c]	N/A[c]	N/A[c]
PEC089a3	poly(isoPrOxa$_{100}$)	40.5 ± 1	39.5 ± 1	1.0
PEC103a1	poly(isoPrOxa$_{98}$-BPOxa$_2$)	23.5 ± 1	23.1 ± 1	0.4
PEC100a5	poly(isoPrOxa$_{95}$-BPOxa$_5$)	13.5 ± 1	11.8 ± 1	1.7
PEC089a2	poly(*n*-PrOxa$_{100}$)	26.3	25.6 ± 1	0.9
PEC100a6	poly(*n*-PrOxa$_{94}$-BPOxa$_6$)	N/A[c]	N/A[c]	N/A[c]

[a]Performed using 0.3 wt% aqueous polymer solutions with a heating rate of 1 K min^{-1}. [b]Calculated by $C_{p,h}$-$C_{p,c}$. [c]Polymer does not dissolve in water

4. Results and Discussion

The results summarized in **Table 8** and depicted in **Figure 21A** show the cloud point dependence on the benzophenone content for the systems poly(EtOxa-co-BPOxa) and poly(isoPrOxa-co-BPOxa). In both cases, a reduction of the cloud point temperature was observed for an increasing BPOxa concentration, caused by the hydrophobic character of the benzophenone moiety. The same trend was observed for poly(*n*-PrOxa) and poly(*n*-PrOxa$_{94}$-BPOxa$_6$) (see **Table 8**). The shift to lower cloud points for an increasing benzophenone concentration result from the less hydrated hydrophobic benzophenone groups of the photocrosslinker unit in comparison to the more polar 2-ethyl- and 2-isopropyl side chains. In addition, $\pi - \pi$ stacking interactions of the aromatic ring systems can lead to partially aggregation of the benzophenone moieties and thus to a decrease of the cloud point (which would also explain the deviation from linearity in **Figure 20C** for the absorption at higher benzophenone content).

Figure 21: Cloud point dependence on benzophenone content (**A**) for poly(EtOxa-co-BPOxa) and poly(isoPrOxa-co-BPOxa). Cloud point error: ± 1 K. Transmittance curves at 550 nm for poly(EtOxa-co-BPOxa) (**B**) and poly(isoPrOxa-co-BPOxa) (**C**). Polymer concentration 3 mg ml^{-1}, heating-/cooling-rate = 1 K min^{-1}, filled circles for heating and open circles for cooling.

4. Results and Discussion

Recorded transmittance curves (**Figure 21B** and **C**) show sharp transitions for heating and cooling, which indicates reversible switching of the respective polymers from a hydrophilic state at low temperatures to a more hydrophobic state at temperatures above their cloud point. In almost all cases, a small hysteresis of approximately 0.5 K was observed between the heating and cooling cycle. Due to insolubility of the copolymer systems poly(n-PrOxa$_{94}$-BPOxa$_6$) in water, cloud point comparison with the respective poly(n-PrOxa) homopolymer could not be performed.

4.2.4 Glass Transition Temperature Dependence on Benzophenone Content

As a final point, the glass transition temperature T_g was determined as a function of benzophenone content using modulated differential scanning calorimetry, as this method allows the separation of simultaneously occurring processes, like glass transition T_g and thermal relaxation. Measurements (kindly performed by Sven Klees during a research lab course, Macromolecular Chemistry, University of Siegen), were conducted for the system poly(EtOxa-BPOxa) of varying benzophenone concentrations from 0°C to 140°C. The heating/cooling rate applied for all measurements was 5 K min^{-1} with a modulation period of 60 s and an amplitude of ±0.796 K. For all measurements at least two heating and cooling cycles were performed and the T_g was determined using the second heating cycle of each experiment.
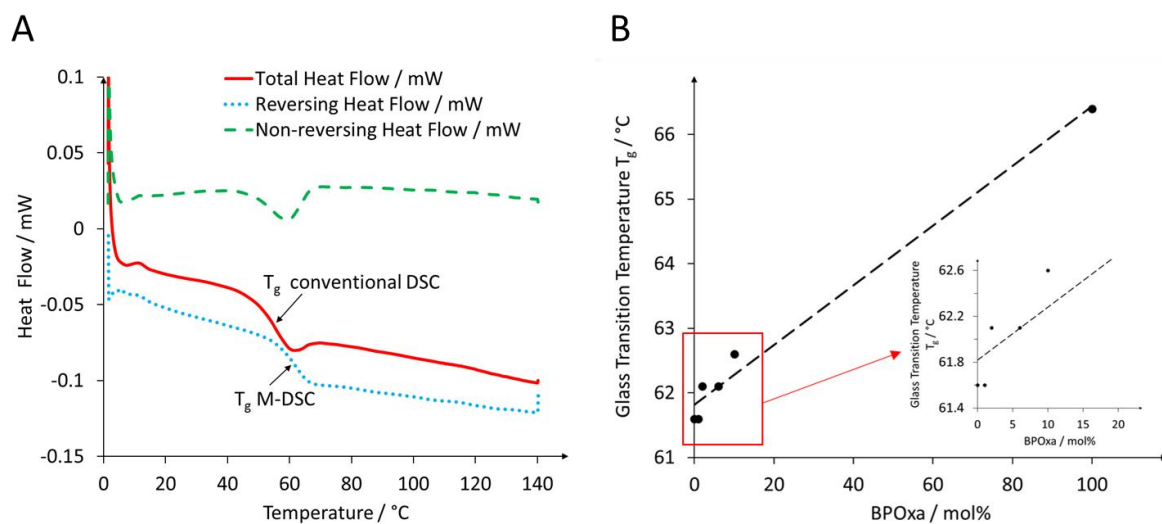
Figure 22: Heat flow traces for the second heating cycle of a M-DSC measurement for poly(EtOxa) with deconvolution of the individual signals (total heat flow, reversing heat flow, non-reversing heat flow). Heating rate M-DSC: 5 K min^{-1} ±0.796 K/60 s (**A**). Measured T_g of the polymer system poly(EtOxa-BPOxa) of different BPOxa concentrations (**B**). All T_g measurements (kindly performed by Sven Klees) and their values were determined by using the second heating cycle of each experiment. T_g error: ±0.1 K.
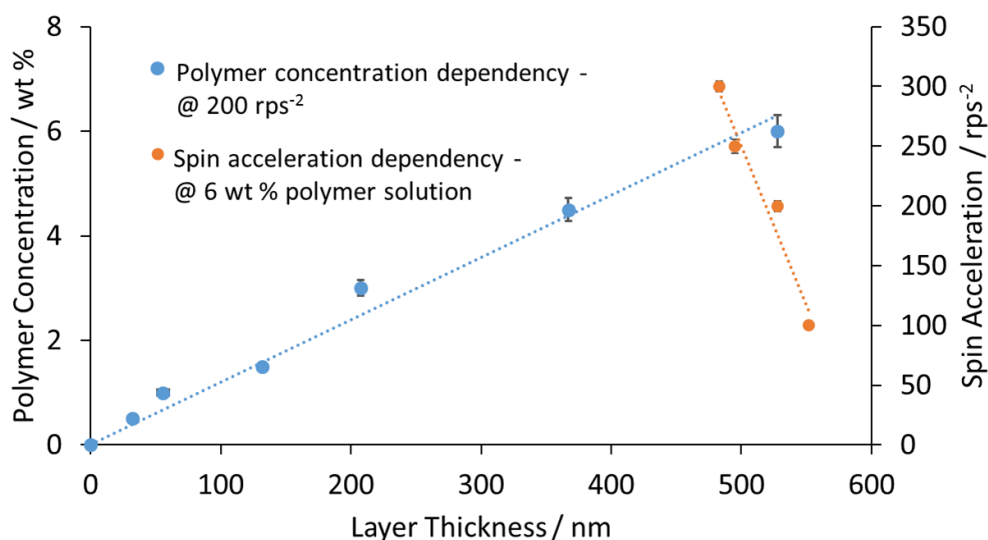
4. Results and Discussion

The M-DSC diagram in **Figure 22A** shows the second heating cycle of poly(EtOxa), with deconvolution of the total heat flow into a reversing and a non-reversing component. The conventional DSC signal, represented by the total heat flow, shows a typical combination of the T_g and an enthalpic relaxation process occurring at nearly equal temperatures, details about this method are described above in **Chapter 3.2**. These two superimposed events can be clearly separated from each other in the reversing and the non-reversing heat flow traces, providing the means of much higher accuracy for the determination of T_g. The process of enthalpy relaxation, observed in the non-reversing heat flow, is assumed to be related to molecular conformational changes, resulting from a decrease of free volume and chain mobility in the glassy state. In other words, the strain from thermal expansion and molecular rearrangements is frozen in the vitrified material upon cooling below the T_g, and released upon heating above the T_g. Corresponding data of the glass transition temperature T_g recorded for the system poly(EtOxa-co-BPOxa) are depicted in **Figure 22B**. It was found, that the benzophenone side chain has a rather minute effect on T_g, as the value for the BPOxa homopolymer lies only 4 K higher than that of the EtOxa homopolymer. In the copolymers a rather linear increase to higher T_g for an increasing benzophenone concentration is observed, as typically found for random copolymers.[173] Here, two opposing factors must be considered. First, the benzophenone group is hydrophobic and rather voluminous, with a substantial dipole moment associated with the carbonyl group, which favors aggregation (e.g. $\pi - \pi$ stacking of the benzophenone ring systems) and thus impede bond rotation of the polymer backbone and result in an increase of T_g. On the other hand, the flexible propylene oxide spacer located between the polymer backbone and the benzophenone group promotes bond rotation and thereby a decrease of T_g. As a result, both factors seem to almost cancel each other and leading to a minor influence on the T_g. of the investigated polymer system.

4.2.5 Optimization of the Spin-Coating Conditions by Ellipsometry

In order to optimize the spin-coating process used for the preparation of surface-attached poly(2-alkyl-2-oxazoline)-based hydrogel systems (for investigation of the temperature dependent swelling), the effect of varying spin-coating conditions was studied by ellipsometry. In this process, fabrication of very homogeneous layers with a dry-state layer thickness of at least 400 nm was targeted, which is needed to support at least two waveguide modes in OWS. For hydrogel immobilization, the cleaned silicon substrates were immersed overnight in an ethanolic solution of the adhesion promoter BPTES (1 mM) and washed with dry ethanol. BPTES-modified substrates were then spin-coated with solutions of poly(EtOxa$_{97}$-BPOxa$_3$) at varying concentrations. After drying of the polymer layers at 50°C under reduced pressure, thickness and homogeneity (as indicated by the fidelity of the fit) were investigated by ellipsometry. Additionally to the polymer concentration, the spin acceleration was varied, while keeping the maximum spin speed constant at 3000 rpm.

Figure 23: Optimization of the spin-coating conditions exemplarily performed for poly(EtOxa$_{97}$-BPOxa$_3$). Spin speed 3000 rpm.

4. Results and Discussion

The results compiled in **Figure 23** show a linear increase of the thickness with higher polymer concentrations, but for such films also the roughness increases, which is indicated by the larger error bar observed for higher polymer concentrations as well as qualitatively assessed from their optical appearance. Spin acceleration has the opposite effect, with a decreasing layer thickness for higher acceleration rates. The data from these measurements enable a rough targeting of the layer thickness by variation of the polymer concentration, but one has to consider that the thickness of the spin-coated layers depends strongly on the viscosity of the polymer solutions, which in turn is mainly influenced by the polymer chain length. Thus, the actual layer thickness obtained by a defined set of spin-coating conditions can vary on a batch-to-batch basis, as well as for polymers of differing composition. Additionally, varying polarity of the polymer systems may require to adapt the solvent type or mixtures, which will have a fundamental effect on the spin coating process. For a more reliable targeting of the desired layer thickness, further optimization of the spin coating conditions for each single polymer type would be necessary. Based on the conditions identified above, the polymer layers studied further below were prepared from 6-8 wt% ethanolic solutions at rotational speed of 3000 rpm and with an acceleration speed of 200 rps^{-2}.

4.2.6 Temperature Dependent Swelling of Hydrogel Layers from Photocrosslinkable Poly(2-Alkyl-2-Oxazoline)s as Investigated by SPR/OWS

Prior to the investigation of the temperature dependent swelling by SPR/OWS, the optical parameters of the Au substrates were determined. This was achieved by fitting the angular-dependent reflectivity $R(\theta)$ of the measured SPR curves for reference samples coated with Ti and Au, only. For this purpose, the light beam of a HeNe laser (λ=633 nm) was directed onto a glass prism, which was optically matched to the respective gold-coated substrate. The resonant excitation of the surface plasmon was observed by measuring changes in reflected intensity R of the laser beam as a function of the angle of incidence θ, using p-polarized light. A series of three individual measurements was performed, with the results summarized in **Table 9** and the corresponding reflectivity curves depicted in **Figure 24**. All reflectivity measurements were performed using the software WASPLAS[174] and the data fitted with the software Winspall 3.02,[175] both developed at the Max Planck Institute for Polymer Research in Mainz (Germany).

Table 9: Optical properties of the gold coating and Ti adhesion layer at 633 nm on LASF9 glass.

Sample–Nr.	Layer Thickness Ti / nm	Refractive Index Ti n	Extinction coefficient Ti k	Layer Thickness Au / nm	Refractive Index Au n	Extinction coefficient Au k
Sample 1	1.1	0.4612	1.9993	48.0	0.2647	3.5060
Sample 2	1.4	0.7088	1.8984	47.4	0.2604	3.5879
Sample 3	1.4	0.442	1.8366	47.3	0.2927	3.6319
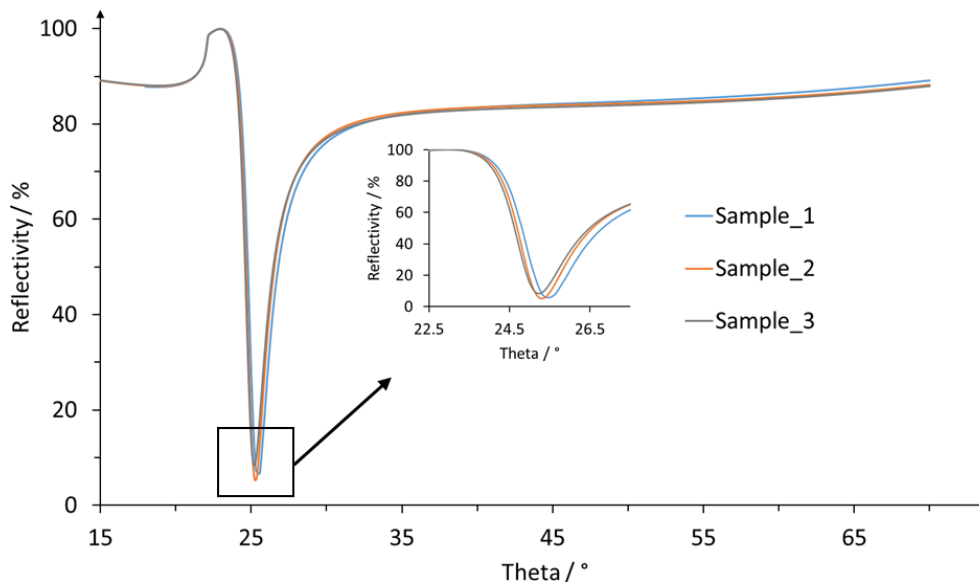
Figure 24: Fit of the angular reflectivity spectra for LASF9 gold substrates for transverse magnetic (TM) polarization.

Analysis of the SPR results indicated a reproducible thickness of 47–48 nm for the Au layer, which was adopted for all further data evaluations. The obtained refractive indices and extinction coefficients are also in good agreement with data from the literature.[95] However, these two parameters have only a minor influence on the data evaluation, especially for the investigation of thick polymer layers, as they only slightly affect the shape but not the position of the reflectivity minimum.

Next, the optical properties of the deposited BPdiS monolayer were evaluated by SPR/OWS. For this purpose, Au-coated glass substrates (LASF9) were immersed into a diluted DMSO solution (1 mM BPdiS) for 24 h and after rinsing and drying the angular reflectivity curves were recorded and compared before and after the deposition process (**Figure 25**).
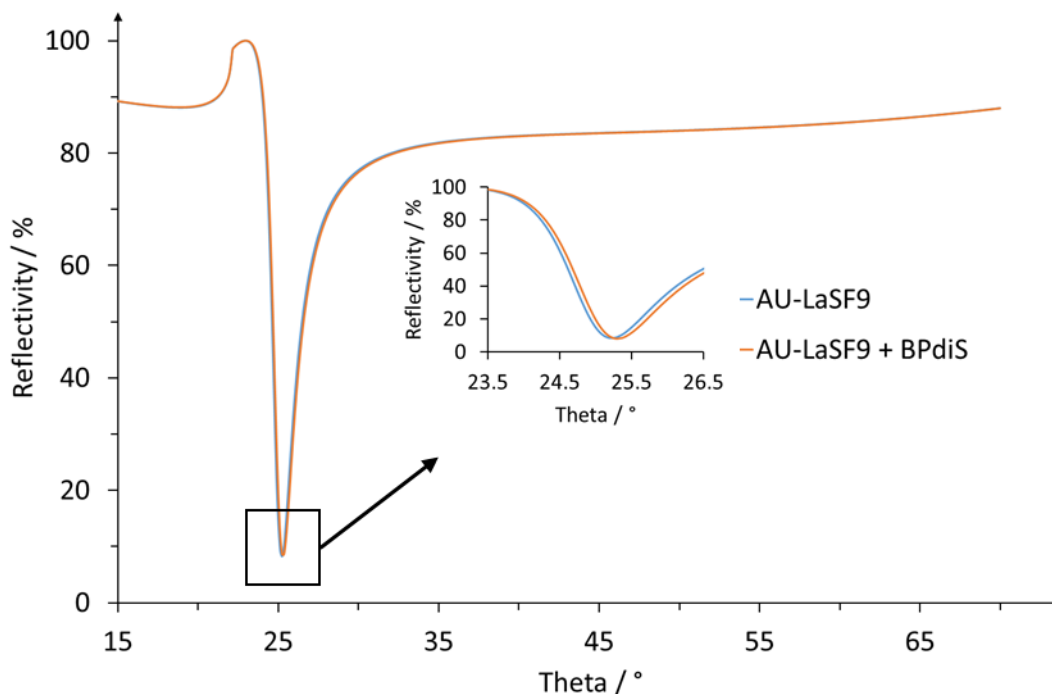
Figure 25: Fit of the angular reflectivity spectra for neat Au-coated LASF9 gold substrates and for modified Au-LASF9 substrates with a BPdiS adhesion layer, using transverse magnetic (TM) polarization.

After the BPdiS deposition process, a slight shift of the surface plasmon was observed, which confirms successful monolayer formation of the adhesion promotor. Fitting of the data sets provided a thickness of $d_{BPdiS} = 0.5$ nm and a refractive index $n_{BPdiS} = 1.55$, which is in good agreement with similar monolayers already described in the literature.[95]

Following complete substrate characterization, the temperature dependent swelling of different poly(2-alkyl-2-oxazoline)-based polymers with a benzophenone concentration between 2-3 mol% and an average molar mass between 30-40 x 10^3 g mol^{-1} (see **Table 7**, M/I ratio 300/1) was investigated. For this purpose, the respective polymers were coated onto BPdiS modified substrates (Au-LASF9 or Au-BK7), which optically matched to the prism used in the SPR setup. Ethanolic solutions of 6-8 wt% polymer concentration were spin-coated at 3000 rpm with an acceleration speed of 200 rps^{-2} on top of the modified substrates, resulting in a dry state layer thickness between 350 nm to 500 nm. The polymer layers were dried at 50°C under reduced pressure for at least 4 h and irradiated with UV light at 365 nm under exclusion of oxygen (**Figure 26A**).

4. Results and Discussion

(A)
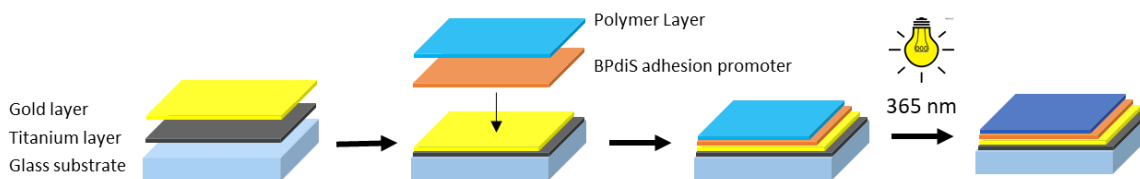
(B) Dry state
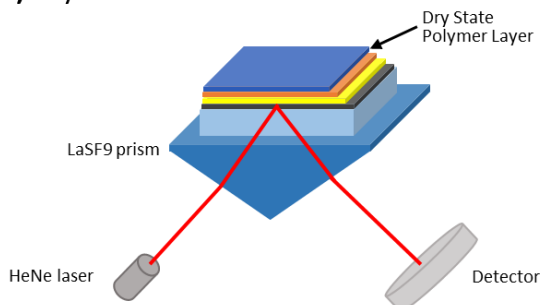
(C) Swollen state
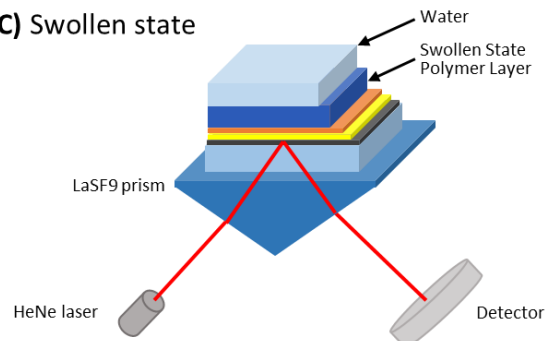
Figure 26: Schematic representation of the coating and surface attachment procedure (**A**) and characterization of the dry polymer film (**B**) and the swollen hydrogel layer (**C**), employing a Kretschmann measurement configuration.

SPR/OWS measurements of the swollen polymer layers were performed using transverse magnetic (TM) polarization of the impinging laser beam. For these experiments, a flow cell was pressed on top of the polymer layer in order to direct a water flux over its surface. The temperature of the flow cell and liquid medium was controlled by an integrated Peltier element. All reflectivity measurements were again performed using the software Wasplas and the data were fitted with the software Winspall 3.02. Here, the model adopted for fitting the hydrogel film assumes a homogenous layer with a given thickness d_h and a refractive index n_h, without considering birefringence. The experiments were designed in a way that the investigated polymer layers support at least two TM waveguide modes (see **Figure 27**), in order to determine the refractive index and the layer thickness independently from each other.
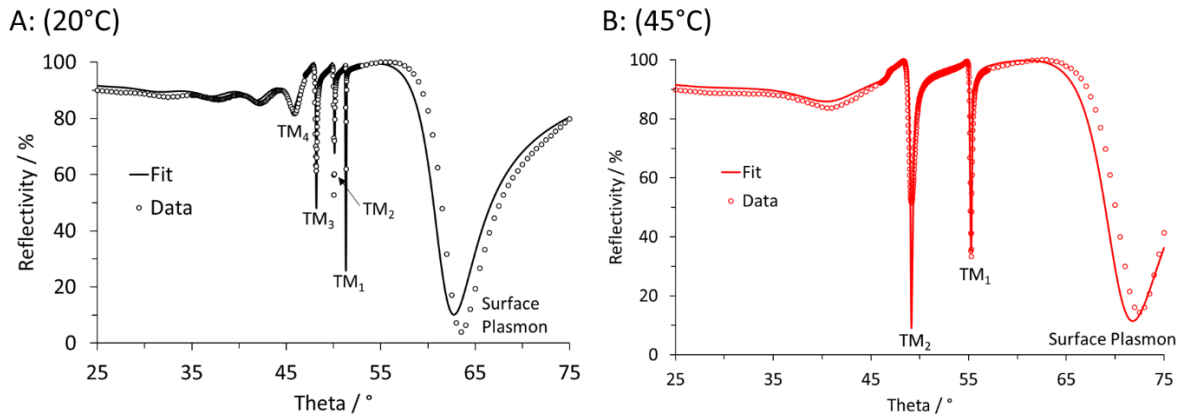
Figure 27: Fit and data points of the angular reflectivity spectra of a swollen (**A**, 20°C) and collapsed (**B**, 45°C) hydrogel layer sustaining at least two waveguide modes, prepared from poly(2-isoPrOxa$_{98}$-BPOxa$_2$) and measured with transverse magnetic (TM) polarization of the incident laser beam. Measurements were performed using LASF9 glass substrates.

For the characterization of polymer layers that support only one TM mode, measurements are additionally performed using transverse electric (TE) polarization. In these cases, data evaluation is performed by fitting both reflectivity curves in conjunction, as it is exemplarily depicted in **Figure 28**.
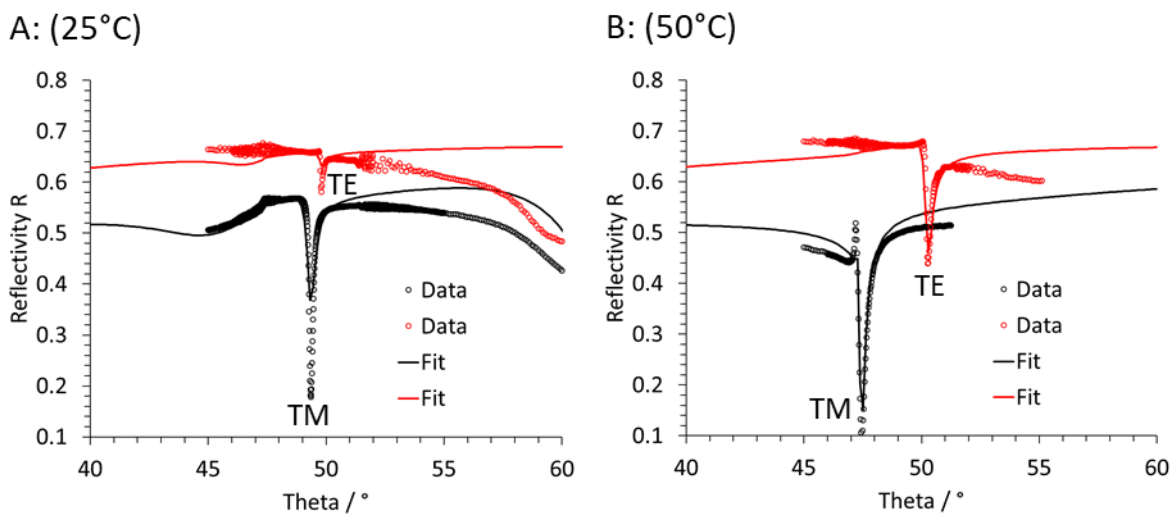
Figure 28: Angular reflectivity spectra of a hydrogel layer in the swollen (**A**, 25°C) and collapsed (**B**, 50°C) state for poly(2-isoPrOxa$_{98}$-BPOxa$_2$), using transverse magnetic (TM) polarization and transverse electric (TE) polarization. Measurements were performed with LASF9 glass substrates.

4. Results and Discussion

The polymer volume fraction ϕ of the investigated hydrogel layers can be calculated from the obtained thickness and refractive index data using effective medium theory.[176]

$$\phi = \frac{n_h^2 - n_{water}^2}{2n_{water}^2 + n_h^2} \Big/ \frac{n_{h-dry}^2 - n_{water}^2}{n_{h-dry}^2 + 2n_{water}^2} \tag{37}$$

Here, n_{dry} represents the refractive index of the dry polymer film, n_h and n_{water} the refractive indices of the swollen film and water, respectively. The polymer swelling ratio (SR) was determined from the measured thickness of dry state d_{dry} and swollen state d_h hydrogel layers as follows:

$$SR = \frac{d_h}{d_{dry}} \tag{38}$$

The crosslinking density-dependent swelling behavior was firstly investigated for poly(EtOxa$_{97}$-BPOxa$_3$) as model system by varying the irradiation dose between 4–20 J cm^{-2}. Films were exposed to the aqueous medium for at least 1 h prior to each measurement, to ensure complete swelling of the hydrogel layers. Swelling ratios were then determined by comparing dry state and swollen state film thicknesses, according to equation (**38**), and the polymer volume fraction was calculated with equation (**37**).
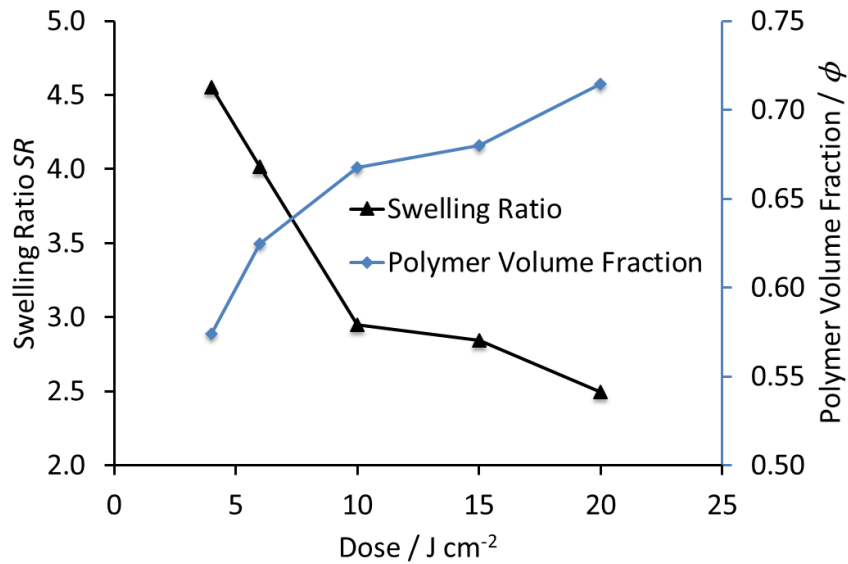
Figure 29: Swelling ratio-dependence on irradiation dose used for crosslinking a poly(EtOxa$_{97}$-BPOxa$_3$) film, as determined by OWS in water at 25°C.

4. Results and Discussion

Results depicted in **Figure 29** show the dependence of the swelling ratio and the polymer volume fraction on the irradiation dose for crosslinking of poly(EtOxa$_{97}$-BPOxa$_3$). It was found that highest swelling ratios were obtained for lowest irradiation doses, while increasing the irradiation dose results in reduction of hydrogel networks swelling. For the polymer volume fraction f, the inverse behavior was observed. Both observations result from the increasing elastic retraction force for shorter chain segments between the crosslink point at higher crosslink densities of the swollen network, as already described for other crosslinked polymer systems.[102, 163] With these results, it could be demonstrated that surface-attached, photocrosslinkable hydrogels of varying swelling ratios can be conveniently fabricated from poly(2-alkyl-2-oxazoline)s by irradiation with UV light at a wavelength of 365 nm.

4. Results and Discussion

In subsequent experiments, the temperature-dependent swelling of hydrogel systems, that were prepared from the novel poly(2-alkyl-2-oxazoline)s, was investigated (**Figure 30A** and **B**). In such experiments, all polymer layers were crosslinked with the same dose of 8 J cm^{-2}. The resulting polymer films were exposed to water for 1 h and reflectivity curves were recorded until a stable baseline was observed. The temperature was increased stepwise and the layers were equilibrated for 15 min before each measurement. Experimental data of the temperature-dependent swelling measurements are exemplarily depicted for poly(isoPrOxa$_{98}$-BPOxa$_2$) in **Chapter 7.7**.
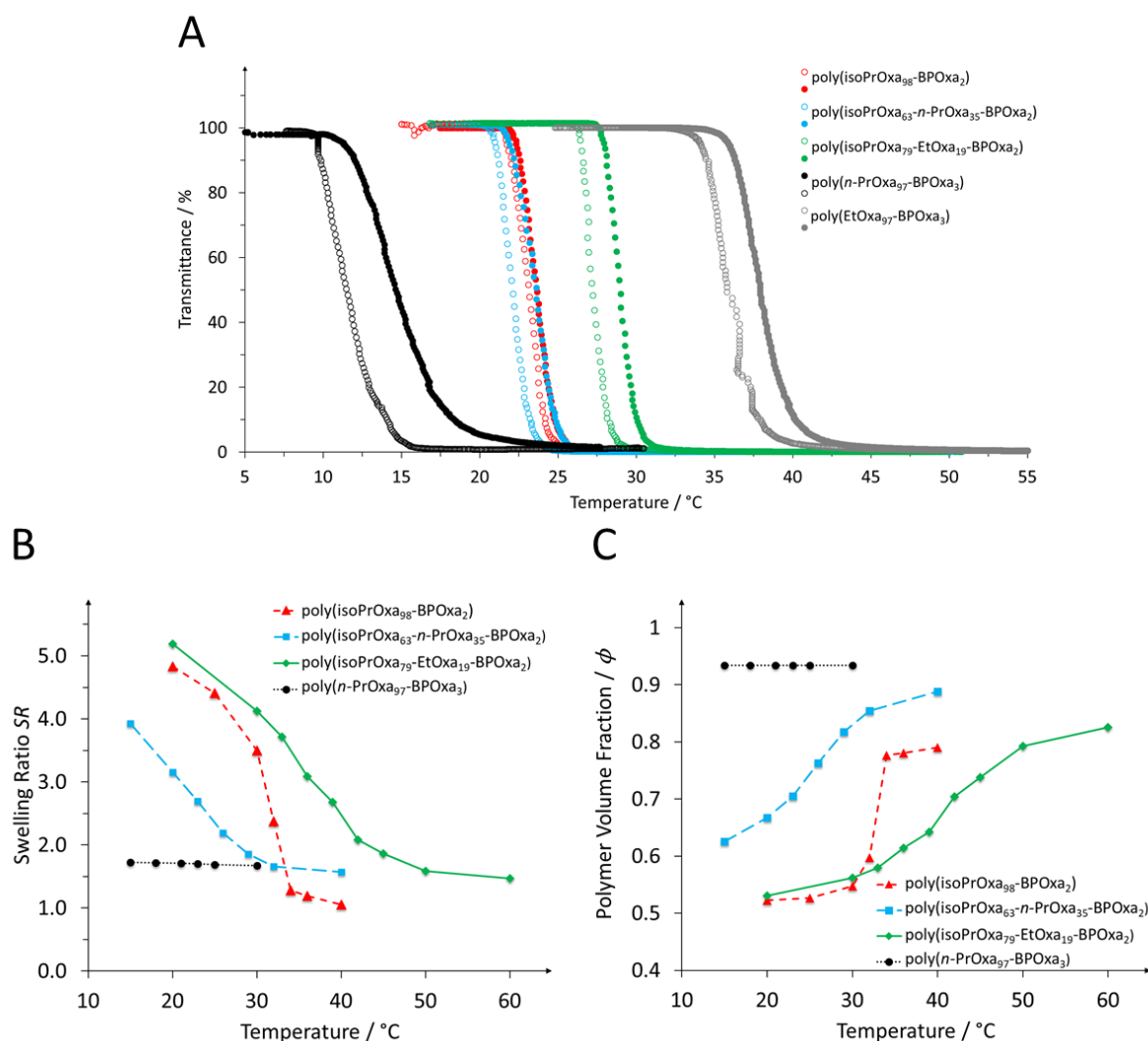
Figure 30: Transmittance curves at 550 nm for different poly(2-alkyl-2-oxazoline-BPOxa) systems (**A**). Polymer concentration 3 mg ml^{-1}, heating-/cooling-rate = 1 K min^{-1}, filled circles for heating and open circles for cooling. Dependence of the swelling ratio (**B**) and the polymer volume fraction (**C**) on temperature for an irradiation dose of 8 J cm^{-2}, as determined by OWS in water.

4. Results and Discussion

Results summarized in **Figure 30A** and **B** depict the temperature-dependent swelling for surface-attached hydrogels from 2-alkyl-2-oxazoline-based co- and terpolymers. By comparing swelling ratios and polymer volume fraction at 20°C of each polymer system, it becomes obvious that their tendency to swell follows the order according to their hydrophobicity, as expressed by their cloud points in aqueous solution (see **Table 10**). The lowest values were observed for poly(n-PrOxa$_{97}$-BPOxa$_3$), with a swelling ratio of 1.7 and a cloud point of 12°C, which is apparently the most hydrophobic system. The highest values were obtained for poly(isoPrOxa$_{79}$-EtOxa$_{19}$-BPOxa$_2$), showing a swelling ratio of 5.2 and a cloud point of 28.4°C as the most hydrophilic system in this series. It has to be noted, that small variations in the BPOxa concentration also effect the swelling ratio, as they may lead to different crosslinking density.

For all investigated polymers, except poly(n-PrOxa$_{97}$-BPOxa$_3$), a volume transition of the hydrogel network was observed with changing temperature, which correlates to the cloud point in solution. For the more hydrophobic poly(isoPrOxa$_{63}$-n-PrOxa$_{35}$-BPOxa$_2$) a phase transition temperature of 23°C was observed, while the more hydrophilic poly(isoPrOxa$_{79}$-EtOxa$_{19}$-BPOxa$_2$) showed a phase transition temperature of 39°C. For both terpolymer systems a broadening of the phase transition was observed, which may result from a contribution of each comonomer with different cloud points for EtOxa and isoPrOxa, or nPrOxa and isoPrOxa, respectively. In contrast, a sharp transition was observed for poly(isoPrOxa$_{98}$-BPOxa$_2$) with only isoPrOxa as single thermoresponsive component.

In general, it was found that cloud points measured for polymer solutions were significantly lower compared to the phase transition temperatures of the corresponding polymers as surface-attached hydrogels, obtained by SPR/OWS (**Table 10**). As already stated in **Chapter 4.2.2**, even small amounts of the benzophenone-2-oxazoline, when copolymerized with 2-alkyl-2-oxazolines, lower the cloud point in aqueous solution. The higher phase transition temperatures observed for the hydrogels by SPR/OWS can be explained by the higher polymer volume fraction in the networks compared to the solutions.

4. Results and Discussion

Table 10: Phase transition temperatures vs. cloud point temperatures for different poly(2-alkyl-2-oxazoline-BPOxa) systems.

Sample	SPR/OWS[a] hydrogel network		Cloud Point[c] polymer solution	
	Heating/°C	Cooling/°C	Heating/°C	Cooling/°C
poly(EtOxa$_{98}$-BPOxa$_2$)	N/A[b]	N/A[b]	37.9	35.8
poly(isoPrOxa$_{98}$-BPOxa$_2$)	32	30	24.0	21.8
poly(isoPrOxa$_{63}$-n-PrOxa$_{34.5}$-BPOxa$_2$)	26	24	22.7	20.6
poly(isoPrOxa$_{79}$-EtOxa$_{19}$-BPOxa$_2$)	41.5	40	28.4	26.6
poly(n-PrOxa$_{97}$-BPOxa$_3$)	N/A[b]	N/A[b]	11.5	14.6

[a]Determined from the inflection point of the temperature-dependent swelling ratio curve. [b]Temperature outside the accessible measurement range of 15-55°C. [c] As determined by turbidity measurements of a 0.3 wt% aqueous solution with a heating/cooling rate of 1 K min^{-1}.

In addition, the cloud point temperature is also concentration dependent, which is demonstrated exemplarily for three different poly(2-alkyl-*co*-2-BPOxa) polymer systems below. The experimental data of the respective transmittance curves are additionally depicted in **Chapter 7.5**.
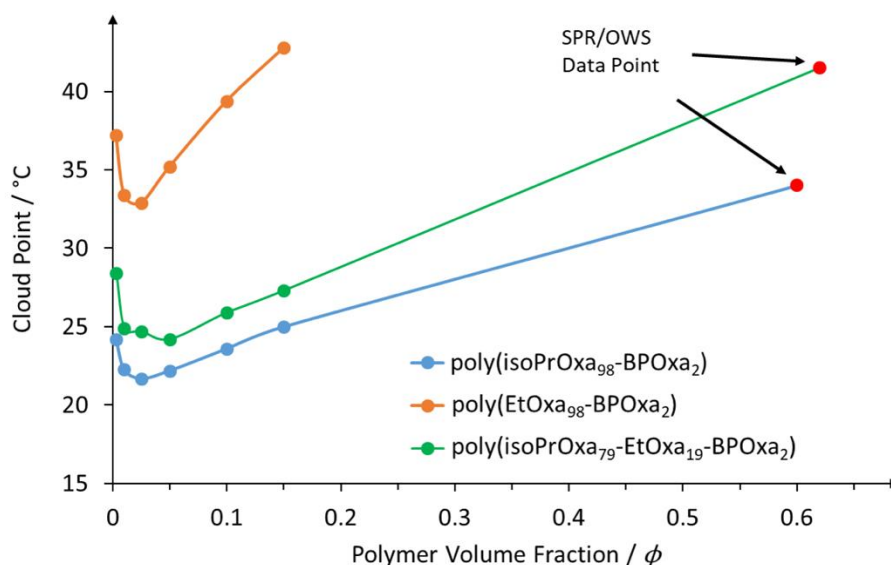
Figure 31: Cloud point dependence on polymer volume fraction for poly(EtOxa$_{98}$-BPOxa$_2$), poly(isoPrOxa$_{79}$-EtOxa$_{19}$-BPOxa$_2$) and poly(isoPrOxa$_{98}$-BPOxa$_2$) as determined by turbidity measurements in aqueous solution (heating only) with a heating rate of 1 K min^{-1}. Phase transition temperatures (indicated as "SPR/OWS data point") were determined by temperature dependent OWS.

4. Results and Discussion

The data in **Figure 31** demonstrate that the cloud point depends on the polymer concentration, as shown for three different polymer-water system. The minima of all three diagrams is observed for a polymer volume fraction of about 0.25, which corresponds to their lower critical solution temperature (LCST). Extrapolation of the measured cloud point data for poly(isoPrOxa$_{79}$-EtOxa$_{19}$-BPOxa$_2$) and poly(isoPrOxa$_{98}$-BPOxa$_2$) coincides with the significantly higher phase transition temperatures found in the SPR/OWS experiments (indicated as "SPR data point"). These higher transition temperatures in the hydrogels are the result of a higher polymer volume fraction in the respective networks.

To demonstrate the reversibility of the temperature-dependent swelling and collapse behavior of the fabricated hydrogel layers, repeated heating and cooling cycles were performed. In these experiments, the layers were equilibrated for 30 min after each temperature step. The recorded data in **Figure 32** were obtained for poly(isoPrOxa$_{98}$-BPOxa$_2$), which was crosslinked with an irradiation dose of 8 J cm^{-2}.
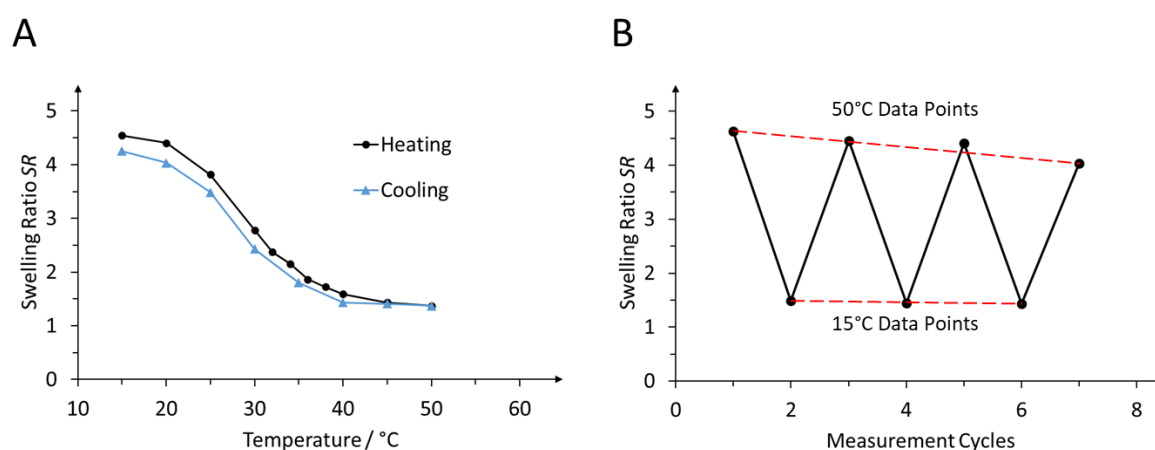
Figure 32: Heating and cooling cycles for poly(isoPrOxa$_{98}$-BPOxa$_2$) for an irradiation dose of 8 J cm^{-2} in water, as determined by OWS.

The curves for the first heating and cooling cycle depicted in **Figure 32A** show a hysteresis, which may result either from material loss of non-covalently bound polymer chains inside the attached hydrogel layer, or from a response time of the system, which is slower than the experimental time frame (cooling rate). The first reason can only be partially relevant, because measurements in dry state before and after the first swelling showed a material loss of only 2-3 wt%, while the SR difference in the swollen state before and after the first cycle amount

to 5-6 %. Furthermore, the layer thickness and refractive index of the collapsed system at higher temperature showed constant values after each cycle **Figure 32B**, while any material loss should also affect the dry layer thickness. The constant SR decrease of the swollen layer with each cycle hints to a kinetic effect with long relaxation times exceeding the time period between each cooling cycle. Potentially, a partial irreversible (on the experimental time scale) aggregation of hydrophobic polymer segments (e.g. benzophenone groups) in the collapsed state take longer to rehydrate during swelling und thus reduce the observed layer thickness.

4.2.7 Mechanical Properties of Surface-Attached Networks from Photocrosslinkable Poly(2-Alkyl-2-Oxazoline)s

Mechanical properties of surface attached poly(2-alkyl-2-oxazoline) based hydrogel systems were investigated by nano-indentation using AFM (kindly performed by Cleiton Kunzler, Macromolecular Chemistry, University of Siegen), exemplarily conducted for poly(isoPrOxa$_{98}$-BPOxa$_2$). The respective polymer was spin-coated from a 1 wt% ethanolic solution onto BPTES-modified glass substrate, dried at 50°C under reduced pressure and crosslinked by UV irradiation at 365 nm with an energy dose of 4 and 8 J cm^{-2}, respectively, under exclusion of oxygen. The thickness of the dry layers, as determined by a scratch test with AFM, was found to be between 750-1400 nm. Both samples were then exposed to water for at least 2 h and the Young's modulus of the swollen films was assessed from force maps (2 x 2 μm or 5 x 5 μm) at 25°C. The same measurements were performed for the hydrogel layers in the collapsed state at 38°C. For each single measurement point, cantilever bending was fixed at 20 nm. This procedure was adopted for both samples, whereby the value of the elastic modulus of the hydrogels was taken as the maximum from a Gaussian fit of the force map distribution, resulting in a representative value for each sample. Fitting of the force curves was performed using a parabolic Hertz cone model based on the shape of the tip and indentation depth, whereby all measurements were performed in the early linear regime of the repulsive region in the approach curve to exclude a contribution of the underlying substrate. Experimental data (Height images and amplitude images, force maps, histograms fitted with Gaussian function for Young's modulus analysis and force curves) are additionally depicted in **Chapter 7.6**.

Table 11: Young's moduli of water-exposed hydrogel films from poly(isoPrOxa$_{98}$-BPOxa$_2$), as measured by AFM nano-indentation in dependence of temperature and UV energy dose for crosslinking.

Dose / J cm^{-2}	Temperature / °C	Young's Modulus / kPa
4	25	193 ± 16
4	38	1140 ± 155
8	25	417 ± 39
8	38	2190 ± 111

All measurements conducted by Cleiton Kunzler were performed for samples in contact with aqueous medium.

In **Table 11** the results are summarized for the dependence of the Young modulus on crosslinking density and temperature. It can be noted, that an increase in irradiation dose by a factor of two (from 4 to 8 J cm^{-2}) results in nearly doubling of the Young's modulus, due to the higher crosslinking density. When switching the polymer layers from a swollen to a collapsed state by rising the temperature above their phase transition temperature, an increase of the Young's modulus by a factor of about six is observed. Here, the increasing Young's modulus results from the substantial increase of the polymer volume fraction in the collapsed hydrogel layers. Since more crosslinked hydrogels absorb less water, due to the higher elastic retraction force of the network, the Young's modulus of such more crosslinked systems is also higher in the collapsed state. Images of the topography of these hydrogel films in the swollen and collapsed state were recorded in tapping mode prior to the evaluation of the Young's modulus by nano-indentation. This operation mode was chosen to identify potential nanoscopic structures present on the sample surface, which could interfere with force map measurements, while minimizing the probability of damaging the sample by the AFM tip.
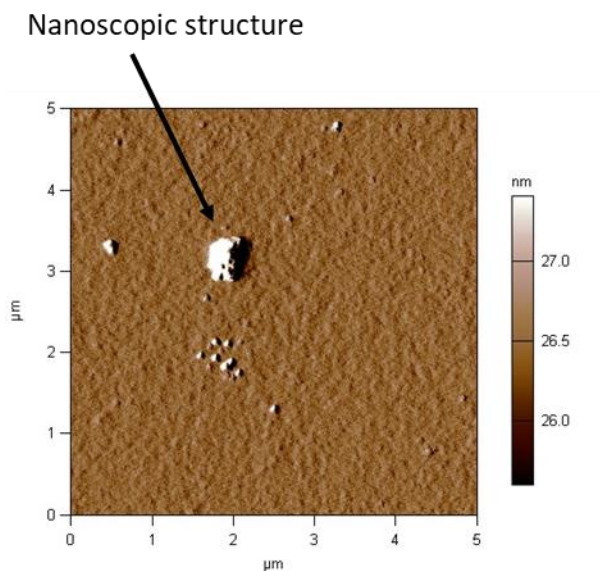
Figure 33: Representative surface topography image for a collapsed poly(isoPrOxa$_{98}$-BPOxa$_2$) hydrogel film in contact with water at 38°C (crosslinked with an irradiation dose of 8 J cm^{-2}).

4. Results and Discussion

The image depicted in **Figure 33** is representative for the investigated poly(isoPrOxa$_{98}$-BPOxa$_2$) hydrogel layers in contact with water. In all cases, nanoscopic structures were observed on top of the sample surface, which were excluded from the analysis of the force maps. It may be assumed that these hemispherical structures result from partially undissolved polymer present during the deposition process in the spin-coating solution.

In summary, AFM results are consistent with observations from SPR/OWS measurements, which demonstrated the influence of the irradiation dose (longer irradiation time lead to denser networks, see **Figure 29**) as well as the influence of the temperature (**Figure 30**) on the swelling behavior of surface-attached, thermoresponsive hydrogel networks prepared from poly(2-oxazoline)s.

4.2.8 Chapter Summary and Conclusion

In the present chapter, fabrication and characterization of surface-attached, thermoresponsive hydrogel layers from novel photocrosslinkable poly(2-alkyl-2-oxazoline)s was demonstrated. For this purpose, a novel benzophenone-2-oxazoline was developed as photocrosslinkable monomer (BPOxa). Cationic ring opening copolymerization of BPOxa with various 2-alkyl-2-oxazolines was performed and the build-in ratio of the benzophenone derivative was assessed. These experiments confirmed that the monomer feed of BPOxa corresponded to its build-in ratio in the polymer chain, which provides the possibility to synthesize poly(2-alkyl-2-oxazoline)-based copolymers with well-defined photocrosslinker concentration.

The dependence of the cloud point temperature on photocrosslinker concentration was investigated for these copolymers in aqueous solution by UV/VIS spectroscopy. Here it was found that the large hydrophobic benzophenone moieties cause a significant decrease of the cloud point temperature compared to the corresponding 2-alkyl-2-oxazoline homopolymers. For this effect, two factors have to be considered: Firstly, hydration of the hydrophobic benzophenone units by water molecules is less favored, compared to smaller and more polar side chains. Secondly, the aromatic benzophenone group with associated dipole of the carbonyl bond may favor π-π-interactions and aggregation in the aqueous environment. Both factors cause a drop of the cloud point and consequently a phase separation at lower temperatures.

The influence of the benzophenone concentration on the glass transition temperature T_g was studied for poly(2-ethyl-2-oxazoline-*co*-2-benzophenone-2-oxazoline) by DSC. Here, the conventional DSC method did not show the typical step-like curve shape normally observed for the glass transition, but more a combination of a first and second order transition due to overlapping processes at almost the same temperature. These processes, potentially a combination of the increase in free volume at the glass transition T_g (quasi-second order transition) and relaxation processes caused by the release of internal stresses (first order transition), are not discernible by conventional DSC. In order to address this limitation, modulated DSC (M-DSC) measurements were conducted, as this method allows deconvolution of the total heat flow into a reversing and a non-reversing component, and

4. Results and Discussion

thereby the separation of overlapping processes. In these experiments it was found that the benzophenone moiety at build-in ratios up to 10 mol% has a minor impact, with the general trend to higher T_g for an increasing benzophenone concentration. Apparently, the voluminous and hydrophobic benzophenone group may lead to aggregation and impedes conformational freedom of the polymer backbone, resulting in an increase of T_g. On the other hand, the flexible propylene spacer between the polymer backbone and the benzophenone group may promote backbone flexibility and thereby a decrease of T_g. Both antagonistic effects seem to cancel and result in an overall small change of T_g for all investigated polymers.

The swelling behavior and volume phase transitions of surface-attached hydrogel films prepared from the thermoresponsive poly(2-alkyl-2-oxazoline)s was studied by SPR/OWS. For efficient surface attachment, a novel benzophenone disulfide (BPdiS) was synthesized and successfully applied as adhesion promotor for the covalent immobilization of the respective polymers onto Au-coated SPR substrates. For the immobilized hydrogel layers, the dependence between crosslinking density and swelling ratio was studied exemplarily with the poly(EtOxa$_{98}$-BPOxa$_2$) system, using varying irradiation doses. As previously observed with PNIPAAm-bases systems it was found, that increasing irradiation doses leads to a decrease in swelling ratio as a direct consequence of the higher crosslinking density in the respective hydrogel network. The phase transition temperature was studied for polymer networks of varying monomer composition (2-ethyl-, 2-n-propy-, 2-isopropyl-2-oxazoline), while keeping the photocrosslinker concentration constant around 2-3 mol%. Only for the binary system poly(isoPrOxa$_{98}$-BPOxa$_2$) a sharp volume phase transition was observed for the surface-attached networks. Ternary polymer systems, composed of combinations of BPOxa with two different 2-alkyl-2-oxazolines, showed a broadening of the volume transition over a larger temperature range, which may result from an overlap of their individual cloud points. For all investigated polymer systems, the surface-attached hydrogel layers showed significantly higher temperatures for the volume phase transition compared to the lower cloud points found in aqueous solution. This behavior is explained with the higher polymer volume fraction in the swollen hydrogel network compared to solution.

The mechanical properties of poly(isoPrOxa$_{98}$-BPOxa$_2$) networks in contact with water were studied by AFM nano-indentation, yielding the Young's modulus (in the range of about 200-2000 kPa) as a function of crosslinking dose and temperature. Here, higher irradiation doses

4. Results and Discussion

(more crosslinked networks) and thermal collapse of the swollen layers result in higher moduli. The obtained results are thus in full agreement with SPR/OWS measurements.

4.3 Modification of Photocrosslinkable Poly(2-oxazoline)s via Azide–Alkyne Click Chemistry for the Preparation of Polymers with Improved Antifouling Properties

Post-modification of polymers has been used frequently for tuning their properties towards specific applications or for the incorporation of analyte-specific ligands within a sensor matrix. For these purposes, various methods have been applied such as thiol-ene[166] reactions, thiol-yne[177] reactions, and NHS active ester reactions[6]. Beside this wide variety of possible post-modification reactions, the copper(I) catalyzed azide-alkyne cycloaddition reaction (CuAAC) has been used most frequently, due to its fast reaction kinetics, high product yields, moderate reaction temperatures, and compatibility with a broad range of different functional groups.[178-180]
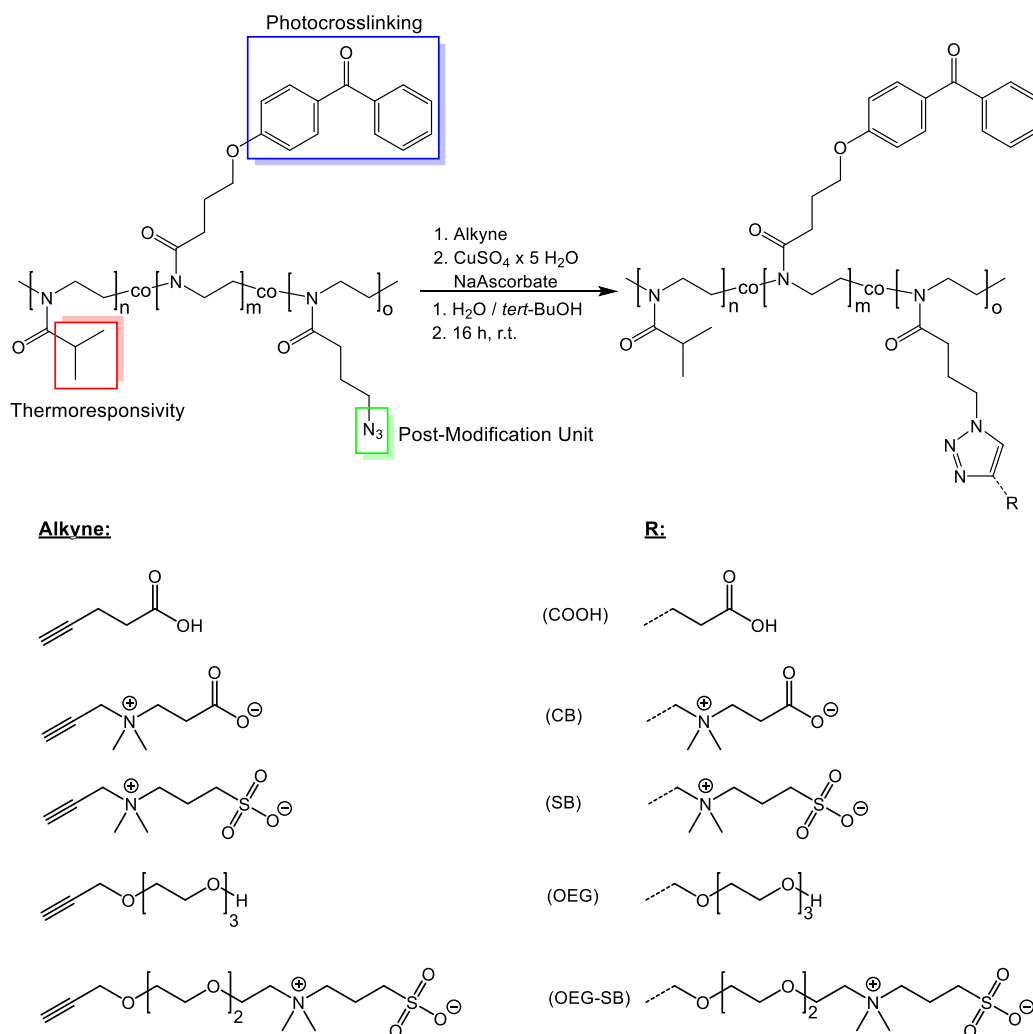
Figure 34: Post-modification of thermoresponsive poly(2-isopropyl-2-oxazoline)-based polymers by CuAAC, as performed in this thesis using different alkyne derivatives.

4. Results and Discussion

One major application target for the hydrogels, which were developed in this dissertation, is a multifunctional sensor matrix in SPR-based biosensors. To prevent unspecific adsorption of proteins onto the sensor surface, it is crucial that the applied hydrogel matrix exhibits minimal fouling properties, especially for the detection of peripheral blood biomarkers. Otherwise false positive signals or even blocking of the sensor matrix may occur. Polymers that have been used for antifouling applications are mostly poly(ethylene glycol) (PEG), poly(2-oxazoline)s, zwitterionic polymers (polybetaines), poly(vinylpyrrolidone) and hydroxy functionalized poly(acrylate)s, to name only a few prominent examples. Improving the already documented low-fouling properties of poly(2-oxazoline)s by combination with short oligoethylene glycol chains or zwitterionic betaine structures seems to be a promising strategy toward hydrogel binding matrices with highly selective analyte interaction.[7, 181-183]

4.3.1 Synthesis of a Functional Post-Modification Unit and Copolymerization with various 2-Alkyl-2-Oxazolines

Based on the advantages stated above, CuAAC was chosen as post-modification method for appropriately functionalized poly(2-alkyl-2-oxazoline)s. The initial step for this approach concerns the synthesis of an alkyne-2-oxazoline derivative, which was first attempted following the reaction scheme depicted below (**Scheme 17**).
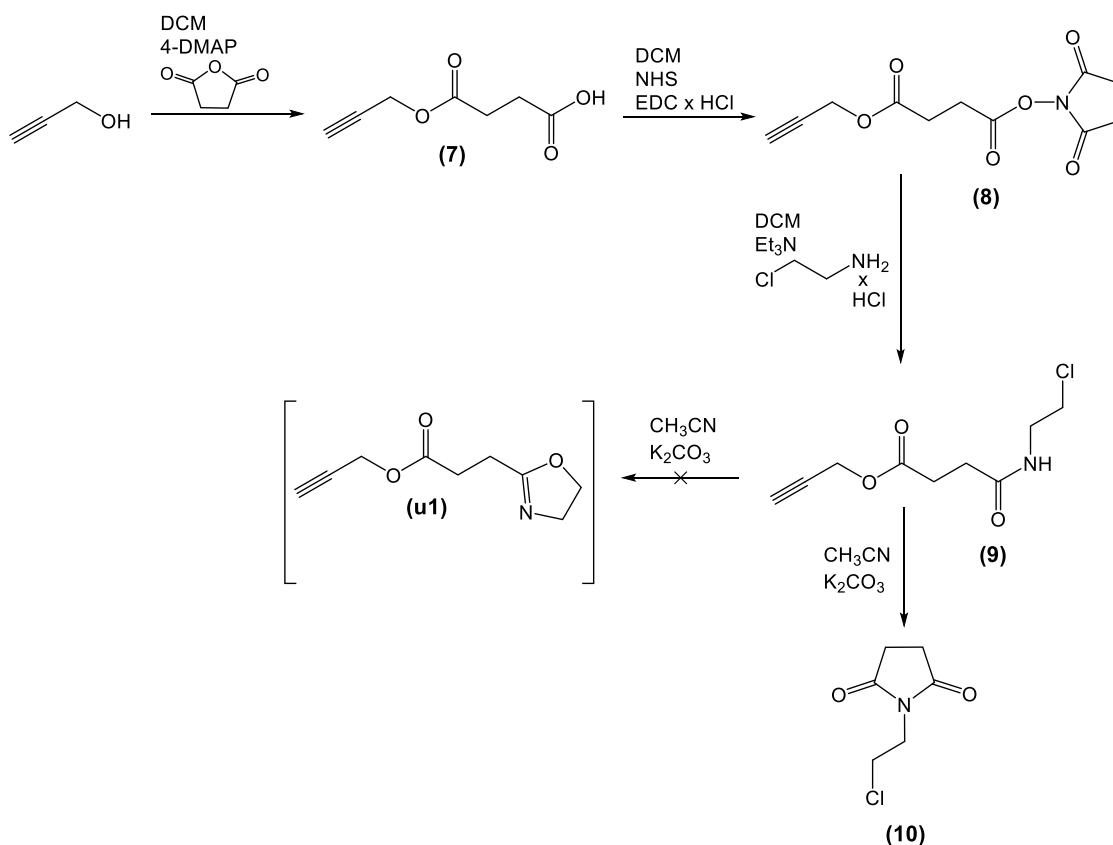
Scheme 17: Attempted synthesis strategy for an alkyne-2-oxazoline as post-modification unit.

The reaction sequence starts by dispersing 4-dimethylaminiopyridine (4-DMAP) and succinic anhydride in dry DCM, followed by the addition of propargyl alcohol. Ring opening of the anhydride is induced by 4-DMAP, which acts as a nucleophilic catalyst for the esterification reaction of succinic anhydride with propargyl alcohol. The resulting carboxylic acid (**7**) functionality is then transformed into an activated species (**8**) by reaction with NHS in the presence of EDC x HCl. Amide coupling of the active ester (**8**) with 2-chloroethylamine hydrochloride is then performed at room temperature, yielding compound (**9**). In the final

step, the respective amide (**9**) was dissolved in MeCN and heated in the presents of anhydrous K$_2$CO$_3$ to attempt the ring closure to the desired alkyne-2-oxazoline derivative (**u1**). Instead, elimination of 2-propyn-1-olate occurred under formation of *N*-(2-chloroethyl)succinimide (**10**), with the proposed reaction mechanism depicted in **Scheme 18**. The product (**10**) was identified by ^{1}H and ^{13}C NMR spectroscopy (see appendix **Figure 112** and **Figure 113**).
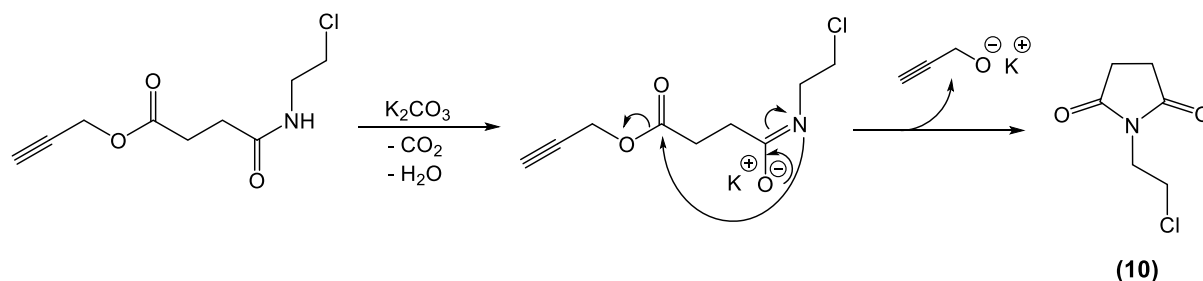
Scheme 18: Proposed mechanism for the elimination of 2-propyn-1-olate and transamidation, yielding *N*-(2-chloroethyl)succinimide.

The above approach for the synthesis of an alkyne-2-oxazoline derivative was abandoned and instead an azido-2-oxazoline derivative was targeted, with similar compounds being already described in the literature.[23, 184] The corresponding reaction scheme of 2-(3-azidopropyl)-4,5-dihydro-1,3-oxazole (AzOxa) is depicted in **Scheme 19**.
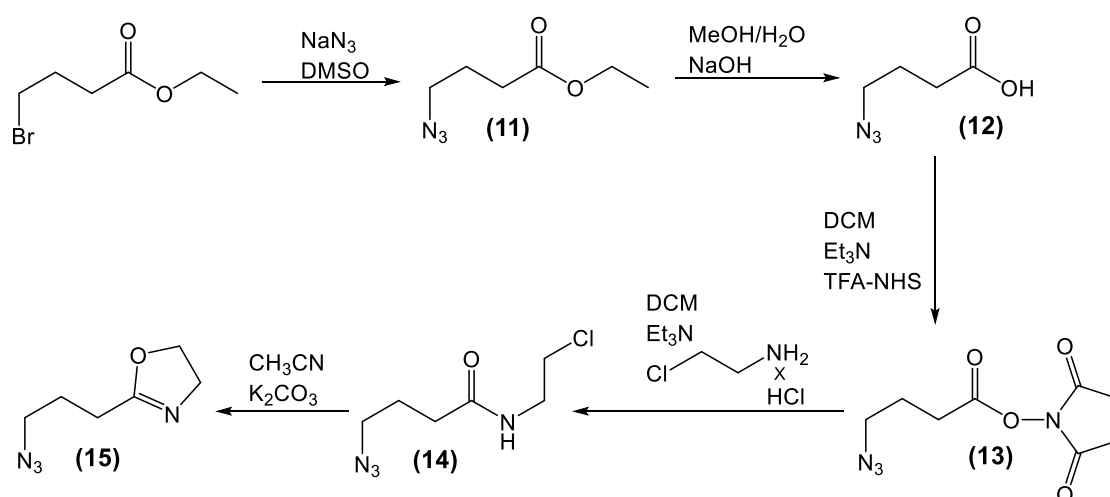
Scheme 19: Synthesis strategy for 2-(3-azidopropyl)-2-oxazoline.

4. Results and Discussion

In this strategy, ethyl 4-bromobuytrate was allowed to react with NaN$_3$ to ethyl 4-azidobutyrate (**11**), followed by alkaline hydrolysis of the corresponding ester to 4-azidobutanoic acid (**12**). 4-azido-*N*-(2-chloroethyl)butanamide (**14**) was obtained by activation of the carboxylic acid functionality with TFA-NHS (**13**) and subsequent reaction with 2-chloroethylamine hydrochloride. Compound (**14**) was then dissolved in MeCN and heated in the presents of anhydrous K$_2$CO$_3$, forming the final product 2-(3-azidopropyl)-2-oxazoline (**15**) with an overall yield of approximately 44 %. The product was characterized by ^{1}H NMR (below) and ^{13}C NMR (**Figure 84**) spectroscopy.
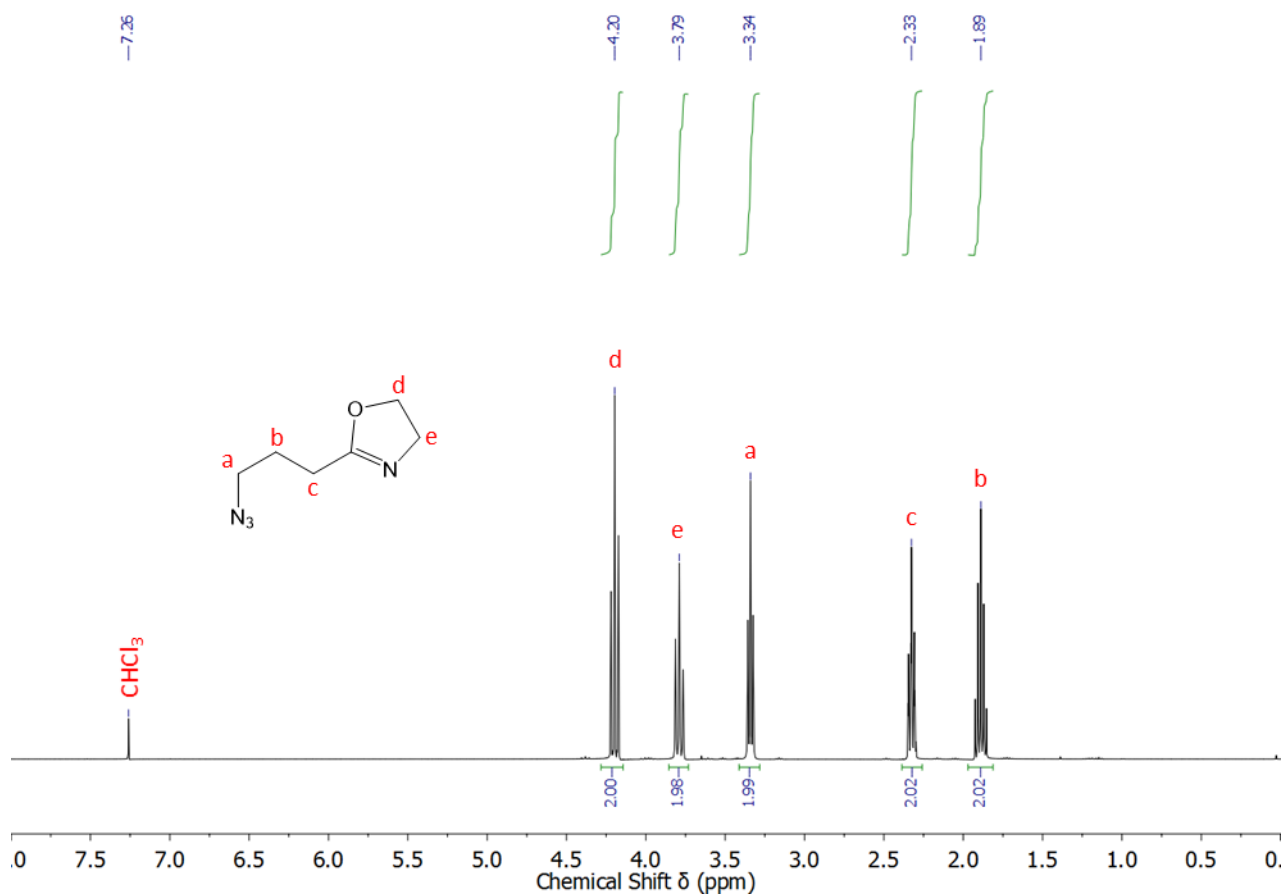
Figure 35: ^{1}H-NMR spectrum of 2-(3-azidopropyl)-2-oxazoline recorded in CDCl$_3$.

4. Results and Discussion

The ^{1}H NMR spectrum depicted in **Figure 35** shows signals at 1.89, 2.33 and 3.34 ppm, which can be assigned to the propylene spacer located between the azide group and the 2-oxazoline ring. The bands for the methylene groups of the 2-oxazoline ring are located at 3.79 and 4.20 ppm. Full agreement of the predicted and experimentally observed chemical shifts of the proton signals, as well as their integrals corroborate the chemical structure and purity of the target compound.

The copolymerization behavior of AzOxa was investigated in monomer feed mixtures with EtOxa and isoPrOxa, respectively, using microwave-assisted CROP. The respective monomers were dissolved in MeCN and the polymerization performed for 90 min at 120°C, using MeOTf as initiator (**Scheme 20**). All polymerization reactions were quenched with morpholine and the resulting copolymers were analyzed by SEC with respect to their average molar mass, and by ^{1}H NMR and IR spectroscopy with respect to their composition.
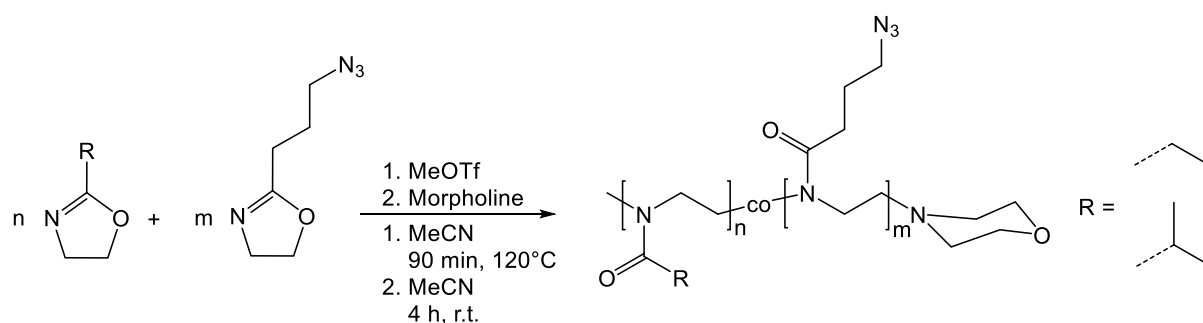
Scheme 20: Copolymerization of AzOxa with various 2-alkyl-2-oxazolines.

4. Results and Discussion

Table 12: Summarized analytical data of poly(isoPrOxa-*co*-AzOxa) and poly(EtOxa-*co*-AzOxa).

ExpNr.	Monomer feed	Polymer composition[a)	$\bar{M}_{w,\,SEC}$[b)] $[\times 10^3 \text{ g mol}^{-1}]$	Dispersity Đ[c)]	Yield / %
PEC097a1	isoPrOxa$_{99}$/AzOxa$_1$	poly(isoPrOxa$_{98}$-AzOxa$_2$)	19.8	1.24	63
PEC097a2	isoPrOxa$_{97}$/AzOxa$_3$	poly(isoPrOxa$_{97}$-AzOxa$_3$)	22.6	1.34	69
PEC097a3	isoPrOxa$_{95}$/AzOxa$_5$	poly(isoPrOxa$_{94}$-AzOxa$_6$)	19.4	1.28	71
PEC097a4	isoPrOxa$_{90}$/AzOxa$_{10}$	poly(isoPrOxa$_{88}$-AzOxa$_{10}$)	20.4	1.30	68
PEC097a5	isoPrOxa$_{70}$/AzOxa$_{30}$	poly(isoPrOxa$_{63}$-AzOxa$_{31}$)	24.3	1.54	75
PEC097a6	isoPrOxa$_{29}$/AzOxa$_{71}$	poly(isoPrOxa$_{29}$-AzOxa$_{72}$)	33.8	1.59	72
PEC097b1	EtOxa$_{99}$/AzOxa$_1$	poly(EtOxa$_{99}$-AzOxa$_1$)	20.8	1.40	92
PEC097b2	EtOxa$_{97}$/AzOxa$_3$	poly(EtOxa$_{98}$-AzOxa$_2$)	29.5	1.69	80
PEC097b3	EtOxa$_{95}$/AzOxa$_5$	poly(EtOxa$_{95}$-AzOxa$_4$)	32.9	1.77	82
PEC097b4	EtOxa$_{89}$/AzOxa$_{11}$	poly(EtOxa$_{90}$-AzOxa$_9$)	37.2	1.84	87
PEC097b5	EtOxa$_{68}$/AzOxa$_{32}$	poly(EtOxa$_{67}$-AzOxa$_{29}$)	44.7	1.80	84
PEC097b6	EtOxa$_{28}$/AzOxa$_{67}$	poly(EtOxa$_{31}$-AzOxa$_{69}$)	50.3	1.82	80
PEC095a1	AzOxa$_{100}$	poly(AzOxa$_{100}$)[e)]	10.5	1.21	71
PEC095a2	AzOxa$_{100}$	poly(AzOxa$_{100}$)[e)]	11.1	1.08	66

Monomer/initiator (M/I) ratio: 150/1. [a)]As calculated from ^{1}H NMR spectra. [b)]As determined by SEC analysis in DMAc/LiBr (1 g L^{-1}). [c)]Đ $= \bar{M}_w/\bar{M}_n$ calculated from SEC analysis. [d)] As determined by turbidity measurements of a 0.3 wt% aq. polymer solution with a heating/cooling rate of 1 K min^{-1}.[e)]Monomer/initiator (M/I) ratio: 50/1.

The data of the corresponding copolymers, summarized in **Table 12**, show an increasing value for the apparent average molar mass from SEC analysis and dispersity for an increasing AzOxa content.
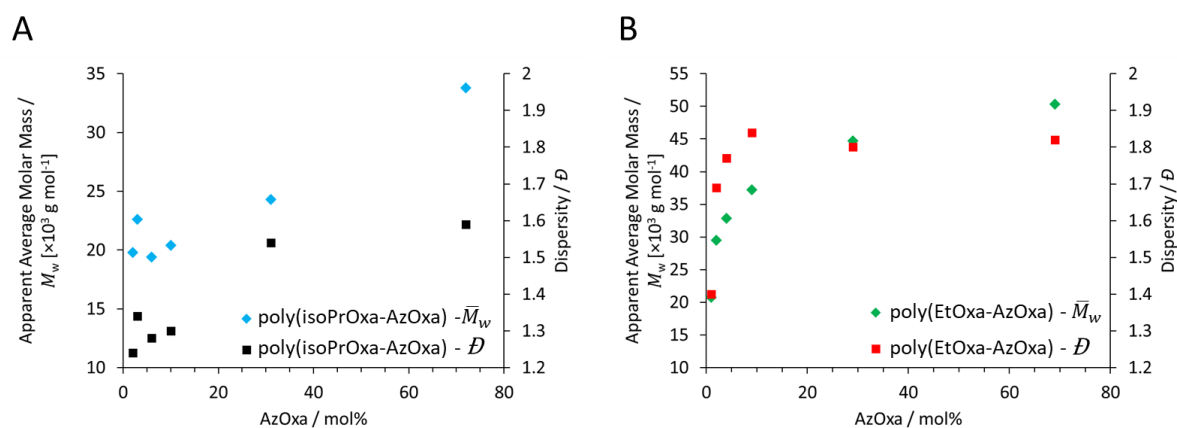
Figure 36: Average molar mass- and dispersity-dependency on AzOxa content for (**A**) poly(2-isoPrOxa-*co*-2-AzOxa) and (**B**) poly(2-EtOxa-*co*-2-AzOxa).

This trend (**Figure 36**) was observed for both copolymer systems and is significantly more pronounced for poly(EtOxa-co-AzOxa), where the average molar mass increased by a factor of 2.5 from 20.8 x 10^3 g mol^{-1} for poly(EtOxa$_{99}$-AzOxa$_1$) to 50.3 x 10^3 g mol^{-1} for poly(EtOxa$_{33}$-AzOxa$_{67}$). This apparent mass increase for otherwise identical polymerization conditions may result from a change in polarity and thereby a different expansion of the polymer coils or their aggregation to micellar structures in the respective mobile phase (DMAc/LiBr (1 g L^{-1})) of the SEC. Thus, the hydrodynamic radius may vary for the polymers with similar degree of polymerization.
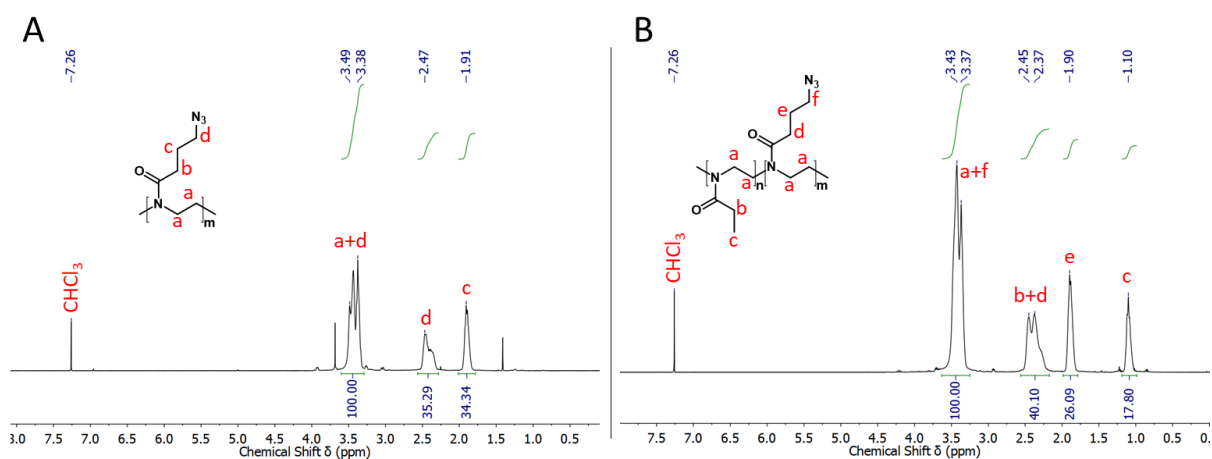
Figure 37: Comparison of ^{1}H NMR spectra between poly(AzOxa$_{100}$) (**A**) and poly(EtOxa$_{69}$-AzOxa$_{31}$) (**B**) recorded in CDCl$_3$.

Composition analysis is performed by ^{1}H NMR spectroscopy, and **Figure 37** shows the comparison between poly(AzOxa$_{100}$) homo- (**A**) and poly(EtOxa-AzOxa) copolymer (**B**). For the homopolymer, overlap of the signals of the polymer backbone and the methylene group adjacent to the azide functionality is observed (3.38-3.49 ppm). Signals at 1.91 (c) and 2.47 (b) ppm belong to the two remaining methylene groups of the azide side chain. Copolymer analysis was performed by comparing the integral of the methylene group at 1.91 ppm next to the azide functionality with the integral of the methyl group of either the 2-ethyl-, or 2-isopropyl-2-oxazoline side chain, both located at 1.10 ppm (e) (see also appendix **Figure 96** and **Figure 97**). The exact composition was then determined by multiplying the integral of the EtOxa methyl group (Signal c at 1.10 ppm, **Figure 37B**) by 3/2 and the obtained value set in relation to the combined value of the integrals of signal e (1.90 ppm, **Figure 37B**) and c (1.10 ppm, **Figure 37B**).

The second, independent method for compositional analysis is based on IR spectroscopy, where the integral of the C=O vibration (in each monomer) at 1660 cm^{-1} is compared with the integral of the N$_3$ vibration (only for AzOxa) at 2100 cm^{-1} (**Figure 38**).
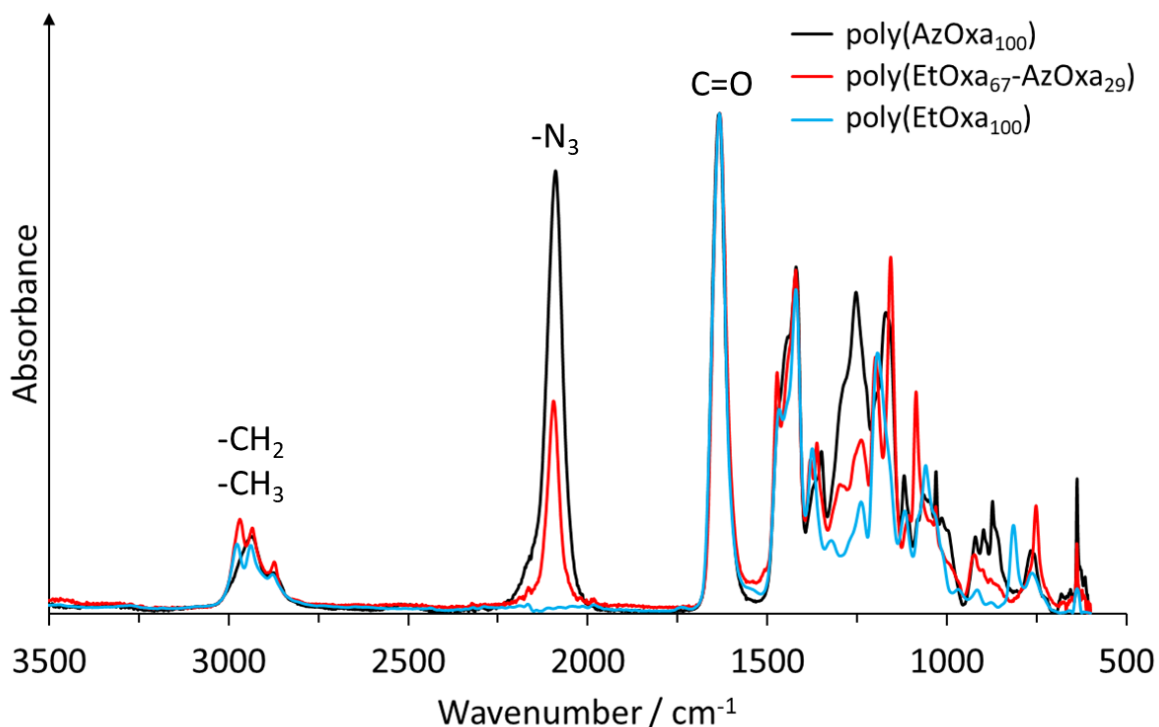
Figure 38: Comparison of IR spectra for poly(AzOxa$_{100}$) (**black**), poly(EtOxa$_{67}$-AzOxa$_{29}$) (**red**) and poly(EtOxa$_{100}$) (**blue**).

Firstly, the ratio between the integral of the C=O and N$_3$ vibration was determined for the poly(AzOxa) homopolymer, which provides a reference value of one N$_3$ group for each repeat unit. Then, the copolymer composition is evaluated by comparison of the N$_3$/C=O ratio for the homopolymer with that of the copolymer. The IR analysis results for the monomer feed (f_{AzOxa}) vs. build-in ratio (F_{AzOxa}) are depicted in **Figure 39** for both polymer systems, poly(EtOxa-co-AzOxa) and poly(isoPrOxa-co-AzOxa).

A

B
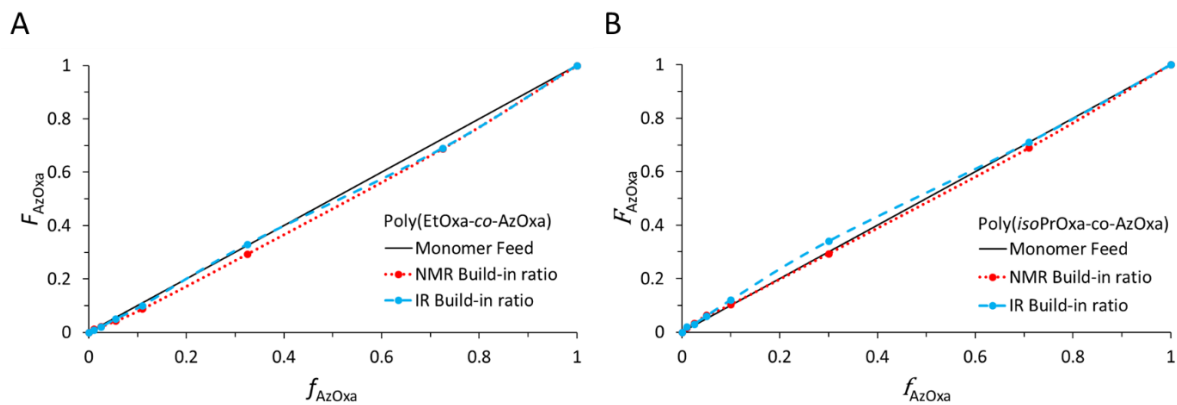
Figure 39: Monomer feed (f_{AzOxa}) vs. build-in ratio (F_{AzOxa}) for poly(EtOxa-co-AzOxa) (**A**) and poly(isoPrOxa-co-AzOxa) (**B**) as determined by ^{1}H NMR spectroscopy in CDCl$_3$ (**red**) and by IR spectroscopy (**blue**).

Both diagrams show an excellent agreement between monomer feed and build-in ratio for both investigated copolymer systems, which supports the assumption, that in both cases random copolymer were obtained. Calculation of the copolymerization parameters was not performed, as the polymerization reactions were always taken to high monomer conversion.

Finally, the dependence of the cloud point of 0.3 wt% aqueous polymer solutions on the AzOxa content was determined by UV/VIS spectroscopy. In these experiments, the temperature-dependent transmittance was recorded for one heating and cooling cycle.
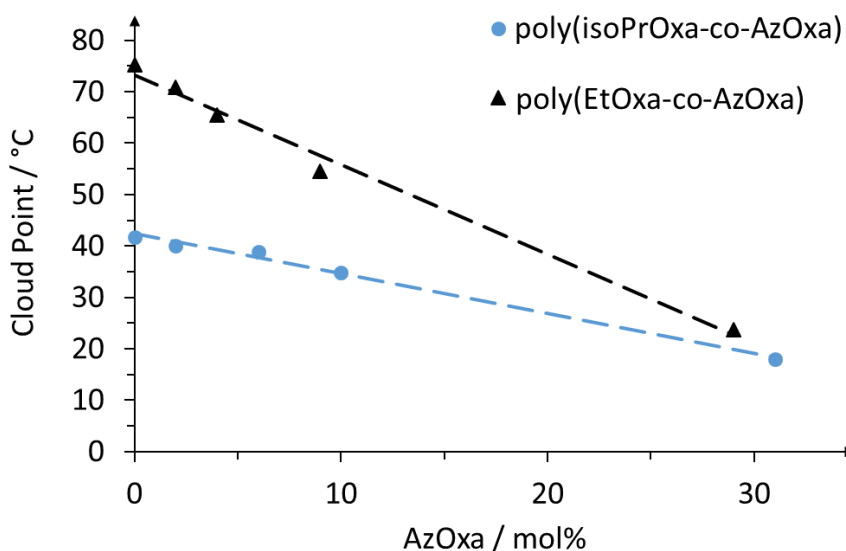
Figure 40: Cloud point dependence on AzOxa content for poly(isoPrOxa-*co*-AzOxa) and poly(EtOxa-*co*-AzOxa), as determined by UV/VIS turbidity measurements of a 0.3 wt% aqueous polymer solution at a wavelength of 550 nm and a heating rate of 1 K min^{-1}.

4. Results and Discussion

Data depicted in **Figure 40** show a linear decrease of the cloud point temperature for an increasing AzOxa content, which is contrary to the expected trend for increased polarity of polymers with higher amounts of the polar azide group, but apparently a higher tendency for chain aggregation is introduced with the N_3 groups. This aggregation of chains may be favored by the dipole-dipole interaction between the azide group, which is polar but may not favor hydrogen bonding with water molecules. Such polar interactions are discussed in the context of increased glass transition temperatures when going from polypropylene to poly(vinyl chloride) and ultimately to polyacrylonitrile.

4.3.2 Synthesis of Various Alkyne-Modified Reagents for the Click-Modification of Poly(2-oxazoline)s with Improved Antifouling Capabilities

In order to improve the antifouling properties of photocrosslinkable poly(2-oxazoline) hydrogels by click-modification with antifouling structure motives, several different alkyne derivatives were prepared. This strategy takes advantage of compounds that are already known for their low fouling properties, namely sulfobetaines, carboxybetaines, oligoethylene glycols and an oligoethylene glycol-sulfobetaine conjugate. At first, alkyne derivatives of the corresponding carboxy- and sulfobetaine were prepared by ring opening reaction of propiolactone or propan-1,3-sulton, respectively with dimethylamino-2-propin (**Scheme 21**). Both reactions were already described in literature[183] and will not be discussed in further detail. Successful isolation of both compounds was confirmed by ^{1}H and ^{13}C NMR (see **Appendix Figure 85**, **Figure 86** and **Figure 87**, **Figure 88**).
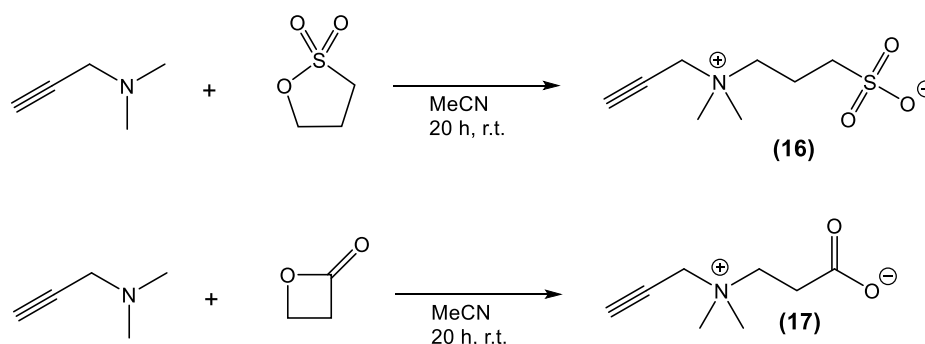
Scheme 21: Synthesis schemes of alkyne-modified sulfo- and carboxybetaine derivatives by ring opening reaction. Both derivatives were synthesized by Bastian Schauerte (Research lab course, Macromolecular Chemistry, University of Siegen).

4. Results and Discussion

Based on these results, an oligoethylene glycol-alkyne and a novel sulfobetaine-oligoethylene glycol-alkyne conjugate were prepared, starting from propargyl bromide. The synthesis route for both alkyne derivatives is depicted in **Scheme 22**.
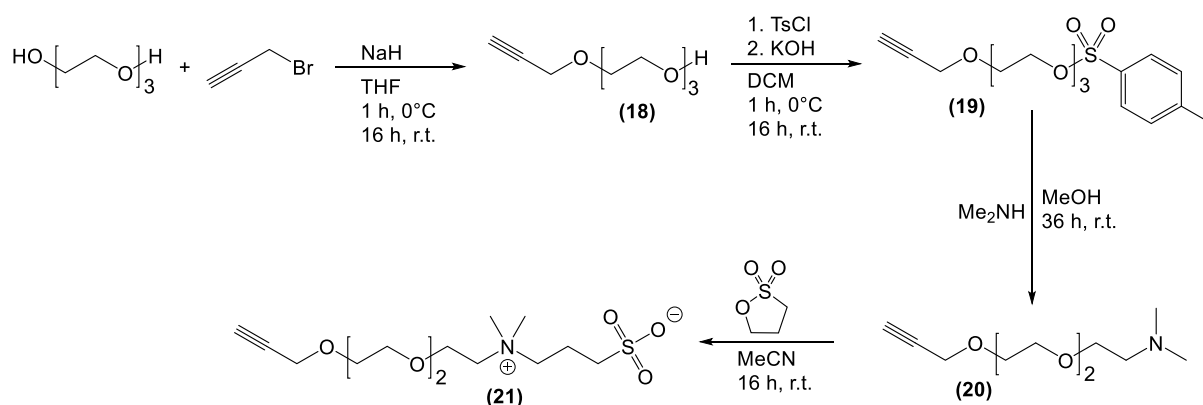
Scheme 22: Synthesis route for an oligoethylene glycol-alkyne and a sulfobetaine-oligoethylene glycol-alkyne derivative. All derivatives were synthesized by Niklas Jung (Research lab course, Macromolecular Chemistry, University of Siegen).

In this synthesis strategy, triethylene glycol is deprotonated with NaH and then coupled to propargyl bromide, yielding 2-{2-[2-(prop-2-yn-1-yloxy)ethoxy]ethoxy}ethan-1-ol (**18**). Next, the hydroxy functionality is transformed into a better leaving group by reaction with tosyl chloride. The subsequent reaction with dimethylamine in methanol leads to compound (**20**), which is subjected to the ring opening reaction with propan-1,3-sulton, resulting in the final product 3-{dimethyl{2-[2-(prop-2-yn-1-yloxy)ethoxy]ethyl}ammonio}propane-1-sulfonate (**21**) (EO-SB). With an overall yield of 41 % of the theory, this four-step synthesis route was still in an acceptable limit, whereby the first reaction step suffered the major loss with only 45 % yield. This is mainly due to the lack of specificity between the two hydroxyl ends of triethylene glycol, resulting in additional disubstitution in the first reaction step. This bis(alkyne) derivative could be removed by column chromatography. Overall, the final product was obtained in good purity, which was confirmed by [1]H (**Figure 41**) and ^{13}C NMR (see Appendix **Figure 94**)
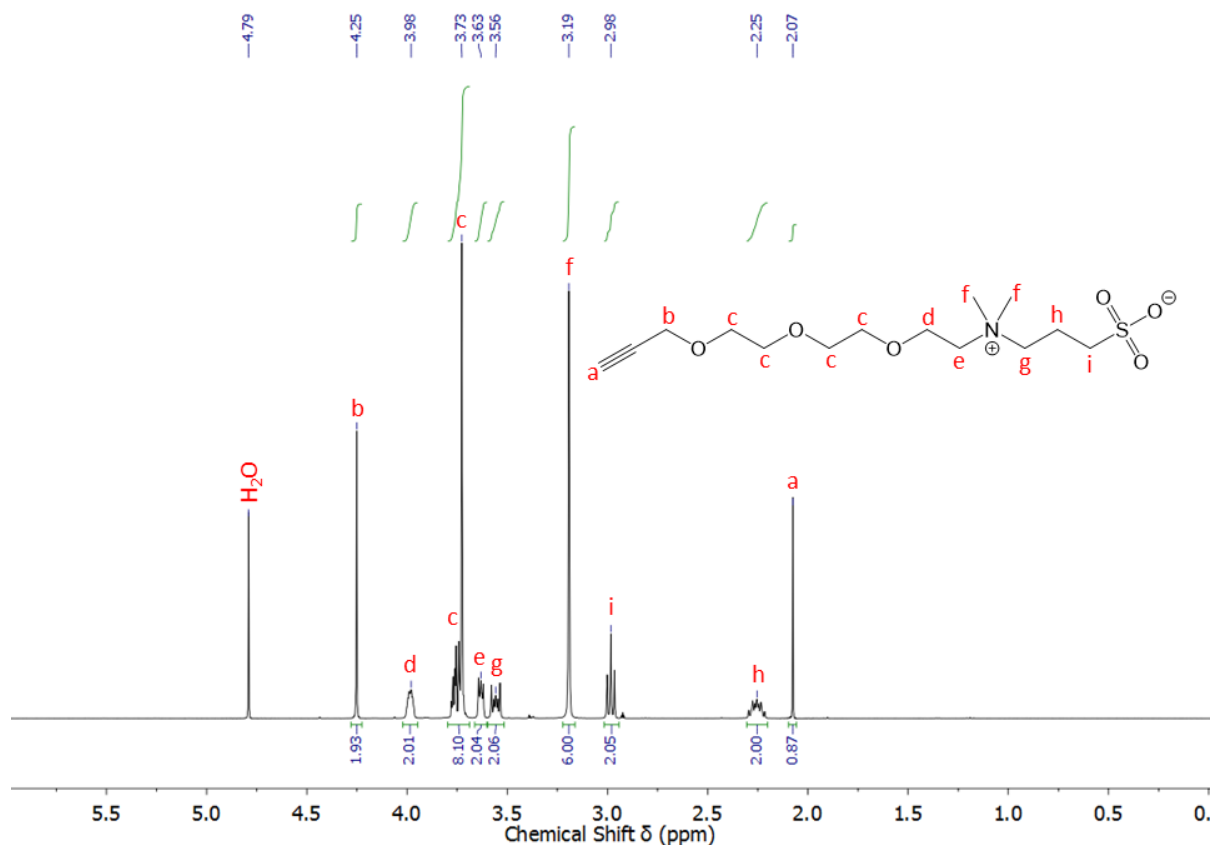
Figure 41: ¹H NMR spectrum of 3-{dimethyl{2-[2-(prop-2-yn-1-yloxy)ethoxy]ethyl}ammonio}propane-1-sulfonate recorded in D₂O.

In the ¹H NMR spectrum, the signal at 2.07 ppm (a) can be assigned to the single proton of the triple bond. The signals for the propylene spacer of the betaine structure appear at 2.25 (h), 2.98 (i) and 3.56 ppm (g). The bands for the methyl groups attached to the nitrogen are located at 3.19 ppm (f) and the ethoxy repeat units show a chemical shift of 3.73 ppm (c). Signals at 3.63 (e) and 3.98 ppm (d) can be assigned to the ethylene group located between the betaine functionality and the ethoxy repeat units. The remaining signal at 4.25 ppm (b) belongs to the methylene group adjacent to the triple bond. All integrals, except the one of the single proton of the triple bond, are in very good agreement with the expected values. The deviation of the integral (a) from its expected value is due to the fact that the weakly acidic proton of the respective triple bond can undergo an interchange with the deuterons of the solvent D₂O, which show no signal in the ¹H NMR spectrum.

4. Results and Discussion

Preparation of a corresponding carboxybetaine-oligoethylene glycol-alkyne conjugate was also attempted in various variations of the synthesis strategy, but surprisingly the desired product could not be obtained. **Figure 42** depicts the unsuccessful synthesis attempts.
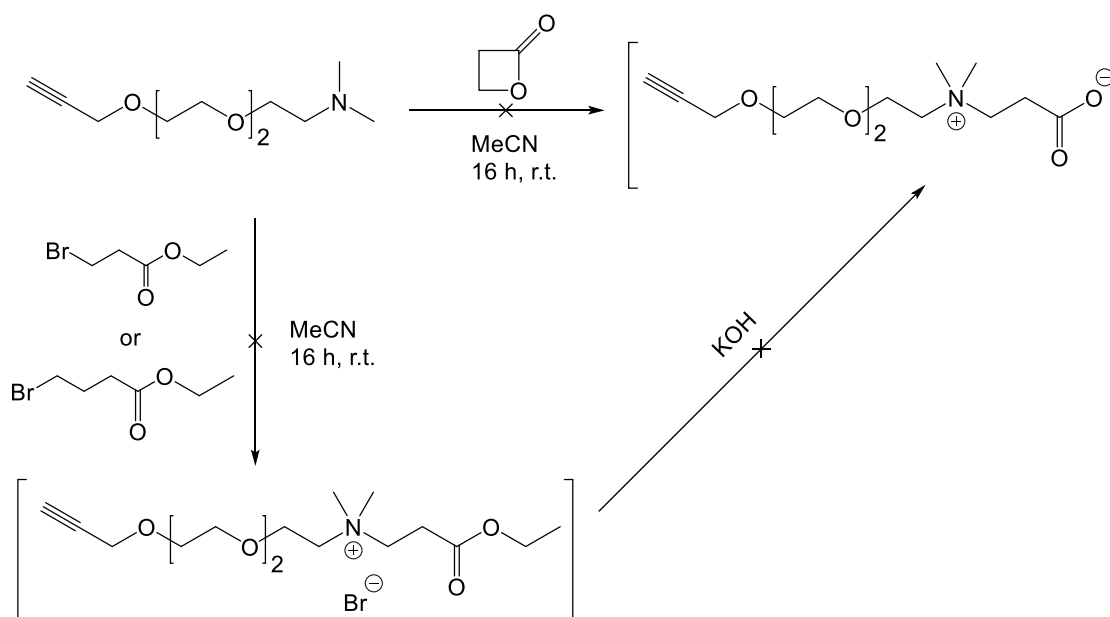
Figure 42: Unsuccessful attempts for the synthesis of a carboxybetaine-oligoethylene glycol-alkyne conjugate in analogy to the sulfobetaine derivative above.

^{1}H NMR analysis of the isolated reaction products showed the signal of the ethylene glycol chain being still present, but the characteristic bands of the alkyne proton and of the methyl groups attached to the nitrogen were absent. However, a reasonable explanation cannot be given at that point and this synthesis route was thus not further pursued.

4. Results and Discussion

With the azide-modified 2-oxazoline AzOxa, two photocrosslinkable poly(2-isopropyl-2-oxazoline)s were synthesized by MWAP, which contained approximately 3 mol% benzophenone and 5 and 10 mol% azide groups (**Figure 43**). The rationale for selecting poly(2-isopropyl-2-oxazoline)s as basis was motivated by the fact, that previously performed temperature-dependent swelling experiments showed a well-defined, sharp transition at 32°C for poly(isoPrOxa-BPOxa).
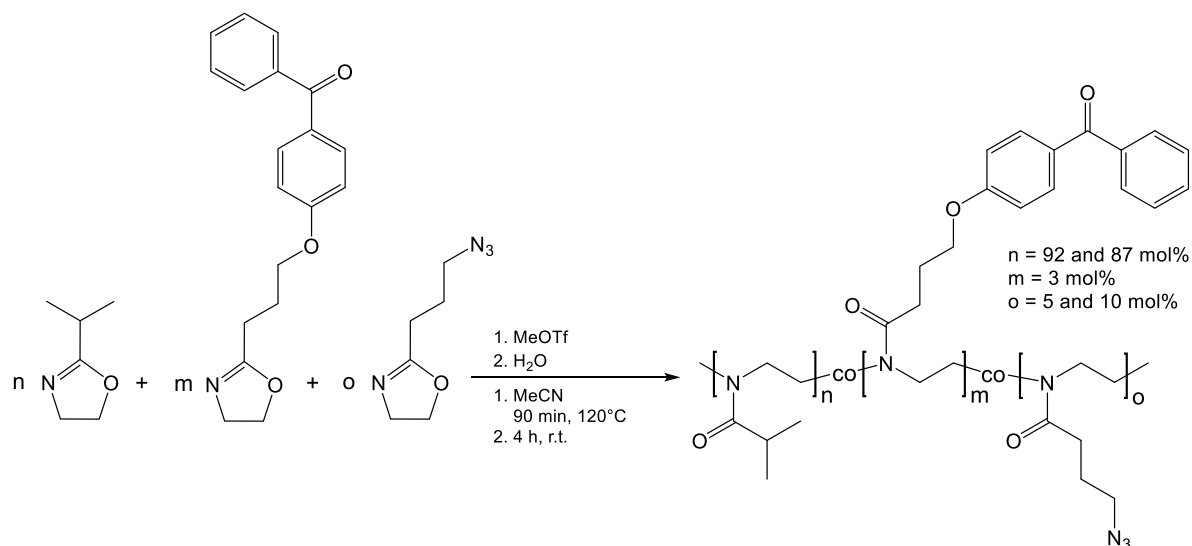
Figure 43: Copolymerization route for a multifunctional poly(2-isopropyl-2-oxazoline) system, which is thermoresponsive, can be photocrosslinked, and modified by click reaction.

With the alkyne products described above, the synthesized azide-polymers were modified via Cu-catalyzed azide-alkyne click coupling (CuAAC). In addition, the commercially available 4-pentynoic acid was also conjugated to the azide polymer by this CuAAC reaction (**Figure 44**). The progress of the reaction was monitored by IR spectroscopy, where complete conversion of the azide functionality was indicated by disappearance of the azide absorption band of the starting material located at around 2100 cm^{-1}. For workup, the modified polymers were dialyzed against water to remove $CuSO_4$, Na ascorbate and any excess of the respective alkynes. All isolated polymers were characterized by ^1H NMR analysis with respect to their composition, and by SEC with respect to their average molar mass. The corresponding analysis data is summarized in **Table 13**.
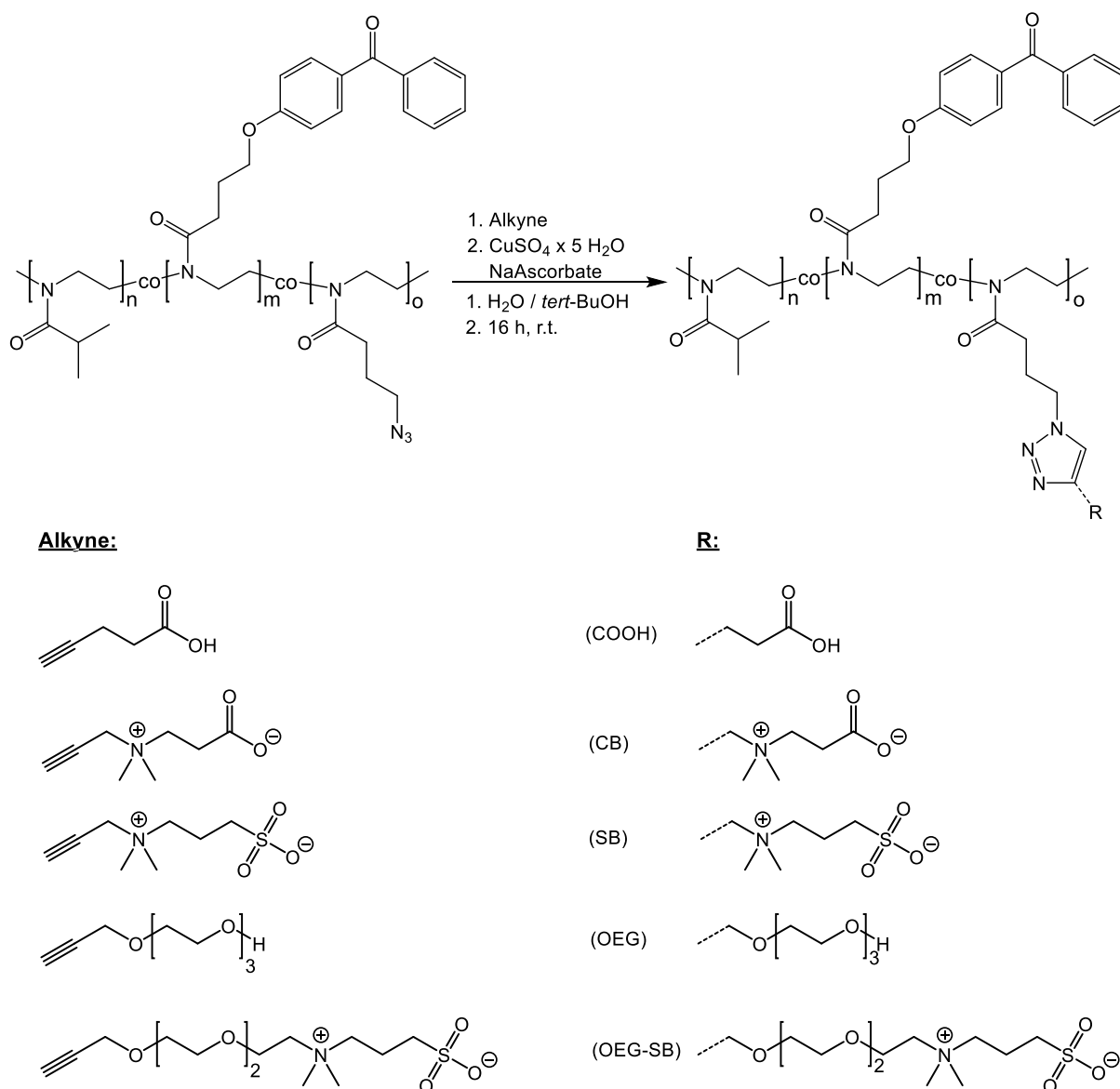
Figure 44: Modification of poly(isoPrOxa-BPOxa-AzOxa) with various non-fouling structure motives by Cu-catalyzed azide-alkyne click coupling.

Table 13: Summarized analytical data of non-modified and modified poly(isoPrOxa-BPOxa-AzOxa).

Exp.-Nr.	Polymer,composition[a]	$\bar{M}_{w, SEC}$[b] [×10³ g mol⁻¹]	Dispersity Đ[c]	Yield / %
PEC112a	poly(isoPrOxa$_{91}$-BPOxa$_3$-AzOxa$_6$)[d]	27.7	1.76	81
PEC112-COOH	poly(isoPrOxa$_{91}$-BPOxa$_3$-COOH$_6$)	27.1	2.17	57
PEC112-SB	poly(isoPrOxa$_{91}$-BPOxa$_3$-SB$_6$)	31.2	2.02	43
PEC112-CB	poly(isoPrOxa$_{91}$-BPOxa$_3$-CB$_6$)	35.8	3.14	41
PEC112-OEG	poly(isoPrOxa$_{91}$-BPOxa$_3$-OEG$_6$)	28.5	2.27	48
PEC112-OEG-SB	poly(isoPrOxa$_{91}$-BPOxa$_3$-OEG-SB$_6$)	30.9	2.03	56
PEC115a	poly(isoPrOxa$_{87}$-BPOxa$_3$-AzOxa$_{10}$)[d]	28.3	1.80	73
PEC115-SB	poly(isoPrOxa$_{87}$-BPOxa$_3$-SB$_{10}$)	21.4	1.82	44
PEC115-CB	poly(isoPrOxa$_{87}$-BPOxa$_3$-CB$_{10}$)	9.5	2.46	39
PEC115-OEG	poly(isoPrOxa$_{87}$-BPOxa$_3$-OEG$_{10}$)	23.4	2.12	52
PEC115-OEG-SB	poly(isoPrOxa$_{87}$-BPOxa$_3$-OEG-SB$_{10}$)	21.5	2.09	51

[a]As calculated from ¹H NMR analysis. [b]As determined by SEC analysis. [c]Đ $= \bar{M}_w/\bar{M}_n$ calculated from SEC analysis. [d]Monomer/initiator (M/I) ratio: 300/1.

The composition of the modified and unmodified terpolymers was determined by ¹H NMR spectroscopy, with particular emphasis on evaluation of the azide conversion in the CuAAC reaction.

The composition of the non-modified terpolymers, here poly(isoPrOxa$_{87}$-BPOxa$_3$-AzOxa$_{10}$) (**Figure 45)**, was determined by comparing the integrals of the methyl groups of the isopropyl chain at 1.09 ppm (c) with the integral of methylene group of the azide side chain at 2.13 ppm (e), and with the in integral of the benzophenone group located between 6.93-7.78 ppm. For this purpose, the integral of the isoPrOxa methyl groups for multiplied by 3/2. The single values of each component were the set in relation to the combined value of all three integrals. ¹H as well as ¹³C NMR spectra of non-modified and modified poly(isoPrOxa$_{87}$-BPOxa$_3$-AzOxa$_{10}$) are depicted in **Figure *45*** and **Figure *46***.
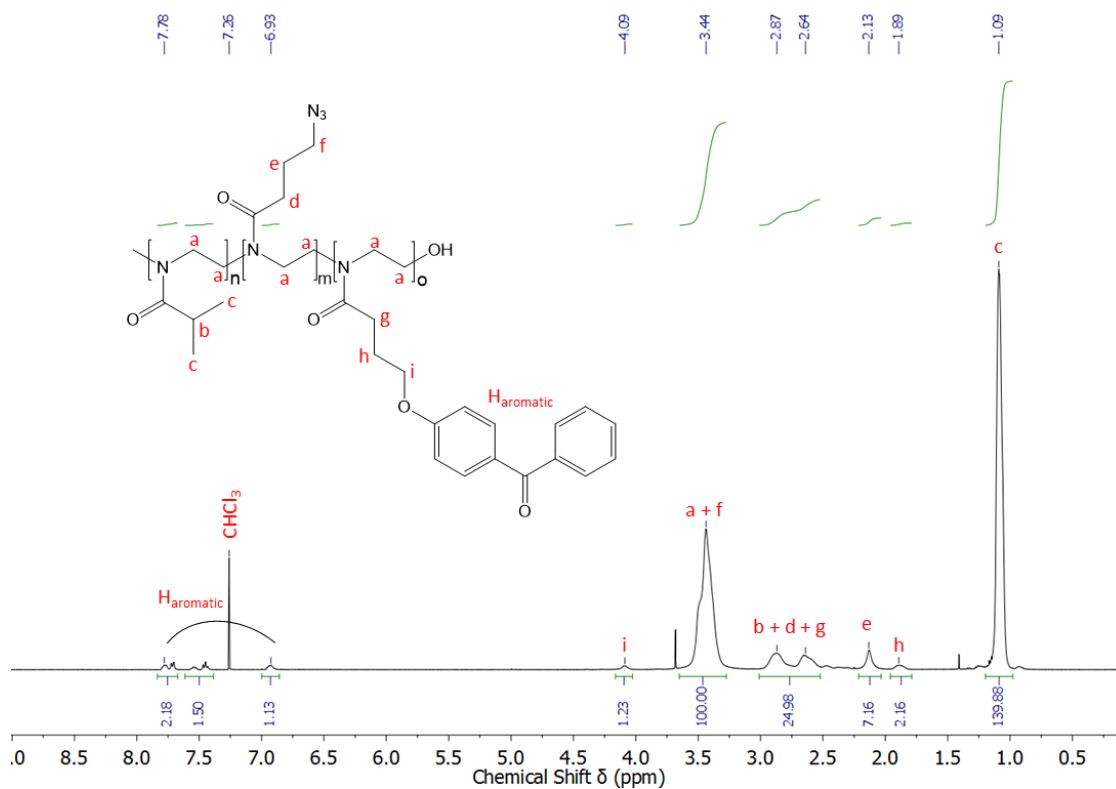
Figure 45: ^{1}H NMR spectra of non-modified poly(isoPrOxa$_{87}$-BPOxa$_3$-AzOxa$_{10}$).

Successful modification is clearly indicated by the signal at 3.17 ppm (**Figure 46**), which can be assigned to the methyl groups of the betaine functionality.
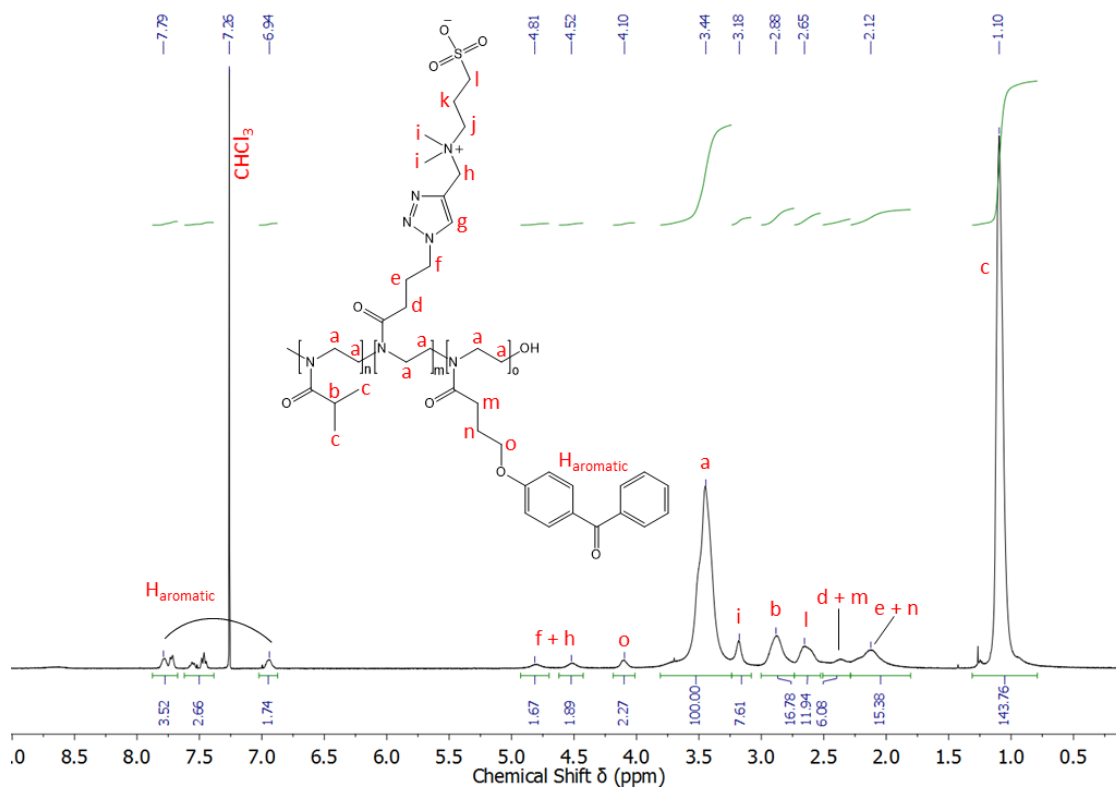

Figure 46: ^{1}H NMR spectra of modified poly(isoPrOxa$_{87}$-BPOxa$_3$-AzOxa$_{10}$).

4. Results and Discussion

^{1}H as well as ^{13}C NMR spectra of sulfobetaine, carboxybetaine, oligoethylene glycol and an oligoethylene glycol-sulfobetaine modified polymers are additionally depicted in **Chapter 7.3**.

The performed SEC measurements indicated interesting differences between the different polymers systems. First, for the 6 mol% azide-modified polymer system poly(isoPrOxa$_{91}$-BPOxa$_3$-AzOxa$_6$) an average molar mass of 27.7 x 10^3 g mol^{-1} was determined, which corresponds very well to the expected values of 30-35 x 10^3 g mol^{-1} for a monomer-initiator ratio of approximately 300/1. After the modification by CuAAC, all investigated polymers showed a trend to higher average molar masses and a considerable increase of their dispersity. In general, the average molar mass increased in the order of N$_3$ < COOH < OEG < OEG-SB < SB < CB. This can be explained by the overall increase in polarity and thus an expansion of the polymer coils, which follows the same order. In contrast to this observation, the modified polymers of the 10 mol% azide system poly(isoPrOxa$_{87}$-BPOxa$_3$-AzOxa$_{10}$) showed the opposite behavior. Here a significant decrease of the average molar mass was observed, from 28.3 x 10^3 g mol^{-1} for poly(isoPrOxa$_{87}$-BPOxa$_3$-AzOxa$_{10}$) to 9.5 x 10^3 g mol^{-1} poly(isoPrOxa$_{87}$-BPOxa$_3$-CB$_{10}$), following the order N$_3$ > OEG > OEG-SB > SB > CB. This reversed trend (**Figure 47**) may be caused by the increased number of charges on the backbone, which possibly leads to an aggregation of single polymer chains (coil to globule transition) and therefore a decrease in hydrodynamic radius and apparent average molar mass in SEC.
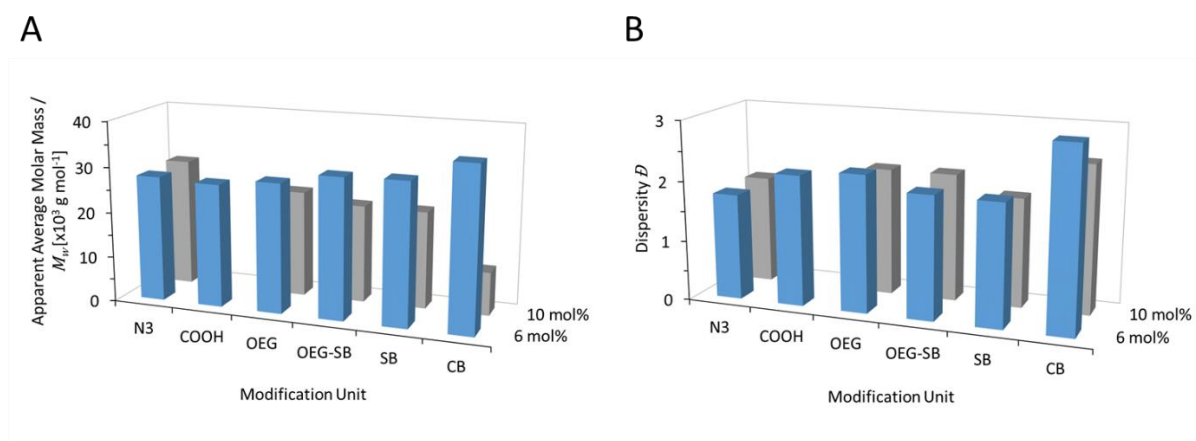
Figure 47: Average molar mass and dispersity dependence on modification unit.

It has to be noted that SEC experiments were performed in DMAc/1 wt% LiBr, which may not allow efficient solvation of the highly polar ethylene glycol, carboxylic acid, and zwitterionic

polymer segments, specifically at higher content in the polymer chain (10 mol% versus 6 mol%). In addition, the charges of the betaine groups may not be shielded efficiently at higher chain content by the presence of LiBr in the mobile phase, which may lead to a collapse of the polymer coil.

Cloud points of the prepared polymers in water were determined by UV/VIS spectroscopy, using 0.3 wt% polymer solution and a heating rate of 1 K min^{-1}, while recording the transmittance at a wavelength of 650 nm. Heating and cooling cycles were performed for each polymer, and the cloud point was defined as the temperature at which a transmittance dropped to 50 %.
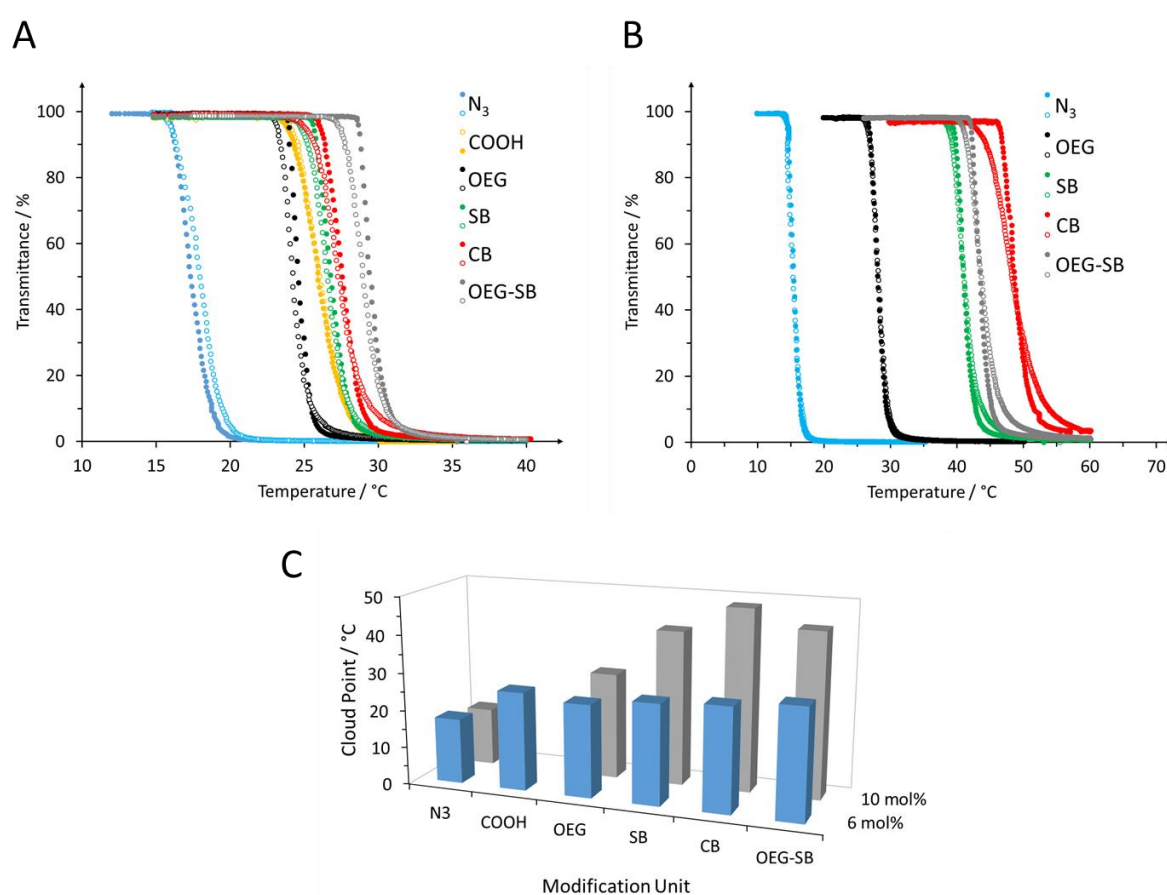
Figure 48: Cloud point dependence on type of functional group for poly(isoPrOxa-BPOxa-AzOxa) systems, as determined by UV/VIS turbidity measurements at a wavelength of 650 nm of a 0.3 wt% aqueous solution and a heating rate of 1 K min^{-1}. Transmittance curves of non-modified and modified poly(isoPrOxa$_{91}$-BPOxa$_3$-AzOxa$_6$) (**A**) and poly(isoPrOxa$_{87}$-BPOxa$_3$-AzOxa$_{10}$) (**B**). Cloud point comparison between non-modified and modified poly(isoPrOxa$_{91}$-BPOxa$_3$-AzOxa$_6$) and poly(isoPrOxa$_{87}$-BPOxa$_3$-AzOxa$_{10}$) (**C**).

4. Results and Discussion

Data depicted in **Figure 48A** and **B** were obtained for unmodified and modified polymers, carrying 6 and 10 mol% of the respective functional groups. It was found that all polymers could be reversibly switched from a hydrophilic to a hydrophobic state, with only a minor hysteresis of 0.5-1 K between the heating and cooling cycle. For all polymers, a significant increase of the cloud point temperature was observed after modification with the anti-fouling motif, with the most significant increase was found for the zwitterionic systems (SB and CB) or the ethylene glycol-betaine combination (OEG-SB). As expected, this trend is more pronounced for higher quantities (10 mol% versus 6 mol%) of the respective functional groups.

The reason for this observation is the fact that the highly polar side chains of the modified polymers are much stronger hydrated (specifically true for the ionizable COOH and even more so for the zwitterionic betaine moieties), which results in a higher contribution to the enthalpy of mixing ΔH_M compared to the non-modified side chains of the starting material.

4.3.3 Film Preparation and Investigation by SPR/OWS

Temperature dependent swelling of hydrogel thin films prepared from the above described non-modified azide and the CuAAC-modified polymers was investigated by OWS, using the same procedure as already described in **Chapter 4.2.3**. Therefore, the respective polymers were spin-coated from a 8-10 wt% ethanolic solution onto BPdiS-modified Au substrates, followed by drying at 50°C under reduced pressure and irradiation with UV light at a wavelength of 365 nm. The resulting dry polymer films exhibit a thickness around 550-850 nm, which is sufficient to support at least two waveguide modes. The polymer-coated substrates were then inserted into the SPR/OWS device and exposed to water for about 1 h, to ensure equilibrium swelling. After each temperature step, the hydrogel layers were again equilibrated for 15 min before the next angular scan was performed. Due to the high polarity of the zwitterionic side chains, polymers were irradiated with 12 J cm^{-2}, to ensure stable layer formation (and prevent hydrogel layer delamination).
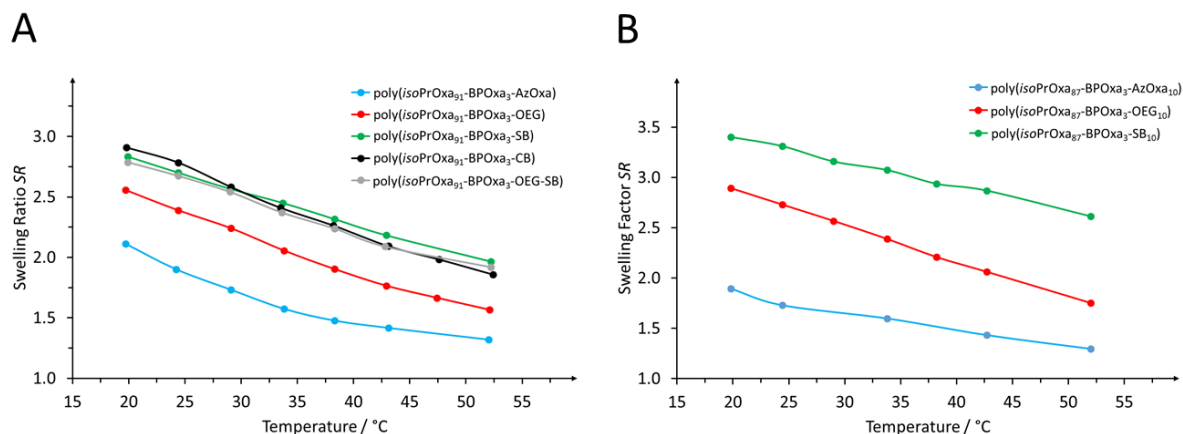
Figure 49: Temperature dependent swelling of hydrogel films made from non-modified and CuAAC-modified poly(isoPrOxa$_{91}$-BPOxa$_3$-AzOxa$_6$) (**A**) and poly(isoPrOxa$_{87}$-BPOxa$_3$-AzOxa$_{10}$) (**B**) as determined by OWS. Irradiation dose 12 J cm^{-2}.

Results depicted in **Figure 49A** and **B** show a significant increase of the initial swelling ratio for CuAAC-modified polymers, specifically for the zwitterionic polymer systems, for which the highest SR values were observed. OEG-modified polymers showed initial swelling ratios between the basic azide-material and the zwitterionic polymer systems. This SR increase is even stronger pronounced for polymers with a higher content of the respective modification unit (10 mol% versus 6 mol%). The same trend was observed for the hydrogel layers when

increasing the temperature over the whole technically accessible range of 20-52°C. At the highest temperature the residual water content was also found to be highest for the zwitterionic polymer systems, followed by the OEG-modified polymer, while the basic azide-material showed the lowest swelling ratio. Most noticeable, it was found that the previously observed sharp volume phase transition in the polymer system poly(isoPrOxa$_{98}$-BPOxa$_2$) (see also **Figure 30**) is no longer present. Instead, a continuous volume transition is observed over the whole temperature range, resulting in an almost linear decrease of the swelling ratio for increasing temperature. Repeated heating and cooling cycles showed full reversibility of the swelling behavior for all investigated polymer systems. The first observation regarding the higher swelling ratios of the polymers modified with the anti-fouling motives can be explained by their increased hydrophilicity, which results in higher rate of water adsorption of the respective polymer networks. The linear decrease of the temperature-dependent swelling for theses modified polymer is apparently a consequence from copolymerization of three different monomers and the additional modification with very polar substituents, which all contribute distinctively to the thermal response with varying kinetics.

Since such polymer systems are targeted for application as biosensor matrix, the influence of buffer, which inevitably will be used in the context of biological analytes and medical samples, on their thermal swelling response needs to be known. For this purpose, the influence of crosslinking density and salt concentration (PBS buffer solution) was investigated for the polymer system poly(isoPrOxa$_{87}$-BPOxa$_3$-SB$_{10}$). Thereby, the temperature-dependent swelling was measured for hydrogel layers photocrosslinked with varying irradiation dose of 5, 8, and 12 J cm^{-2} (**Figure 50A**), and the initial swelling ratio was recorded for PBS-buffer concentrations of 0, 1, 5 and 10 M (**Figure 50B**), respectively.
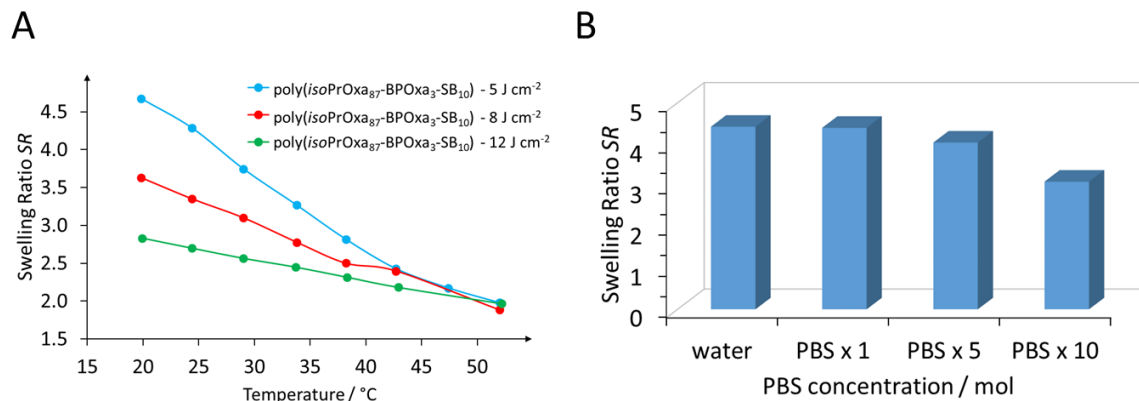
Figure 50: Swelling ratio dependence on irradiation dose (in water) (**A**) and varying PBS buffer concentration (for an irradiation dose of 5 J cm^{-2}) (**B**) for poly(isoPrOxa$_{87}$-BPOxa$_3$-SB$_{10}$) hydrogel films, as determined by OWS.

It was found that the swelling ratio was significantly influenced by the irradiation dose, which increased from SR = 2.8 for 12 J cm^{-2} up to SR = 4.7 for 5 J cm^{-2}, which follows the expected trend for increasing crosslinking density. Similar results were already described for the polymer system poly(EtOxa$_{97}$-BPOxa$_3$) above (see Chapter 4.2.3). For all three irradiation doses, a linear decrease of the swelling ratio with increasing temperature was observed, as already described for the 12 J cm^{-2} sample in **Figure 49B** above. At the highest temperature of 52°C all three systems reach almost equal swelling ratios of 1.9-2.0, which can be assigned to the fully collapsed state of these hydrogel systems. These measurements indicate the strong influence of the elastic retraction force of the hydrogel network, which is much more pronounced for highly crosslinked networks. The swelling ratio measurements performed for different PBS-buffer concentrations showed a decreasing swelling ratio for an increasing salt concentration. Here, charge screening of the betaine groups by the ions from the PBS buffer reduces repulsive forces between identical charges and leads to a compaction of the hydrogel layer.

4.3.4 Chapter Summary and Conclusion

In this chapter, the successful synthesis of azide-modified poly(2-alkyl-2-oxazoline)s and the fabrication of a multifunctional hydrogel layer system by photocrosslinking and post-modification by copper(I) catalyzed azide-alkyne cycloaddition reaction (CuAAC) was demonstrated. The temperature-dependent swelling properties were assessed for these CuAAC-modified hydrogels by SPR/OWS. As clickable monomer, the synthesis route to a novel azido-2-oxazoline was developed and its copolymerization behavior with 2-ethyl-2-oxazoline and 2-isopropyl-2-oxazoline was studied. It was found that the build-in ratio corresponds very well to the monomer feed, suggesting random copolymerization took place.

For these polymers in aqueous solution, the cloud point dependence with respect to the content of the azide post-modification unit in the polymer backbone was investigated by UV/VIS spectroscopy. Here a decrease of the cloud point for an increasing concentration of azide-containing repeat units was found for both studied copolymer systems (EtOxa and isoPrOxa), which is contrary to the expected trend but may result from an increased tendency to aggregate with higher azide content due to the attractive dipole interaction between the azide group. For the fabrication of thermoresponsive and photocrosslinkable poly(2-oxazoline)-based hydrogels with improved anti-fouling properties, the two different terpolymers poly(isoPrOxa$_{91}$-BPOxa$_3$-AzOxa$_6$) and poly(isoPrOxa$_{87}$-BPOxa$_3$-AzOxa$_{10}$) were synthesized. Both terpolymers were then modified by CuAAC with several different alkyne derivatives carrying functional groups like ethylene glycol, carboxylic acid, sulfo- and carboxybetaine and a novel oligo ethylene glycol-sulfobetaine conjugate. The investigation of the cloud point of the respective non-modified and CuAAC-modified polymers in aqueous solution was performed by UV/VIS spectroscopy. These measurements showed a significant increase of the cloud point temperature with the introduction of the very polar anti-fouling motives (N_3 < COOH < OEG < OEG-SB < SB < CB), and the strongest increase was observed for zwitterionic polymer systems. The cloud point of oligo ethylene glycol- and carboxylic acid-modified polymers was found in between the values for the basic azide-containing material and the zwitterionic polymer systems.

This general cloud point increase in the CuAAc-modified polymer systems can be explained by the fact that the substantially more polar side chains are more strongly hydrated, which results

in a higher contribution of the enthalpy of mixing ΔH_M compared to the non-modified side chains of the starting material.

For the photocrosslinked, surface-attached hydrogel layers, prepared from the non-modified and CuAAC-modified terpolymers, the temperature dependent swelling was investigated by SPR/OWS, following the same procedure already described before (**Chapter 4.2.3**). Here, a significant increase of the initial swelling ratio was found for the respective CuAAC-modified polymers, with the highest values observed for zwitterionic systems, namely sulfobetaine- and carboxybetaine-modified polymers as well as the oligo ethylene glycol-sulfobetaine conjugate. As expected, the swelling ratio of oligo ethylene glycol-modified polymers is located in between the swelling ratios of the zwitterionic systems and the respective basic azide-material. In addition, this change was more pronounced for polymers with a higher content of the azide-modification unit. As for the cloud point measurements above, these results can be explained by an increased hydrophilicity, resulting in a stronger hydration of the polymer network. In contrast to the hydrogel of the binary copolymer system poly(isoPrOxa$_{98}$-BPOxa$_2$), which showed a sigmoidal volume phase transition around 32°C, a very linear decrease of the swelling ratio with increasing temperature was found for non-modified and modified terpolymer hydrogels. Apparently, each of the monomeric species contributes individually to the volume phase transition and the combined effects lead to this linearized temperature dependence.

The dependence of the swelling ratio on the crosslinking density, which was exemplarily studied for poly(isoPrOxa$_{91}$-BPOxa$_3$-SB$_6$) networks, yielded similar results like already observed for the poly(EtOxa$_{98}$-BPOxa$_2$) system. Also here a decrease of the hydrogel swelling was observed for an increasing irradiation dose, which results from the higher crosslink density in the hydrogel layer. Swelling dependence on salt concentration was studied for the same poly(isoPrOxa$_{91}$-BPOxa$_3$-SB$_6$) system, showing a decreasing swelling ratio for an increasing PBS-buffer concentration. This trend results from charge screening of the repulsive interactions between the zwitterionic sulfobetaine groups in the polymer chain by the ions of the PBS buffer.

4.4 Published Application Examples of Photocrosslinkable Hydrogels
4.4.1 Photocrosslinkable Poly(*N*-isopropylacrylamide)-based Hydrogel Systems

In this chapter, various applications of the photocrosslinkable and thermoresponsive poly(*N*-isopropylacrylamide)-based coatings are highlighted by the joint publications that emerged from the collaboration with Jakub Dostalek and Wolfgang Knoll in the context of the Austrian Institute of Technology (AIT) partner group. Synthesis and characterization of the respective hydrogel materials and adhesion promoters were performed by Christian Petri in the group of Macromolecular Chemistry at the University of Siegen, while the different applications in optical sensing were carried out at the AIT.

The thermoresponsive properties of poly(*N*-isopropylacrylamide) (pNIPAAm) were described first by Heskins and Guillet in 1968 and since this time it has become the most intensely studied polymer, showing phase separation upon temperature increase in aqueous solution.[185-186] The reason why pNIPAAm has gained such a great interest is not least the fact that its LCST of 32°C is close to physiological conditions, which makes it suitable for biomedical applications, such as tissue engineering, drug delivery systems or as biosensor matrix material.[5, 186-187]

For the implementation of pNIPAAm-based hydrogels as a potential biosensor matrix, a benzophenone group and a carboxylic acid functionality were incorporated, where benzophenone serves as photocrosslinking unit and the carboxylic acid moiety allows post-modification with appropriate ligands (such as antibodies). The preparation of these materials is performed in analogy to published synthesis procedures, with the corresponding synthesis route depicted in **Scheme 23**.
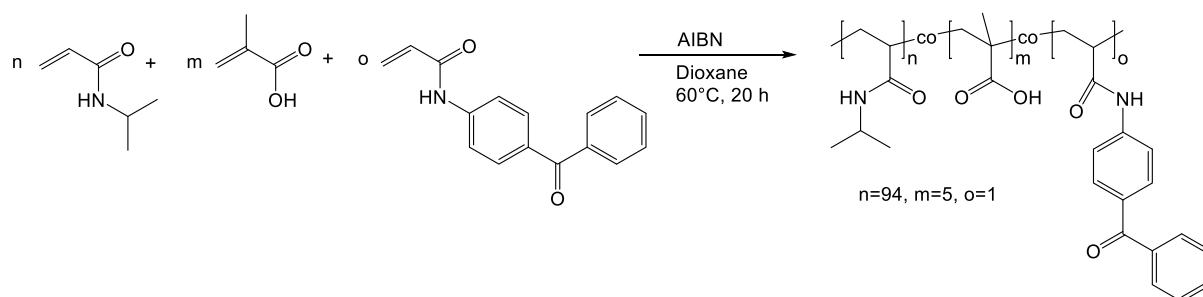
Scheme 23: Synthesis of the pNIPAAm-based terpolymer poly(*N*-isopropylacrylamide-*co*-methacrylic acid-*co*-benzophenone acrylamide).

4. Results and Discussion

For this purpose, *N*-isopropylacrylamide (NIPAAm), methacrylic acid (MAA) and benzophenone acrylamide (BPAAm) were copolymerized by free radical polymerization in 1,4-dioxane at 60°C for 20 h, using AIBN as initiator. After finishing of the reaction the resulting polymer was isolated by precipitation in diethyl ether, followed by freeze-drying from dioxane. The polymer was then analyzed by ^{1}H NMR spectroscopy, showing a very good correlation between polymer composition of poly(NIPPAm$_{94}$-MAA$_5$-BPAAm$_1$) and a monomer feed ratio NIPPAm/MAA/BPAAm of 94/5/1. In addition, the polymer was analyzed by SEC, resulting in an average molar mass $\overline{M}_w$ of 250 x 10^3 g mol^{-1} and a dispersity Đ of 2.55. In the following, the published application examples will be presented (as reference citation, abstract, and illustrating figure) using this terpolymer as a binding matrix for the detection of analyte molecules and exploiting its thermoresponsive properties.

4. Results and Discussion

Optical Waveguide-Enhanced Diffraction for Observation of Responsive Hydrogel Nanostructures

Federica Pirani, Nityanand Sharma, Alberto Moreno-Cencerrado, Stefan Fossati, Christian Petri, Emiliano Descrovi, José L. Toca-Herrera, Ulrich Jonas, Jakub Dostalek

Abstract-Optical diffraction measurements are reported for in situ observation of swelling and collapsing of responsive hydrogel nanostructures. The optical signal is enhanced by probing the surface carrying periodic arrays of hydrogel nanostructures by resonantly excited optical waveguide modes. UV-nanoimprint lithography is employed for the preparation of the arrays of nanopillars from photo-crosslinked *N*-isopropylacrylamide (pNIPAAm)-based hydrogel that are covalently tethered to a gold surface. The thermo-responsive properties of such pNIPAAm nanopillars that swell in 3D are compared to those of a thin film prepared from the identical material and that is allowed to swell predominantly in 1D. The nanopillars with a diameter of ≈100 nm and aspect ratio of 2 swell by a factor of ≈6 as determined by optical measurements supported by simulations that are compared to morphological characteristics obtained from atomic force microscopy. Bending of nanopillars above the lower critical solution temperature (LCST), erasure of the topographic structure by drying at temperature below the LCST, and recovery by subsequent swelling below the LCST and drying at temperature above the LCST are observed.
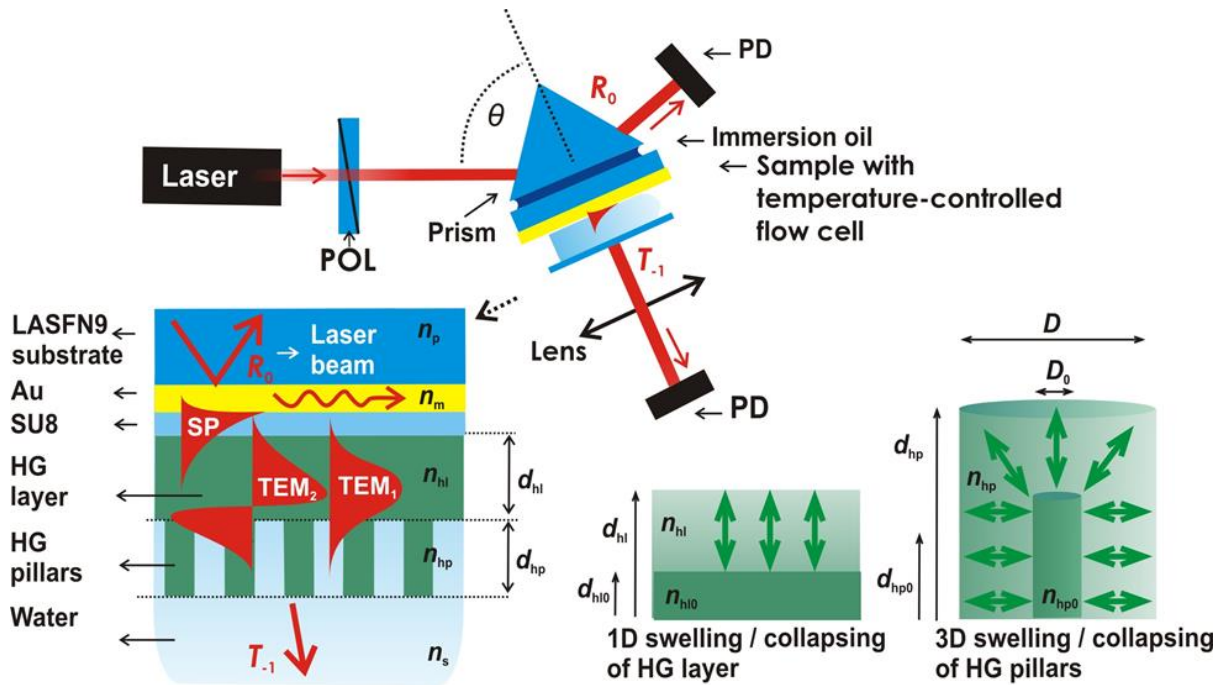
Figure 51: Optical system that was employed for the probing of swelling and collapsing of pNIPAAm-based hydrogel (HG) nanopillar arrays by optical waveguide spectroscopy and optical waveguide-enhanced diffraction. The system utilized a polarizer (POL) and a photodiode (PD), and the sensor surface was probed by surface plasmon (SP) and optical waveguide (TEM) modes travelling along the surface.
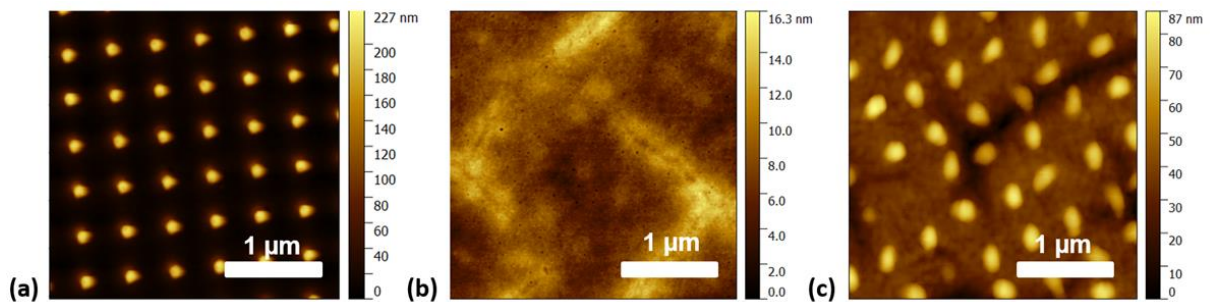
Figure 52: Ex situ AFM observation of a) freshly prepared pNIPAAm nanopillar arrays (before any swelling process) in air compared to the structure that was swollen in water and dried at temperature b) of T = 22°C below the LCST (of around 32°C) and c) of T = 38°C above the LCST. The scale bar is the same for the three microscopy images.

4. Results and Discussion

Tunable Plasmonic Nanohole Arrays Actuated by a Thermoresponsive Hydrogel Cushion

Nityanand Sharma, Hamid Keshmiri, Xiaodong Zhou, Ten It Wong, Christian Petri, Ulrich Jonas, Bo Liedberg, and Jakub Dostalek

Abstract-New plasmonic structure with actively tunable optical characteristics based on thermoresponsive hydrogel is reported. It consists of a thin, template-stripped Au film with arrays of nanoholes that is tethered to a transparent support by a cross-linked poly(*N*-isopropylacrylamide) (pNIPAAm)-based polymer network. Upon a contact of the porous Au surface with an aqueous environment, a rapid flow of water through the pores enables swelling and collapsing of the underlying pNIPAAm network. The swelling and collapsing could be triggered by small temperature changes around the lower critical solution temperature (LCST) of the hydrogel. The process is reversible, and it is associated with strong refractive index changes of $\Delta n \sim 0.1$, which characteristically alters the spectrum of surface plasmon modes supported by the porous Au film. This approach can offer new attractive means for optical biosensors with flow-through architecture and actively tunable plasmonic transmission optical filters.
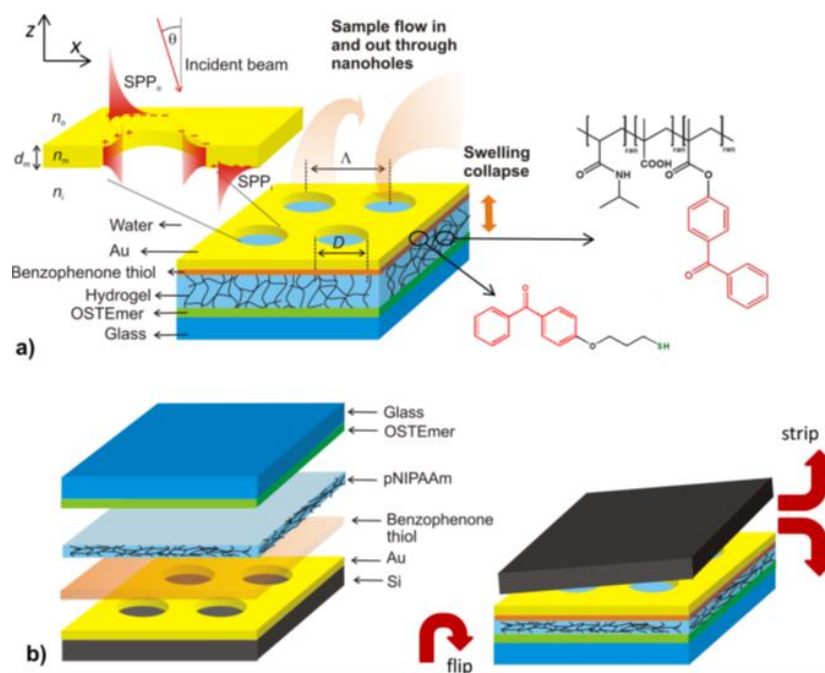
Figure 53: (**a**) Schematics of the investigated structure that comprise Au film with NHA that is attached to a glass substrate by a responsive pNIPAAm-based hydrogel cushion. (**b**) Preparation procedure of the structure by using template stripping from a Si wafer.

Molecularly Imprinted Polymer Waveguides for Direct Optical Detection of Low-Molecular-Weight Analytes

Nityanand Sharma, <u>Christian Petri</u>, Ulrich Jonas , Monika Bach, Günter Tovar, Katerina Mrkvová, Milan Vala, Jirí Homola,Wolfgang Knoll, Jakub Dostálek

Abstract-New composite layer architecture of 3D hydrogel polymer network that is loaded with molecularly imprinted polymer nanoparticles (nanoMIP) is reported for direct optical detection of low-molecular-weight compounds. This composite layer is attached to the metallic surface of a surface plasmon resonance (SPR) sensor in order to simultaneously serve as an optical waveguide and large capacity binding-matrix for imprinted target analyte. Optical waveguide spectroscopy (OWS) is used as a labelfree readout method allowing direct measurement of refractive index changes that are associated with molecular binding events inside the matrix. This approach is implemented by using a photocrosslinkable poly(N-isopropylacrylamide)-based hydrogel and poly[(ethylene glycol dimethylacrylate)-(methacrylic acid)] nanoparticles that are imprinted with ʟ-Boc-phenylalanine-anilide (ʟ-BFA, molecular weight 353 g mol^{-1}). Titration experiments with the specific target and other structurally similar reference compounds show good specificity and limit of detection for target ʟ-BFA as low as 2 x 10^{-6} M.
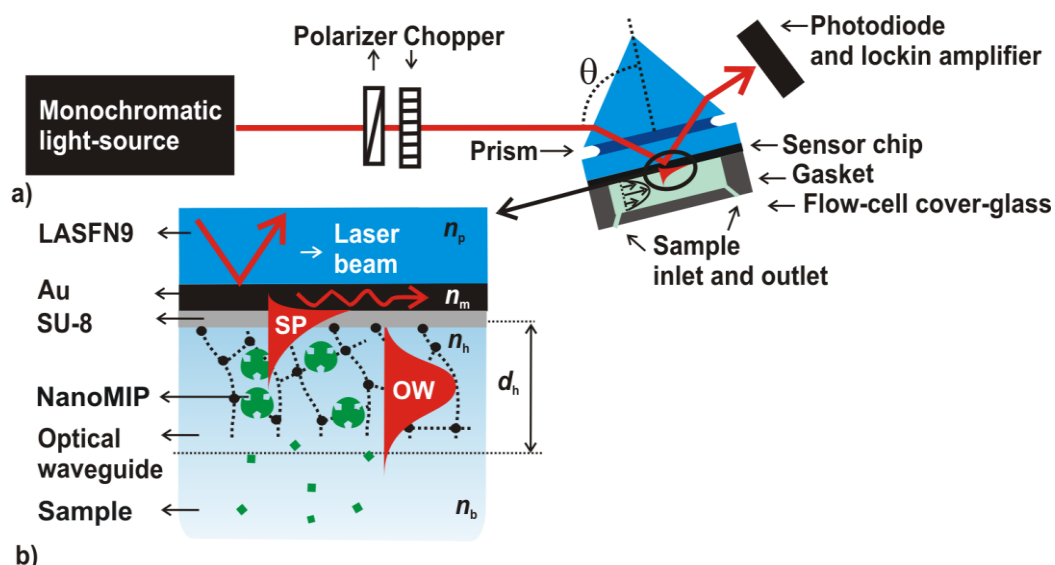
Figure 54: Schematic of sensor surface architecture and optical setup used for optical waveguide spectroscopy utilizing a surface plasmon resonance spectrometer with: **a)** angular interrogation. **b)** Detail of the sensor surface architecture with the polymer composite waveguide.

4. Results and Discussion

Reversibly tunable plasmonic bandgap by responsive hydrogel grating

Nityanand Sharma, Christian Petri, Ulrich Jonas, and Jakub Dostalek

Abstract-Reversible actuating of surface plasmon propagation by responsive hydrogel grating is reported. Thermo-responsive poly(*N*-isopropylacrylamide)-based (pNIPAAm) hydrogel nanostructure was designed and tethered to a gold surface in order to switch on and off Bragg scattering of surface plasmons which is associated with an occurrence of a bandgap in their dispersion relation. pNIPAAm-based grating with a period around 280 nm was prepared by using photo-crosslinkable terpolymer and laser interference lithography and it was brought in contact with water. The temperature induced swelling and collapse of pNIPAAm hydrogel grating strongly modulates its refractive index ($\Delta n \sim 0.1$) which leads to the reversible opening and closing of a plasmonic bandgap. The experiments demonstrate partial opening of a bandgap with the width of 12 nm at wavelength around 800 nm where SPR exhibited the spectral width of about 75 nm.
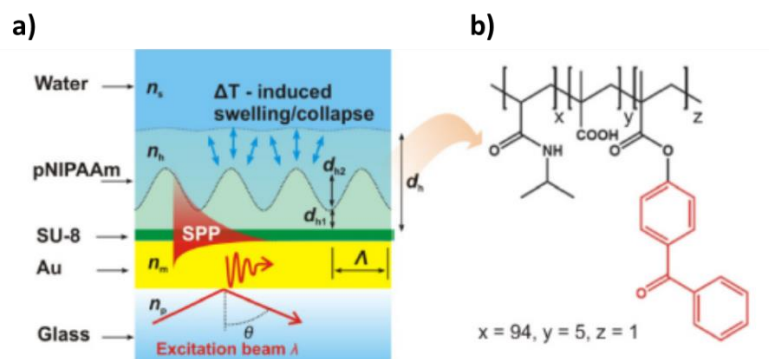
Figure 55: a) Schematics of the prepared pNIPAAm-based grating that is probed by travelling surface plasmon polaritons (SPPs). **b)** Chemical structure of the photocrosslinkable pNIPAAm terpolymer used in the interference lithography process.
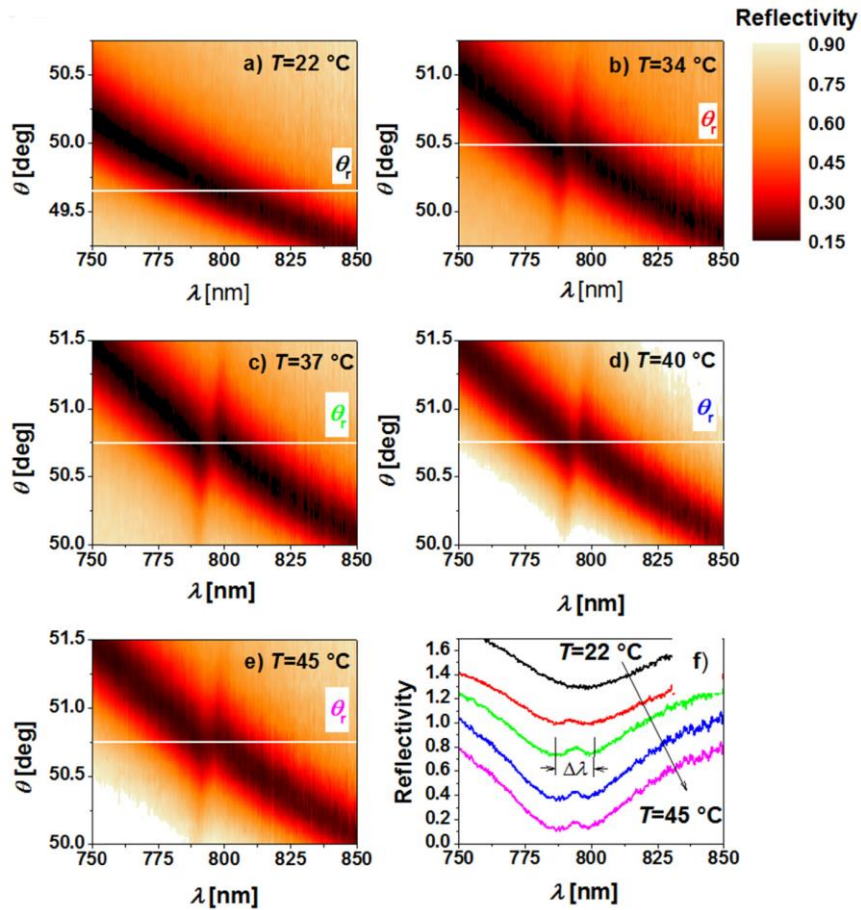
Figure 56: Measured reflectivity dependence on θ and λ for a pNIPAAm grating with the period Λ= 280 nm and temperature a) T = 22°C, b) T = 34°C, c) T = 37°C, d) T = 40°C, and e) T = 45°C. f) Cross-section of reflectivity at each temperature for the indicated angle of incidence θ_{res} at which the bandgap occurs for a pNIPAAm grating with the periodicity Λ = 280 nm. Subsequent reflectivity curves are offset by 0.3 along the reflectivity axis. Reflectivity spectra measured for TM polarization were normalized with those obtained for TE polarization in all graphs.

4. Results and Discussion

Free-standing hydrogel-particle composite membrane with dynamically controlled permeability for lab-on-chip applications

Khulan Sergelen, Christian Petri, Ulrich Jonas, Jakub Dostalek

Abstract-The preparation and investigation of a free-standing membrane made from a composite of thermoresponsive poly(*N*-isopropylacrylamide) (pNIPAAm) and polystyrene nanoparticles (PS NP) with temperature-controlled permeability is reported. The method exploits the light-induced crosslinking of the photo-reactive pNIPAAm-based polymer and mechanical reinforcement of the membrane structure by the polystyrene nanoparticles. About micrometer thick layers were either directly attached to a gold surface or prepared as free-standing layers spanning over arrays of microfluidic channels with a width of about hundred microns by using template stripping. Diffusion of liquid medium, low molecular weight molecules, and large molecular weight proteins contained in blood through the composite membrane was observed with combined surface plasmon resonance (SPR) and optical waveguide spectroscopy (OWS). The swelling ratio, permeability, and non-specific sorption to these composite membranes were investigated by SPR and OWS as a function of molecular weight of analyte, loading of PS NP in the composite film, and temperature. We show successful preparation of a defect-free membrane structure that acts as a thermoresponsive filter with nanoscale pores spanning over an area of several square millimeters. This membrane can be reversibly switched to block or allow the diffusion of low mass molecules to the sensor surface by temperature-triggered swelling and collapsing of the hydrogel component. Low unspecific sorption and blocking of diffusion of proteins contained in blood serum is observed. These features make this platform interesting for potential future applications in continuous monitoring biosensors for the analysis of low molecular weight drug analytes or for advanced cell-on-chip microfluidic studies.
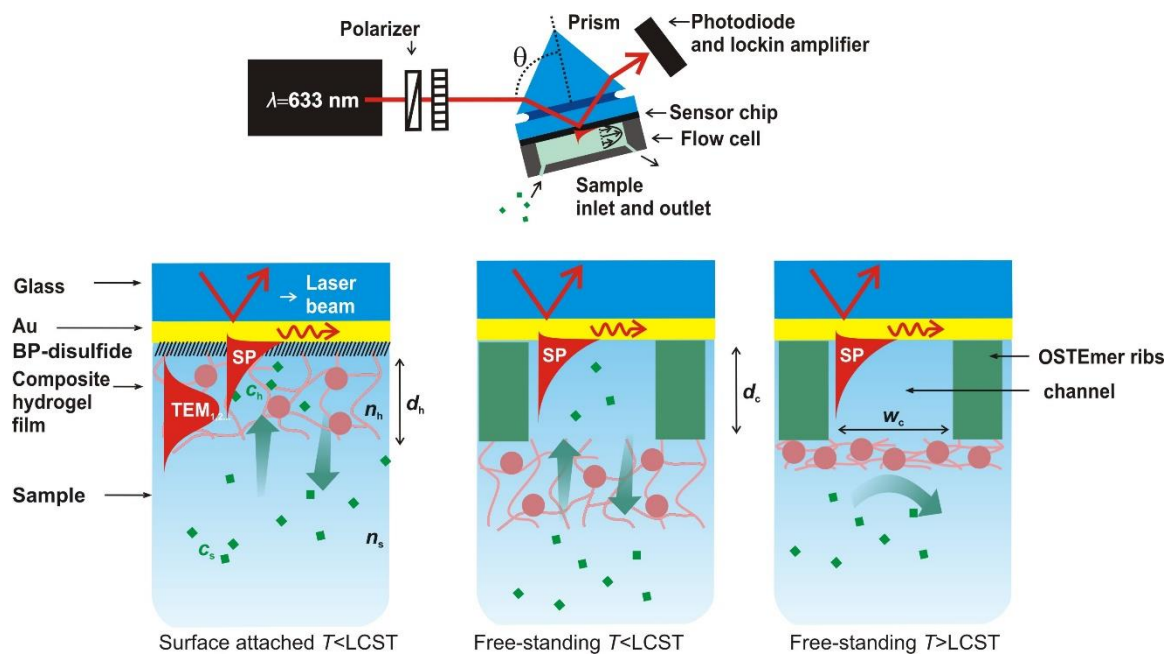
Figure 57: Optical setup for the observation of thin hydrogel films and diffusion of biomolecules based on combined surface plasmon resonance (SPR) and optical waveguide spectroscopy (OWS).

4.4.2 Photocrosslinkable Dextran-based Hydrogel Systems

This chapter describes the fabrication of a photocrosslinkable dextran-based hydrogel system, which was applied for the label free detection of Angiopoetin-1, whereby synthesis and characterization of the hydrogel material were performed by Christian Petri at the University of Siegen. The sensor application was carried out at the Politecnico di Torino in the group of Emiliano Descrovi and Francesca Frascella.[6]

Due to their beneficial properties (e.g. biocompatibility and degradability), naturally occurring polymers can be highly attractive for the fabrication of hydrogels. In particular the water solubility of dextran makes it an ideal candidate for the fabrication of hydrogel sensing matrices. Its chemical structure comprises glucose repeat units featuring α-1,6 glycosidic linkages in the main chain and additional branches emanating from α-1,3 linkages. Each repeat unit carries three hydroxyl groups, which can be used for post-modification reactions, whereas a modification of the hydroxyl groups in 2- and 4-position is most probable.[188] For the application of dextran as biosensor matrix, a benzophenone unit was incorporated to perform crosslinking by irradiation with UV light at a wavelength of 365 nm. In addition, a carboxylic acid functionality was introduced for post-modification, in this case with Angiopoietin-1-specific antibody (Anti-Ang-1), for the label free detection of Angiopoietin-1 (Ang-1), which is assumed to play a key role in tumor progression.[189] The preparation of the respectively modified dextran was performed in analogy to published synthesis procedures (**Scheme 24**).[86]

4. Results and Discussion

α-1,6 main chain linkage

α-1,3 branching

R = R₁, R₂

R₁ = H

R₂ =

R₃ =

R = R₁, R₂, R₃
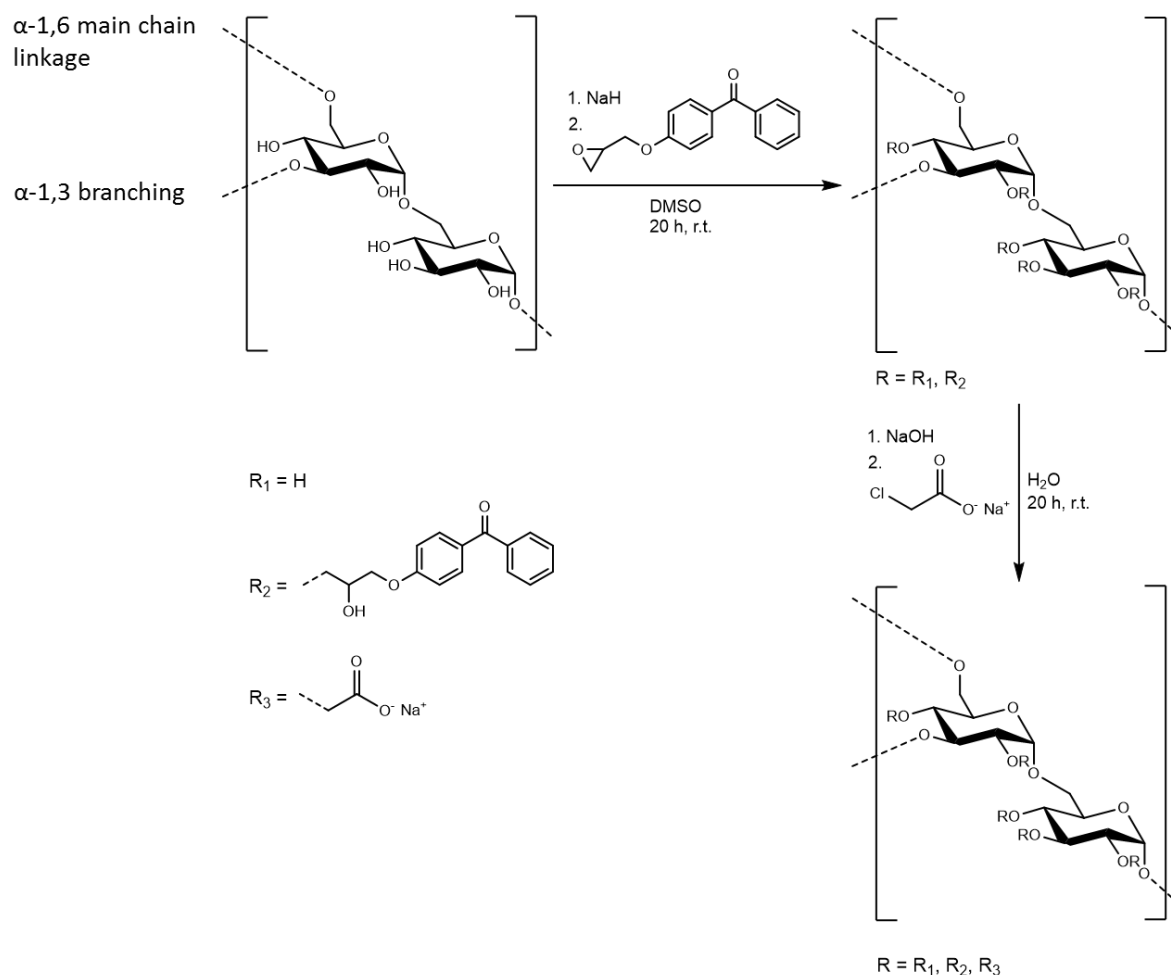
Scheme 24: General structure of dextran and synthesis of photocrosslinkable carboxymethylated dextran (EBP-CMD).

First, dextran was dissolved in dry DMSO, followed by deprotonation of the hydroxyl functionalities with sodium hydride (NaH). The benzophenone moiety was then introduced by ring opening reaction of the negative charged oxygen of the glucose units with the epoxy functionality of 4-(2,3-epoxypropyloxy)benzophenone (EBP). In the final step, the carboxylic acid group is incorporated by deprotonation of the non-modified hydroxyl functionalities, followed by nucleophilic substitution of the respective chlorine of sodium chloroacetate. The described modification reactions were performed with several dextran fractions of different average molar mass (20, 75, 200 and 2000 x 10^3 g mol^{-1}). Finally, the decision was made to use dextran of $\bar{M}_w$= 75 x 10^3 g mol^{-1} for hydrogel fabrication, since this material could be further purified by filtration using a 0.2 µm syringe filter, which was necessary to remove non-dissolved components. In comparison to dextran of lower $\bar{M}_w$, this material showed still good photocrosslinking capabilities.

4. Results and Discussion

Hydrogel-Terminated Photonic Crystal for Label-Free Detection of Angiopoietin-1

Francesca Frascella, Christian Petri, Serena Ricciardi, Lucia Napione, Peter Munzert, Ulrich Jonas, Jakub Dostalek, Federico Bussolino, Candido Fabrizio Pirri, and Emiliano Descrovi

Abstract-We report on a label-free time-resolved biosensing technique based on refractometric measurements. A one-dimensional photonic crystal (1-DPC) constituted by a planar stack of dielectric layers is used for supporting Bloch surface waves. These electromagnetic surface waves probe the aqueous environment within few hundreds of nanometers from the photonic crystal surface, which is functionalized with a hydrogel binding matrix. Therein, selected antibodies are grafted for the specific recognition of the tumoral biomarker Angiopoietin-1. A model bioassay is established demonstrating a detection of Antiopoiegin-1 as low as picomolar concentrations.
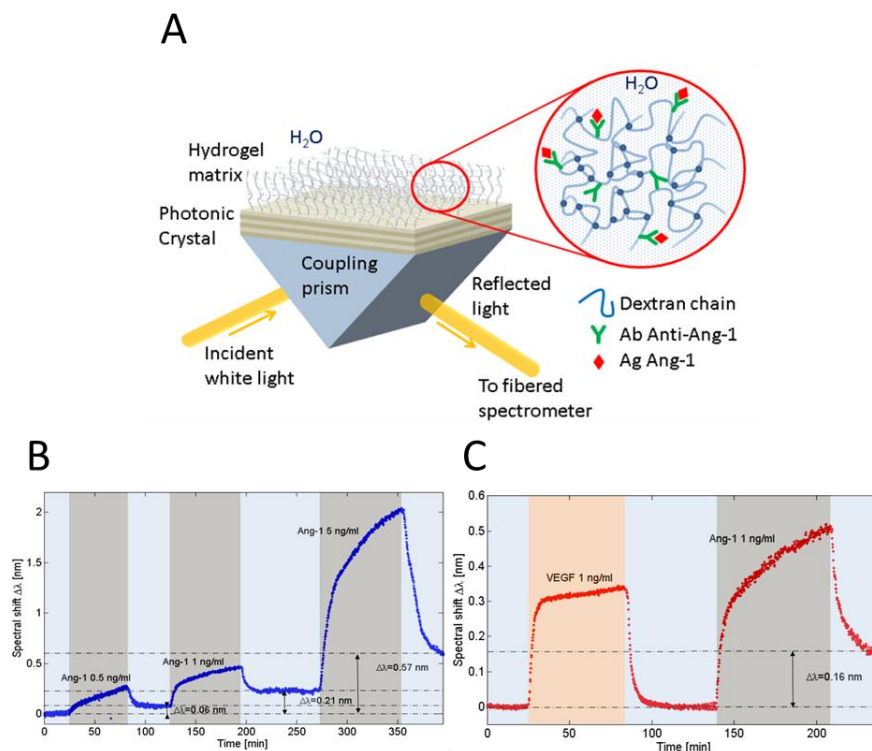
Figure 58: (**A**) Detection principle of Ang-1 via Bloch surface waves (BSWs) using modified dextran hydrogels as binding matrix (**B**) Illustrative time-resolved sensorgram related to the incubation and binding of Ang-1 in solution at sequential concentrations of 0.5 ng ml^{-1}, 1 ng ml^{-1}, 5 ng ml^{-1}. Darker bands correspond to antigen incubation periods. (**C**) Illustrative time-resolved sensorgram related to the incubation of a VEGF-A solution (negative control) and an Ang-1 solution at a concentration of 1 ng ml^{-1}. Contrary to the case wherein Angiopoietin is incubated, VEGF-A results in a substantially negligible spectral shift, meaning that no binding is observed.

5. Experimental Part

5. Experimental Part

5.1 Materials

Chemicals were purchased from Alfa Aesar (trifluoroacetic anhydride, *N*-hydroxysuccinimide, 2-aminoethanol, (4-(aminomethyl)phenyl)(phenyl)methanone, butyronitrile, isobutyronitrile, 4-hydroxybenzophenone, 2-chloroethylamine hydrochloride, sodium azide, ethyl 4-bromobutyrate, *N*-isopropylacrylamide, methacrylic acid, acryloyl chloride, 2 2'-azobisisobutyronitrile, sodium chloroacetate, 4-hydroxybenzophenone, sodium hydride, epichlorhydrine, ethylene diamine, phenyl isocyanate, morpholine, propargyl alcohol, propargyl bromide, succinic anhydride, 4-dimethylaminopyridine, pyridine, dichloromethane, 3,3'-dithiodipropionic acid, 3-dimethylamino-1-propyne, 4-toluenesulfonyl chloride, 1,3-propane sultone, β-propiolactone, and 2-ethyl-2-oxazoline), Fluorochem (Methyltriflate), Sigma Aldrich (Dextran, anhydrous ethanol), Carl Roth (1-(3-dimethylaminopropyl)-3-ethylcarbodiimid hydrochloride) and Prolabo (anhydrous acetonitrile) and were used as received, unless otherwise noted. 2-Ethyl-, 2-isopropyl- and 2-*n*-propyl-2-oxazoline were refluxed over CaH_2 and stored under dry nitrogen atmosphere. 2-Aminoethanol, morpholine, ethylene diamine were distilled under reduced pressure prior to use. The synthesis of the monomers as well as the synthesis of the BPdiS adhesion promoter were carried out under dry argon gas atmosphere, unless otherwise noted. Anhydrous sodium carbonate K_2CO_3 was dried in vacuum at 130°C prior to use. The synthesis of poly(2-oxazoline)-based polymers was carried out under dry nitrogen atmosphere using microwave assisted polymerization and the synthesis of poly(N-isopropylacrylamide)-based polymers was carried out under dry argon atmosphere.

5.2 Instrumentation

^{1}H NMR (400MHz) and ^{13}C NMR (100 MHz) spectra were recorded on a Bruker AV 400 spectrometer, with an estimated coupling constant of ±0.3 Hz. FT-IR spectroscopy was carried out on a Bruker Tensor 27. Gel permeation chromatography (SEC) was carried out on a PSS-System consisting of a degasser, an isocratic pump, an autosampler (Agilent 1200), a UV-detector Lambda 1010 (Bishoff), a RI-detector RI-71 (Shodex) and a SDV Linear M column. All SEC measurements were performed at 60°C using a 0.1 wt% solution of LiBr dissolved in

5. Experimental Part

dimethylacetamide (DMAc) as eluent, with a flow rate of 1 ml/min. PMMA standards (PSS Polymer Standard Services) were used as reference material. Poly(2-oxazoline)-based polymers were synthesized by microwave assisted cationic ring opening polymerization, using a microwave reactor type Discover LabMate. Thermal Analysis was performed on a Differential Scanning Calorimeter (DSC) TA Instruments Q 1000. Cloud point analysis was performed on a UV/VIS spectrophotometer type Thermo Scientfic Evolution 201/220, using 0.3 wt% aqueous polymer solution with a heating and cooling rate of 1 K min^{-1}. Spin coating of the silicon wafers and of the Au coated LASF9 glass slides was performed on a SPS SPIN200i spin coater. Photochemical crosslinking of the deposited polymer layers was performed using a Stratalinker UV photocrosslinker at wavelength of 365 nm under nitrogen atmosphere. SPR/OWS measurements were performed on a Res-Tec RT 2005 spectrometer (Resonant Technologies GmbH) using Kretschmann configuration. Plasmon and waveguide excitation is achieved with a monochromatic He-Ne-laser beam of wavelength 632.8 nm. The incident light beam is reflected at the base of the prism and the reflected intensity recorded as a function of the angle of incidence θ by a photodiode detector connected to a lock-in amplifier. The temperature inside the flow cell was controlled by a heatable and coolable computer controlled Peltier element, with an operating temperature range from 15-50°C. The coated polymer layers were attached to the prim by using immersion oil of $n = 1.700$. The prism with the glass slide was then mounted on a rotating plate in the SPR/OWS. SPR/OWS substrates were bought form Hellma Optics Jena. The thickness of the polymer layer coated onto silicon substrates was determined using a J. A. Woolman ellipsometer type Alpha-SE, with a He-Ne laser of wavelength 632.8 nm as light source. The data sets were evaluated with the software CompleteEASE 4.48. AFM measurements were performed on an Asylum MFP-3D and the data evaluated with the software Igor Pro.

5.3 Synthesis of Monomers and Functionalization Units

5.3.1 Au Substrate Anchor Synthesis

Bis(2,5-dioxopyrrolidin-1-yl) 3,3'-disulfanediyldipropanoate (1) was synthesized referring to literature[22]:

Reagents and conditions: Pyridine, NHS, TFAA, DCM, 0.5 h, 0°C, 16 h, r.t.

Left: 210.3 g mol⁻¹, 1.05 g, 4.99 mmol. Right: 404.4 g mol⁻¹, 1.66 g, 4.09 mmol.
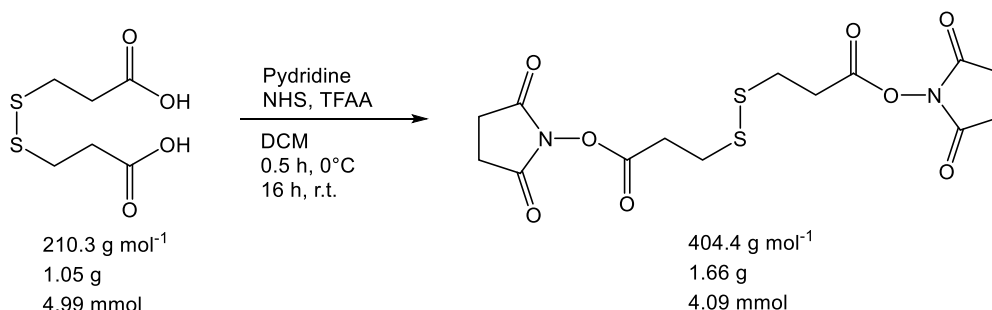
To a mixture of 3,3'-dithiodipropionic acid (4.99 mmol, 1.05 g) and DCM (35 ml), pyridine (62.0 mmol, 4.90 g) and NHS (16.8 mmol, 1.93 g) was added. The resulting solution was cooled with an ice-water bath to 0°C, followed by the addition of TFAA (16.3 mmol, 3.43 g). After 30 min the solution was allowed to warm to room temperature and stirred for additional 16 h. DCM (60 ml) was added to the solution and the organic layer washed with aq. HCl (0.5 M, 3 x 60 ml) and saturated $NaHCO_3$ (2 x 60 ml). The separated organic layer was dried over $MgSO_4$ and the solvent evaporated, giving the title compound as a slightly brownish solid.

Yield 82 % (4.09 mmol, 1.66 g).

IR (cm⁻¹) = 2998 (C-H), 1808, 1779, 1730 (C=O).

¹H NMR (400 MHz, Chloroform-*d*): δ [ppm] = 3.13 – 2.97 (m, 8H), 2.96 – 2.73 (m, 8H).

¹³C NMR (101 MHz, Chloroform-*d*): δ [ppm] = 169.1, 167.2, 32.4, 31.2, 25.7.

5. Experimental Part

3,3'-disulfanediylbis(*N*-(4-benzoylbenzyl)propanamide) (2) was synthesized referring to literature:[190]
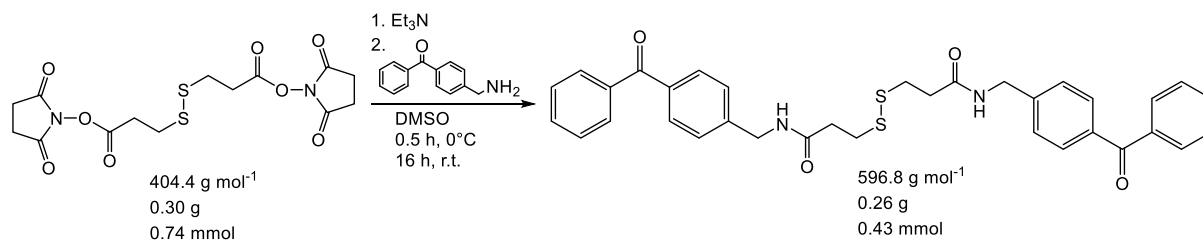
Compound **(1)** (0.74 mmol, 0.30 g) was dissolved in DMSO (14 ml) and cooled with an ice-water bath to 0°C. (4-(aminomethyl)phenyl)(phenyl)methanone (3.30 mmol, 0.70 g) dissolved in DMSO (6 ml) and Et₃N (3.20 mmol, 0.45 ml) were added and the solution stirred for 16 h at room temperature. DCM (20 ml) was added and the organic layer was washed with water (2 x 20 ml). The formed precipitate in the organic layer was filtered off and washed with small portions of DCM several times. The remaining product was dried in vacuum overnight.

Yield: 51 % (0.43 mmol, 0.26 g) of a white solid.

IR (cm^{-1}) = 3295 (N-H), 3052 (C-H$_{aromatic}$), 2907 (C-H), 1641 (C=O).

^{1}H NMR (400 MHz, DMSO-d_6): δ [ppm] = 8.60 (t, *J* = 6.0 Hz, 1H), 7.76 – 7.62 (m, 5H), 7.55 (t, *J* = 7.6 Hz, 2H), 7.43 (d, *J* = 8.0 Hz, 2H), 4.38 (d, *J* = 5.9 Hz, 2H), 2.96 (t, *J* = 7.1 Hz, 2H), 2.60 (t, *J* = 7.1 Hz, 2H).

^{13}C NMR (101 MHz, DMSO-d_6): δ [ppm] = 196.7, 171.5, 145.8, 138.4, 136.8, 133.8, 131.1, 130.8, 129.8, 128.4, 43.2, 36.2, 35.1.

5.3.2 Photocrosslinker Monomer Synthesis

4-(4-benzoylphenoxy)butanoic acid (3) was synthesized according to literature[191]:
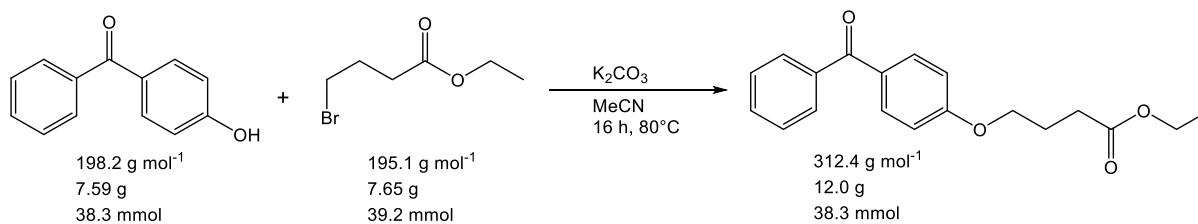
Anhydrous K_2CO_3 (43.5 mmol, 6.01 g) was added to a solution of 4-hydroxybenzophenone (38.3 mmol, 7.59 g) in MeCN (250 ml). After stirring for 30 min, ethyl 4-brombutanoate (39.2 mmol, 7.65 g) was added and the mixture was heated up to 80°C until TLC (Thin layer chromatography) indicated complete conversion of the educt, which was obtained after 16 h. The solvent was evaporated and the residue dissolved in EtOAc (100 ml), followed by washing with water (3 x 50 ml). The solvent was again evaporated and the crude ester was used without further purification in the next reaction step. TLC (n-hexane/EtOAc, 4:1): R_f = 0.41.

312.4 g mol^{-1}	284.3 g mol^{-1}
12.0 g	9.97 g
38.3 mmol	35.2 mmol
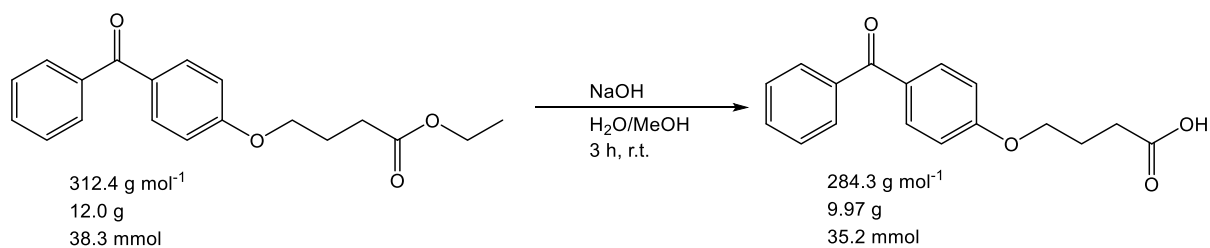
The crude product of the corresponding ester (38.3 mmol) was dissolved in a mixture of MeOH (320 ml) and aqueous NaOH (320 mmol, 12.8 g, 320 ml H_2O) solution and stirred at ambient temperature until TLC indicated complete conversion of the educt, which was obtained after 3 h. The solution was acidified with 4 M HCl to pH = 1 and the formed precipitate filtered off and washed several times with small portions of cold water. The remaining product was dried in vacuum at 60°C over P_2O_5.

Yield: 92% (9.97 g, 35.2 mmol) of a white solid.

TLC (n-hexane/EtOAc/AcOH, 1:1:0.1): R_f = 0.62; m.p. 84 – 86°C.

IR (cm^{-1}) = 3119 (COOH), 1596 (C=O), 1282, 1227, 1142.

^{1}H NMR (400 MHz, Chloroform-*d*): δ [ppm] = 7.90 – 7.68 (m, 4H), 7.63 – 7.40 (m, 3H), 7.01 – 6.88 (m, 2H), 4.11 (t, *J* = 6.1 Hz, 2H), 2.61 (t, *J* = 7.2 Hz, 2H), 2.22 – 2.08 (m, 2H).

^{13}C NMR (101 MHz, Chloroform-*d*): δ [ppm] = 196.5, 179.9, 163.2, 139.0, 133.4, 132.8, 131.0, 130.6, 129.0, 114.8, 67.6, 31.2, 25.0.

4-(benzoylphenoxy)butanoate 2,5-dioxopyrrolidinon-1-yl (4) was synthesized referring to literature[22]:
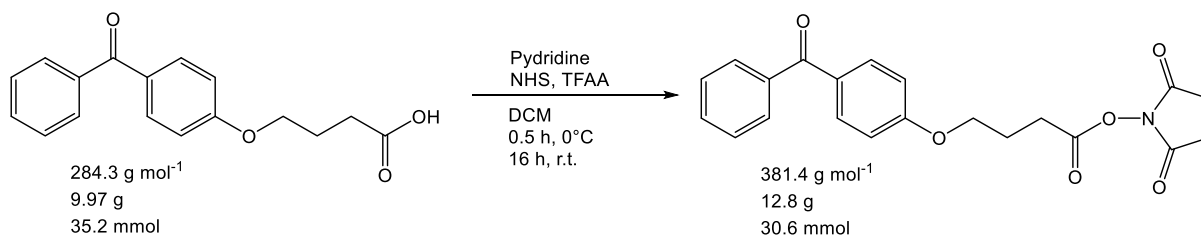
Pyridine (619 mmol, 50 ml) and NHS (86.6 mmol, 17.0 g) were added to a solution of compound **(3)** (35.2 mmol, 9.97 g) in DCM (150 ml). The solution was cooled to 0°C and TFAA (149 mmol, 21 ml) was added. After 30 min the solution was allowed to warm to room temperature and stirred for additional 16 h. DCM (100 ml) was added and the organic layer was washed with aq. 0.5 M HCl (3 x 200 ml) and saturated aqueous $NaHCO_3$ (2 x 200 ml). The separated organic layer was dried over $MgSO_4$ and the solvent evaporated, giving the title compound as a slightly brownish solid.

Yield: 87% (30.6 mmol, 12.8 g).

TLC (n-hexane/EtOAc, 1:1): R_f = 0.42.

IR (cm^{-1}) = 3063 (C-H$_{aromatic}$), 2945 (C-H), 1813, 1782, 1728 (C=O).

^{1}H NMR (400 MHz, Chloroform-*d*): δ [ppm] = 7.88 – 7.68 (m, 4H), 7.61 – 7.40 (m, 3H), 7.02 – 6.91 (m, 2H), 4.15 (t, *J* = 6.0 Hz, 2H), 2.93 – 2.77 (m, 6H), 2.27 (tt, *J* = 7.3, 6.0 Hz, 2H).

^{13}C NMR (101 MHz, Chloroform-*d*): δ [ppm] = 195.7, 169.2, 168.4, 162.3, 138.4, 132.7, 132.0, 130.5, 129.9, 128.3, 114.2, 66.3, 27.83, 25.7, 24.4.

4-(4-benzoylphenoxy)-*N*-(2-chloroethyl)butanamide (5) was synthesized referring to literature:[190]
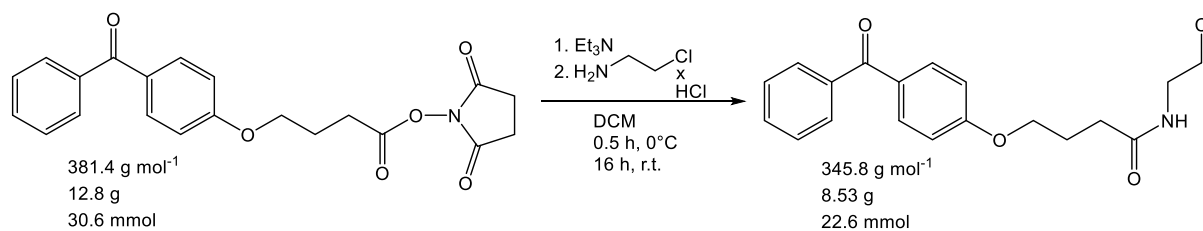
Compound **(4)** (30.6 mmol, 12.8 g) was dissolved in DCM (150 ml) and cooled to 0°C. 2-chloroethylamine hydrochloride (86.2 mmol, 10.0 g) and Et_3N (86.6 mmol, 8.76 g, 12.0 ml) were added. After 45 min the ice water bath was removed and the reaction mixture stirred at room temperature until TLC indicated complete conversion of the educts, which was obtained after 16 h. The reaction mixture was diluted with DCM (150 ml) and aqueous 1 M HCl (200 ml) was added. The layers were separated and the organic layer was washed with aqueous 1 M HCl (2 x 200 ml) followed by washing with saturated aqueous $NaHCO_3$ (2 x 200 ml). The organic layer was dried over $MgSO_4$ and the solvent evaporated.

Yield: 74% (22.6 mmol, 8.53 g) of a white solid.

TLC (n-hexane/EtOAc, 1:1: R_f = 0.24.

IR (cm^{-1}) = 3302 (NH), 3068 (C-$H_{aromatic}$), 2963 (C-H), 1728 (C=O).

^{1}H NMR (400 MHz, Chloroform-*d*): δ [ppm] = 7.77 (ddd, *J* = 26.8, 7.6, 1.8 Hz, 4H), 7.61 – 7.40 (m, 3H), 7.01 – 6.84 (m, 2H), 4.09 (t, *J* = 6.0 Hz, 2H), 3.61 (d, *J* = 3.7 Hz, 4H), 2.44 (t, *J* = 7.2 Hz, 2H), 2.17 (p, *J* = 6.6 Hz, 2H).

^{13}C NMR (101 MHz, Chloroform-*d*): δ [ppm] = 195.7, 172.4, 162.6, 138.3, 132.7, 132.1, 130.30, 129.8, 128.3, 114.1, 67.2, 44.2, 41.3, 32.7, 25.0.

5. Experimental Part

2-[3-(4-benzoylphenoxy)propyl]-2-oxazoline (6) was synthesized referring to literature[19]:
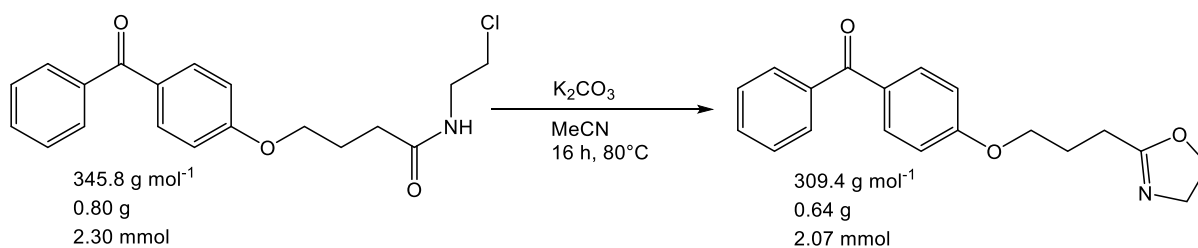
Compound **(5)** (2.30 mmol, 0.80 g) was dissolved in MeCN (25 ml) and K_2CO_3 (4.60 mmol, 0.64 g) was added under argon atmosphere. The reaction mixture was stirred at 80°C until TLC indicated complete conversion of the educt, which was obtained after 16 h. The insoluble K_2CO_3 was removed by filtration and the solvent evaporated to obtain the product as a slightly brownish viscous oil.

Yield: 87% (2.07 mmol, 0.62 g).

TLC (n-hexane/EtOAc, 1:1): R_f = 0.35.

IR (cm^{-1}) = 3057 (C-H$_{aromatic}$), 2939 (C-H), 1651 (C=O), 1597 (C=N).

^{1}H NMR (400 MHz, Chloroform-d): δ [ppm] = 7.87 − 7.66 (m, 4H), 7.61 − 7.38 (m, 3H), 7.01 − 6.88 (m, 2H), 4.31 − 4.18 (m, 2H), 4.11 (t, J = 6.1 Hz, 2H), 3.89 − 3.76 (m, 2H), 2.49 (tt, J = 7.3, 1.5 Hz, 2H), 2.21 − 2.09 (m, 2H).

^{13}C NMR (101 MHz, Chloroform-d): δ [ppm] = 195.7, 167.8, 162.7, 138.4, 132.7, 132.0, 130.2, 129.8, 128.3, 114.1, 67.4, 67.1, 54.5, 25.6, 24.5.

5.3.3 Alkyne Containing Monomer Synthesis

4-oxo-4-(prop-2-yn-1-yloxy)butanoic acid (7) was synthesized according to literature.[192]

56.1 g mol^{-1}	100.1 g mol^{-1}	156.1 g mol^{-1}
5.05 g	11.2 g	7.49 g
89.9 mmol	112 mmol	48.0 mmol
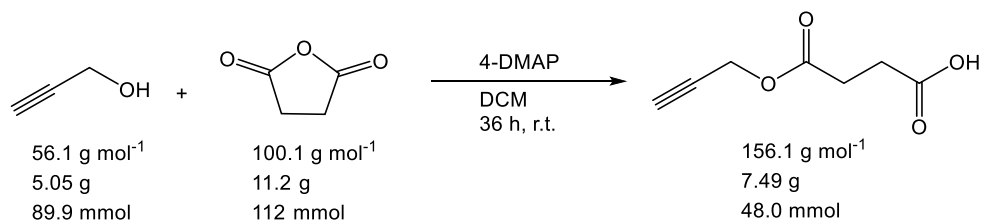
4-DMAP (20 mmol, 2.45 g) and succinic anhydride (111.6 mmol, 11.2 g) were dispersed in dry DCM (15 ml). Propargyl alcohol (89.9 mmol, 5.05 g, 5.20 ml) was slowly added to the suspension over a period of 30 min, which became a clear yellowish solution and the reaction mixture was stirred for 36 h at room temperature. The solution was diluted with DCM (50 ml) and water (50 ml) was added, followed by washing of the organic layer with aqueous NaHSO$_4$ (10 wt%, 3 x 50 ml). The organic layer was separated and dried over anhydrous MgSO$_4$, filtered and concentrated. The remaining yellowish liquid was allowed to crystallize at -15°C and the resulting solid dried under reduced pressure.

Yield: 59 % (48.0 mmol, 7.49 g).
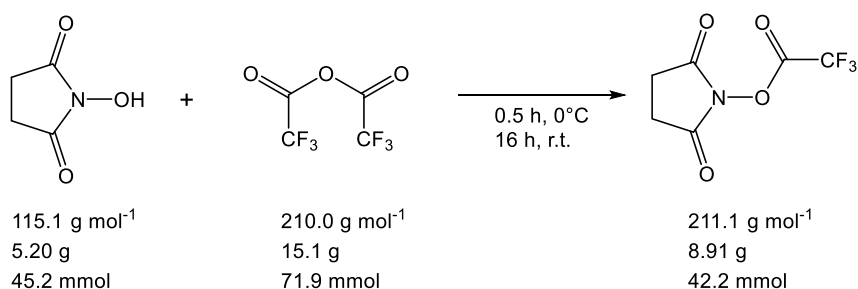
TLC (n-hexane/EtOAc: 1/1): R$_f$ = 0.57.

^{1}H NMR (400 MHz, Chloroform-*d*): δ [ppm] = 4.71 (s, 2H), 2.69 (m, 4H), 2.51 (s, 1H).

^{13}C NMR (101 MHz, Chloroform-*d*): δ [ppm] = 177.3, 170.4, 76.4, 74.1, 51.3, 27.8, 27.6.

5. Experimental Part

2,5-dioxopyrrolidin-1-yl prop-2-yn-1-yl succinate (8) was synthesized referring to literature.[22]
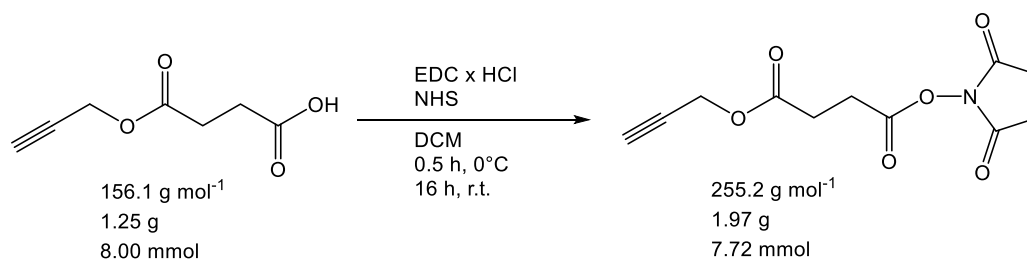
Compound (**7**) (8.00 mol, 1.25 g) was dissolved in dry DCM (50 ml). EDC x HCl (11.3 mmol, 2.19 g) and NHS (17.6 mmol, 2.02 g) were added and the resulting solution stirred at room temperature until TLC (n-hexane/EtOAc: 1/1) indicated complete conversion of the educt, which was obtained after 16 h. The solution was diluted with DCM (50 ml) and washed with water (3 x 50 ml). The organic layer was separated and dried over anhydrous MgSO$_4$, filtered and the solvent evaporated, giving the title compound white crystalline solid.

Yield: 59 % (48.0 mmol, 7.49 g).

TLC (n-hexane/EtOAc: 1/1): R$_f$ = 0.32.

^{1}H NMR (400 MHz, Chloroform-*d*): δ [ppm] = 4.73 (s, 2H), 2.65 (m, 4H), 2.50 – 2.42 (m, 4H)

^{13}C NMR (101 MHz, Chloroform-*d*): δ [ppm] = 170.7, 169.3, 168.0, 77.7, 75.6, 52.9, 28.9, 26.5, 26.0.

Prop-2-yn-1-yl 4-[(2-chloroethyl)amino]-4-oxobutanoate (9) was synthesized referring to literature.[23]

255.2 g mol^{-1}
1.97 g
7.72 mmol

217.7 g mol^{-1}
993 mg
4.56 mmol
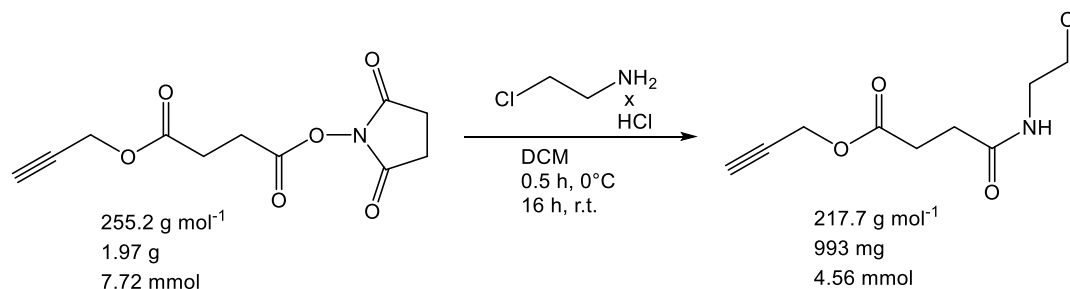
Compound (**8**) was dissolved in DCM and the solution cooled with an ice-water bath for 30 min. 2-chloroethylamine hydrochloride (16.8 mmol, 1.95 g) and Et$_3$N (17.3 mmol, 1.75 g, 2.40 ml) was added and the solution stirred at 0°C for 1 h. The solution was then allowed to warm to room temperature and stirred until TLC (n-hexane/EtOAc: 1/2) indicated complete conversion of the educt, which was obtained after 3 h. The solution was diluted with DCM (50 ml) and washed with 0.5 M aq. HCl (3 x 50 ml) and saturated aq. NaHCO$_3$ soluiton (2 x 50 ml). The organic layer was separated and dried over anhydrous MgSO$_4$, filtered and the solvent evaporated, giving the title compound white crystalline solid.

Yield: 59 % (4.56 mmol, 993 mg).

TLC (n-hexane/EtOAc: 1/2): R$_f$ = 0.54.

^{1}H NMR (400 MHz, Chloroform-*d*): δ [ppm] = 6.09 (b, 1H, NH), 4.69 (s, 2H), 3.61 (m, 4H), 2.73 (t, 2H), 2.53 (t, 2H), 2.47 (s, 1H).

^{13}C NMR (101 MHz, Chloroform-*d*): δ [ppm] = 171.1, 170.3, 76.5, 74.0, 51.2, 43.0, 40.3, 29.7, 28.2.

1-(2-chloroethyl)pyrrolidine-2,5-dione (10) was synthesized according to literature.[19]
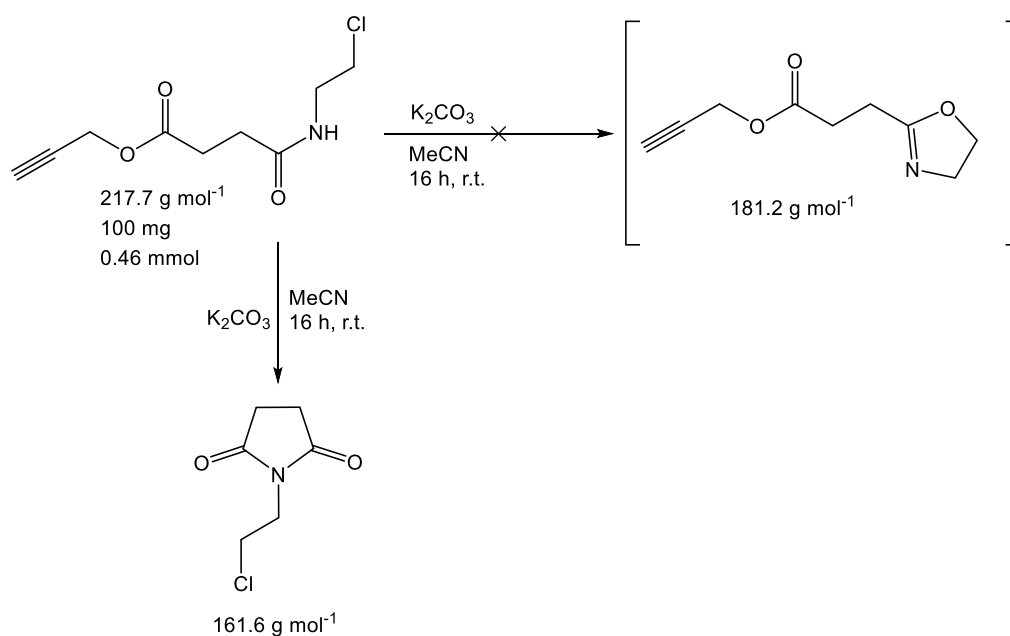
Compound (**9**) (0.46 mmol, 100 mg) was dissolved in acetonitrile (10 ml). Then K_2CO_3 (0.92 mmol, 127 mg) was added and the mixture was stirred at room temperature until TLC indicated complete conversion of the educt, which was obtained after 1h. The mixture was filtered and the solvent evaporated.

Yield: 62 % (0.29 mmol, 47 mg).

TLC (n-hexane/EtOAc: 1/1): R_f = 0.92.

^{1}H NMR (400 MHz, Chloroform-*d*): δ [ppm] = 3.87 (t, 2H), 3.69 (t, 2H), 2.75 (s, 4H).

^{13}C NMR (101 MHz, Chloroform-*d*): δ [ppm] = 176.9, 40.2, 40.1, 28.2.

5.3.4 Azide Containing Monomer Synthesis

2,5-dioxopyrrolidin-1-yl 2,2,2-trifluoroacetate was synthesized according to literature:[193]

115.1 g mol⁻¹	210.0 g mol⁻¹	211.1 g mol⁻¹

115.1 g mol^{-1}
5.20 g
45.2 mmol

210.0 g mol^{-1}
15.1 g
71.9 mmol

211.1 g mol^{-1}
8.91 g
42.2 mmol

A 50 ml Schlenk flask was charged with TFAA (71.9 mmol, 15.1 g) and cooled to 0°C. Then NHS (45.2 mmol, 5.20 g) was added and the reaction stirred for 30 min at this temperature, followed by stirring at room temperature for additional 16 h. The excess of TFAA was removed by rotary evaporator and the residue redissolved twice in toluene (20 ml) and the solvent evaporated. Yield: 93 % (42.2 mmol, 8.90 g)

Ethyl 4-azidobutanoate (11) was synthesized referring to literature:[23]

195.1 g mol^{-1}
20.3 g
104 mmol

157.2 g mol^{-1}
14.9 g
94.6 mmol
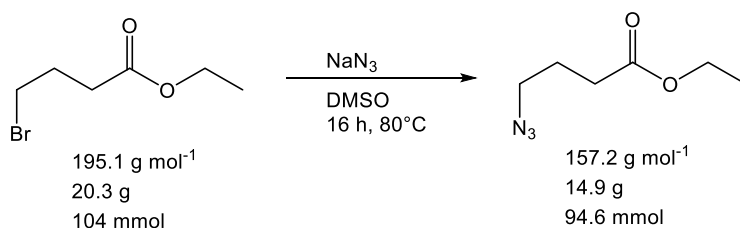
Ethyl 4-bromobutanoate (104 mmol, 20.3 g, 15 ml) and NaN$_3$ (365 mmol, 23.7 g) were added to DMSO (100 ml) and the mixture was heated up to 80°C for 16 h. After cooling to room temperature, DCM (200 ml) was added and the organic layer was washed with water (5 x 100 ml), dried over MgSO$_4$ and the solvent evaporated.

Yield: 91 % (94.6 mmol, 14.9 g).

IR (cm^{-1}) = 2939 (C-H), 2094 (N$_3$), 1729 (C=O).

^{1}H NMR (400 MHz, Chloroform-*d*): δ [ppm] = 4.10 (q, *J* = 7.1 Hz, 2H), 3.31 (t, *J* = 6.7 Hz, 2H), 2.36 (t, *J* = 7.2 Hz, 2H), 1.87 (p, *J* = 7.0 Hz, 2H), 1.22 (td, *J* = 7.1, 0.5 Hz, 3H).

^{13}C NMR (101 MHz, Chloroform-*d*): δ [ppm] = 172.7, 60.6, 50.7, 31.2, 24.3, 14.2.

5. Experimental Part

4-azidobutanoic acid (12) was synthesized referring to literature:[191]
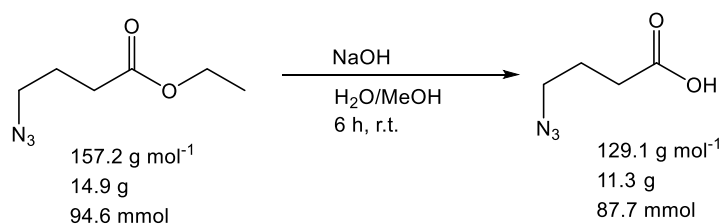
To compound **(11)** aq. NaOH (200 mmol, 8.0 g, 200 ml) and MeOH (40 ml) was added. The solution was stirred at room temperature for 6 h, acidified with 4 M HCl to pH = 1 and extracted with Et$_2$O (4 x 100 ml). The organic layer was dried over MgSO$_4$ and the solvent evaporated.

Yield: 93 % (87.7 mmol, 11.3 g).

IR (cm^{-1}) = 3095 (OH), 2939 (C-H), 2093 (N$_3$), 1705 (C=O).

^{1}H NMR (400 MHz, Chloroform-*d*): δ [ppm] = 11.48 (s, 1H), 3.35 (t, *J* = 6.7 Hz, 2H), 2.45 (t, *J* = 7.2 Hz, 2H), 1.98 – 1.81 (m, 2H).

^{13}C NMR (101 MHz, Chloroform-*d*): δ [ppm] = 179.4, 50.5, 31.0, 23.9.

5. Experimental Part

2,5-dioxopyrrolidin-1-yl 4-azidobutanoate (13) was synthesized referring to literature:[193]
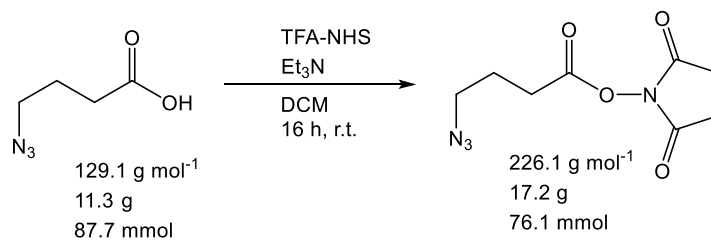
Compound **(12)** (87.7 mmol, 11.3 g) was dissolved in DCM (200 ml) and TFA-NHS (128 mmol, 27.0 g) and Et$_3$N (500 mmol, 51.0 g) were added. The solution was stirred at room temperature for 16 h, followed by the addition of DCM (100 ml). The organic layer was washed with aq. 0.1 M HCl (3 x 100 ml), saturated NaHCO$_3$ (2 x 100 ml) solution and dried over MgSO$_4$. After evaporation of the solvent, a highly viscous yellowish liquid remained, which became solid after 3 days.

Yield: 87 % (76.1 mmol, 17.2 g).

IR (cm^{-1}) = 2947 (C-H), 2097 (N$_3$), 1813, 1783, 1729 (C=O).

^{1}H NMR (400 MHz, Chloroform-d): δ [ppm] = 3.41 (t, J = 6.6 Hz, 2H), 2.80 (s, 4H), 2.69 (t, J = 7.2 Hz, 2H), 1.98 (p, J = 6.9 Hz, 2H).

^{13}C NMR (101 MHz, Chloroform-d): δ [ppm] = 169.2, 168.0, 50.0, 28.1, 25.6, 24.1.

5. Experimental Part

4-azido-*N*-(2-chloroethyl)butanamide (14) was synthesized according to literature:[23]
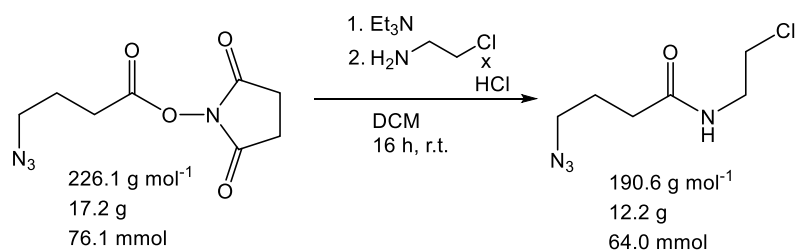
Compound **(13)** (76.1 mmol, 17.2 g) was dissolved in DCM (150 ml) and 2-chloroethylamine hydrochloride (150 mmol, 17.4 g) and Et_3N (360 mmol, 36.5 g, 50 ml) were added. The solution was stirred at room temperature for 16 h, followed by the addition of DCM (100 ml). The organic layer was washed with aq. 1 M HCl (3 x 100 ml) and $NaHCO_3$ (2 x 100 ml), dried over $MgSO_4$ and the solvent evaporated, giving the product as highly viscous yellowish liquid.

Yield: 84 % (64.0 mmol, 12.2 g).

IR (cm^{-1}) = 3296 (NH), 2935 (C-H), 2093 (N_3), 1646 (C=O).

^{1}H NMR (400 MHz, Chloroform-*d*): δ [ppm] = 6.57 (d, *J* = 5.8 Hz, 1H), 3.59 – 3.45 (m, 4H), 3.29 (t, *J* = 6.6 Hz, 2H), 2.25 (t, *J* = 7.3 Hz, 2H), 1.92 – 1.79 (m, 2H).

^{13}C NMR (101 MHz, Chloroform-*d*): δ [ppm] = 172.3, 50.7, 43.6, 41.2, 32.9, 24.7.

2-(3-azidopropyl)-2-oxazoline (15) was synthesized referring to literature:[19]
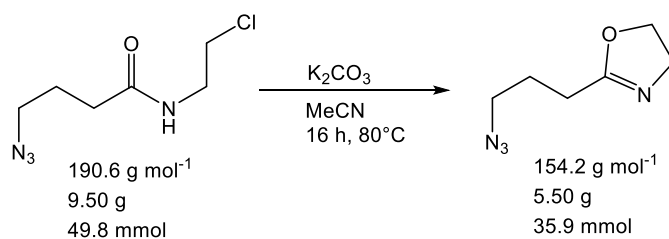
Compound **(14)** (49.8 mmol, 9.50 g) was dissolved in anhydrous MeCN (120 ml) and K_2CO_3 (65.8 mmol, 9.10 g) was added. The reaction mixture was heated up to 80°C for 16 h. Then the reaction mixture was allowed to cool to room temperature, filtered (0.4 µm syringe filter) and the solvent evaporated. The resulting product was then connected to fine vacuum line overnight. CaH_2 was added and the mixture stirred at room temperature for 16 h, followed by distillation under reduced pressure (0.5 mbar), giving the product as a colorless liquid.

Yield: 72 % (35.9 mmol, 5.50 g).

IR (cm^{-1}) = 2940 (C-H), 2093 (N_3), 1667 (N=C-O).

^{1}H NMR (400 MHz, Chloroform-*d*): δ [ppm] = 4.28 – 4.14 (m, 2H), 3.85 – 3.73 (m, 2H), 3.34 (t, *J* = 6.7 Hz, 2H), 2.33 (tt, *J* = 7.3, 1.4 Hz, 2H), 1.97 – 1.81 (m, 2H).

^{13}C NMR (101 MHz, Chloroform-*d*): δ [ppm] = 167.3, 77.2, 67.3, 54.5, 25.3, 25.0.

5.3.5 Synthesis of Alkyne Derivatives

3-[dimethyl(prop-2-yn-1-yl)ammonio]propane-1-sulfonate (16) was synthesized according to literature:[183]

83.1 g mol⁻¹	122.1 g mol⁻¹	205.2 g mol⁻¹

$83.1\ \text{g mol}^{-1}$ / $122.1\ \text{g mol}^{-1}$ / $205.2\ \text{g mol}^{-1}$
2.23 g / 3.60 g / 3.16 g
26.8 mmol / 29.5 mmol / 15.4 mmol
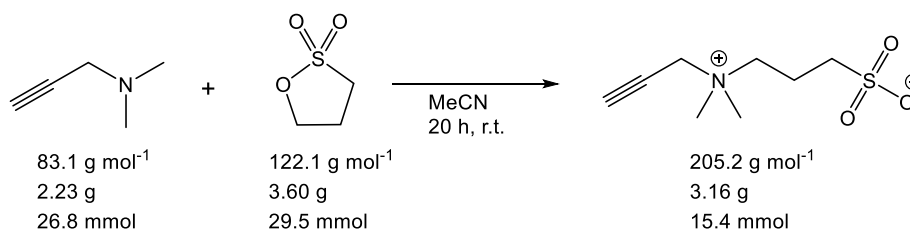
Propan-1,3-sulton (29.5 mmol, 3.6 g) was added to a solution of dimethylamino-2-propin (26.8 mmol, 2.23 g) in MeCN (57 ml) and stirred for 24 h at room temperature. The formed precipitate was filtered off, washed with small portions of cold MeCN and dried under reduced pressure.

Yield: 58 % (15.6 mmol, 3.2 g) of a white solid.

IR (cm⁻¹) = 3190 (H-C≡C), 2963 (C-H) 2123 (C≡C).

^{1}H NMR (400 MHz, Deuterium Oxide): δ [ppm] = 4.30 (s, 2H), 3.68 – 3.57 (m, 2H), 3.22 (s, 6H), 3.01 (t, J = 7.2 Hz, 2H), 2.33 – 2.20 (m, 2H).

^{13}C NMR (101 MHz, Deuterium Oxide + DMSO-d_6): δ [ppm] = 83.2, 71.9, 63.9, 55.9, 48.8, 19.8.

3-[dimethyl(prop-2-yn-1-yl)ammonio]propanoate (17) was synthesized according to literature:[183]

83.1 g mol^{-1}	72.1 g mol^{-1}	155.2 g mol^{-1}
1.99 g	1.90 g	3.24 g
24.0 mmol	26.5 mmol	20.9 mmol
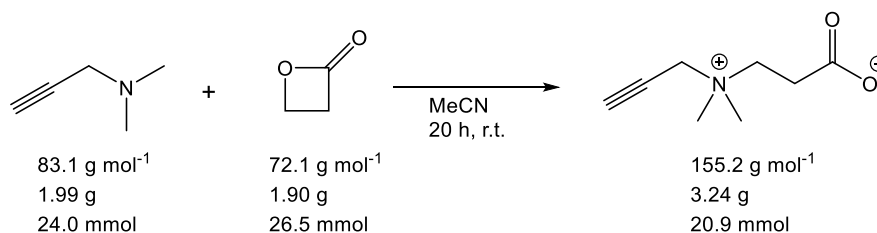
β-Propiolactone (26.5 mmol, 1.90 g) was added to a solution of dimethylamino-2-propin (24.0 mmol, 1.99 g) in MeCN (57 ml) and stirred for 18 h at room temperature. The formed precipitate was filtered off, washed with small portions of cold MeCN and dried under reduced pressure.

Yield: 88 % (20.6 mmol, 3.3 g) of a white solid.

IR (cm^{-1}) = 3190 (H-C≡C), 2963 (C-H) 2123 (C≡C).

^{1}H NMR (400 MHz, Deuterium Oxide): δ [ppm] = 4.25 (d, *J* = 2.0 Hz, 2H), 3.74 – 3.63 (m, 2H), 3.17 (s, 6H), 2.74 – 2.64 (m, 2H).

^{13}C NMR (101 MHz, Deuterium Oxide + DMSO-d_6): δ [ppm] = 177.5, 83.3, 62.9, 55.9, 51.9, 32.4.

5. Experimental Part

2-{2-[2-(prop-2-yn-1-yloxy)ethoxy]ethoxy}ethan-1-ol (18) was synthesized according to literature:[194]

150.2 g mol^{-1}	119.0 g mol^{-1}	188.3 g mol^{-1}
60.5 g	20.0 g	13.8 g
400 mmol	133 mmol	73.3 mmol
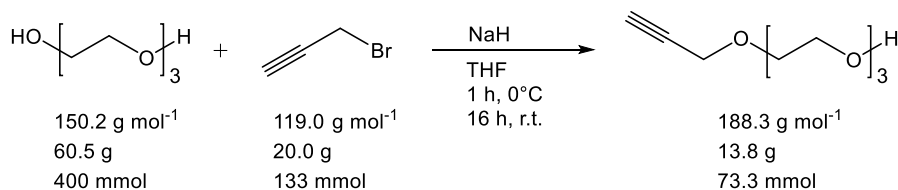
Triethylene glycol (400 mmol, 60.5 g, 54.0 ml) was dissolved in THF (200 ml) and NaH was added portion wise at 0°C. The reaction was stirred at 0 °C for 1 h and propargyl bromide (133 mmol, 20.0 g, 12.7 ml) was added, followed by stirring at room temperature for additional 16 h. During the reaction, the solution turned brownish and a white solid was formed. The reaction was quenched with ice cold water (100 ml) and the mixture extracted with dichloromethane (3 x 50 ml). The organic layer was washed with brine (2 x 50 ml), dried over anhydrous Na_2SO_4 and the solvent evaporated. The product was isolated by column chromatography (silica gel, EtOAc /n-hexane: 3/1), giving the title compound as a slightly yellowish oil.

Yield: 55 % (73.3 mmol, 13.8 g).

^{1}H NMR (400 MHz, Chloroform-*d*): δ [ppm] = 4.20 (d, *J* = 2.4 Hz, 2H), 3.75 – 3.64 (m, 10H), 3.63 – 3.59 (m, 2H), 2.60 – 2.45 (m, 1H), 2.43 (t, *J* = 2.4 Hz, 1H).

^{13}C NMR (101 MHz, Chloroform-*d*) δ [ppm] = 79.7, 74.7, 72.6, 70.8, 70.50, 70.47, 69.2, 61.9, 58.5.

2-{2-[2-(prop-2-yn-1-yloxy)ethoxy]ethoxy}ethyl 4-methylbenzenesulfonate (19) was synthesized according to literature:[195]
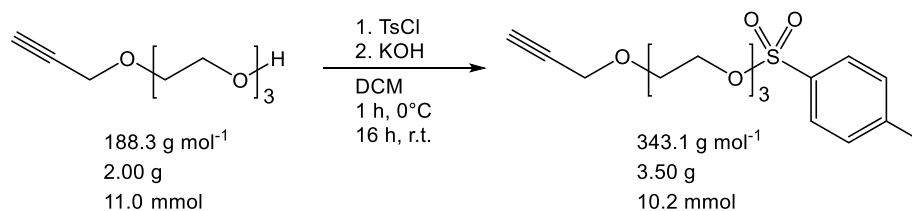
Compound **(19)** (11.0 mmol, 2.00 g) and 4-toluenesulfonyl chloride (12.0 mmol, 2.22 g) were dissolved in DCM (10 ml) and KOH (43.3 mmol, 2.38 g) was added at 0°C. The reaction mixture was stirred at room temperature until TLC indicated complete conversion of the educt, which was obtained after 16 h, and quenched with ice cold water (25 ml). The product was extracted with DCM (3 x 100 ml). The organic phases were combined and dried over $MgSO_4$ and solvent was removed under reduced pressure. The product appeared as colorless liquid.

Yield: 93 % (10.2 mmol, 3.50 g).

^{1}H NMR (400 MHz, Chloroform-*d*): δ [ppm] = 7.84 – 7.74 (m, 2H), 7.37 – 7.30 (m, 2H), 4.18 (d, *J* = 2.4 Hz, 2H), 4.17 – 4.14 (m, 2H), 3.71 – 3.66 (m, 4H), 3.66 – 3.61 (m, 2H), 3.58 (s, 4H), 2.44 (d, *J* = 0.6 Hz, 3H), 2.42 (t, *J* = 2.4 Hz, 1H).

^{13}C NMR (101 MHz, Chloroform-*d*) δ [ppm] = 144.9, 133.2, 130.0, 128.1, 79.7, 74.7, 70.9, 70.7, 70.6, 69.4, 69.2, 68.8, 58.5.

5. Experimental Part

N,N-dimethyl-2-{2-[2-(prop-2-yn-1-yloxy)ethoxy]ethoxy}ethan-1-amine **(20)** was synthesized according to literature:[196]

343.1 g mol^{-1}
8.65 g
25.0 mmol

215.4 g mol^{-1}
4.48 g
20.8 mmol
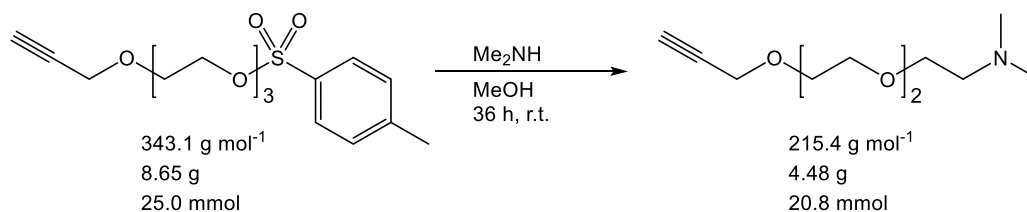
Compound **(20)** (25.0 mmol, 8.65 g) was dissolved in methanolic dimethylamine (100 mmol, 50.0 ml). The reaction was stirred at room temperature for 35 h and the solvent removed under reduced pressure. The remaining brownish residue was dissolved in water (50 ml ml) and extracted with DCM (5 x 30 ml). The combined organic phase was washed with slightly basic water (2 x 50 + 5 ml NH$_4$OH (25 % wt %)) and brine (2 x 50 ml), dried over MgSO$_4$ and the solvent evaporated.

Yield: 83 % (20.8 mmol, 4.48 g) of a yellowish oil.

^{1}H NMR (400 MHz, Chloroform-d): δ [ppm] = 4.19 (d, J = 2.4 Hz, 2H), 3.71 – 3.59 (m, 8H), 3.56 (t, J = 5.9 Hz, 2H), 2.49 (t, J = 5.9 Hz, 2H), 2.44 – 2.39 (m, 1H), 2.24 (s, 6H), 2.22 (d, J = 3.1 Hz, 6H).

^{13}C NMR (101 MHz, Chloroform-d): δ [ppm] = 79.8, 74.6, 70.7, 70.5, 70.5, 69.5, 69.2, 59.0, 58.5, 46.0.

3-{dimethyl{2-[2-(prop-2-yn-1-yloxy)ethoxy]ethyl}ammonio}propane-1-sulfonate (21) was synthesized according to literature:[183]

215.4 g mol⁻¹
2.00 g
9.29 mmol

337.0 g mol⁻¹
2.76 g
8.19 mmol
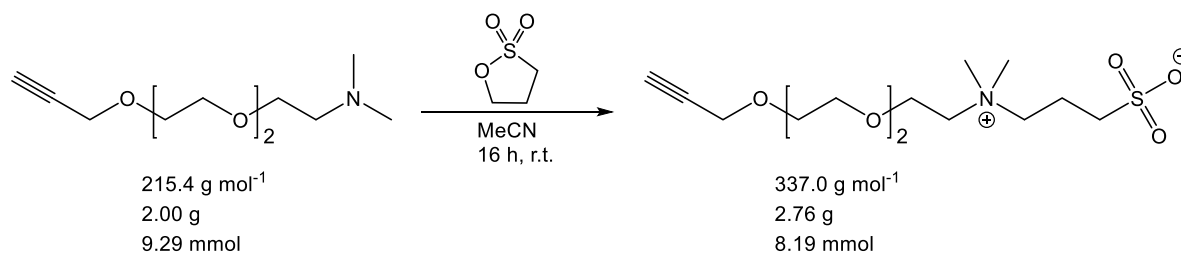
Compound **(21)** (9.29 mmol, 2.00 g) and 1,3-propane sultone (8.45 mmol, 1.03 g) were dissolved in MeCN (7 ml) and the resulting mixture stirred at room temperature for 16 h. A white precipitate was formed, which was filtered off and washed with diethyl ether (3 x 30 ml). The product was then dried under reduced pressure.

Yield: 97 % (8.19 mmol, 2.98 g).

^{1}H NMR (400 MHz, Deuterium Oxide): δ [ppm] = 4.25 (s, 2H), 3.98 (dq, J = 5.0, 2.5 Hz, 2H), 3.80 – 3.69 (m, 8H), 3.66 – 3.60 (m, 2H), 3.60 – 3.52 (m, 2H), 3.19 (s, 6H), 2.98 (t, J = 7.3 Hz, 2H), 2.30 – 2.20 (m, 2H), 2.07 (s, 1H).

^{13}C NMR (101 MHz, Deuterium Oxide + DMSO-d_6): δ [ppm] = 80.6, 77.7, 71.2, 71.0, 71.0, 70.2, 65.6, 65.0, 64.64, 64.61, 64.58, 59.4, 53.1, 53.1, 53.0, 48.9, 19.9.

5.3.6 Synthesis of 2-Alkyl-2-Oxazolines Monomers

2-isopropyl-2-oxazoline (22) and 2-*n*-propyl-2-oxazoline (23) were synthesized according to literature:[18]
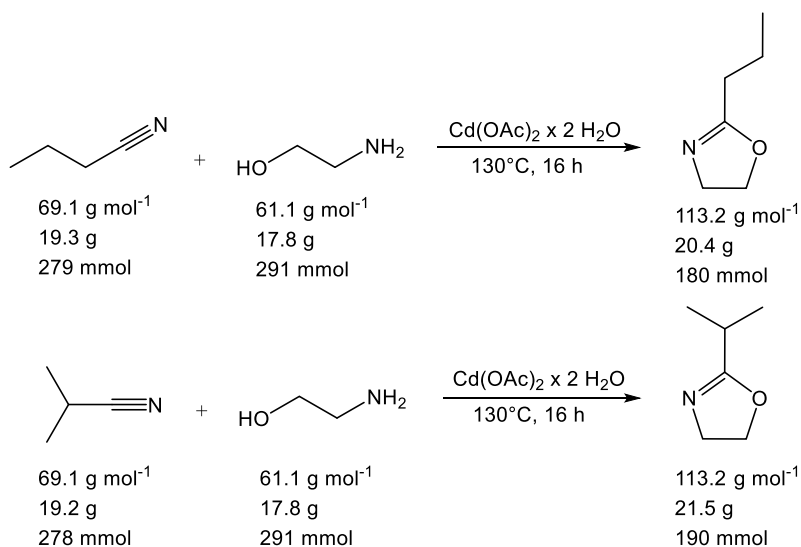
To 2-aminoethanol (291 mmol; 17.8 g) either butyronitrile (279 mmol, 19.3 g) or isobutryonitrile (278 mmol, 19.2 g), and $Cd(OAc)_2$ x 2 H_2O (15.0 mmol, 4.01 g) were added. The obtained solution was heated up to 130°C for 16 h and the respective products isolated by fractional distillation under reduced pressure.

Yield (2-*n*-propyl-2-oxazoline): 68 % (21.5 g, 190 mmol).

^{1}H NMR (400 MHz, Chloroform-*d*): δ [ppm] = 4.22 (td, *J* = 9.4, 0.5 Hz, 2H), 3.89 – 3.76 (m, 2H), 2.25 (tt, *J* = 7.8, 1.3 Hz, 2H), 1.74 – 1.59 (m, 2H), 0.97 (t, *J* = 7.4 Hz, 3H).

^{13}C NMR (101 MHz, Chloroform-*d*): δ [ppm] = 168.2, 66.9, 54.2, 29.7, 19.2, 13.6.

Yield (2-isopropyl-2-oxazoline): 65 % (20.4 g, 180 mmol).

^{1}H NMR (400 MHz, Chloroform-*d*): δ [ppm] = 4.30 – 4.17 (m, 2H), 3.88 – 3.76 (m, 2H), 2.56 (ddtd, *J* = 13.9, 8.1, 7.0, 5.8 Hz, 1H), 1.19 (d, *J* = 7.1 Hz, 6H).

^{13}C NMR (101 MHz, Chloroform-*d*): δ [ppm] = 172.2, 66.9, 54.0, 27.8, 19.3.

5.4 Synthesis of Photocrosslinkable Poly(2-Alkyl-2-Oxazoline)s

All polymers were synthesized by microwave assisted CROP, using MeOTf as initiator and acetonitrile (MeCN) as solvent. The general procedure is as follows:

For the microwave assisted CROP of the respective 2-oxazolines, an initiator stock solution of varying concentrations (0.016-0.127 mmol ml^{-1}) was prepared. The respective 2-oxazolines as well as the initiator stock solution were mixed under inert gas conditions (glove box) in a microwave reaction vessel and the polymerization performed by using a specific temperature program (specific details are provided for each polymer system further below). After the polymerization process, the reaction was quenched with either morpholine, water or Et$_3$N and stirred at room temperature for additional 4 h. The polymers were then precipitated in ice-cold diethyl ether and isolated by either freeze-drying from 1,4-dioxane or drying under reduced pressure at 50°C.

5.4.1 Synthesis of Poly(2-Alkyl-2-Oxazoline)s

Dependence of Molar Mass Distribution on Nature of the Monomer:

Temperature Program:
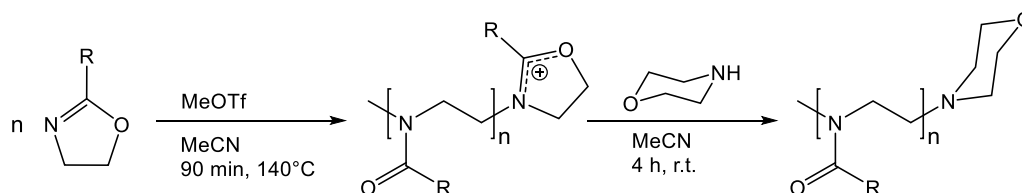
Power: 140 Watt, Ramp: 2 min, Hold Time: 90 min, Temperature: 140°C.

All polymerization reactions were quenched with morpholine (2.29 mmol, 0.20 g, 0.2 ml) and isolated by freeze-drying form 1,4-dioxane.

Table 14: Dependence of molar mass distribution on nature of the monomer.

Exp.-Nr.	Monomer	Monomer,$_{feed}$ [mg/mmol]	Yield [%/mg]	$\bar{M}_{w,\,SEC}$[a] [$\times 10^3$ g mol^{-1}]	Dispersity Đ[b]
PEC089a1	EtOxa	537 / 5.42	78 / 478	36.9	1.17
PEC089a2	*n*-PrOxa	605 / 5.35	61 / 369	33.3	1.18
PEC089a3	isoPrOxa	607 / 5.36	81 / 433	21.6	1.13

Initiator stock solution (MeCN/MeOTf): 2 ml (0.035 mmol, 5.8 mg ≙ 2.9 mg ml^{-1} of MeOTf). Monomer/Initiator (M/I) Ratio: 155/1. [a]As determined by SEC analysis. [b]Đ as calculated by SEC analysis.

5. Experimental Part

Dependence of Molar Mass Distribution on Monomer-Initiator Ratio:

Temperature Program:
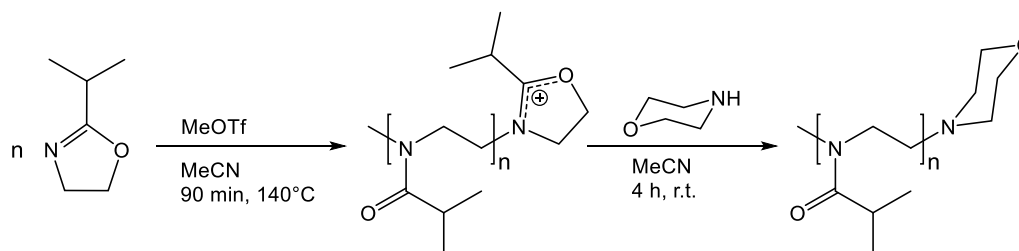
Power: 140 Watt, Ramp: 2 min, Hold Time: 90 min, Temperature: 140°C.

All polymerization reactions were quenched with morpholine (2.29 mmol, 0.20 g, 0.2 ml) and isolated by drying at 50°C under reduced pressure.

Table 15: Dependence of molar mass distribution on monomer-initiator ratio.

Exp.-Nr.	M/I Ratio and c (MeOTf) [mmol][a]	Monomer,$_{feed}$ [mg/mmol]	Yield [%/mg]	$\bar{M}_{w,\,SEC}$[b] [× 10^3 g mol^{-1}]	Dispersity Đ[c]
PEC092a1	45 / 0.127	644 / 5.70	66 / 425	8.38	1.14
PEC092b2	67 / 0.085	645 / 5.71	71 / 458	11.7	1.14
PEC092b1	82 / 0.069	641 / 5.67	72 / 468	13.7	1.15
PEC092c1	156 / 0.037	652 / 5.77	61 / 397	20.8	1.12

[a]Initiator stock solution (MeCN/MeOTf): 2 ml. [b]As determined by SEC analysis. [c]Đ as calculated by SEC analysis.

5. Experimental Part

Dependence of Molar Mass Distribution on Reaction Temperature:

Temperature Program:

Power: 140 Watt, Ramp: 2 min, Hold Time: 90 min, Temperature: 120, 130 and 140°C.
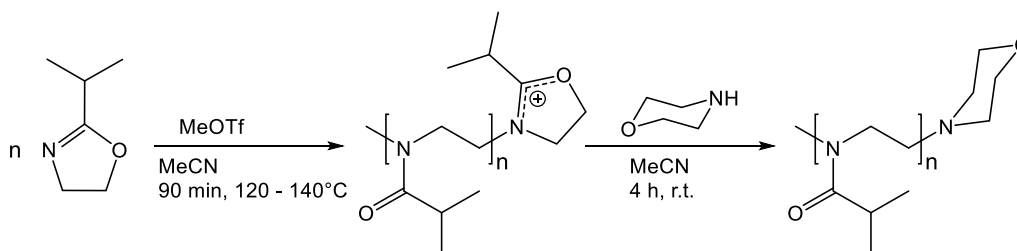
All polymerization reactions were quenched with morpholine (2.29 mmol, 0.20 g, 0.2 ml) and isolated by drying under reduced pressure at 50°C.

Table 16: Dependence of molar mass distribution on reaction temperature.

Exp.-Nr.	Reaction Temp. / °C	Monomer,feed [mg/mmol]	Yield [%/mg]	$\bar{M}_{w, SEC}$[a] [$\times 10^3$ g mol^{-1}]	Dispersity Đ[b]
PEC093d2	120	648 / 5.73	67 / 430	10.9	1.11
PEC093d1	130	639 / 5.65	70 / 447	11.4	1.20
PEC093b2	140	645 / 5.71	65 / 419	11.7	1.14

Initiator stock solution (MeCN/MeOTf): 2 ml (0.079 mmol, 13.0 mg ≙ 6.5 mg ml^{-1} of MeOTf). Monomer/Initiator (M/I) Ratio: 72/1. [a]As determined by SEC analysis. [b]Đ as calculated by SEC analysis.

End group Functionalization of Poly(2-Alkyl-2-Oxazoline):

Temperature Program:

Power: 140 Watt, Ramp: 2 min, Hold Time: 90 min, Temperature: 120.
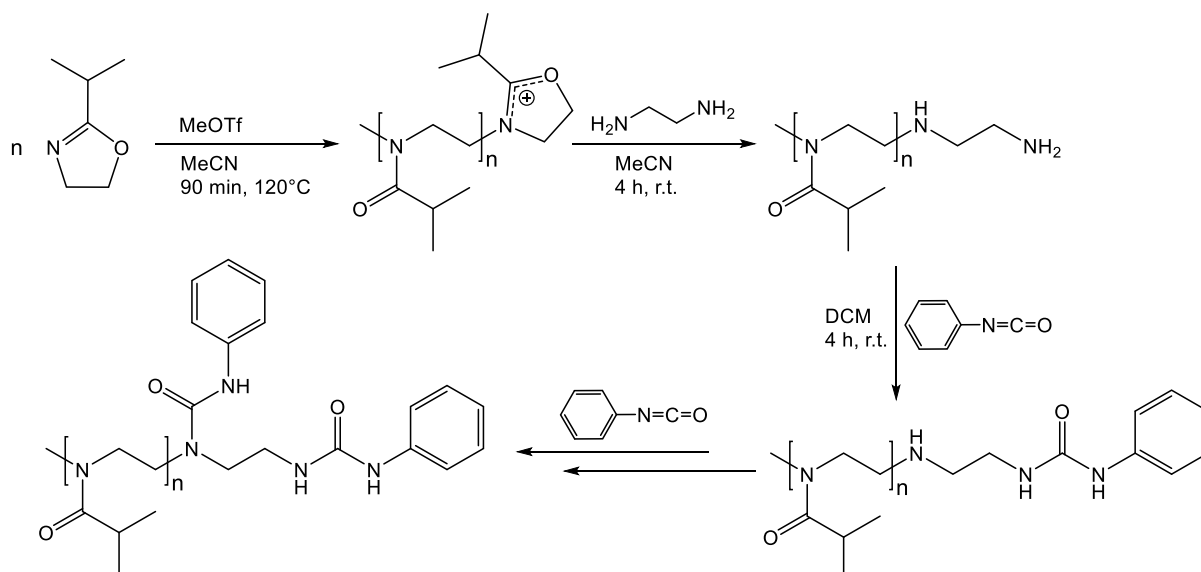
The polymerization reaction was quenched with morpholine (2.29 mmol, 0.20 g, 0.2 ml) and isolated by drying under reduced pressure at 50°C.

Table 17: End group modification of poly(2-alkyl-2-oxazoline)s.

Exp.-Nr.	Reaction Temp. / °C	Monomer,$_{feed}$ [mg/mmol]	Yield [%/mg]	$\overline{M}_{w, SEC}$[a] [$\times 10^3$ g mol^{-1}]	Dispersity Đ[b]
PEC094a1	120	635 / 5.62	75 / 476	11.1	1.11

Initiator stock solution (MeCN/MeOTf): 2 ml (0.079 mmol, 13.0 mg ≙ 6.5 mg ml^{-1} of MeOTf). Monomer/Initiator (M/I) Ratio: 72/1. [a]As determined by SEC analysis. [b]Đ as calculated by SEC analysis.

For the determination of the amine end group functionality, the respective polymer (100 mg; PEC094a1) was dissolved in DCM (7.5 ml) and phenyl isocyanate (1 ml; distilled from P$_2$O$_5$ before use) was added. The resulting reaction mixture was stirred over night at room temperature and the polymer precipitated in ice-cold diethyl ether, followed by drying overnight under reduced pressure.

Yield: 63 % (63 mg)

5.4.2 Synthesis of Photocrosslinkable Poly(2-Alkyl-2-Oxazoline)s

Temperature Program:

Power: 140 Watt, Ramp: 2 min, Hold Time: 90 min, Temperature: 140°C
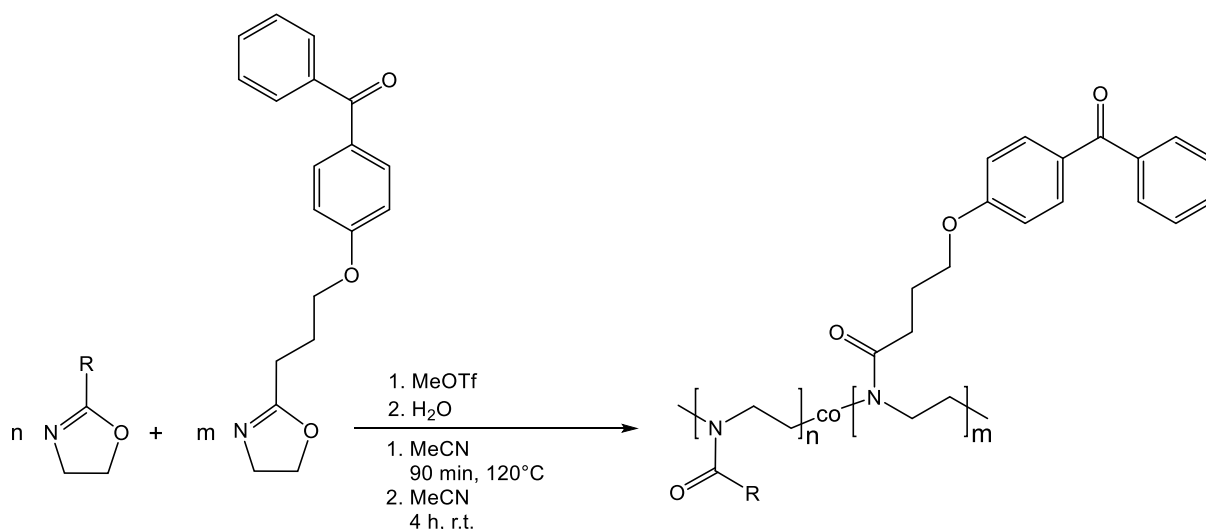
All polymerization reactions were quenched with water (12.5 mmol, 0.20 g, 0.2 ml) and isolated by drying under reduced pressure at 50°C.

Table 18: Monomer feed synthesis of photocrosslinkable poly(2-alkyl-2-oxazoline)s, M/I = 150.

Exp.-Nr.	Monomer,$_{feed}$ [mg/mmol]				M/I
	n-PrOxa	isoPrOxa	EtOxa	BPOxa	Ratio[a]
PEC100a1	-	-	601 / 6.07	20.0 / 0.06	149
PEC100a2	-	-	597 / 6.02	50.0 / 0.16	150
PEC100a3	-	-	592 / 5.97	100 / 0.32	152
PEC100a4	-	-	537 / 5.42	200 / 0.65	147
PEC100a5	-	650 / 5.75	-	100 / 0.32	148
PEC100a6	643 / 5.68	-	-	100 / 0.32	146
PEC100a7	326 / 2.88	327 / 2.89	-	100 / 0.32	143
PEC100a8	-	485 / 4.89	154 / 1.55	110 / 0.36	159
PEC116a	-	-	-	425 / 1.38	152[b]

[a]Initiator stock solution (MeCN/MeOTf): 2 ml (0.041 mmol, 6.75 mg ≙ 3.38 mg ml^{-1} of MeOTf). Monomer/Initiator (M/I) Ratio: 150/1. [b]Initiator stock solution (MeCN/MeOTf): 2 ml (0.005 mmol, 1.49 mg ≙ 0.75 mg ml^{-1} of MeOTf).

5. Experimental Part

<u>Temperature Program:</u>

Power: 140 Watt, Ramp: 2 min, Hold Time: 90 min, Temperature: 140°C

All polymerization reactions were quenched with water (12.5 mmol, 0.20 g, 0.2 ml) and isolated by drying under reduced pressure at 50°C.

Table 19: Monomer feed synthesis of photocrosslinkable poly(2-alkyl-2-oxazoline)s, M/I = 300.

Exp.-Nr.	Monomer,$_{feed}$ [mg/mmol]				M/I Ratio[a]
	n-PrOxa	isoPrOxa	EtOxa	BPOxa	
PEC103a1	-	1390 / 12.3	-	71 / 0.23	293
PEC103a2	-	1310 / 11.6	-	158 / 0.51	283
PEC103a3	230 / 2.03	1120 / 9.90	-	83 / 0.27	286
PEC103a4	460 / 4.07	910 / 8.04	-	87 / 0.28	290
PEC103a5	-	1108 / 9.79	231 / 2.33	83 / 0.27	290
PEC103a6	-	905 / 8.00	395 / 3.98	71 / 0.23	304
PEC103a7	894 / 7.90	456 / 4.03	-	92 / 0.30	287
PEC103a8	-	700 / 6.19	600 / 6.05	95 / 0.31	294
PEC103a9	1350 / 11.9	-	-	86 / 0.28	286
PEC103a10	-	355 / 3.14	908 / 9.16	96 / 0.31	296
PEC103a11	-	-	1268 / 12.8	96 / 0.31	307

[a]Initiator stock solution (MeCN/MeOTf): 4 ml (0.043 mmol, 7 mg $\triangleq$ 1.75 mg ml^{-1} of MeOTf). Monomer/Initiator (M/I) Ratio: 300/1.

5.4.3 Synthesis of Azide Containing Poly(2-Alkyl-2-Oxazoline)s

Copolymerization of 2-ethyl-2-oxazoline and 2-isopropyl-2-oxazoline with 2-(3-azidopropyl)-2-oxazoline:

Temperature Program:

Power: 140 Watt, Ramp: 2 min, Hold Time: 90 min, Temperature: 120°C
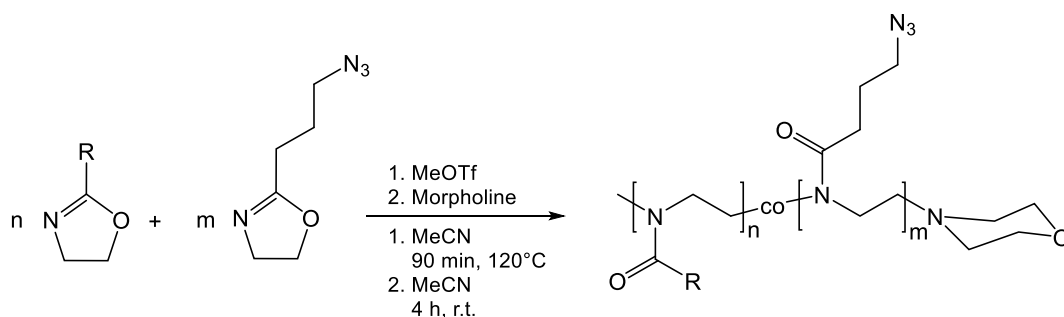
All polymerization reactions were quenched with morpholine (12.5 mmol, 0.20 g, 0.2 ml) and isolated by drying under reduced pressure at 50°C.

Table 20: Monomer feed copolymerization of 2-alkyl-2-oxazolines and 2-AzOxa.

Exp.-Nr.	Monomer,$_{feed}$ [mg/mmol]			M/I Ratio[a]
	isoPrOxa	EtOxa	AzOxa	
PEC097a1	604 / 5.37	-	10 / 0.06	155
PEC097a2	598 / 5.31	-	20 / 0.13	155
PEC097a3	580 / 5.23	-	46 / 0.30	158
PEC097a4	549 / 4.88	-	82 / 0.53	155
PEC097a5	427 / 3.79	-	253 / 1.64	147
PEC097a6	183 / 1.53	-	589 / 3.82	145
PEC097b1	-	607 / 5.30	9 / 0.06	143
PEC097b2	-	600 / 4.59	19 / 0.12	143
PEC097b3	-	592 / 4.47	39 / 0.25	143
PEC097b4	-	552 / 4.29	80 / 0.52	146
PEC097b5	-	428 / 3.31	245 / 1.59	140
PEC097b6	-	173 / 1.45	585 / 3.79	150
PEC095a1	-	-	630 / 4.09	48
PEC095a2	-	-	660 / 4.28	56

[a]Initiator stock solution (MeCN/MeOTf): 2 ml (0.037 mmol, 6 mg ≙ 3 mg ml^{-1} of MeOTf). Monomer/Initiator (M/I) Ratio: 150/1 and 2 ml (0.080 mmol, 13 mg ≙ 6.5 mg/ml of MeOTf) Monomer/Initiator (M/I) Ratio: 50/1.

5.4.4 Synthesis of Photocrosslinkable and Azide Containing Poly(2-Alkyl-2-Oxazoline)s

Temperature Program:

Power: 140 Watt, Ramp: 2 min, Hold Time: 90 min, Temperature: 120°C
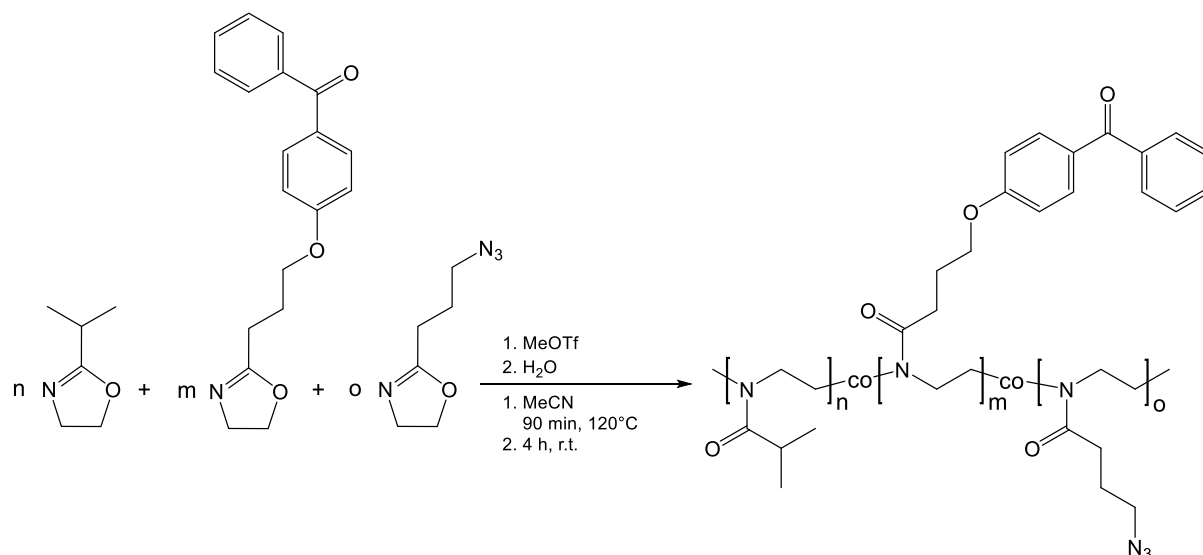
All polymerization reactions were quenched with water (12.5 mmol, 0.20 g, 0.2 ml) and isolated by drying under reduced pressure at 50°C.

Table 21: Monomer feed copolymerization of 2-alkyl-2-oxazolines, BPOxa and 2-AzOxa

Exp.-Nr.	Monomer,feed [mg/mmol]			M/I Ratio[a]
	isoPrOxa	BPOxa	AzOxa	
PEC112a1	782 / 6.92	62 / 0.20	60 /0.39	313
PEC112a2	778 / 6.88	59 / 0.19	59 / 0.38	311
PEC112a3	780 / 6.90	69 / 0.22	62 / 0.40	314
PEC112a4	783 / 6.93	62 / 0.20	60 / 0.39	313
PEC112a5	788 / 6.97	60 / 0.19	61 / 0.40	315
PEC115a1	794 / 7.01	59 / 0.19	126 / 0.82	334
PEC115a2	791 / 6.99	57 / 0.18	118 / 0.77	331
PEC115a3	793 / 7.00	58 / 0.19	123 / 0.80	333
PEC115a4	791 / 6.99	58 / 0.19	121 / 0.78	332

[a]Initiator stock solution (MeCN/MeOTf): 1.5 ml (0.024 mmol, 3.50 mg $\triangleq$ 2.70 mg ml^{-1} of MeOTf). Monomer/Initiator (M/I) Ratio: 300/1.

Yield: 81 % (3.65 g) for the combined reaction yields of PEC112a1-a5

Composition: Poly(isoPrOxa$_{91}$-BPOxa$_3$-AzOxa$_6$)

Yield: 73 % (2.85 g) for the combined reaction yields of PEC115a1-a5

Composition: Poly(isoPrOxa$_{87}$-BPOxa$_3$-AzOxa$_{10}$)

5.5 Click Reaction of Photocrosslinkable and Azide Containing Poly(2-Alkyl-2-Oxazoline)s

For the modification 500 mg (PEC112) and 400 mg (PEC115) of the respective azide containing polymers were dissolved at room temperature in a mixture of H_2O/t.-BuOH (20 ml; 1/1 ratio). Then the respective alkyne was added, followed by the addition of $CuSO_4$ x 5 H_2O (0.28 mmol; 70 mg) and NaAscorbat (0.50 mmol; 100 mg). The reaction solution was stirred for 16 h and then dialyzed against water (Membrane MWCO = 3500 Da) for 3 days. The modified polymer was then isolated by freeze-drying from water.

Alkyne:

R:
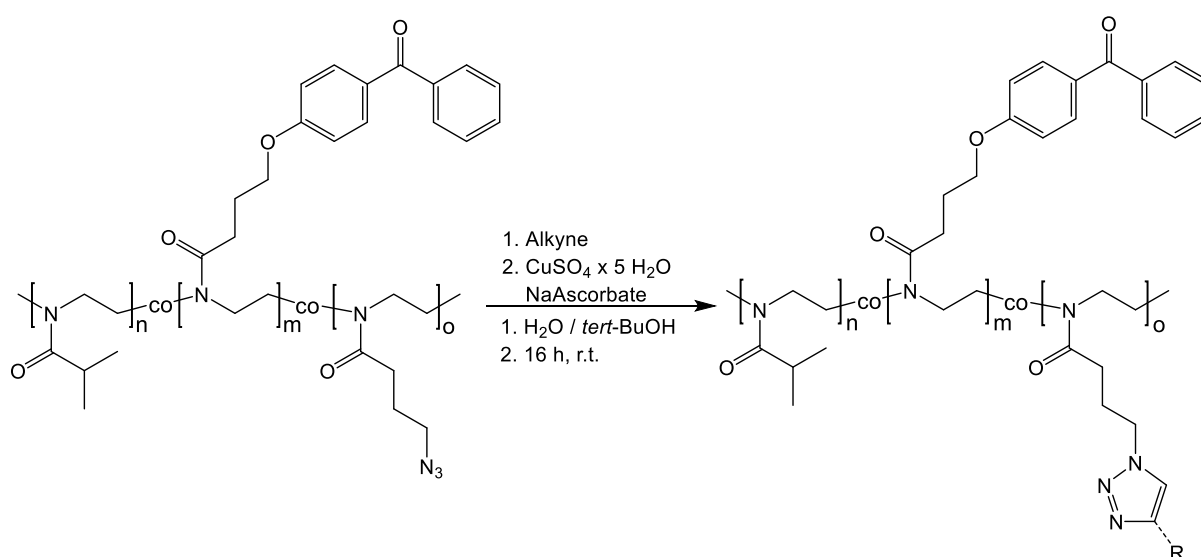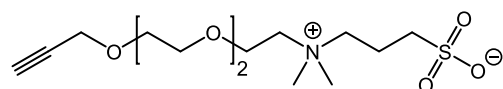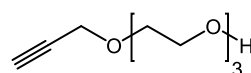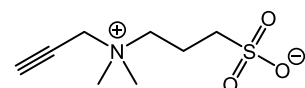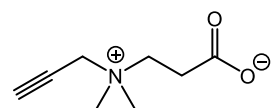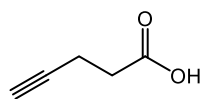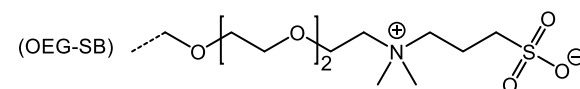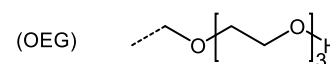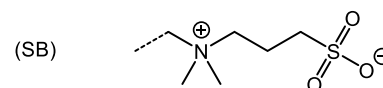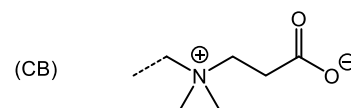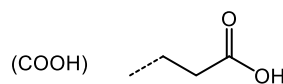
Table 22: Click reaction of poly(isoPrOxa$_{91}$-BPOxa$_3$-AzOxa$_6$)

			Modification Unit			
	PEC112-N$_3$	PEC112-COOH	PEC112-SB	PEC112-CB	PEC112-OEG	PEC112-OEG-SB
Alkyne,$_{Feed}$ [mg/mmol]	-/-	80 / 0.82	85 / 0.42	85 / 0.45	100 / 0.53	125 / 0.37
Polymer Yield [mg/%]	-/-	391 / 78	407 / 81	444 / 89	370 / 74	472 / 94

Table 23: Click reaction of poly(isoPrOxa$_{87}$-BPOxa$_3$-AzOxa$_{10}$)

			Modification Unit			
	PEC115-N$_3$	PEC115-COOH	PEC115-SB	PEC115-CB	PEC115-OEG	PEC115-OEG-SB
Alkyne,$_{Feed}$ [mg/mmol]	-/-	80 / 0.82	85 / 0.42	85 / 0.45	100 / 0.53	125 / 0.37
Polymer Yield [mg/%]	-/-	-/-	400 / 100	340 / 85	310 / 78	300 / 75

5.6 Synthesis of Photocrosslinkable Poly(*N*-isopropylacrylamide)

N-(4-benzoylphenyl)acrylamide (24) was synthesized according to literature:[197]

197.2 g mol^{-1}	90.5 g mol^{-1}	251.3 g mol^{-1}
4.00 g	2.39 g	1.69 g
20.3 mmol	26.4 mmol	6.73 mmol
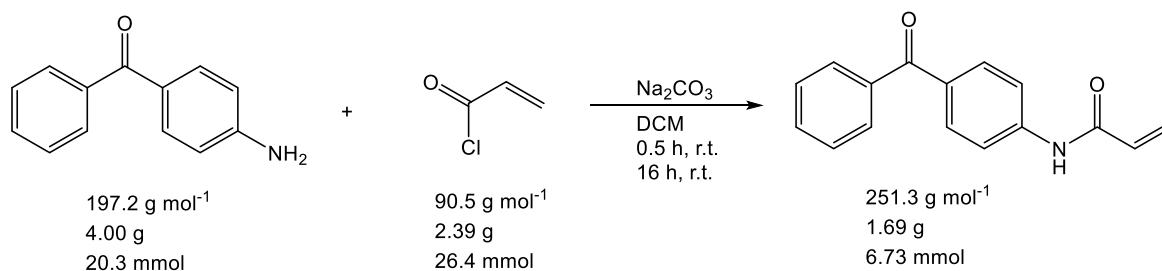
For the synthesis of the title compound, 4-aminobenzophenone (20.3 mmol, 4.00 g) was dissolved in DCM (50 ml) and the solution cooled with an ice-water bath to 0°C. Na$_2$CO$_3$ (20.3 mmol, 2.15 g) was added and the resulting dispersion stirred for 20 min at 0°C. Acryloyl chloride (26.4 mmol, 2.39g, 2.12 ml) was diluted with DCM (50 ml) and added dropwise to the dispersion at 0°C. After complete addition, the reaction mixture was allowed to warm to room temperature at stirred for additional 16 h. The formed solid was filtered off and the reaction extracted with aq. NaHCO$_3$ solution (5 wt%, 3 x 100 ml) and water (3 x 100 ml). The organic layer was separated and dried over MgSO$_4$, filtered and the solvent evaporated, giving the title compound as a brownish solid.

Yield: 33 % (6.73 mmol, 1.69 g).

^{1}H-NMR (400 MHz, Chloroform-*d*): δ [ppm] = 7.85 – 7.46 (m, 9H); 6.51 – 6.47 (dd, 1H); 6.31 – 6.24 (dd, 1H); 5.85 – 5.83 (dd, 1H)

5. Experimental Part

Terpolymer Synthesis

113.2 g mol^{-1}	86.1 g mol^{-1}	251.3 g mol^{-1}
2.01 g	100 mg	45 mg
17.8 mmol	1.20 mmol	0.18 mmol
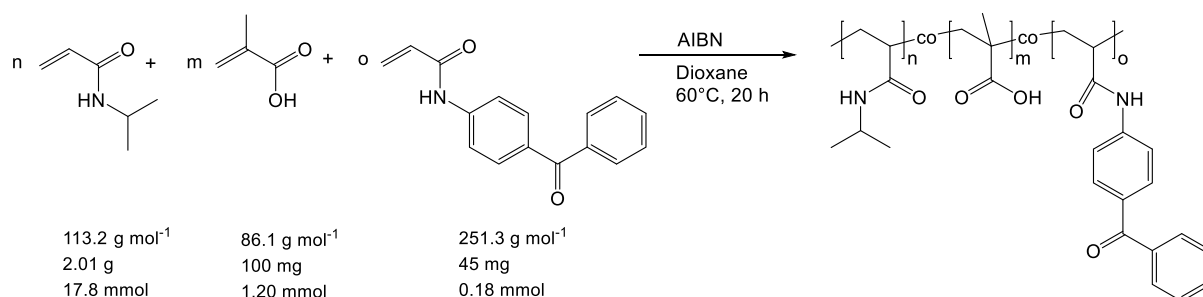
A 50 ml Schlenk flask was charged with 1,4-dioxane (20 ml). Oxygen was then removed by degassing of the solvent and flushing with Argon. This procedure was repeated three times, followed by the addition of NIPPAm (17.8 mmol, 2.01 g), MAA (1.2 mmol, 0.1 g) and BPAAm (0.18 mmol, 0.045 g). After stirring of the solution at room temperature for 30 min, AIBN (0.22 mmol, 0.036 g) was added and the solution was heated up 60°C for 18 h. After cooling to room temperature, the resulting polymer was precipitated in ice cold Et$_2$O, filtered off and washed again with Et$_2$O several times. The polymer was the isolated by drying at 50°C under reduced pressure.

Yield: 77 % (1.66 g)

5.7 Synthesis of Photocrosslinkable Carboxymethyl Dextran

4-(2,3-epoxypropyloxy)-benzophenone (25) was synthesized according to literature:[86]

198.2 g mol^{-1}	92.5 g mol^{-1}	254.3 g mol^{-1}
10.0 g	35.4 g	9.00 g
50.5 mmol	383 mmol	35.4 mmol
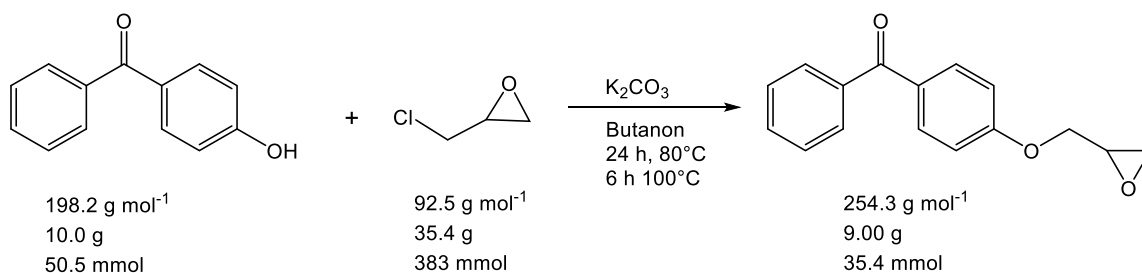
For the synthesis of the title compound, 4-hydroxybenzophenone (50.5 mmol, 10.0 g) was dissolved in freshly distilled butanone (160 ml) and anhydrous K_2CO_3 (120 mmol, 12.0 g) was added. Then epichlorohydrin (383 mmol, 30 ml, 35.4 g) was added dropwise (5 ml/min) and the reaction mixture stirred at 80°C for 24 h, followed by stirring at 100°C for additional 6 h. After cooling to room temperature, the obtained solid material was filtered off, washed with small portions of butanone and discarded. The excess of epichlorohydrin and butanone was removed under reduced pressure and the remaining residue redissolved in DCM (15 ml). The organic layer was washed with water (3 x 10 ml), separated and dried over $MgSO_4$. DCM was removed under reduced pressure and the obtained raw product recrystallized from ethanol.

Yield: 71 % (35.4 mmol, 9.00 g).

^{1}H-NMR (400 MHz, Chloroform-*d*): δ [ppm] = 7.00 – 7.99 (various m, Ar H), 4.33 (d, 1H), 4.04 (d, 1H), 3.39 (m, 1H), 2.94 (m, 1H), 2.79 (d, 1H).

5. Experimental Part

Dextran Modification

For the synthesis of photocrosslinkable carboxymethylated dextrans, dextrans of different molecular weights were chosen. The general modification procedure is as follows:

Benzophenone modified Dextran

The respective dextran was dissolved in DMSO (100 ml) and NaH was added. The obtained solution was stirred for 30 min at room temperature, followed by the addition of EBP and stirring of the solution for another 20 h at room temperature. Then water (200 ml) was added and the dextran precipitated in acetone (750 ml), filtered off and washed with acetone until a colorless filtrate was obtained. The obtained product was then dried under reduced pressure.

Exp.-Nr.	Dextran $\bar{M}_w$ [$\times 10^3$ g mol^{-1}]	Weighed Portions			Degree of Substitution EBP	Yield / %
		Dextran [g]	NaH [g /mmol]	EBP [g /mmol]		
PEC055a	2000	1.07	0.50 / 20.83	0.81 / 3.15	NMR inaccurate	71
PEC055b	200	1.06	0.50 / 20.83	0.80 / 3.15	0.35	65
PEC055c	75	1.00	0.49 / 20.42	0.80 / 3.15	0.35	66
PEC055d	20	1.08	0.50 / 20.83	0.79 / 3.15	0.29	70

Carboxymethylation of EBP-Dextran

The modified dextran of step one was dissolved in water and NaOH (8 M) was added. After 1 h stirring at room temperature NaClOAc was added and the mixture stirred for another 5 d. The slightly yellowish solution was dropped into MeOH (200 ml). The precipitated polymer was filtered off and washed several times with MeOH/Water (Ratio 90:10) until a negative chloride ion test was obtained and finally dried under reduced pressure.

Exp.-Nr.	Dextran $\bar{M}_w$ [$\times 10^3$ g mol^{-1}]	Weighed Portions				Degree of Substitution AcO$^-$Na$^+$	Yield / %
		EBP-Dextran [g]	Water [ml]	NaOH 8M [ml]	AcClO$^-$Na$^+$ [g / mmol]		
PEC055n	2000	0.25	5.0	1.60	0.55 / 4.72	0.75	55
PEC055o	200	0.25	5.0	1.60	0.55 / 4.72	0.81	59
PEC055p	75	0.25	5.0	1.60	0.55 / 4.72	0.79	51
PEC055q	20	0.25	5.0	1.60	0.55 / 4.72	0.93	61

5.8 Unsuccessful Synthesis

5.8.1 Synthesis of 3-{dimethyl{2-[2-(prop-2-yn-1-yloxy)ethoxy]ethyl}ammonio}propanoate

This chapter describes different approaches for the synthesis of EO_2-carboxybetaine combinations, similar to the compound synthesized in **Chapter 5.3.5**.

1.)

215.4 g mol^{-1}
2.00 g
9.29 mmol

287.4 g mol^{-1}
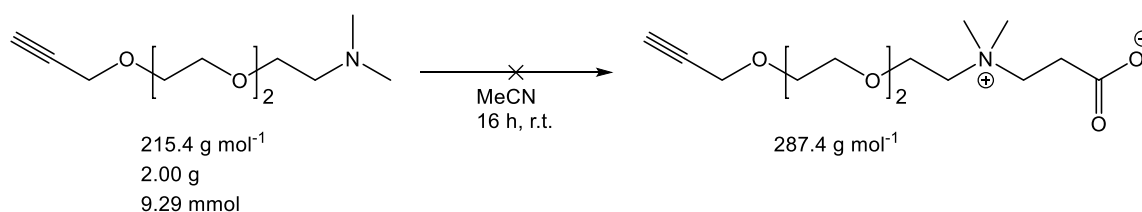
EO_2-DMAm (0.93 mmol, 200 mg) and β-propiolactone (1.02 mmol, 73.6 mg) were dissolved in MeCN (2 ml) and stirred for 16 h at room temperature. As TLC indicated no conversion of the educt, the reaction temperature was raised to 50°C for 24 h. TLC indicated still no conversion of the educt.

In a second approach, the reaction was performed, using β-propiolactone as solvent. The reaction mixture was stirred for 16 h at room temperature. A white precipitate was formed, which was filtered off and dried under reduced pressure. ^{1}H-NMR indicated that the title compound was not obtained.

2.)

215.4 g mol^{-1}
2.00 g
9.29 mmol

287.4 g mol^{-1}
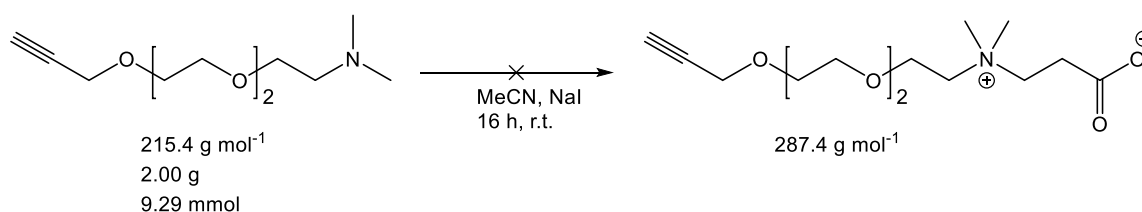
A third approach included the addition of NaI, which was added to get a better leaving group. Therefore, EO_2-DMAm (0.45 mmol, 100 mg) and β-propiolactone (051 mmol, 36.8 mg) were dissolved in MeCN. The sodium iodide (0.046 mmol, 6.90 mg) was added and the resulting solution was stirred at room temperature for 16 h. A white solid was formed during the reaction, which was removed and analyzed. The recorded ^{1}H-NMR spectrum indicated that the desired product was not formed.

5. Experimental Part

3.)

215.4 g mol^{-1}
2.00 g
9.29 mmol

316.4 g mol^{-1}

287.4 g mol^{-1}
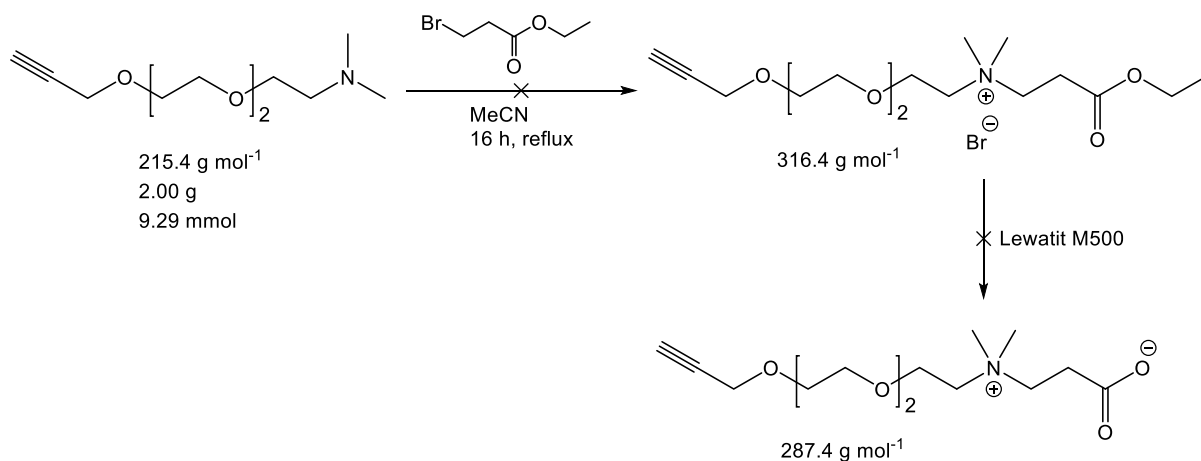
For the synthesis of the title compound, another approach was tested, using EO$_2$-DMAm (0.90 mmol, 200 mg) and ethyl 3-bromopropionate (0.95 mmol, 172 mg) dissolved in MeCN (1.5 ml). The resulting reaction mixture was stirred at 60°C for 3 days.

The same reaction was performed by dissolving EO$_2$-DMAm (0.90 mmol, 200 mg) in ethyl 3-bromopropionate (3.80 mmol, 680 mg). The resulting reaction mixture was also stirred at 60°C for days. In both cases, the desired product was not formed.

5. Experimental Part

5.8.2 Synthesis of 3-{dimethyl{2-[2-(prop-2-yn-1-yloxy)ethoxy]ethyl}ammonio}butanoate

4.)

215.4 g mol^{-1}
2.00 g
9.29 mmol

330.4 g mol^{-1}

301.4 g mol^{-1}
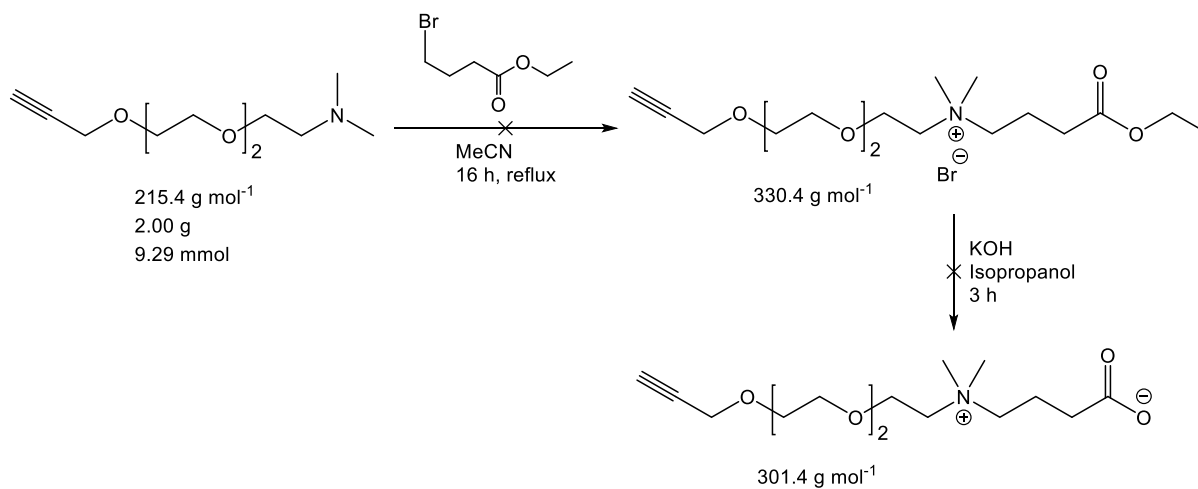
The last approach of synthesizing a combination of a carboxybetaine and oligoethylene glycol, was done by dissolving EO$_2$-DMAm (0.70 mmol, 150 mg) and ethyl 4-bromobutyrate (0.77 mmol, 150 mg) in MeCN (2 ml). The resulting reaction mixture was heated to reflux for 16 h and then allowed to cool to room temperature. MeCN was evaporated under reduced pressure, but the desired product was not formed.

6. References

6. References

1.   Fan, X.; White, W. M.; Shopova, S. I.; Zhu, H.; Suter, J. D.; Sun, Y., Sensitive optical biosensors for unlabeled targets: A review. *Analytica Chimica Acta* **2008,** (620), 8-26.

2.   Sang, S.; Zhang, W.; Zhao, Y., Review on the Design Art of Biosensors. In *State of the Art in Biosensors - General Aspects*, Rinken, T., Ed. InTech: Rijeka, 2013; p Ch. 04.

3.   Borisov, S. M.; Wolfbeis, O. S., Optical Biosensors. *Chemical Reviews* **2008,** *108* (2), 423-461.

4.   Damborský, P.; Švitel, J.; Katrlík, J., Optical biosensors. *Essays In Biochemistry* **2016,** *60* (1), 91-100.

5.   Toma, M.; Jonas, U.; Mateescu, A.; Knoll, W.; Dostalek, J., Active Control of SPR by Thermoresponsive Hydrogels for Biosensor Applications. *J Phys Chem C Nanomater Interfaces* **2013,** *117* (22), 11705-11712.

6.   Frascella, F.; Petri, C.; Ricciardi, S.; Napione, L.; Munzert, P.; Jonas, U.; Dostalek, J.; Bussolino, F.; Pirri, C. F.; Descrovi, E., Hydrogel-Terminated Photonic Crystal for Label-Free Detection of Angiopoietin-1. *Journal of Lightwave Technology* **2016,** *34* (15), 3641-3645.

7.   Lowe, S.; O'Brien-Simpson, N. M.; Connal, L. A., Antibiofouling polymer interfaces: poly(ethylene glycol) and other promising candidates. *Polym. Chem.* **2015,** *6* (2), 198-212.

8.   Kobayashi, S.; Uyama, H., Polymerization of cyclic imino ethers: From its discovery to the present state of the art. *Journal of Polymer Science Part A: Polymer Chemistry* **2002,** *40* (2), 192-209.

9.   Gabriel, S., Zur Kenntniss des Bromäthylamins. *Berichte der deutschen chemischen Gesellschaft* **1889**, 1139 - 1154.

10.   Rossegger, E.; Schenk, V.; Wiesbrock, F., Design Strategies for Functionalized Poly(2-oxazoline)s and Derived Materials. *Polymers* **2013,** *5* (3), 956-1011.

11.   de la Rosa, V. R., Poly(2-oxazoline)s as materials for biomedical applications. *J Mater Sci Mater Med* **2014,** *25* (5), 1211-25.

12.   Tomalia, D. A.; Sheetz, D. P., Homopolymerization of 2-Alkyl- and 2-Aryl-2-Oxazolines. *Journal of Polymer Science Part A: Polymer Chemistry* **1966,** *4*, 2253 - 2265.

13.   Tsutomu, K.; Shizuo, N.; Taneo, M.; Kenichi, F., Ring-Opening Polymerization of 2-Substituted 2-Oxazolines. *Polymer Letters* **1966,** *4*, 441 - 445.

14.   Bassiri, T. G.; Levy, A.; Litt, M., Polymerization of Cyclic Imino Ethers. I. Oxazolines. *Polymer Letters* **1697,** *5*, 871 - 879.

15.   Meyers, A. I.; Mihelich, E. D., The Synthetic Utility of 2-Oxazolines. *Angew. Chem. Int. Ed. Engl.* **1976,** *15* (5), 270 - 281.

16.   Frump, J. A., OXAZOLINES. THEIR PREPARATION, REACTIONS, AND APPLICATIONS. *Chemical Reviews* **1971,** *71* (5), 483 - 505.

17.   Bansal, S.; Halve, A. K., OXAZOLINES: THEIR SYNTHESIS AND BIOLOGICAL ACTIVITY. *International Journal of Pharmaceutical Sciences and Research* **2014,** *5* (11), 4601 - 4616.

18.   Seeliger, H. W. u. W., Cyclische Imidsäureester aus Nitrilen und Aminoalkoholen. *Liebigs Ann. Chem.* **1974**, 996 - 1009.

19.   Zarka, M. T.; Nuyken, O.; Weberskirch, R., Amphiphilic polymer supports for the asymmetric hydrogenation of amino acid precursors in water. *Chemistry* **2003,** *9* (14), 3228-34.

20.   Holerca, Marian N.; Percec, V., 1H NMR Spectroscopic Investigation of the Mechanism of 2-Substituted-2-Oxazoline Ring Formation and of the Hydrolysis of the Corresponding Oxazolinium Salts. *European Journal of Organic Chemistry* **2000,** *2000* (12), 2257-2263.

21.   Seeliger, W.; Aufderhaar, E.; Diepers, W.; Feinauer, R.; Nehring, R.; Thier, W.; Hellmann, H., Neuere Synthesen und Reaktionen cyclischer Imidsäureester. *Angewandte Chemie* **1966,** *78* (20), 913-927.

22.   Leonard, N. M.; Brunckova, J., In situ formation of N-trifluoroacetoxy succinimide (TFA-NHS): one-pot formation of succinimidyl esters, N-trifluoroacetyl amino acid succinimidyl esters, and N-maleoyl amino acid succinimidyl esters. *J Org Chem* **2011,** *76* (21), 9169-74.

23.   Lav, T.-X.; Lemechko, P.; Renard, E.; Amiel, C.; Langlois, V.; Volet, G., Development of a new azido-oxazoline monomer for the preparation of amphiphilic graft copolymers by combination of cationic ring-opening polymerization and click chemistry. *Reactive and Functional Polymers* **2013,** *73* (8), 1001-1008.

6. References

24.   Gant, T. G.; Meyers, A. I., The chemistry of 2-oxazolines (1985–present). *Tetrahedron* **1994,** *50* (8), 2297-2360.

25.   Fry, E. M., OXAZOLINES. *The Journal of Organic Chemistry* **1949,** *14* (5), 887-894.

26.   Västilä, P.; Pastor, I. M.; Adolfsson, H., 2-(Aminomethyl)-oxazolines: Highly Modular Scaffolds for the Preparation of Novel Asymmetric Ligands. *The Journal of Organic Chemistry* **2005,** *70* (8), 2921-2929.

27.   Rajaram, S.; Sigman, M. S., Modular Synthesis of Amine-Functionalized Oxazolines. *Organic Letters* **2002,** *4* (20), 3399-3401.

28.   Aoi, K.; Okada, M., Polymerization of oxazolines. *Progress in Polymer Science* **1996,** *21* (1), 151-208.

29.   Kobayashi, S., Ethylenimine polymers. *Progress in Polymer Science* **1990,** *15* (5), 751-823.

30.   Miyamoto, M.; Aoi, K.; Yamaga, S.; Saegusa, T., Double isomerization polymerization of 2-amino-2-oxazolines: a novel ring-opening polymerization accompanying isomerization of growing species. *Macromolecules* **1992,** *25* (19), 5111-5114.

31.   Miyamoto, M.; Shimakura, M.; Tsutsui, K.; Hasegawa, K.; Aoi, K.; Yamaga, S.; Saegusa, T., Double isomerization polymerization of 2-amino-2-oxazolines having four- to eight-membered cyclic imino substituents. *Macromolecules* **1993,** *26* (26), 7116-7124.

32.   Saegusa, T.; Ikeda, H.; Fujii, H., Isomerization Polymerization of 2-Oxazoline. IV. Kinetic Study of 2-Methyl-2-oxazoline Polymerization. *Macromolecules* **1972,** *5* (4), 359-362.

33.   Saegusa, T.; Ikeda, H.; Fujii, H., Isomerization Polymerization of 2-Oxazoline. III. Reactivities of Unsisbstituted and 2-Substittited 2-Oxazoline Monomers. *Polym J* **1973,** *4* (1), 87-92.

34.   Saegusa, T.; Ikeda, H.; Fujii, H., Isomerization Polymerization of 2-Oxazoline. V. Kinetic Studies on the Polymerization of 2-Oxazoline. *Macromolecules* **1973,** *6* (3), 315-319.

35.   Kobayashi, S.; Isobe, M.; Saegusa, T., Spontaneous 2:1 sequence-regulated copolymerization of cyclic imino ethers with cyclic carboxylic anhydrides. *Macromolecules* **1982,** *15* (3), 703-707.

36.   Miyamoto, M.; Aoi, K.; Saegusa, T., Mechanisms of ring-opening polymerization of 2-(perfluoroalkyl)-2-oxazolines initiated by sulfonates: a novel covalent-type electrophilic polymerization. *Macromolecules* **1988,** *21* (6), 1880-1883.

37.   Miyamoto, M.; Aoi, K.; Saegusa, T., Novel covalent-type electrophilic polymerization of 2-(perfluoroalkyl)-2-oxazolines initiated by sulfonates. *Macromolecules* **1991,** *24* (1), 11-16.

38.   Luxenhofer, R.; Han, Y.; Schulz, A.; Tong, J.; He, Z.; Kabanov, A. V.; Jordan, R., Poly(2-oxazoline)s as Polymer Therapeutics. *Macromolecular rapid communications* **2012,** *33* (19), 1613-1631.

39.   Hoogenboom, R.; Fijten, M. W. M.; Schubert, U. S., Parallel kinetic investigation of 2-oxazoline polymerizations with different initiators as basis for designed copolymer synthesis. *Journal of Polymer Science Part A: Polymer Chemistry* **2004,** *42* (8), 1830-1840.

40.   Park, J.-S.; Kataoka, K., Precise Control of Lower Critical Solution Temperature of Thermosensitive Poly(2-isopropyl-2-oxazoline) via Gradient Copolymerization with 2-Ethyl-2-oxazoline as a Hydrophilic Comonomer. *Macromolecules* **2006,** *39* (19), 6622-6630.

41.   Miyamoto, M.; Naka, K.; Tokumizu, M.; Saegusa, T., End capping of growing species of poly(2-oxazoline) with carboxylic acid: a novel and convenient route to prepare vinyl- and carboxy-terminated macromonomers. *Macromolecules* **1989,** *22* (4), 1604-1607.

42.   Reif, M.; Jordan, R., α,ω-Functionalized Poly(2-Oxazoline)s Bearing Hydroxyl and Amino Functions. *Macromolecular Chemistry and Physics* **2011,** *212* (16), 1815-1824.

43.   Huber, S.; Hutter, N.; Jordan, R., Effect of end group polarity upon the lower critical solution temperature of poly(2-isopropyl-2-oxazoline). *Colloid and Polymer Science* **2008,** *286* (14), 1653-1661.

44.   Cesana, S.; Auernheimer, J.; Jordan, R.; Kessler, H.; Nuyken, O., First Poly(2-oxazoline)s with Pendant Amino Groups. *Macromolecular Chemistry and Physics* **2006,** *207* (2), 183-192.

45.   Fijten, M. W. M.; Haensch, C.; van Lankvelt, B. M.; Hoogenboom, R.; Schubert, U. S., Clickable Poly(2-Oxazoline)s as Versatile Building Blocks. *Macromolecular Chemistry and Physics* **2008,** *209* (18), 1887-1895.

46.   Einzmann, M.; Binder, W. H., Novel functional initiators for oxazoline polymerization. *Journal of Polymer Science Part A: Polymer Chemistry* **2001,** *39* (16), 2821-2831.

6. References

47.   Li, H.; Zhu, Z.; Fahrenbach, A. C.; Savoie, B. M.; Ke, C.; Barnes, J. C.; Lei, J.; Zhao, Y.-L.; Lilley, L. M.; Marks, T. J.; Ratner, M. A.; Stoddart, J. F., Mechanical Bond-Induced Radical Stabilization. *Journal of the American Chemical Society* **2013,** *135* (1), 456-467.

48.   Litt, M.; Levy, A.; Herz, J., Polymerization of Cyclic Imino Ethers. X. Kinetics, Chain Transfer, and Repolymerization. *Journal of Macromolecular Science: Part A - Chemistry* **1975,** *9* (5), 703-727.

49.   Hoogenboom, R.; Fijten, M. W. M.; Brändli, C.; Schroer, J.; Schubert, U. S., Automated Parallel Temperature Optimization and Determination of Activation Energy for the Living Cationic Polymerization of 2-Ethyl-2-oxazoline. *Macromolecular Rapid Communications* **2003,** *24* (1), 98-103.

50.   Wiesbrock, F.; Hoogenboom, R.; Leenen, M. A. M.; Meier, M. A. R.; Schubert, U. S., Investigation of the Living Cationic Ring-Opening Polymerization of 2-Methyl-, 2-Ethyl-, 2-Nonyl-, and 2-Phenyl-2-oxazoline in a Single-Mode Microwave Reactor. *Macromolecules* **2005,** *38* (12), 5025-5034.

51.   Legros, C., Engineering of poly (2-oxazoline)s for potential use in biomedical applications. *Universite de Bordeaux* **2015**, 24 - 27.

52.   Ganta, S.; Devalapally, H.; Shahiwala, A.; Amiji, M., A review of stimuli-responsive nanocarriers for drug and gene delivery. *Journal of Controlled Release* **2008,** *126* (3), 187-204.

53.   Eslahi, N.; Abdorahim, M.; Simchi, A., Smart Polymeric Hydrogels for Cartilage Tissue Engineering: A Review on the Chemistry and Biological Functions. *Biomacromolecules* **2016,** *17* (11), 3441-3463.

54.   Jonas, U.; Brom, C. R. v. d.; Brunsen, A.; Roskamp, R. F., Surface-Attached Polymeric Hydrogel Films. In *Handbook of Biofunctional Surfaces*, Knoll, W., Ed. Pan Stanford Publishing: Singapore 2012, 2012; pp 277-361.

55.   Sharma, N.; Keshmiri, H.; Zhou, X.; Wong, T. I.; Petri, C.; Jonas, U.; Liedberg, B.; Dostalek, J., Tunable Plasmonic Nanohole Arrays Actuated by a Thermoresponsive Hydrogel Cushion. *The Journal of Physical Chemistry C* **2016,** *120* (1), 561-568.

56.   Vagias, A.; Sergelen, K.; Koynov, K.; Košovan, P.; Dostalek, J.; Jonas, U.; Knoll, W.; Fytas, G., Diffusion and Permeation of Labeled IgG in Grafted Hydrogels. *Macromolecules* **2017,** *50* (12), 4770-4779.

57.   Junk, M. J.; Berger, R.; Jonas, U., Atomic force spectroscopy of thermoresponsive photo-cross-linked hydrogel films. *Langmuir* **2010,** *26* (10), 7262-9.

58.   Sharma, N.; Petri, C.; Jonas, U.; Bach, M.; Tovar, G.; Mrkvová, K.; Vala, M.; Homola, J.; Knoll, W.; Dostálek, J., Molecularly Imprinted Polymer Waveguides for Direct Optical Detection of Low-Molecular-Weight Analytes. *Macromolecular Chemistry and Physics* **2014,** *215* (23), 2295-2304.

59.   Ward, M. A.; Georgiou, T. K., Thermoresponsive Polymers for Biomedical Applications. *Polymers* **2011,** *3* (4), 1215-1242.

60.   Bawa, P.; Pillay, V.; Choonara, Y. E.; du Toit, L. C., Stimuli-responsive polymers and their applications in drug delivery. *Biomed Mater* **2009,** *4* (2), 022001.

61.   Kishi, R.; Miura, T.; Kihara, H.; Asano, T.; Shibata, M.; Yosomiya, R., Fast pH-thermo-responsive copolymer hydrogels with micro-porous structures. *Journal of Applied Polymer Science* **2003,** *89* (1), 75-84.

62.   Schmaljohann, D., Thermo- and pH-responsive polymers in drug delivery. *Adv Drug Deliv Rev* **2006,** *58* (15), 1655-70.

63.   Gandhi, A.; Paul, A.; Sen, S. O.; Sen, K. K., Studies on thermoresponsive polymers: Phase behaviour, drug delivery and biomedical applications. *Asian Journal of Pharmaceutical Sciences* **2015,** *10* (2), 99-107.

64.   Cabane, E.; Zhang, X.; Langowska, K.; Palivan, C. G.; Meier, W., Stimuli-responsive polymers and their applications in nanomedicine. *Biointerphases* **2012,** *7* (1-4), 9.

65.   Young, R. J.; Lovell, P. A., *Introduction to Polymers*. Taylor & Francis Group: 2011; Vol. 3.

66.   Tieke, B., *Makromolekulare Chemie*. Third Edition ed.; WILEY - VCH: 2014.

67.   Veis, A., A review of the early development of the thermodynamics of the complex coacervation phase separation. *Advances in Colloid and Interface Science* **2011,** *167* (1), 2-11.

6. References

68. Bischofberger, I.; Calzolari, D. C. E.; De Los Rios, P.; Jelezarov, I.; Trappe, V., Hydrophobic hydration of poly-N-isopropyl acrylamide: a matter of the mean energetic state of water. *Scientific Reports* **2014,** *4*, 4377.

69. Moelbert, S.; De Los Rios, P., Hydrophobic Interaction Model for Upper and Lower Critical Solution Temperatures. *Macromolecules* **2003,** *36* (15), 5845-5853.

70. Ashbaugh, H. S.; Paulaitis, M. E., Monomer Hydrophobicity as a Mechanism for the LCST Behavior of Poly(ethylene oxide) in Water. *Industrial & Engineering Chemistry Research* **2006,** *45* (16), 5531-5537.

71. Hoogenboom, R.; Thijs, H. M.; Jochems, M. J.; van Lankvelt, B. M.; Fijten, M. W.; Schubert, U. S., Tuning the LCST of poly(2-oxazoline)s by varying composition and molecular weight: alternatives to poly(N-isopropylacrylamide)? *Chem Commun (Camb)* **2008,** (44), 5758-60.

72. Weber, C.; Hoogenboom, R.; Schubert, U. S., Temperature responsive bio-compatible polymers based on poly(ethylene oxide) and poly(2-oxazoline)s. *Progress in Polymer Science* **2012,** *37* (5), 686-714.

73. Trinh, L. T. T.; Lambermont-Thijs, H. M. L.; Schubert, U. S.; Hoogenboom, R.; Kjøniksen, A.-L., Thermoresponsive Poly(2-oxazoline) Block Copolymers Exhibiting Two Cloud Points: Complex Multistep Assembly Behavior. *Macromolecules* **2012,** *45* (10), 4337-4345.

74. Slaughter, B. V.; Khurshid, S. S.; Fisher, O. Z.; Khademhosseini, A.; Peppas, N. A., Hydrogels in regenerative medicine. *Adv Mater* **2009,** *21* (32-33), 3307-29.

75. Hoare, T. R.; Kohane, D. S., Hydrogels in drug delivery: Progress and challenges. *Polymer* **2008,** *49* (8), 1993-2007.

76. Caló, E.; Khutoryanskiy, V. V., Biomedical applications of hydrogels: A review of patents and commercial products. *European Polymer Journal* **2015,** *65*, 252-267.

77. Janik, I. G. a. H., REVIEW: SYNTHETIC POLYMER HYDROGELS FOR BIOMEDICAL APPLICATIONS. *CHEMISTRY & CHEMICAL TECHNOLOGY* **2010,** *4* (4), 297 - 304.

78. Wichterle, O.; Lim, D., Hydrophilic Gels for Biological Use. *Nature* **1960,** *185* (4706), 117-118.

79. Kyle, R. A.; Steensma, D. P.; Shampo, M. A., Otto Wichterle—Inventor of the First Soft Contact Lenses. *Mayo Clinic Proceedings* **2016,** *91* (3), e45-e46.

80. Pal, K.; Banthia, A. K.; Majumdar, D. K., Polymeric Hydrogels: Characterization and Biomedical Applications. *Designed Monomers and Polymers* **2009,** *12* (3), 197-220.

81. Gulrez, S. K. H.; Al-Assaf, S.; Phillips, G. O., Hydrogels: Methods of Preparation, Characterisation and Applications. In *Progress in Molecular and Environmental Bioengineering - From Analysis and Modeling to Technology Applications*, Capri, P. A., Ed. InTech: 2011.

82. Mateescu, A.; Wang, Y.; Dostalek, J.; Jonas, U., Thin hydrogel films for optical biosensor applications. *Membranes (Basel)* **2012,** *2* (1), 40-69.

83. Okay, O., General Properties of Hydrogels. In *Hydrogel Sensors and Actuators: Engineering and Technology*, Gerlach, G.; Arndt, K.-F., Eds. Springer Berlin Heidelberg: Berlin, Heidelberg, 2010; pp 1-14.

84. Ebara, M.; Kotsuchibashi, Y.; Uto, K.; Aoyagi, T.; Kim, Y.-J.; Narain, R.; Idota, N.; Hoffman, J. M., Smart Hydrogels. In *Smart Biomaterials*, Published by Springer: National Institute for Materials Science, Japan., 2014.

85. Drury, J. L.; Mooney, D. J., Hydrogels for tissue engineering: scaffold design variables and applications. *Biomaterials* **2003,** *24* (24), 4337-4351.

86. Brunsen, A.; Ritz, U.; Mateescu, A.; Höfer, I.; Frank, P.; Menges, B.; Hofmann, A.; Rommens, P. M.; Knoll, W.; Jonas, U., Photocrosslinkable dextran hydrogel films as substrates for osteoblast and endothelial cell growth. *Journal of Materials Chemistry* **2012,** *22* (37), 19590.

87. Lee, K. Y.; Mooney, D. J., Alginate: properties and biomedical applications. *Progress in polymer science* **2012,** *37* (1), 106-126.

88. Nokhodchi, A.; Tailor, A., In situ cross-linking of sodium alginate with calcium and aluminum ions to sustain the release of theophylline from polymeric matrices. *Il Farmaco* **2004,** *59* (12), 999-1004.

6. References

89.   Van Vlierberghe, S.; Dubruel, P.; Schacht, E., Biopolymer-based hydrogels as scaffolds for tissue engineering applications: a review. *Biomacromolecules* **2011,** *12* (5), 1387-408.

90.   Shen, X.; Shamshina, J. L.; Berton, P.; Gurau, G.; Rogers, R. D., Hydrogels based on cellulose and chitin: fabrication, properties, and applications. *Green Chemistry* **2016,** *18* (1), 53-75.

91.   Dargaville, T. R.; Forster, R.; Farrugia, B. L.; Kempe, K.; Voorhaar, L.; Schubert, U. S.; Hoogenboom, R., Poly(2-oxazoline) hydrogel monoliths via thiol-ene coupling. *Macromol Rapid Commun* **2012,** *33* (19), 1695-700.

92.   Dargaville, T. R.; Hollier, B. G.; Shokoohmand, A.; Hoogenboom, R., Poly(2-oxazoline) hydrogels as next generation three-dimensional cell supports. *Cell Adhesion & Migration* **2014,** *8* (2), 88-93.

93.   Gao, X.; Cao, Y.; Song, X.; Zhang, Z.; Xiao, C.; He, C.; Chen, X., pH- and thermo-responsive poly(N-isopropylacrylamide-co-acrylic acid derivative) copolymers and hydrogels with LCST dependent on pH and alkyl side groups. *Journal of Materials Chemistry B* **2013,** *1* (41), 5578.

94.   Beines, P. W.; Klosterkamp, I.; Menges, B.; Jonas, U.; Knoll, W., Responsive Thin Hydrogel Layers from Photo-Cross-Linkable Poly(N-isopropylacrylamide) Terpolymers. *Langmuir* **2007,** *23* (4), 2231-2238.

95.   Aulasevich, A.; Roskamp, R. F.; Jonas, U.; Menges, B.; Dostálek, J.; Knoll, W., Optical Waveguide Spectroscopy for the Investigation of Protein-Functionalized Hydrogel Films. *Macromolecular Rapid Communications* **2009,** *30* (9-10), 872-877.

96.   Muthiah, P.; Hoppe, S. M.; Boyle, T. J.; Sigmund, W., Thermally tunable surface wettability of electrospun fiber mats: polystyrene/poly(N-isopropylacrylamide) blended versus crosslinked poly[(N-isopropylacrylamide)-co-(methacrylic acid)]. *Macromol Rapid Commun* **2011,** *32* (21), 1716-21.

97.   Hoffman, A. S., Hydrogels for biomedical applications. *Advanced Drug Delivery Reviews* **2002,** *54* (1), 3-12.

98.   Fariba Ganji, S. V.-F., and Ebrahim Vasheghani-Farahani, Theoretical Description of Hydrogel Swelling: A Review. *Iranian Polymer Journal* **2010,** *19* (5), 375 - 398.

99.   Christensen, S. K.; Chiappelli, M. C.; Hayward, R. C., Gelation of Copolymers with Pendent Benzophenone Photo-Cross-Linkers. *Macromolecules* **2012,** *45* (12), 5237-5246.

100.   Tanaka, T.; Fillmore, D. J., Kinetics of swelling of gels. *The Journal of Chemical Physics* **1979,** *70* (3), 1214-1218.

101.   Bajpai, S. K., Swelling Studies on Hydrogel Networks - A Review. *Journal of Scientific & Industrial Research* **2001,** *60*, 451 - 462.

102.   Toomey, R.; Freidank, D.; Rühe, J., Swelling Behavior of Thin, Surface-Attached Polymer Networks. *Macromolecules* **2004,** *37* (3), 882-887.

103.   Advincula, W. K. a. R. C., *Functional Polymer Films*. WILEY-VCH Verlag GmbH & Co. KGaA: 2011.

104.   Faust, B., 4. Ultraviolet/visible spectroscopy. In *Modern Chemical Techniques : An Essential Reference for Students and Teachers* CHEMISTRY, T. R. S. O., Ed. Unilever: 1997; pp 92 - 115.

105.   Owen, T.; Technologies, A., *Fundamentals of Modern UV-visible Spectroscopy: Primer*. Agilent Technologies: 2000.

106.   Tissue, B. M., Ultraviolet and Visible Absorption Spectroscopy. In *Characterization of Materials*, John Wiley & Sons, Inc.: 2002.

107.   Shah, R. S.; Shah, R. R.; Pawar, R. B.; Gayakar, P. P., UV-VISIBLE SPECTROSCOPY- A REVIEW. *International Journal of Institutional Pharmacy and Life Sciences* **2015,** *5* (5), 490 - 505.

108.   Harris, D. C., *Lehrbuch der Quantitativen Analyse*. Springer-Verlag Berlin Heidelberg New York: 1998.

109.   Bloksma, M. M.; Bakker, D. J.; Weber, C.; Hoogenboom, R.; Schubert, U. S., The Effect of Hofmeister Salts on the LCST Transition of Poly(2-oxazoline)s with Varying Hydrophilicity. *Macromol Rapid Commun* **2010,** *31* (8), 724-8.

110.   Hofmann, C.; Schönhoff, M., Do additives shift the LCST of poly (N-isopropylacrylamide) by solvent quality changes or by direct interactions? *Colloid and Polymer Science* **2009,** *287* (12), 1369-1376.

6. References

111.   Meiswinkel, G.; Ritter, H., Polymers from 1-Vinyl-2-(hydroxymethyl)imidazole in Water: Altering from UCST to LCST Behavior via O-Ethylation. *Macromolecular Chemistry and Physics* **2014,** *215* (7), 682-687.

112.   Chiu, M.; Prenner, E., Differential scanning calorimetry: An invaluable tool for a detailed thermodynamic characterization of macromolecules and their interactions. *Journal of Pharmacy And Bioallied Sciences* **2011,** *3* (1), 39-59.

113.   M. D. Lechner, K. G., E. H. Nordmeier, *Makromolekulare Chemie*. Birkhäuser Verlag: Basel – Boston – Berlin, 2009; Vol. 4.

114.   Coleman, N. J.; Craig, D. Q. M., Modulated temperature differential scanning calorimetry: A novel approach to pharmaceutical thermal analysis. *International Journal of Pharmaceutics* **1996,** *135* (1), 13-29.

115.   Riga, A.; Collins, R., Differential Scanning Calorimetry and Differential Thermal Analysis. In *Encyclopedia of Analytical Chemistry*, John Wiley & Sons, Ltd: 2006.

116.   Simon, S. L., Temperature-modulated differential scanning calorimetry: theory and application. *Thermochimica Acta* **2001,** *374* (1), 55-71.

117.   Reading, M.; Luget, A.; Wilson, R., Modulated differential scanning calorimetry. *Thermochimica Acta* **1994,** *238*, 295-307.

118.   Broady, S. D.; Rexhausen, J. E.; Thomas, E. J., Total synthesis of AI-77-B: stereoselective hydroxylation of 4-alkenylazetidinones. *Journal of the Chemical Society, Perkin Transactions 1* **1999,** (8), 1083-1094.

119.   MacCallum, J. R., Thermogravimetric analysis of polymers for assessing thermal degradation. *Thermochimica Acta* **1985,** *96* (2), 275-281.

120.   Sepe, M. P.; Limited, R. T., *Thermal Analysis of Polymers*. Rapra Technology Limited: 1997.

121.   Prime, R. B.; Bair, H. E.; Vyazovkin, S.; Gallagher, P. K.; Riga, A., Thermogravimetric Analysis (TGA), in Thermal Analysis of Polymers: Fundamentals and Applications. In *Thermal Analysis of Polymers*, Prime, J. D. M. a. R. B., Ed. John Wiley & Sons, Inc.: Hoboke, NJ, USA, 2009.

122.   Trathnigg, B., Size-Exclusion Chromatography of Polymers. In *Encyclopedia of Analytical Chemistry*, John Wiley & Sons, Ltd: 2006.

123.   Porath, J.; Flodin, P. E. R., Gel Filtration: A Method for Desalting and Group Separation. *Nature* **1959,** *183* (4676), 1657-1659.

124.   Kostanski, L. K.; Keller, D. M.; Hamielec, A. E., Size-exclusion chromatography—a review of calibration methodologies. *Journal of Biochemical and Biophysical Methods* **2004,** *58* (2), 159-186.

125.   Barth, H. G.; Boyes, B. E.; Jackson, C., Size Exclusion Chromatography and Related Separation Techniques. *Analytical Chemistry* **1998,** *70* (12), 251-278.

126.   Binnig, G.; Quate, C. F.; Gerber, C., Atomic Force Microscope. *Physical Review Letters* **1986,** *56* (9), 930-933.

127.   Magonov, S. N.; Reneker, D. H., CHARACTERIZATION OF POLYMER SURFACES WITH ATOMIC FORCE MICROSCOPY. *Annual Review of Materials Science* **1997,** *27* (1), 175-222.

128.   Maver, U.; Velnar, T.; Gaberšček, M.; Planinšek, O.; Finšgar, M., Recent progressive use of atomic force microscopy in biomedical applications. *TrAC Trends in Analytical Chemistry* **2016,** *80*, 96-111.

129.   Jalili, N.; Laxminarayana, K., A review of atomic force microscopy imaging systems: application to molecular metrology and biological sciences. *Mechatronics* **2004,** *14* (8), 907-945.

130.   Maver, U.; Maver, T.; Peršin, Z.; Mozetič, M.; Vesel, A.; Gaberšček, M.; Stana-Kleinschek, K., Polymer Characterization with the Atomic Force Microscope. InTech, Ed. InTech: 2013; Vol. Chapter 4, pp 113 - 132.

131.   Magonov, S. N., Atomic Force Microscopy in Analysis of Polymers. In *Encyclopedia of Analytical Chemistry*, John Wiley & Sons, Ltd: 2006.

132.   D. Tranchida, Z. K., and S. Piccarolo, Atomic Force Microscope Nanoindentations to Reliably Measure the Young's Modulus of Soft Matter. *Modern Research and Educational Topics in Microscopy. Méndez-Vilas and J. Díaz (Eds.) ©FORMATEX 2007* **2007**, 737 - 746.

6. References

133.   Tse, J. R.; Engler, A. J., Preparation of Hydrogel Substrates with Tunable Mechanical Properties. In *Current Protocols in Cell Biology*, John Wiley & Sons, Inc.: 2001.

134.   Soofi, S. S.; Last, J. A.; Liliensiek, S. J.; Nealey, P. F.; Murphy, C. J., The elastic modulus of Matrigel™ as determined by atomic force microscopy. *Journal of Structural Biology* **2009,** *167* (3), 216-219.

135.   Butt, H.-J.; Cappella, B.; Kappl, M., Force measurements with the atomic force microscope: Technique, interpretation and applications. *Surface Science Reports* **2005,** *59* (1–6), 1-152.

136.   Shahin, V.; Hafezi, W.; Oberleithner, H.; Ludwig, Y.; Windoffer, B.; Schillers, H.; Kühn, J. E., The genome of HSV-1 translocates through the nuclear pore as a condensed rod-like structure. *Journal of Cell Science* **2005,** *119* (1), 23.

137.   Sagle, L. B.; Ruvuna, L. K.; Ruemmele, J. A.; Van Duyne, R. P., Advances in localized surface plasmon resonance spectroscopy biosensing. *Nanomedicine* **2011,** *6* (8), 1447-1462.

138.   Englebienne, P.; Hoonacker, A. V.; Verhas, M., Surface plasmon resonance: principles, methods and applications in biomedical sciences. *Spectroscopy* **2003,** *17* (2,3), 255-273.

139.   Cheskis, B.; Freedman, L. P., Modulation of Nuclear Receptor Interactions by Ligands: Kinetic Analysis Using Surface Plasmon Resonance. *Biochemistry* **1996,** *35* (10), 3309-3318.

140.   Harmon, M. E.; Jakob, T. A. M.; Knoll, W.; Frank, C. W., A Surface Plasmon Resonance Study of Volume Phase Transitions in N-Isopropylacrylamide Gel Films. *Macromolecules* **2002,** *35* (15), 5999-6004.

141.   Green, R. J.; Frazier, R. A.; Shakesheff, K. M.; Davies, M. C.; Roberts, C. J.; Tendler, S. J. B., Surface plasmon resonance analysis of dynamic biological interactions with biomaterials. *Biomaterials* **2000,** *21* (18), 1823-1835.

142.   Tang, Y.; Zeng, X.; Liang, J., Surface Plasmon Resonance: An Introduction to a Surface Spectroscopy Technique. *Journal of Chemical Education* **2010,** *87* (7), 742-746.

143.   Zhu, S.; Yu, A. W.; Hawley, D.; Roy, R., Frustrated total internal reflection: A demonstration and review. *American Journal of Physics* **1986,** *54* (7), 601-607.

144.   Sambles, J. R.; Bradbery, G. W.; Yang, F., Optical excitation of surface plasmons: An introduction. *Contemporary Physics* **1991,** *32* (3), 173-183.

145.   Knoll, W., INTERFACES AND THIN FILMS AS SEEN BY BOUND ELECTROMAGNETIC WAVES. *Annu. Rev. Phys. Chem.* **1998,** *49*, 569–638.

146.   Kretschmann, E., Die Bestimmung optischer Konstanten von Metallen durch Anregung von Oberflächenplasmaschwingungen. *Zeitschrift für Physik A Hadrons and nuclei* **1971,** *241* (4), 313-324.

147.   Homola, J., Surface Plasmon Resonance Sensors for Detection of Chemical and Biological Species. *Chemical Reviews* **2008,** *108* (2), 462-493.

148.   Sigal, G. B.; Bamdad, C.; Barberis, A.; Strominger, J.; Whitesides, G. M., A Self-Assembled Monolayer for the Binding and Study of Histidine-Tagged Proteins by Surface Plasmon Resonance. *Analytical Chemistry* **1996,** *68* (3), 490-497.

149.   Sigal, G. B.; Mrksich, M.; Whitesides, G. M., Using Surface Plasmon Resonance Spectroscopy To Measure the Association of Detergents with Self-Assembled Monolayers of Hexadecanethiolate on Gold. *Langmuir* **1997,** *13* (10), 2749-2755.

150.   Mrksich, M.; Sigal, G. B.; Whitesides, G. M., Surface Plasmon Resonance Permits in Situ Measurement of Protein Adsorption on Self-Assembled Monolayers of Alkanethiolates on Gold. *Langmuir* **1995,** *11* (11), 4383-4385.

151.   Silin, V.; Weetall, H.; Vanderah, D. J., SPR Studies of the Nonspecific Adsorption Kinetics of Human IgG and BSA on Gold Surfaces Modified by Self-Assembled Monolayers (SAMs). *Journal of Colloid and Interface Science* **1997,** *185* (1), 94-103.

152.   Jung, L. S.; Nelson, K. E.; Stayton, P. S.; Campbell, C. T., Binding and Dissociation Kinetics of Wild-Type and Mutant Streptavidins on Mixed Biotin-Containing Alkylthiolate Monolayers. *Langmuir* **2000,** *16* (24), 9421-9432.

153.   Nelson, K. E.; Gamble, L.; Jung, L. S.; Boeckl, M. S.; Naeemi, E.; Golledge, S. L.; Sasaki, T.; Castner, D. G.; Campbell, C. T.; Stayton, P. S., Surface Characterization of Mixed Self-Assembled Monolayers Designed for Streptavidin Immobilization. *Langmuir* **2001,** *17* (9), 2807-2816.

6. References

154. Förch, R.; Schönherr, H.; Jenkins, A. T. A., Appendix I: Optical Waveguide Spectroscopy (OWS) – μm-Thick Films. In *Surface Design: Applications in Bioscience and Nanotechnology*, Wiley-VCH Verlag GmbH & Co. KGaA: 2009; pp 488-490.

155. Hug, T. S.; Prenosil, J. E.; Maier, P.; Morbidelli, M., Optical waveguide lightmode spectroscopy (OWLS) to monitor cell proliferation quantitatively. *Biotechnology and Bioengineering* **2002,** *80* (2), 213-221.

156. Mendes, S. B.; Scott Saavedra, S., On probing molecular monolayers: a spectroscopic optical waveguide approach of ultra-sensitivity. *Opt. Express* **1999,** *4* (11), 449-456.

157. Sinnwell, S.; Ritter, H., Recent Advances in Microwave-Assisted Polymer Synthesis. *Australian Journal of Chemistry* **2007,** *60* (10), 729-743.

158. Wiesbrock, F.; Hoogenboom, R.; Schubert, U. S., Microwave-Assisted Polymer Synthesis: State-of-the-Art and Future Perspectives. *Macromolecular Rapid Communications* **2004,** *25* (20), 1739-1764.

159. Hoogenboom, R.; Wiesbrock, F.; Huang, H.; Leenen, M. A. M.; Thijs, H. M. L.; van Nispen, S. F. G. M.; van der Loop, M.; Fustin, C.-A.; Jonas, A. M.; Gohy, J.-F.; Schubert, U. S., Microwave-Assisted Cationic Ring-Opening Polymerization of 2-Oxazolines: A Powerful Method for the Synthesis of Amphiphilic Triblock Copolymers. *Macromolecules* **2006,** *39* (14), 4719-4725.

160. Hoogenboom, R.; Schlaad, H., Bioinspired Poly(2-oxazoline)s. *Polymers* **2011,** *3* (4), 467-488.

161. Hoogenboom, R., Poly(2-oxazoline)s: a polymer class with numerous potential applications. *Angew Chem Int Ed Engl* **2009,** *48* (43), 7978-94.

162. Gianneli, M.; Roskamp, R. F.; Jonas, U.; Loppinet, B.; Fytas, G.; Knoll, W., Dynamics of swollen gel layers anchored to solid surfaces. *Soft Matter* **2008,** *4* (7), 1443.

163. Prucker, O.; Naumann, C. A.; Rühe, J.; Knoll, W.; Frank, C. W., Photochemical Attachment of Polymer Films to Solid Surfaces via Monolayers of Benzophenone Derivatives. *Journal of the American Chemical Society* **1999,** *121* (38), 8766-8770.

164. Samuel, J. D. J. S.; Brenner, T.; Prucker, O.; Grumann, M.; Ducree, J.; Zengerle, R.; Rühe, J., Tailormade Microfluidic Devices Through Photochemical Surface Modification. *Macromolecular Chemistry and Physics* **2010,** *211* (2), 195-203.

165. Dhende, V. P.; Samanta, S.; Jones, D. M.; Hardin, I. R.; Locklin, J., One-step photochemical synthesis of permanent, nonleaching, ultrathin antimicrobial coatings for textiles and plastics. *ACS Appl Mater Interfaces* **2011,** *3* (8), 2830-7.

166. Dargaville, T. R.; Forster, R.; Farrugia, B. L.; Kempe, K.; Voorhaar, L.; Schubert, U. S.; Hoogenboom, R., Poly(2-oxazoline) Hydrogel Monoliths via Thiol-ene Coupling. *Macromolecular Rapid Communications* **2012,** *33* (19), 1695-1700.

167. Gress, A.; Völkel, A.; Schlaad, H., Thio-Click Modification of Poly[2-(3-butenyl)-2-oxazoline]. *Macromolecules* **2007,** *40* (22), 7928-7933.

168. Korchia, L.; Bouilhac, C.; Lapinte, V.; Travelet, C.; Borsali, R.; Robin, J.-J., Photodimerization as an alternative to photocrosslinking of nanoparticles: proof of concept with amphiphilic linear polyoxazoline bearing coumarin unit. *Polym. Chem.* **2015,** *6* (33), 6029-6039.

169. Tanaka, Y.; Bond, M. R.; Kohler, J. J., Photocrosslinkers illuminate interactions in living cells. *Molecular BioSystems* **2008,** *4* (6), 473-480.

170. van den Brom, C. R.; Anac, I.; Roskamp, R. F.; Retsch, M.; Jonas, U.; Menges, B.; Preece, J. A., The swelling behaviour of thermoresponsive hydrogel/silica nanoparticle composites. *Journal of Materials Chemistry* **2010,** *20* (23), 4827.

171. Fijten, M. W. M.; Hoogenboom, R.; Schubert, U. S., Initiator effect on the cationic ring-opening copolymerization of 2-ethyl-2-oxazoline and 2-phenyl-2-oxazoline. *Journal of Polymer Science Part A: Polymer Chemistry* **2008,** *46* (14), 4804-4816.

172. Brissault, B.; Kichler, A.; Leborgne, C.; Danos, O.; Cheradame, H.; Gau, J.; Auvray, L.; Guis, C., Synthesis, Characterization, and Gene Transfer Application of Poly(ethylene glycol-b-ethylenimine) with High Molar Mass Polyamine Block. *Biomacromolecules* **2006,** *7* (10), 2863-2870.

173. Young, R. J.; Lovell, P. A., *Introduction to Polymers*. Taylor & Francis Group: 2011; Vol. 3, p 359.

174. Scheller, A., WASPLAS. *Max Planck Institute for Polymer Research* **2005**.

175. Winspall. *http://www.res-tec.de/downloads.html*.

6. References

176.	Aspnes, D. E., Optical properties of thin films. *Thin Solid Films* **1982,** *89* (3), 249-262.

177.	Hoogenboom, R., Thiol–Yne Chemistry: A Powerful Tool for Creating Highly Functional Materials. *Angewandte Chemie International Edition* **2010,** *49* (20), 3415-3417.

178.	Shi, Y.; Cao, X.; Gao, H., The use of azide-alkyne click chemistry in recent syntheses and applications of polytriazole-based nanostructured polymers. *Nanoscale* **2016,** *8* (9), 4864-4881.

179.	Binder, W. H.; Sachsenhofer, R., 'Click' Chemistry in Polymer and Materials Science. *Macromolecular Rapid Communications* **2007,** *28* (1), 15-54.

180.	Binder, W. H.; Sachsenhofer, R., 'Click' Chemistry in Polymer and Material Science: An Update. *Macromolecular Rapid Communications* **2008,** *29* (12-13), 952-981.

181.	Blaszykowski, C.; Sheikh, S.; Thompson, M., Surface chemistry to minimize fouling from blood-based fluids. *Chem Soc Rev* **2012,** *41* (17), 5599-612.

182.	Li, G.; Cheng, G.; Xue, H.; Chen, S.; Zhang, F.; Jiang, S., Ultra low fouling zwitterionic polymers with a biomimetic adhesive group. *Biomaterials* **2008,** *29* (35), 4592-7.

183.	Tauhardt, L.; Pretzel, D.; Kempe, K.; Gottschaldt, M.; Pohlers, D.; Schubert, U. S., Zwitterionic poly(2-oxazoline)s as promising candidates for blood contacting applications. *Polymer Chemistry* **2014,** *5* (19), 5751.

184.	Le Fer, G.; Amiel, C.; Volet, G., Copolymers based on azidopentyl-2-oxazoline: Synthesis, characterization and LCST behavior. *European Polymer Journal* **2015,** *71*, 523-533.

185.	Heskins, M.; Guillet, J. E., Solution Properties of Poly(N-isopropylacrylamide). *Journal of Macromolecular Science: Part A - Chemistry* **1968,** *2* (8), 1441-1455.

186.	Halperin, A.; Kröger, M.; Winnik, F. M., Poly(N-isopropylacrylamide) Phase Diagrams: Fifty Years of Research. *Angewandte Chemie International Edition* **2015,** *54* (51), 15342-15367.

187.	Klouda, L.; Mikos, A. G., Thermoresponsive hydrogels in biomedical applications - a review. *European journal of pharmaceutics and biopharmaceutics : official journal of Arbeitsgemeinschaft fur Pharmazeutische Verfahrenstechnik e.V* **2008,** *68* (1), 34-45.

188.	Tommasina Coviello, P. M., Carlotta Marianecci, Franco Alhaique, Polysaccharide hydrogels for modified release formulations. *Journal of Controlled Release* **2007,** (119), 5-24.

189.	Metheny-Barlow, L. J.; Li, L. Y., The enigmatic role of angiopoietin-1 in tumor angiogenesis. *Cell Res* **2003,** *13* (5), 309-317.

190.	Shumpei, S.; Noriyoshi, I., The Trifluoroacetate Method of Peptide Synthesis. I. The Synthesis and Use of Trifluoroacetate Reagents. *Bulletin of the Chemical Society of Japan* **1965,** *38* (11), 1979-1984.

191.	Scott, R. J.; Lian, L.-Y.; Muharram, S. H.; Cockayne, A.; Wood, S. J.; Bycroft, B. W.; Williams, P.; Chan, W. C., Side-chain-to-tail thiolactone peptide inhibitors of the staphylococcal quorum-sensing system. *Bioorganic & Medicinal Chemistry Letters* **2003,** *13* (15), 2449-2453.

192.	Percec, V.; Leowanawat, P.; Sun, H.-J.; Kulikov, O.; Nusbaum, C. D.; Tran, T. M.; Bertin, A.; Wilson, D. A.; Peterca, M.; Zhang, S.; Kamat, N. P.; Vargo, K.; Moock, D.; Johnston, E. D.; Hammer, D. A.; Pochan, D. J.; Chen, Y.; Chabre, Y. M.; Shiao, T. C.; Bergeron-Brlek, M.; André, S.; Roy, R.; Gabius, H.-J.; Heiney, P. A., Modular Synthesis of Amphiphilic Janus Glycodendrimers and Their Self-Assembly into Glycodendrimersomes and Other Complex Architectures with Bioactivity to Biomedically Relevant Lectins. *Journal of the American Chemical Society* **2013,** *135* (24), 9055-9077.

193.	Andreev, S. M.; Pavlova, L. A.; Davidovich, Y. A.; Rogozhin, S. V., Synthesis of N-trifluoroacetoxysuccinimide and its reaction with organic bases. *Bulletin of the Academy of Sciences of the USSR, Division of chemical science* **1980,** *29* (5), 785-789.

194.	Asano, S.; Gavrilyuk, J.; Burton, D. R.; Barbas, C. F., 3rd, Preparation and activities of macromolecule conjugates of the CCR5 antagonist Maraviroc. *ACS Med Chem Lett* **2014,** *5* (2), 133-137.

195.	Norberg, O.; Deng, L.; Yan, M.; Ramström, O., Photo-Click Immobilization of Carbohydrates on Polymeric Surfaces—A Quick Method to Functionalize Surfaces for Biomolecular Recognition Studies. *Bioconjugate Chemistry* **2009,** *20* (12), 2364-2370.

196.	Della, E. W.; Smith, P. A., Synthesis of Bridgehead Nitrogen Heterocycles via Cyclization of α-Ammonio 5-Hexenyl Radicals. *The Journal of Organic Chemistry* **1999,** *64* (6), 1798-1806.

6. References

197.   Roy, D.; Sumerlin, B. S., Glucose-Sensitivity of Boronic Acid Block Copolymers at Physiological pH. *ACS Macro Letters* **2012,** *1* (5), 529-532.

7. Appendix

7.1 Additional ^{1}H- and ^{13}C-NMR Spectra Monomers and Functionalization Units

7.1.1 Synthesis of 2-Alkyl-2-Oxazolines
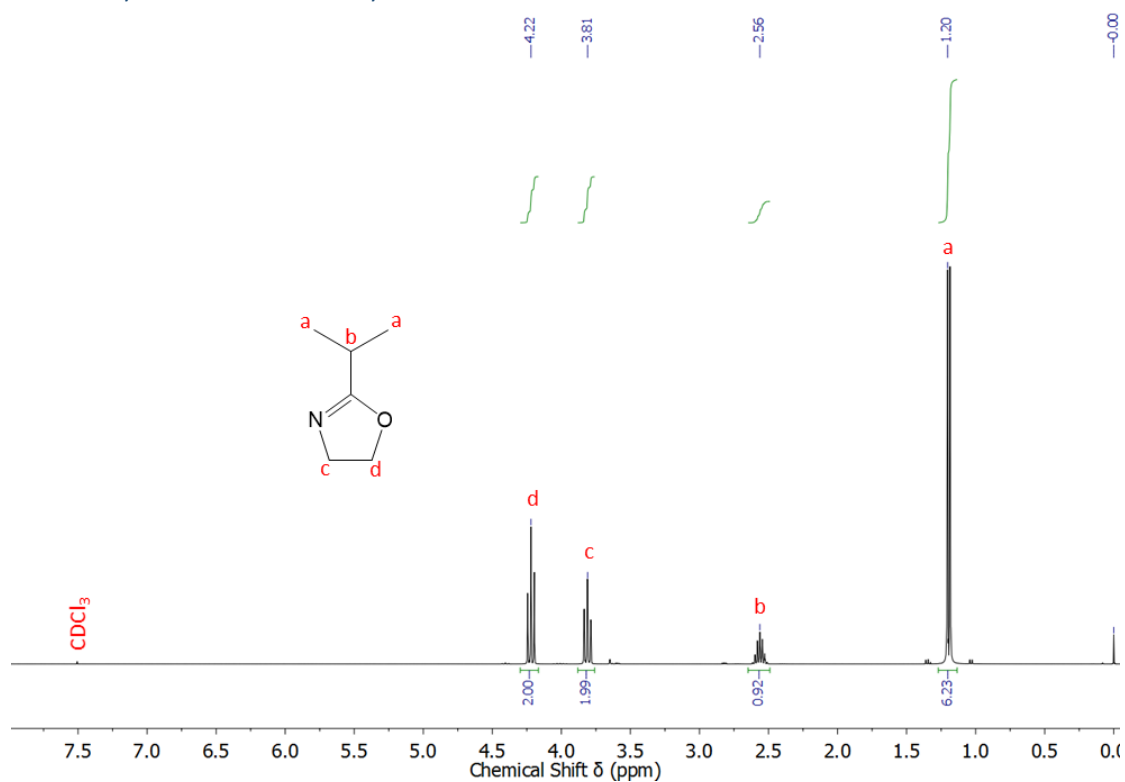
Figure 59: ^{1}H-NMR spectrum of 2-isopropyl-2-oxazoline (CDCl$_3$).
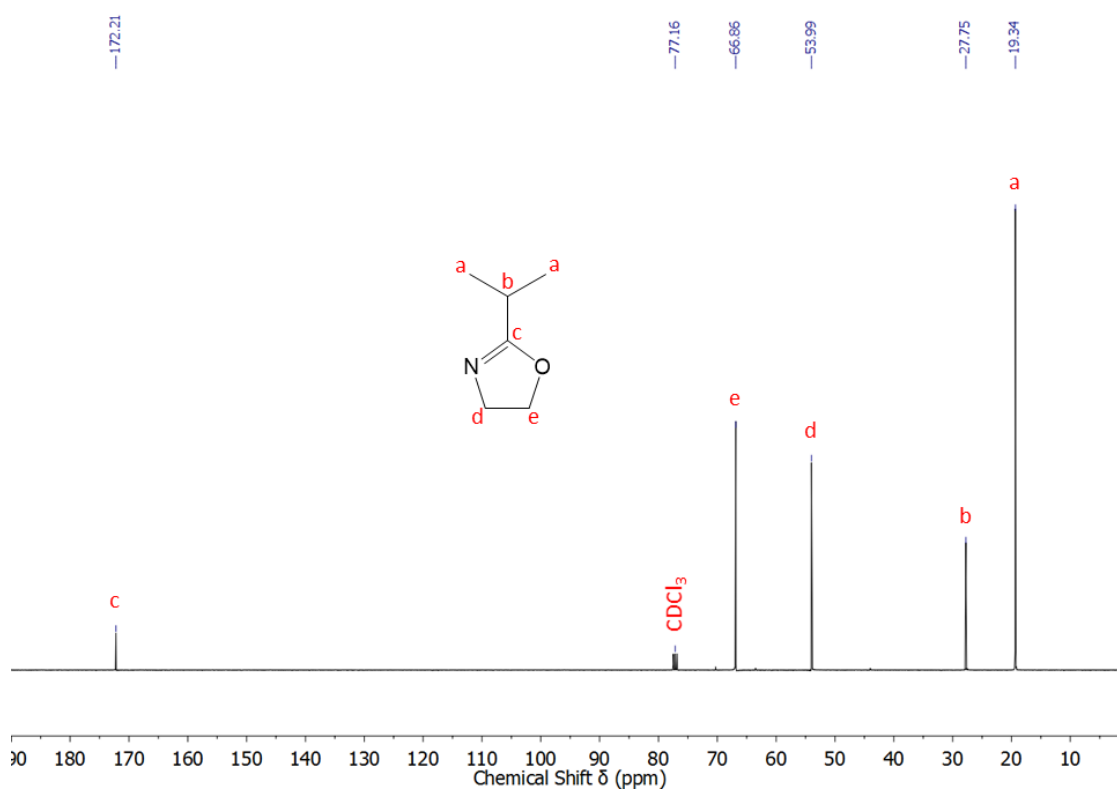
Figure 60: ^{13}C-NMR spectrum of 2-isopropyl-2-oxazoline (CDCl$_3$).
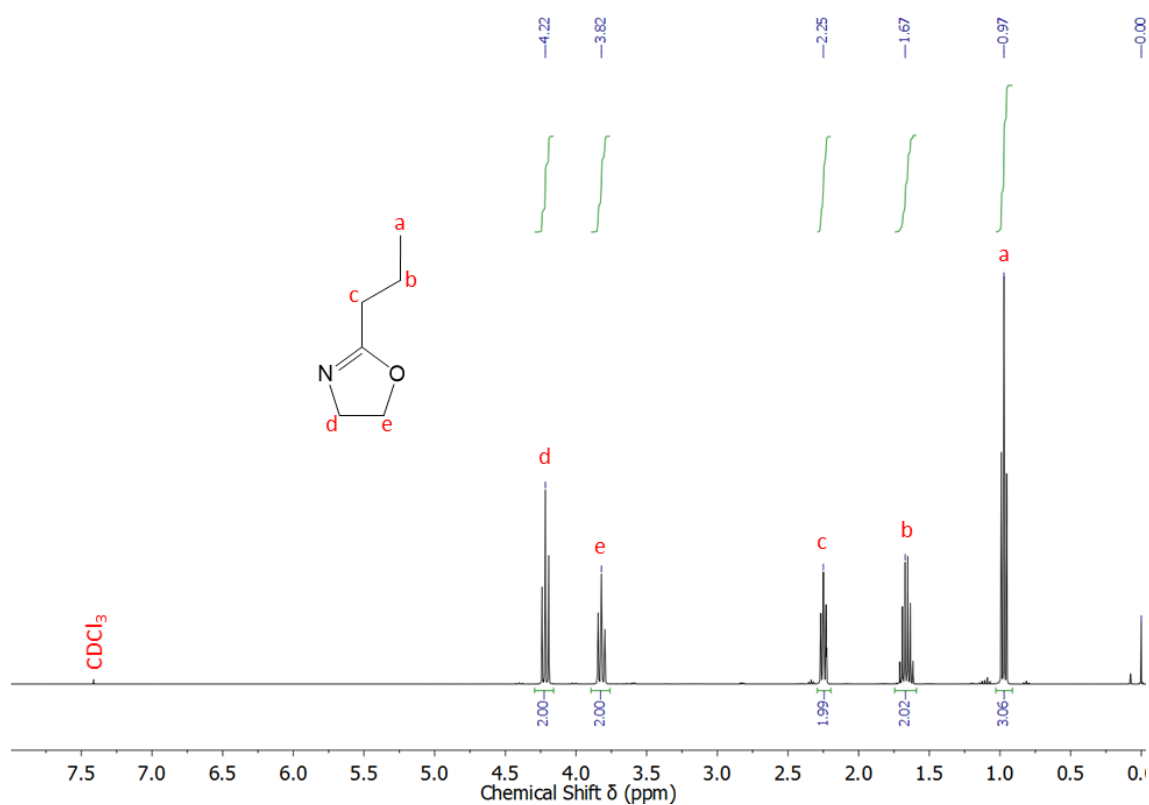
Figure 61: ^{1}H-NMR spectrum of 2-*n*-propyl-2-oxazoline (CDCl₃).
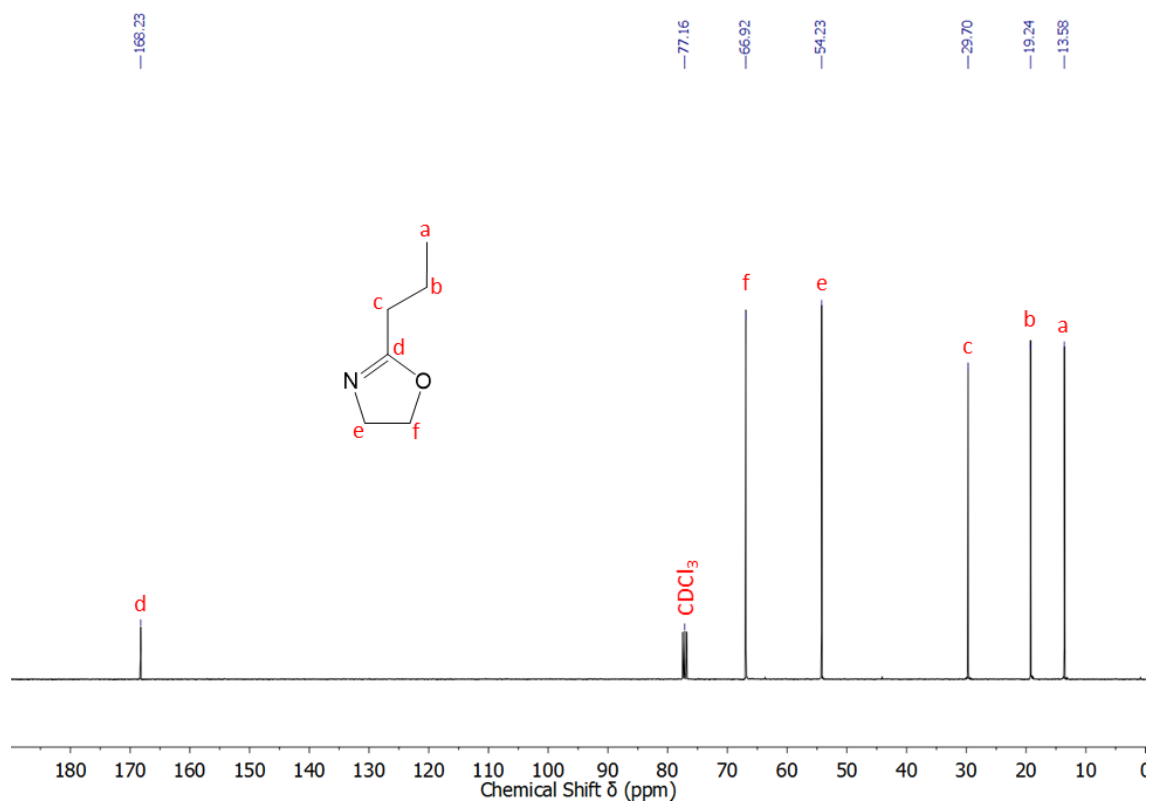
Figure 62: ^{13}C-NMR spectrum of 2-*n*-propyl-2-oxazoline (CDCl₃).

7.1.2 Photocrosslinker Monomer Synthesis

Figure 63: ^{1}H-NMR spectrum of 4-(4-benzoylphenoxy)butanoic acid (CDCl$_3$).

Figure 64: ^{13}C-NMR spectrum of 4-(4-benzoylphenoxy)butanoic acid (CDCl$_3$).
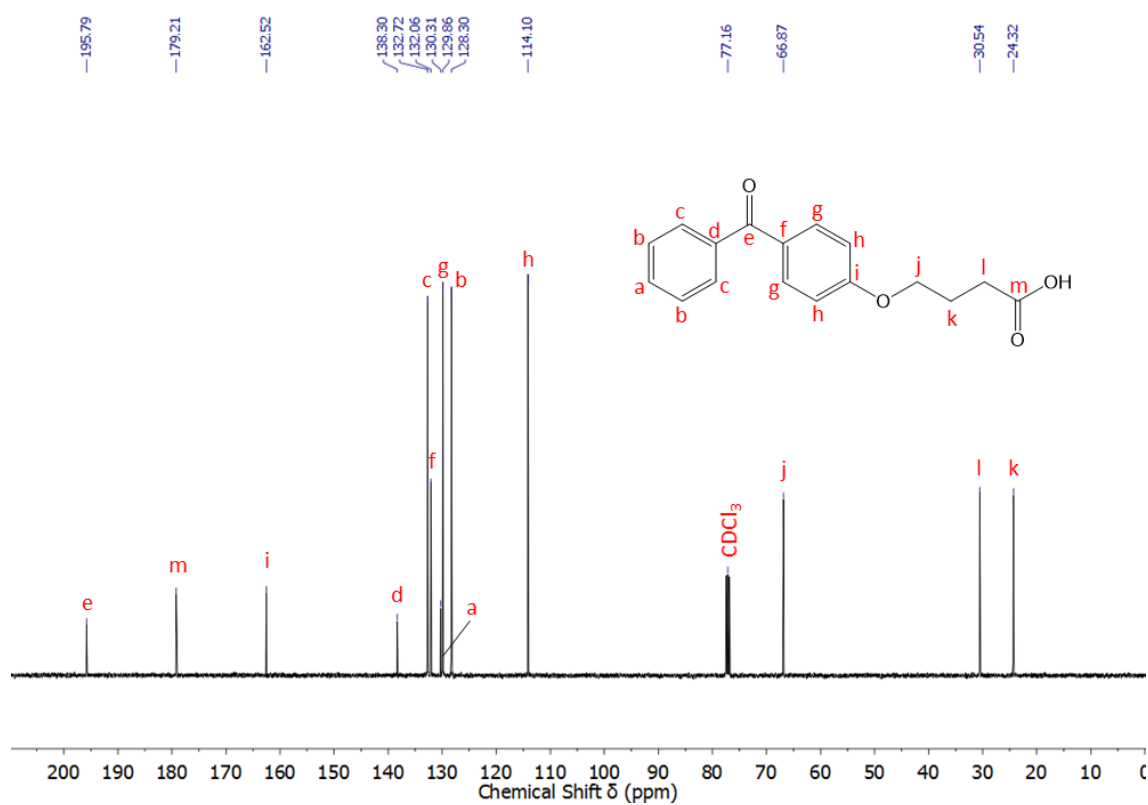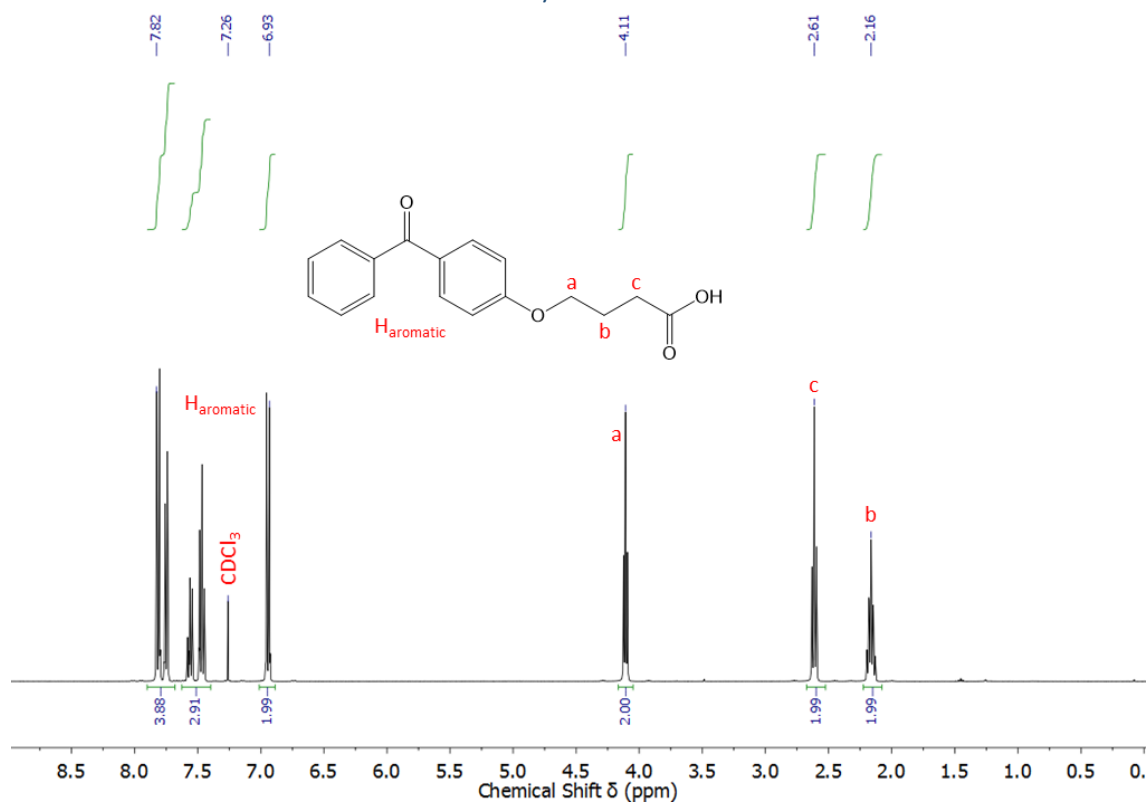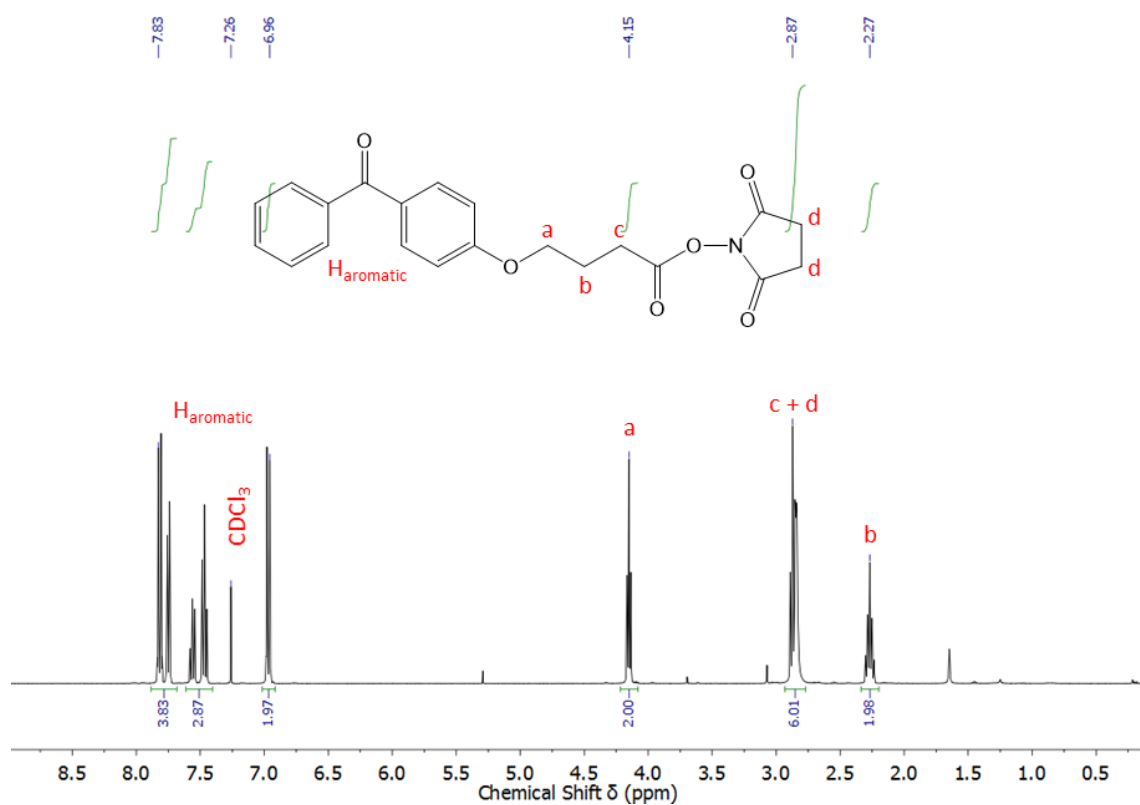
Figure 65: ^{1}H-NMR spectrum of 4-(benzoylphenoxy)butanoate 2,5-dioxopyrrolidinon-1-yl (CDCl$_3$).
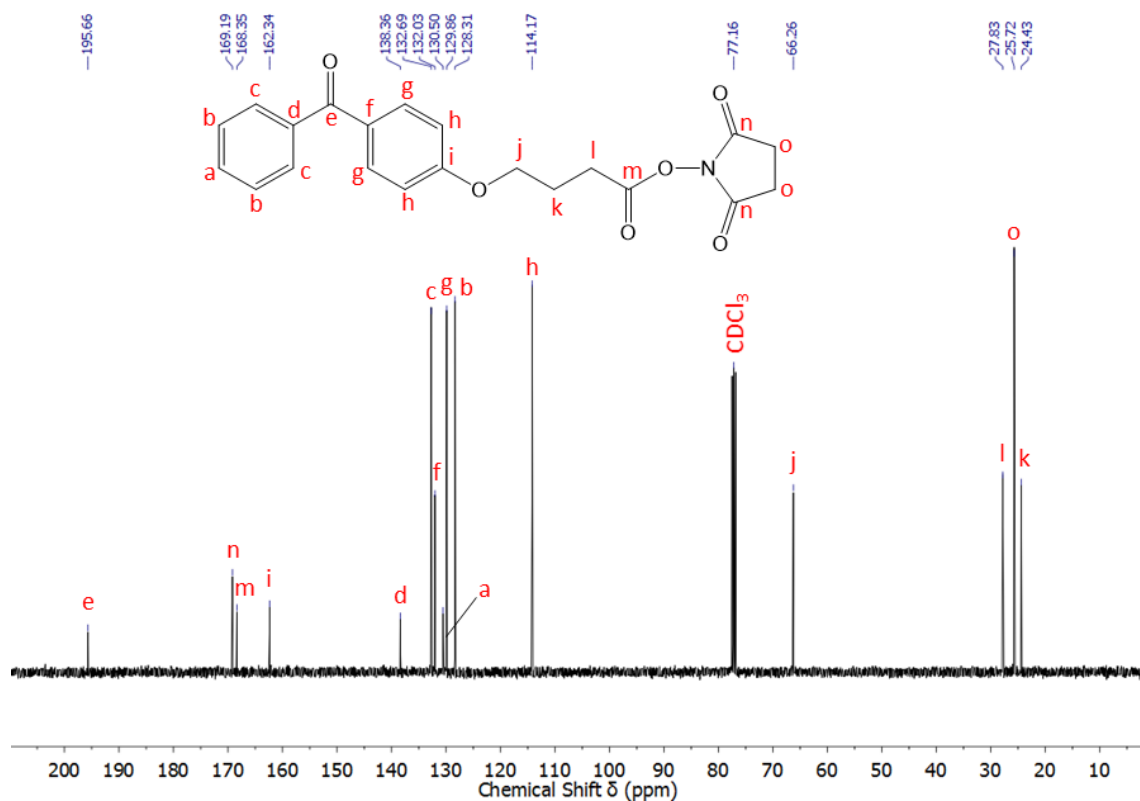
Figure 66: ^{13}C-NMR spectrum of 4-(benzoylphenoxy)butanoate 2,5-dioxopyrrolidinon-1-yl (CDCl$_3$).
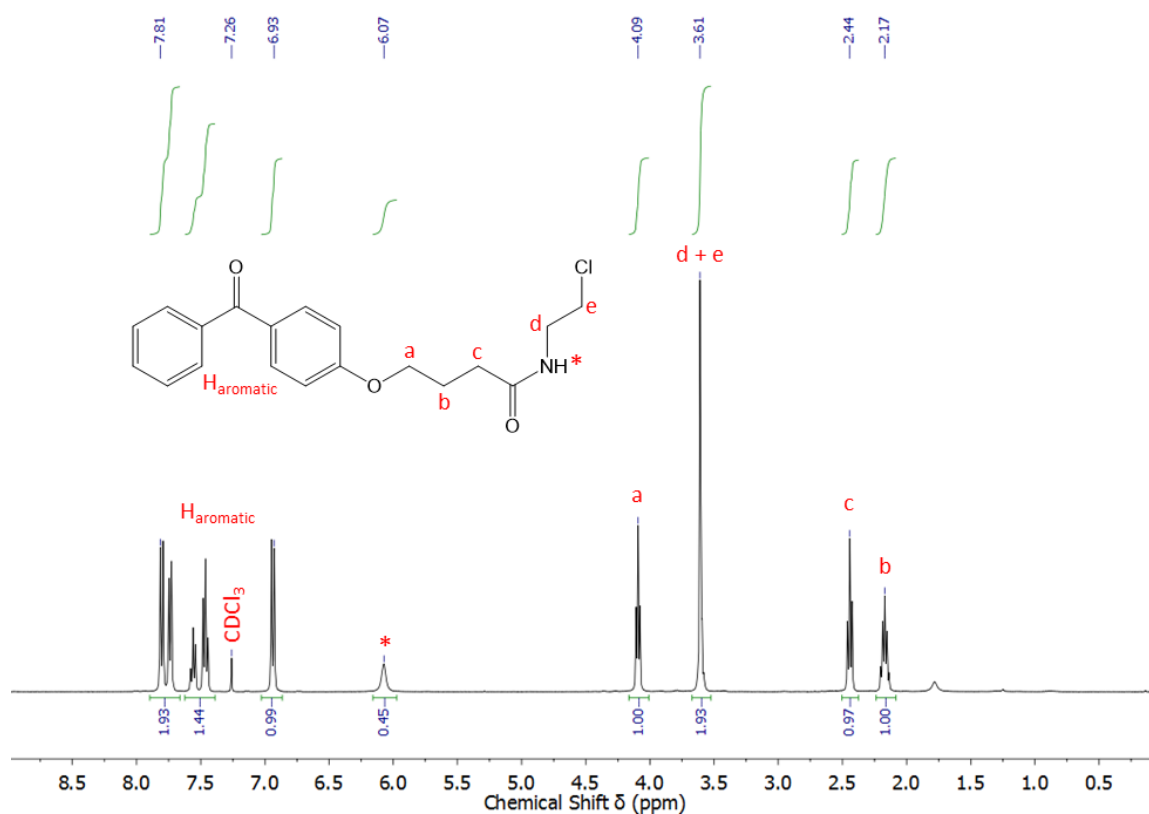
Figure 67: ^{1}H-NMR spectrum 4-(4-benzoylphenoxy)-*N*-(2-chloroethyl)butanamide (CDCl$_3$).
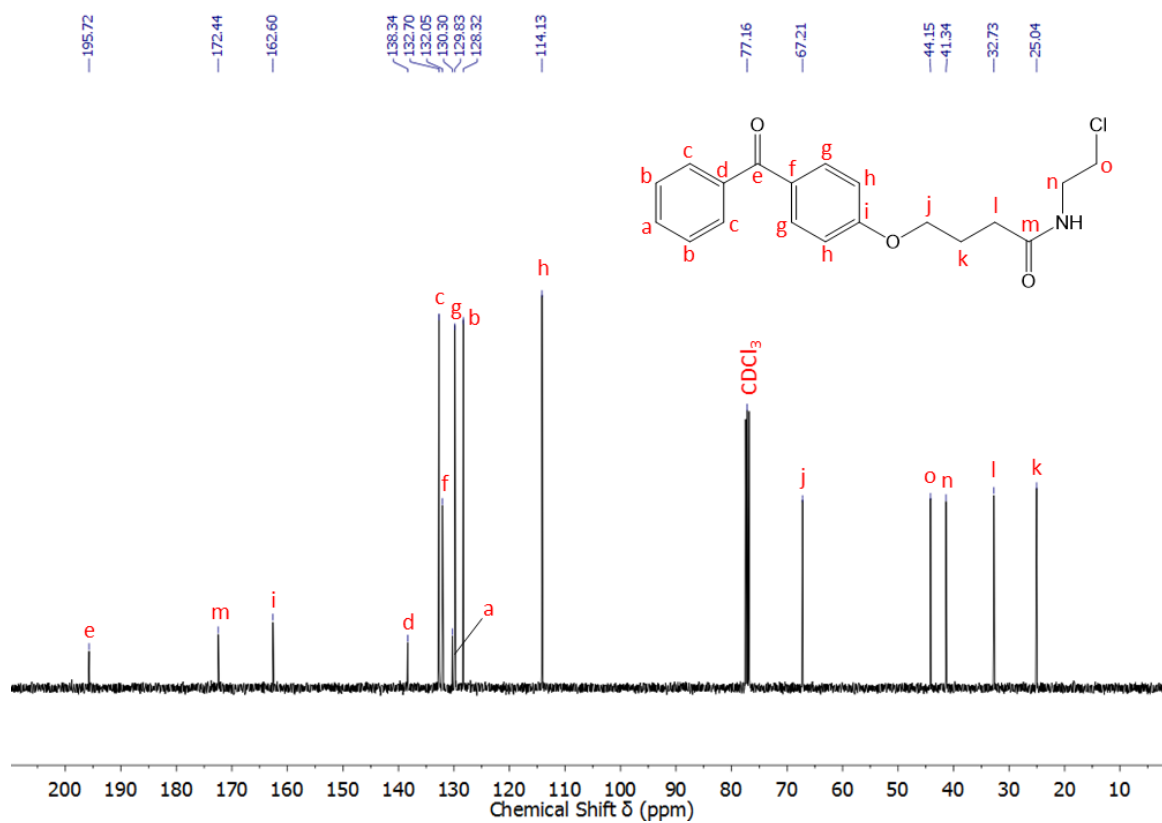
Figure 68: ^{13}C-NMR spectrum of 4-(4-benzoylphenoxy)-*N*-(2-chloroethyl)butanamide (CDCl$_3$).
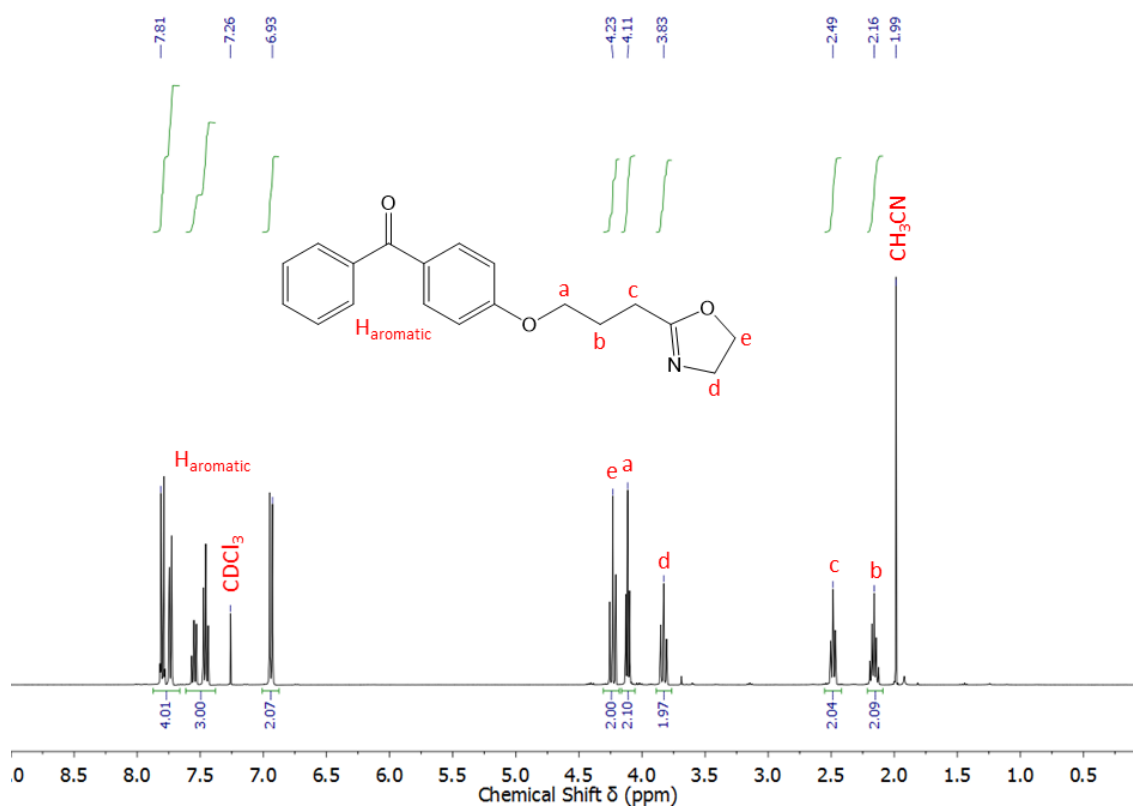
Figure 69: ^{1}H-NMR spectrum of 2-[3-(4-benzoylphenoxy)propyl]-2-oxazoline (CDCl$_3$).
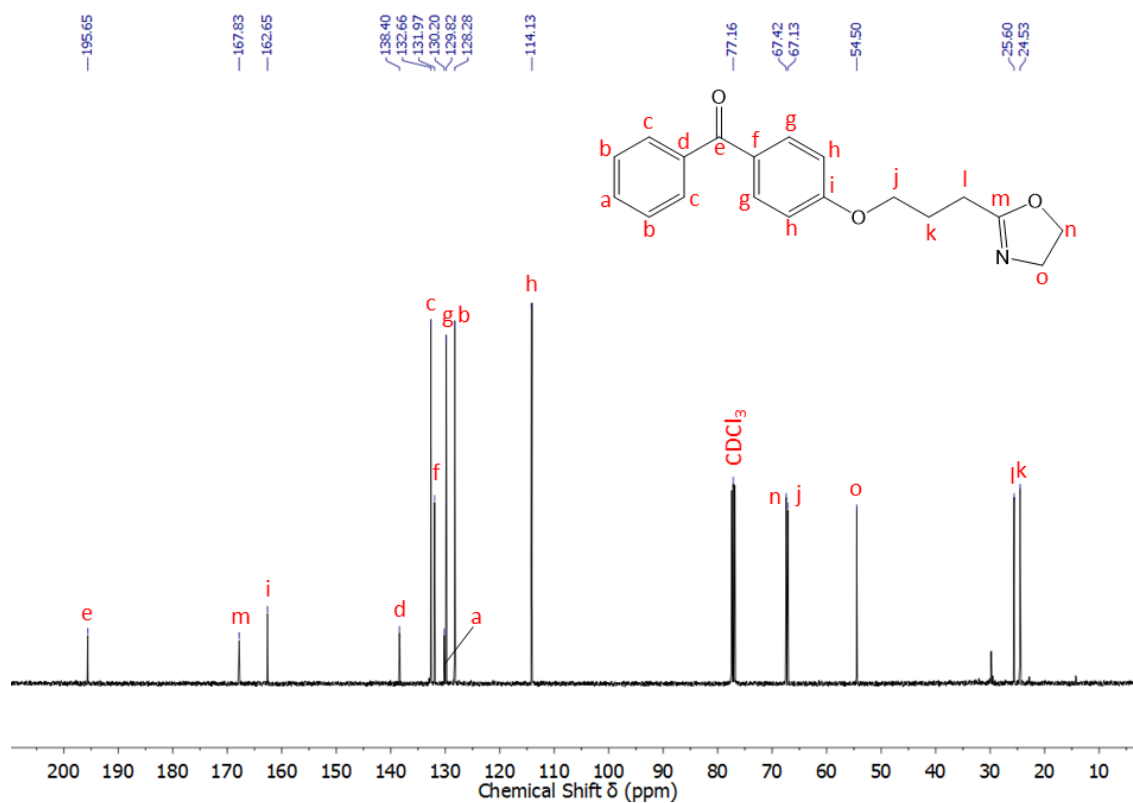
Figure 70: ^{13}C-NMR spectrum of 2-[3-(4-benzoylphenoxy)propyl]-2-oxazoline (CDCl$_3$).

7.1.3 Au Substrate Anchor Synthesis
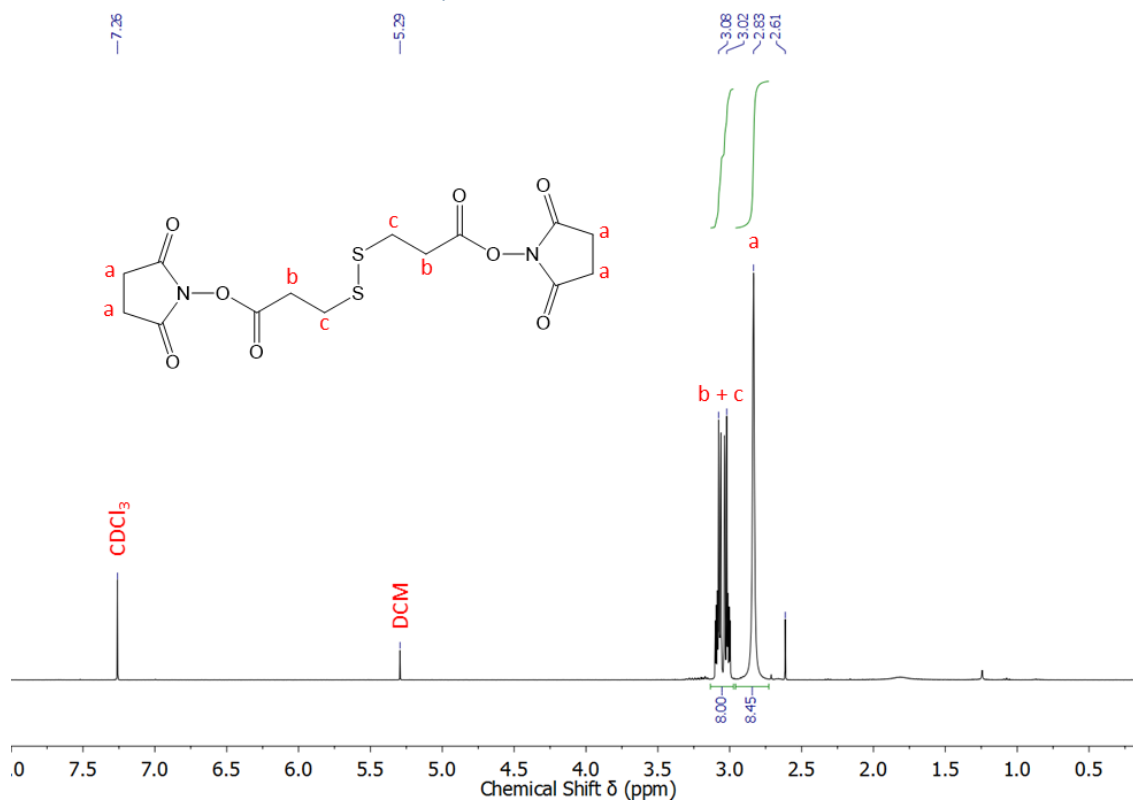
Figure 71: ^{1}H-NMR spectrum of bis(2,5-dioxopyrrolidin-1-yl) 3,3'-disulfanediyldipropanoate (CDCl$_3$).
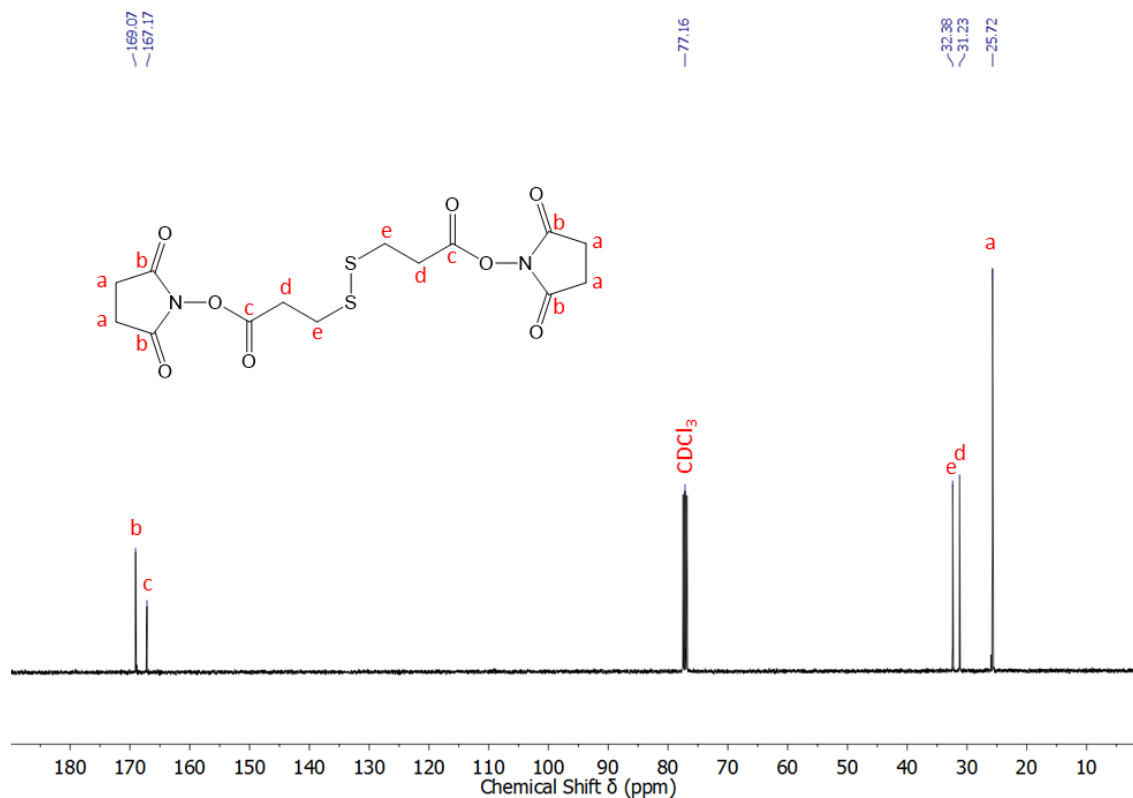
Figure 72: ^{13}C-NMR spectrum of bis(2,5-dioxopyrrolidin-1-yl) 3,3'-disulfanediyldipropanoate (CDCl$_3$).
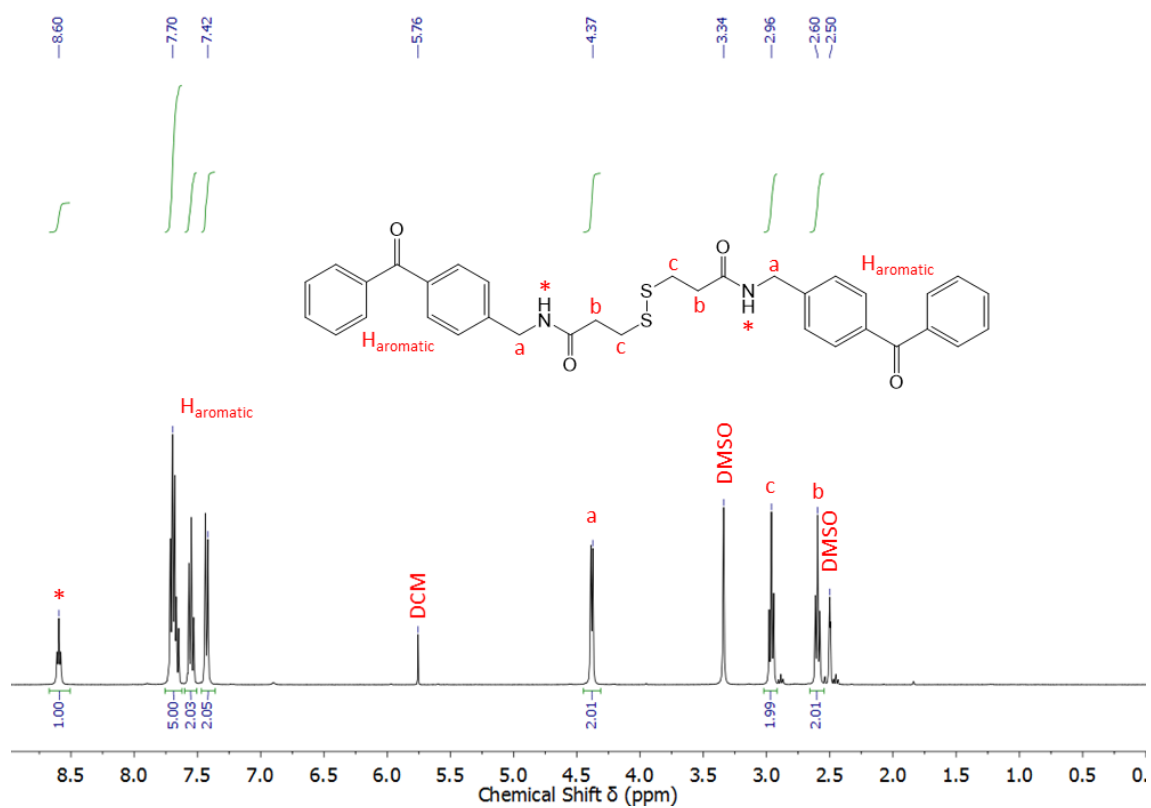
Figure 73: ^{1}H-NMR spectrum of 3,3'-disulfanediylbis[*N*-(4-benzoylbenzyl)propanamide] (DMSO).
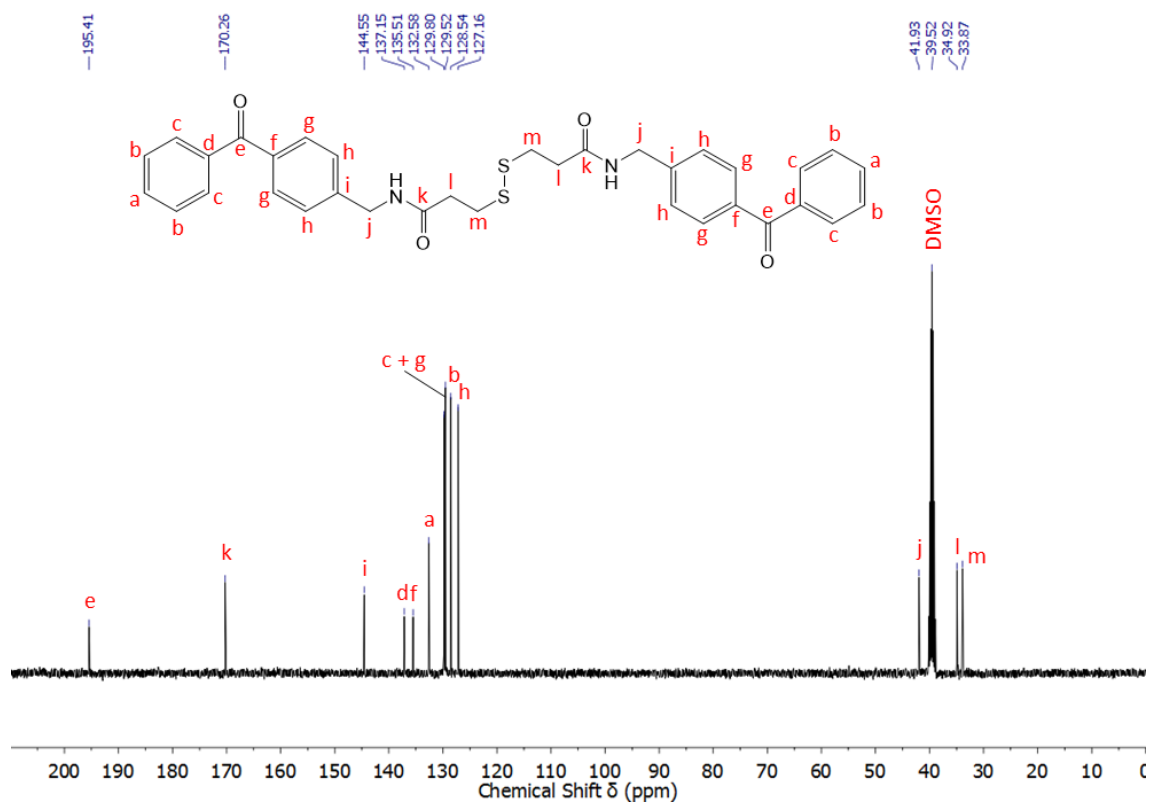
Figure 74: ^{1}H-NMR spectrum of 3,3'-disulfanediylbis[*N*-(4-benzoylbenzyl)propanamide] (DMSO).

7.1.4 Azide Containing Monomer Synthesis
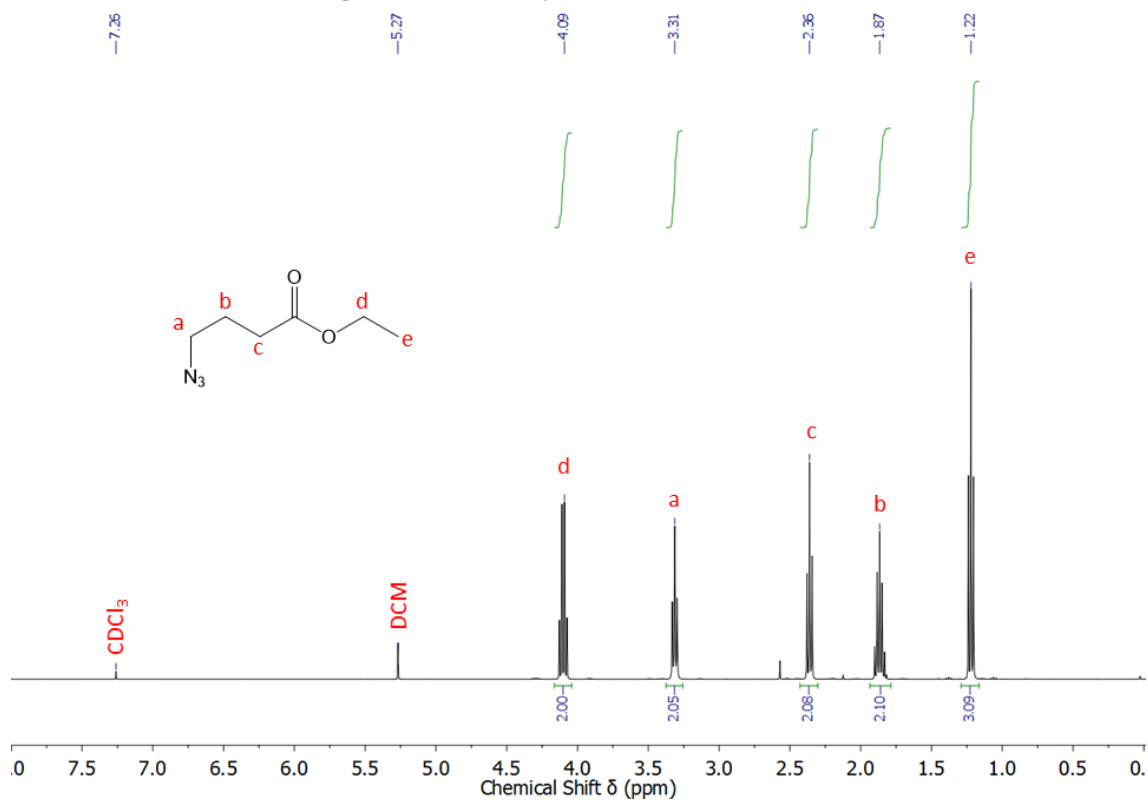
Figure 75: ^{1}H-NMR spectrum of Ethyl 4-azidobutanoate (CDCl$_3$).
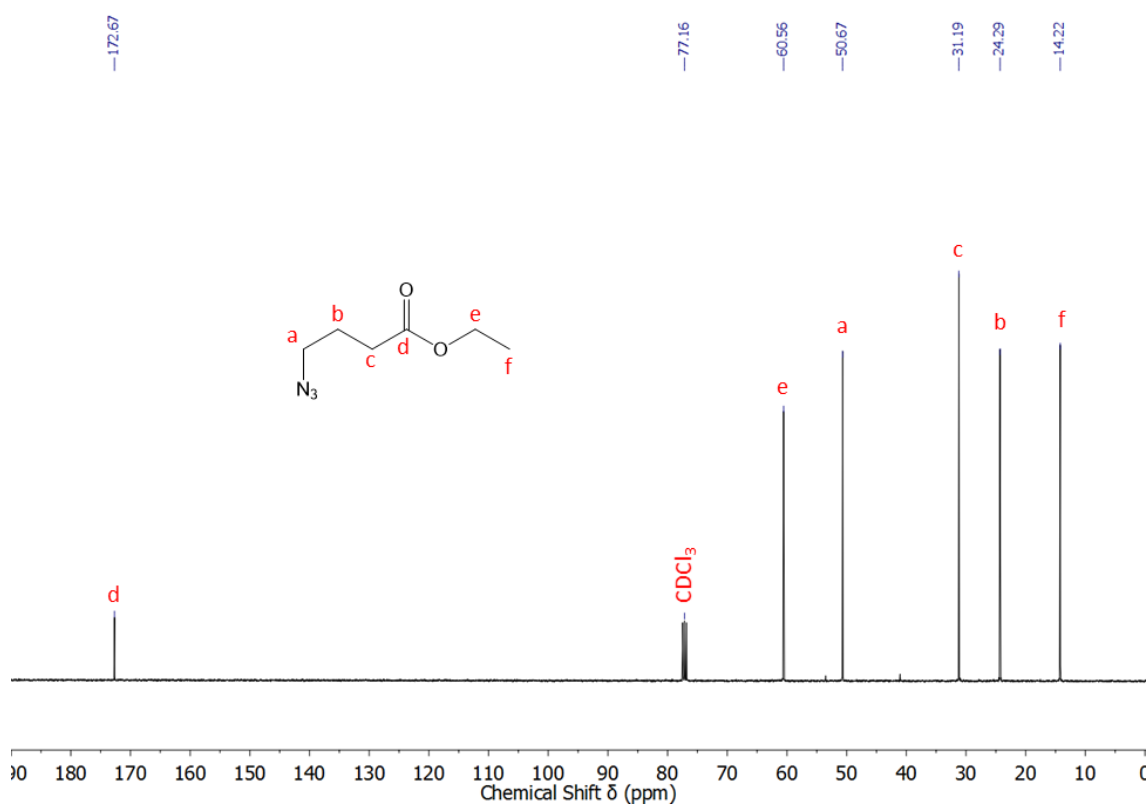
Figure 76: ^{13}C-NMR spectrum of Ethyl 4-azidobutanoate (CDCl$_3$).
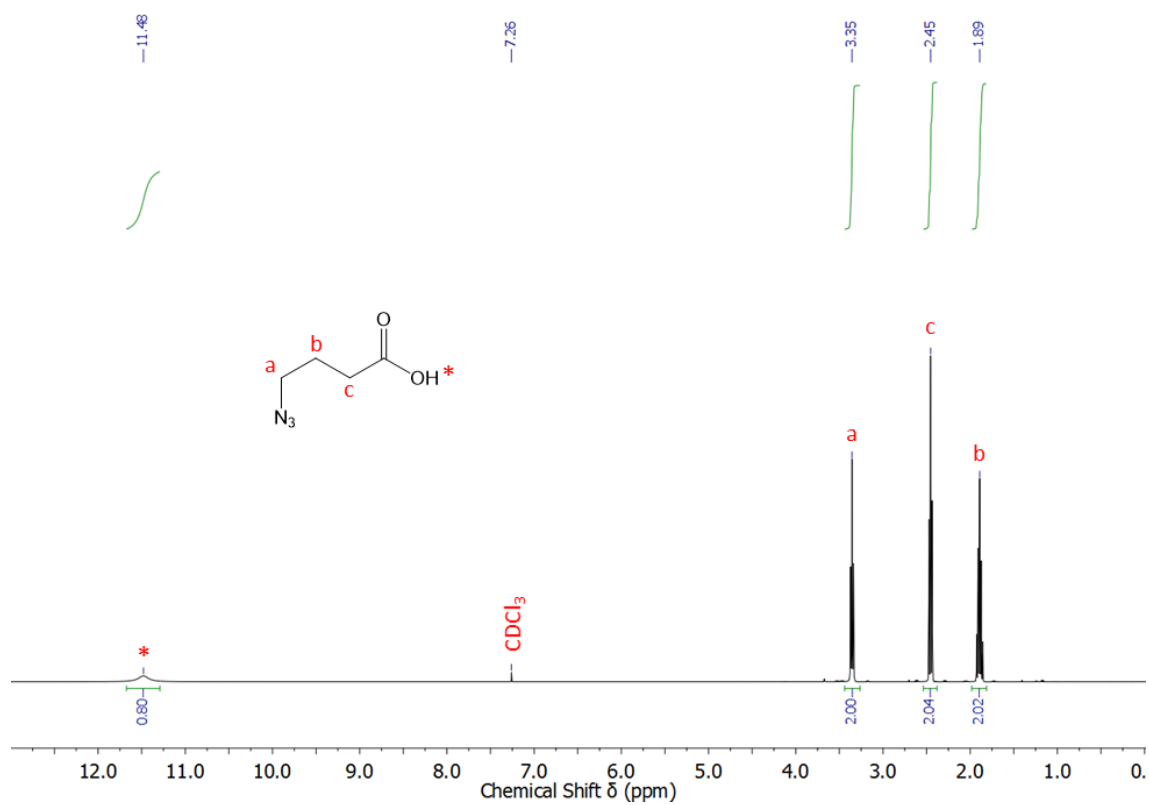
Figure 77: ^{1}H-NMR spectrum of ethyl 4-azidobutanoic acid (CDCl$_3$).
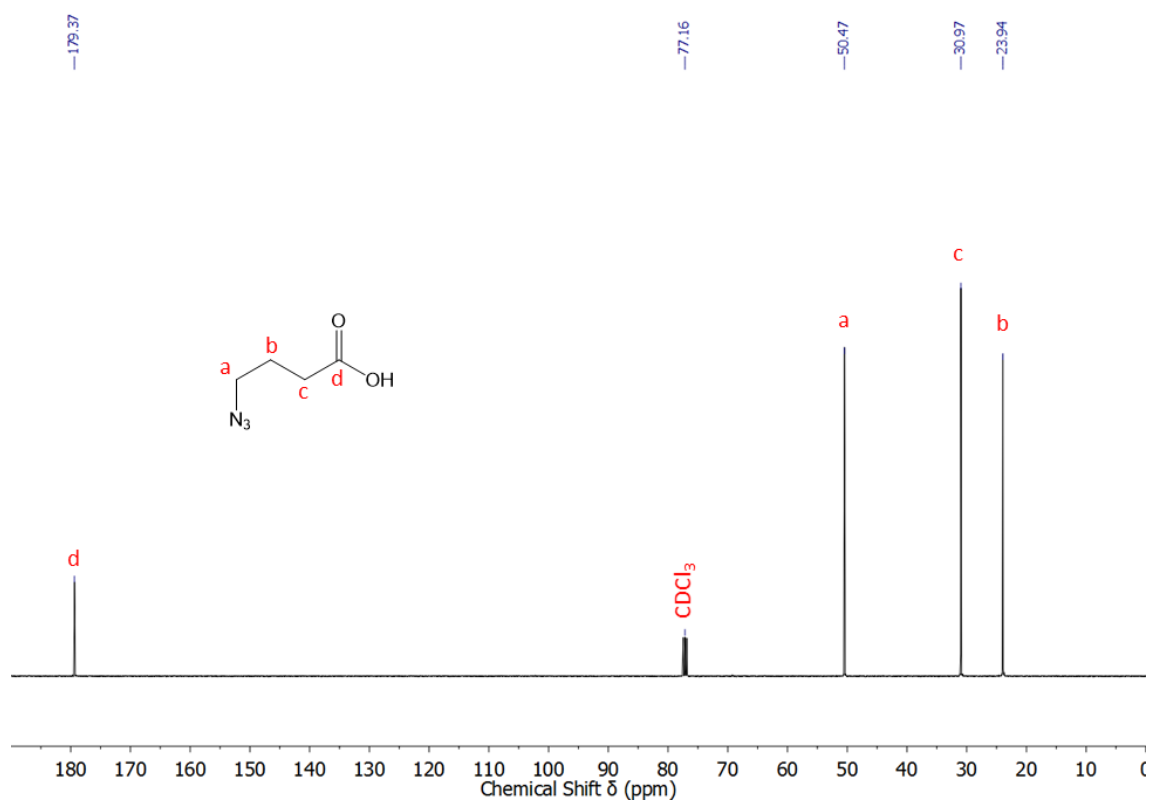
Figure 78: ^{13}C-NMR spectrum of ethyl 4-azidobutanoic acid (CDCl$_3$).
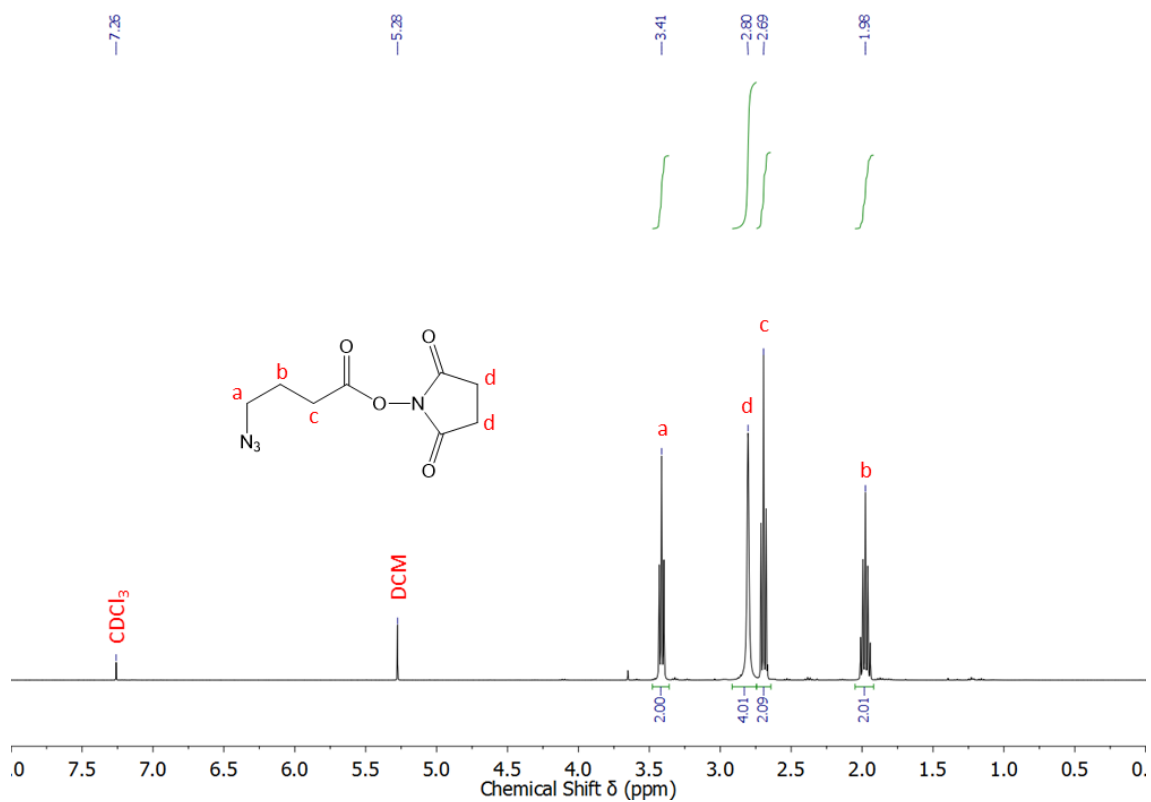
Figure 79: ¹H-NMR spectrum of 2,5-dioxopyrrolidin-1-yl 4-azidobutanoate (CDCl₃).
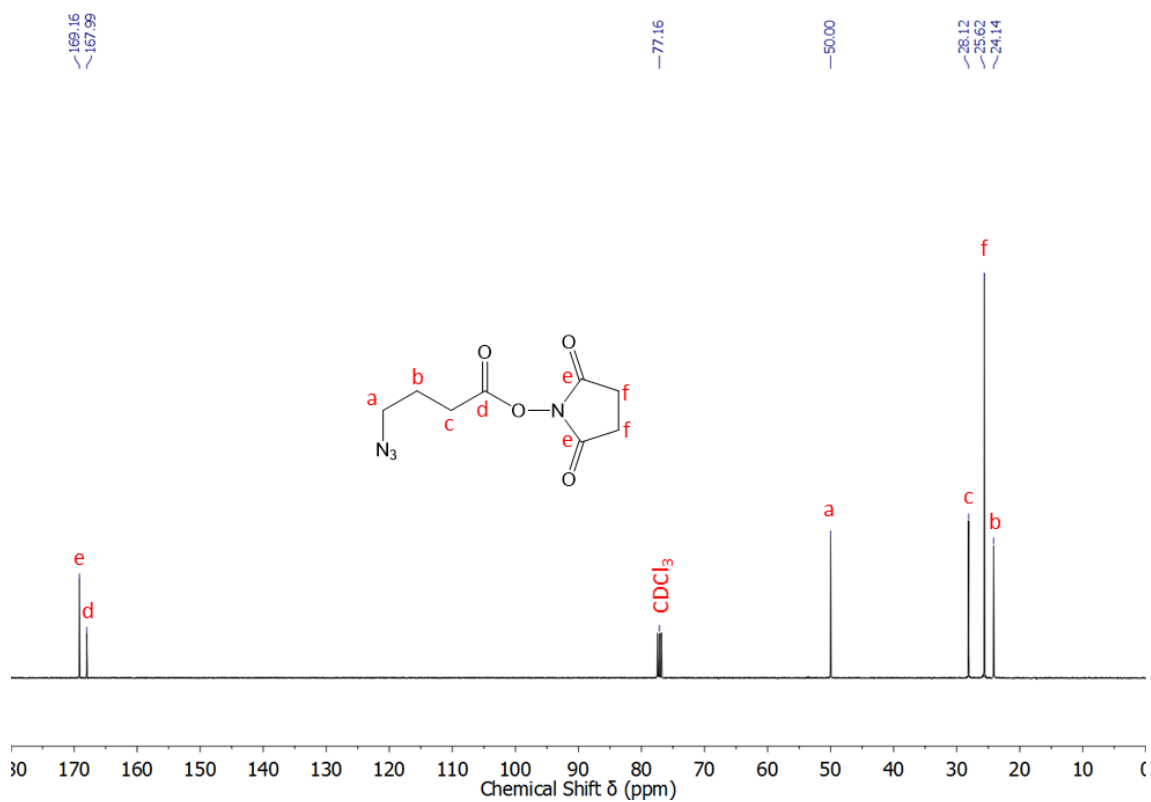
Figure 80: ¹³C-NMR spectrum of 2,5-dioxopyrrolidin-1-yl 4-azidobutanoate (CDCl₃).
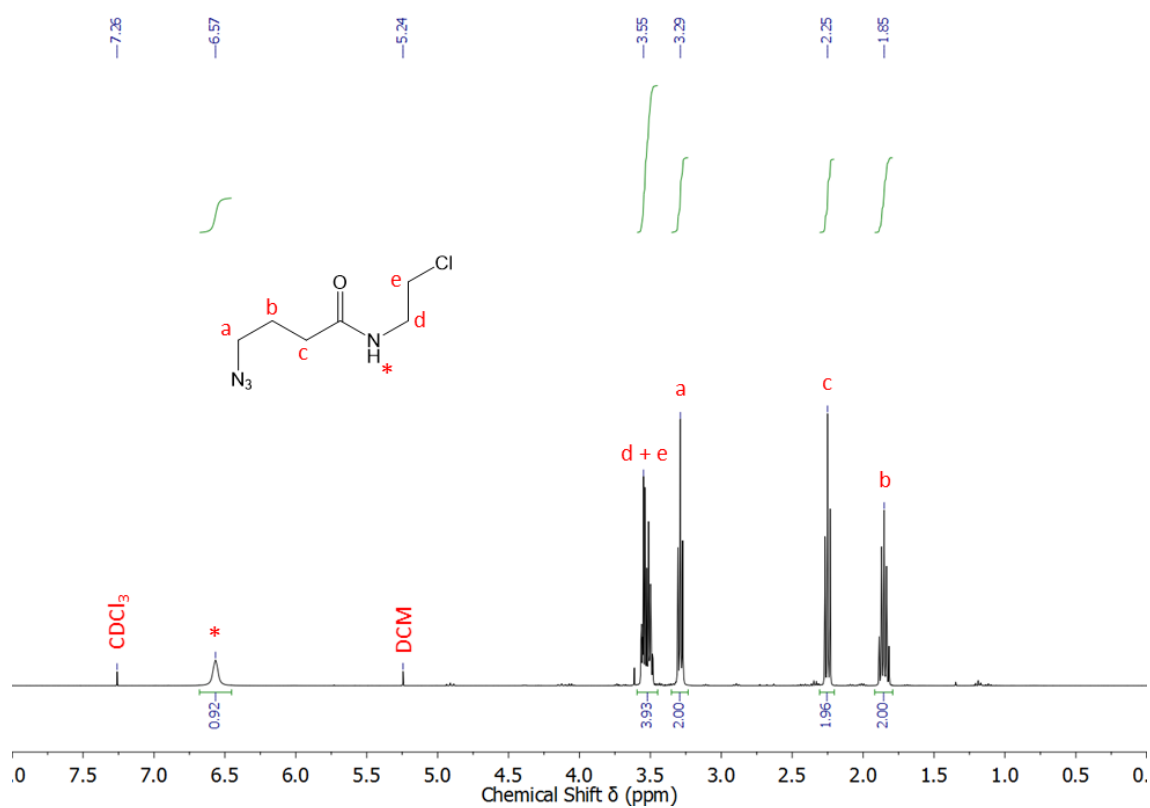
Figure 81: ^{1}H-NMR spectrum of 4-azido-*N*-(2-chloroethyl)butanamide (CDCl$_3$).
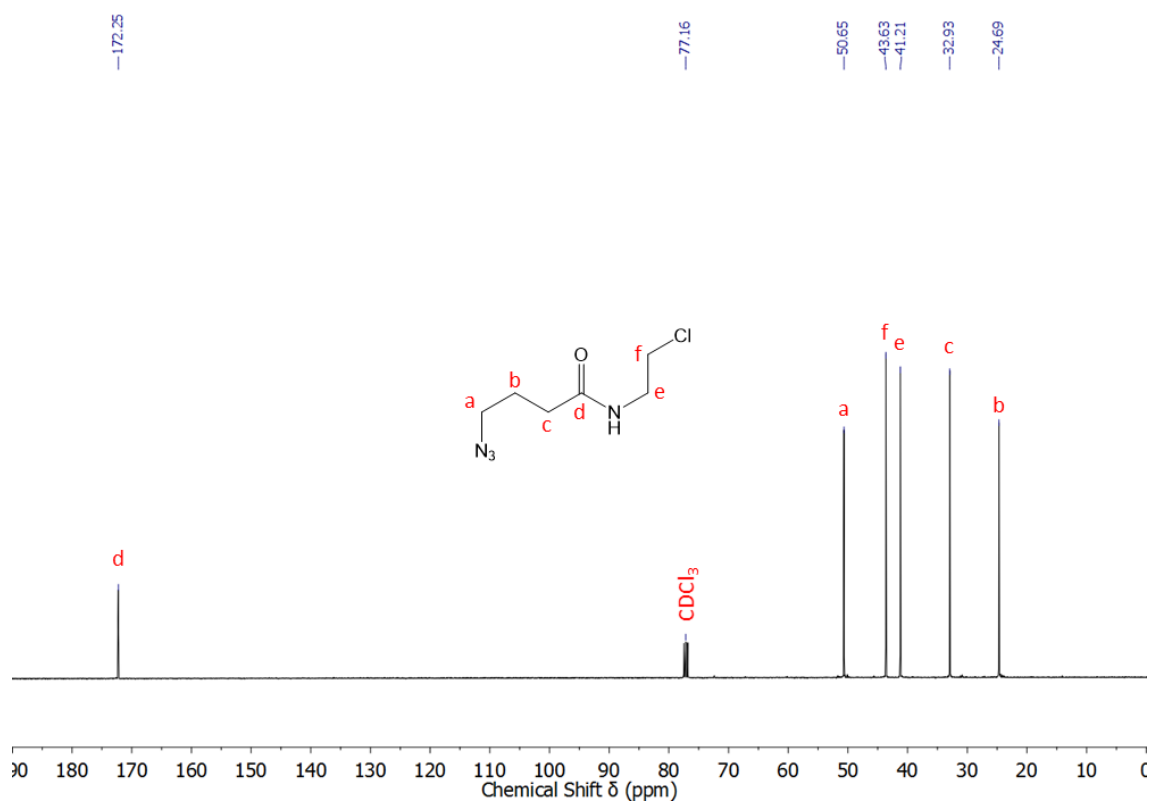
Figure 82: ^{13}C-NMR spectrum of 4-azido-*N*-(2-chloroethyl)butanamide (CDCl$_3$).
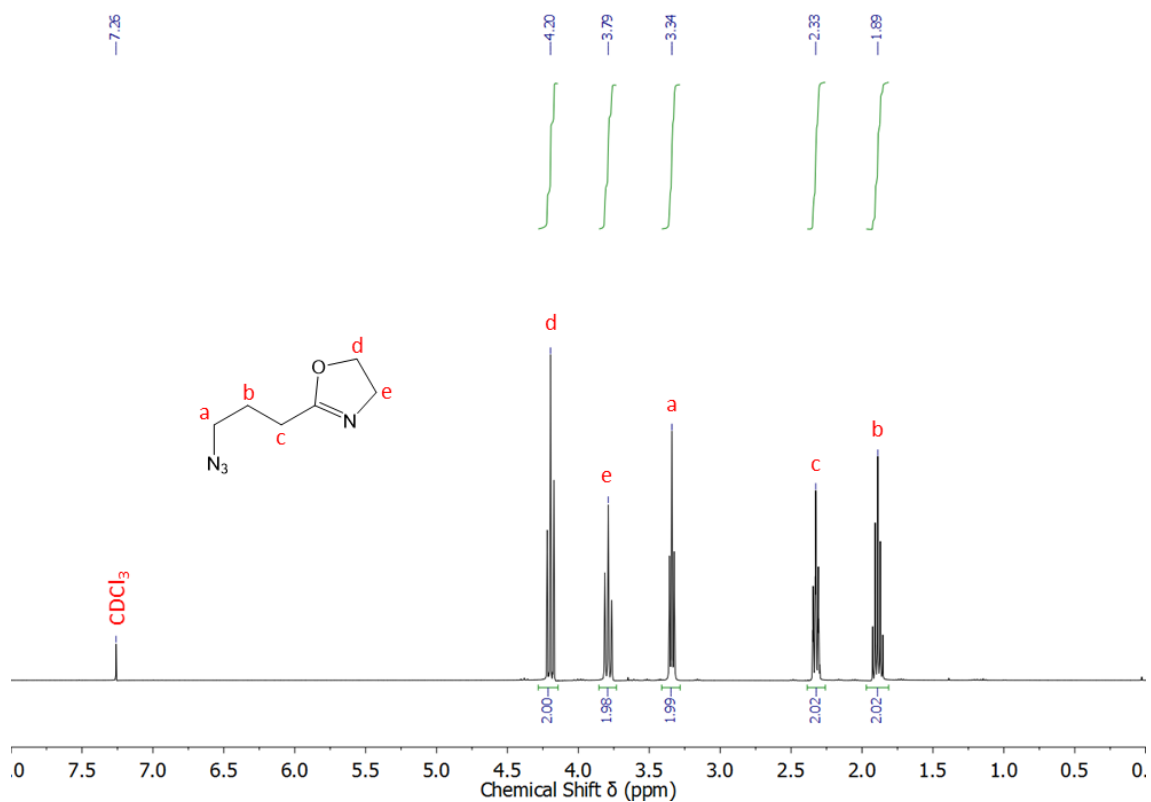
Figure 83: ¹H-NMR spectrum of 2-(3-azidopropyl)-2-oxazoline (CDCl₃).
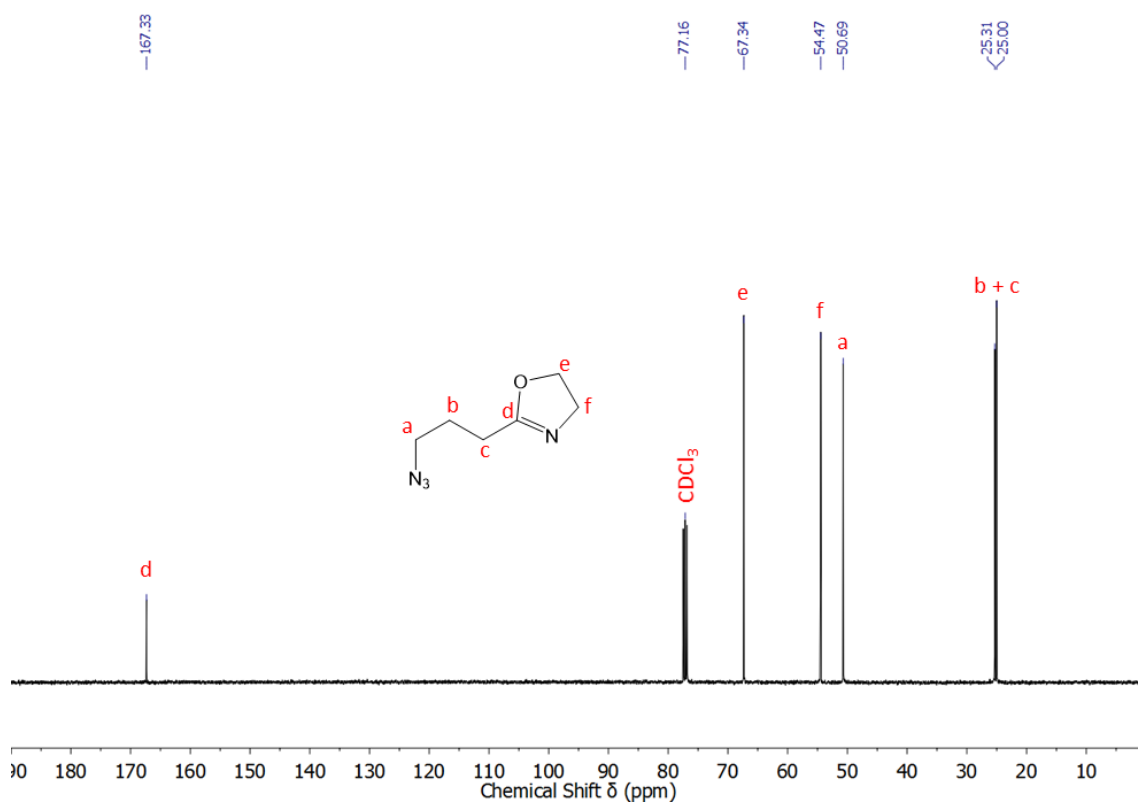
Figure 84: ¹³C-NMR spectrum of 2-(3-azidopropyl)-2-oxazoline (CDCl₃).

7.1.5 Synthesis of Alkyne Derivatives
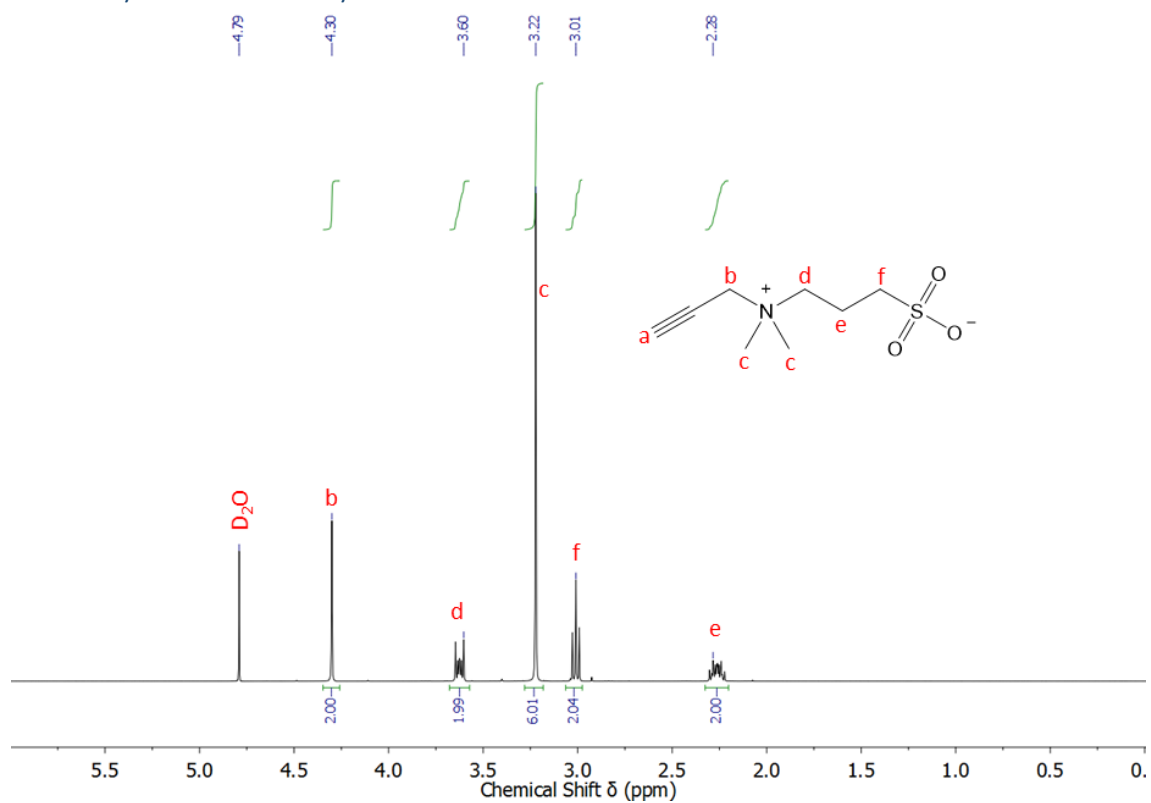
Figure 85: ^{1}H-NMR spectrum of 3-[dimethyl(prop-2-yn-1-yl)ammonio]propane-1-sulfonate (D_2O).
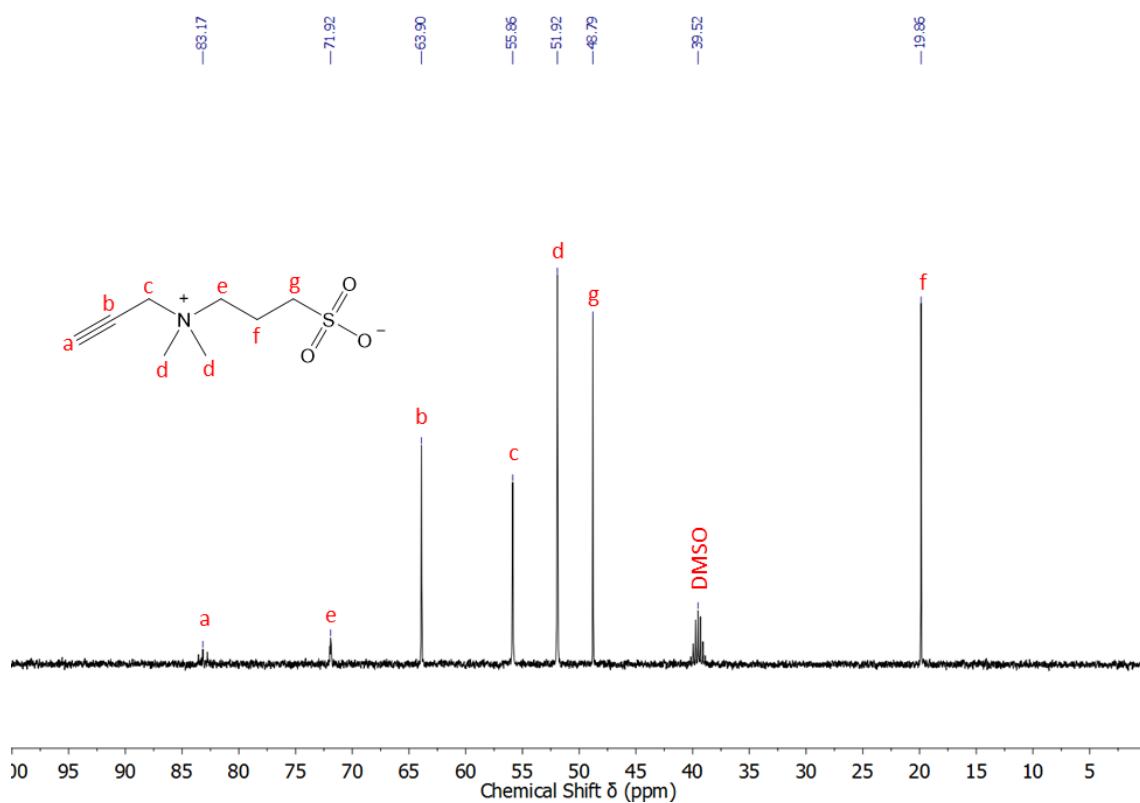
Figure 86: ^{13}C-NMR spectrum of 3-[dimethyl(prop-2-yn-1-yl)ammonio]propane-1-sulfonate (D_2O + DMSO).
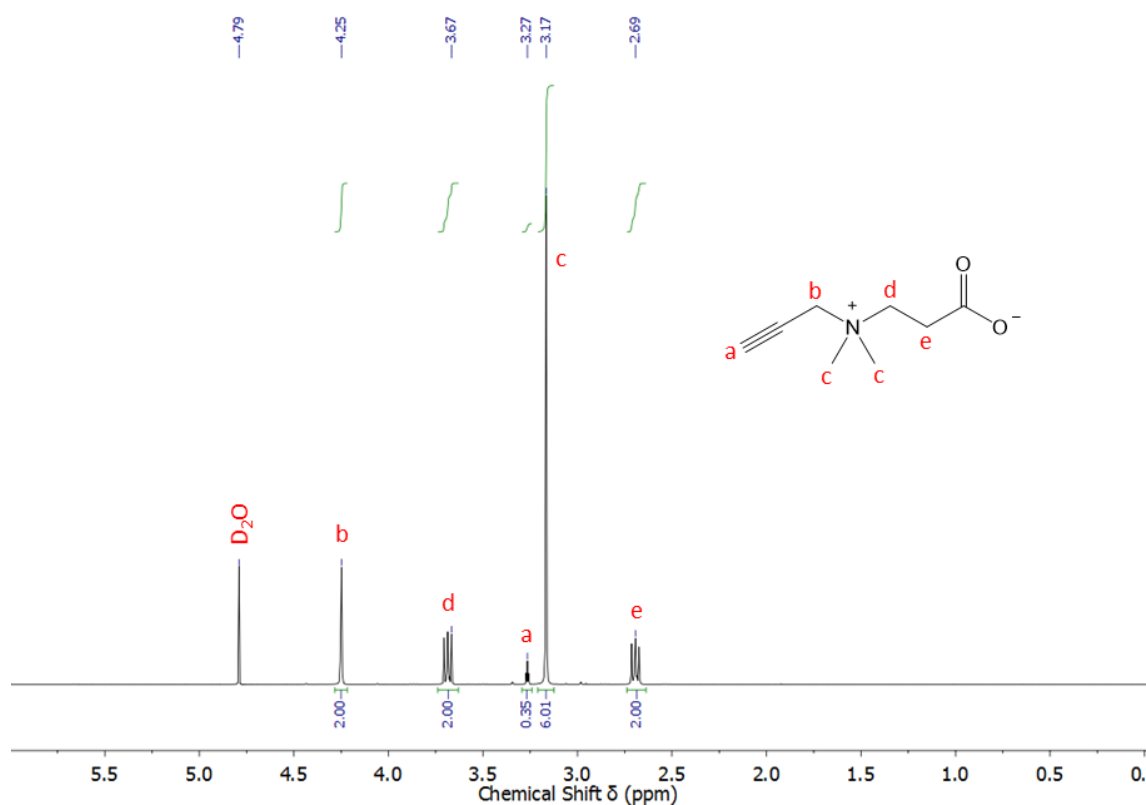
Figure 87: ^{1}H-NMR spectrum of 3-[dimethyl(prop-2-yn-1-yl)ammonio]propane-1-propanoate (D₂O).
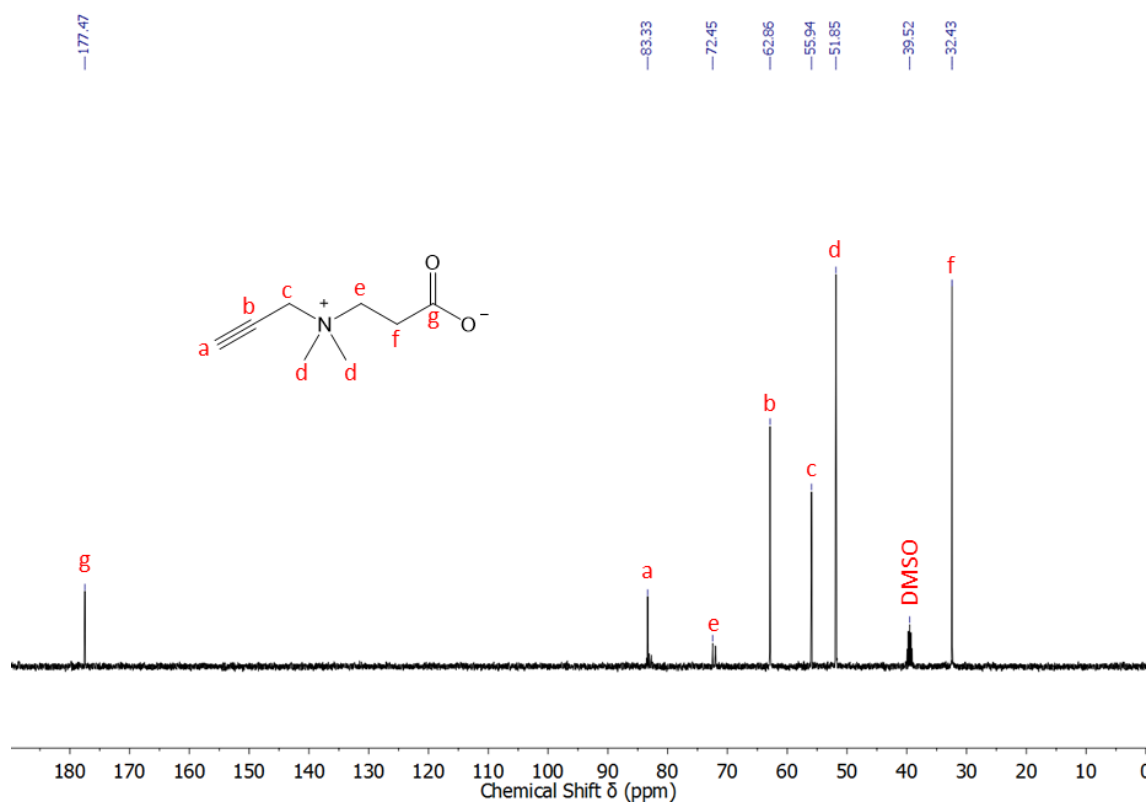
Figure 88: ^{13}C-NMR spectrum of 3-[dimethyl(prop-2-yn-1-yl)ammonio]propane-1-propanoate (D₂O + DMSO).
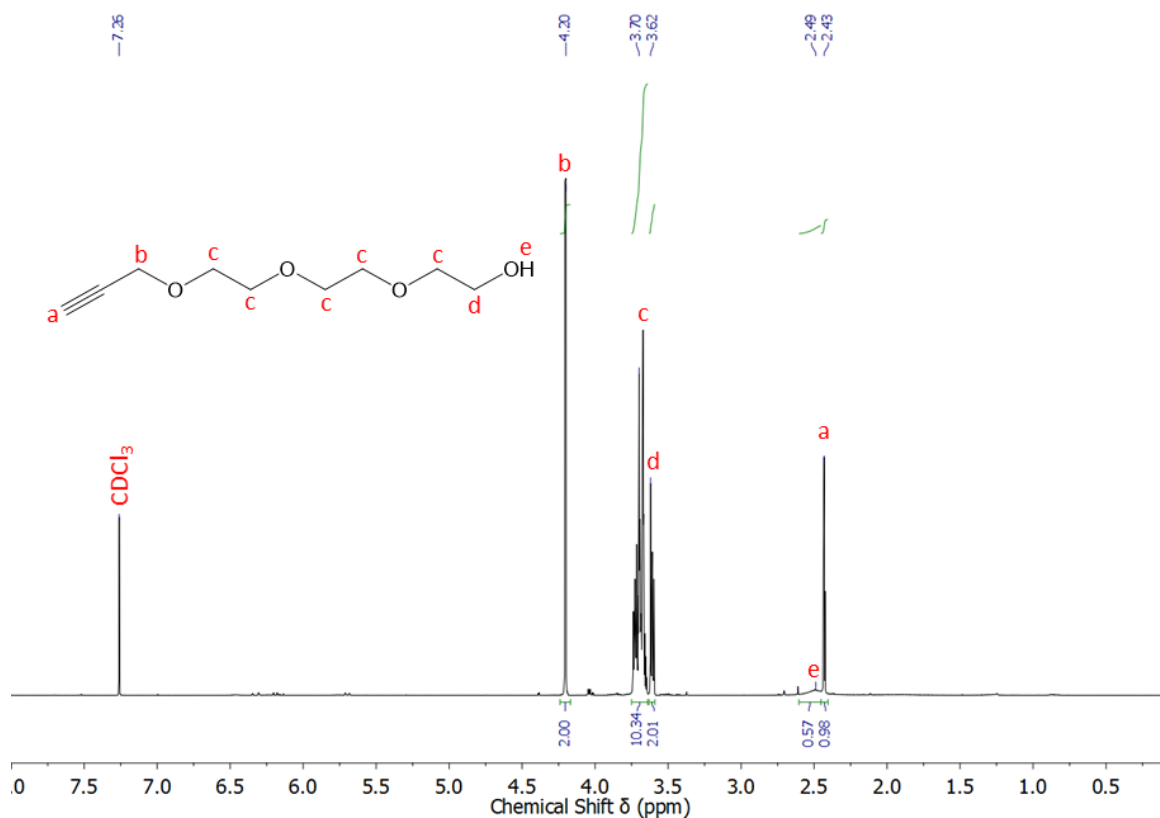
Figure 89: ^{1}H-NMR spectrum of 2-{2-[2-(prop-2-yn-1-yloxy)ethoxy]ethoxy}ethan-1-ol (CDCl$_3$).
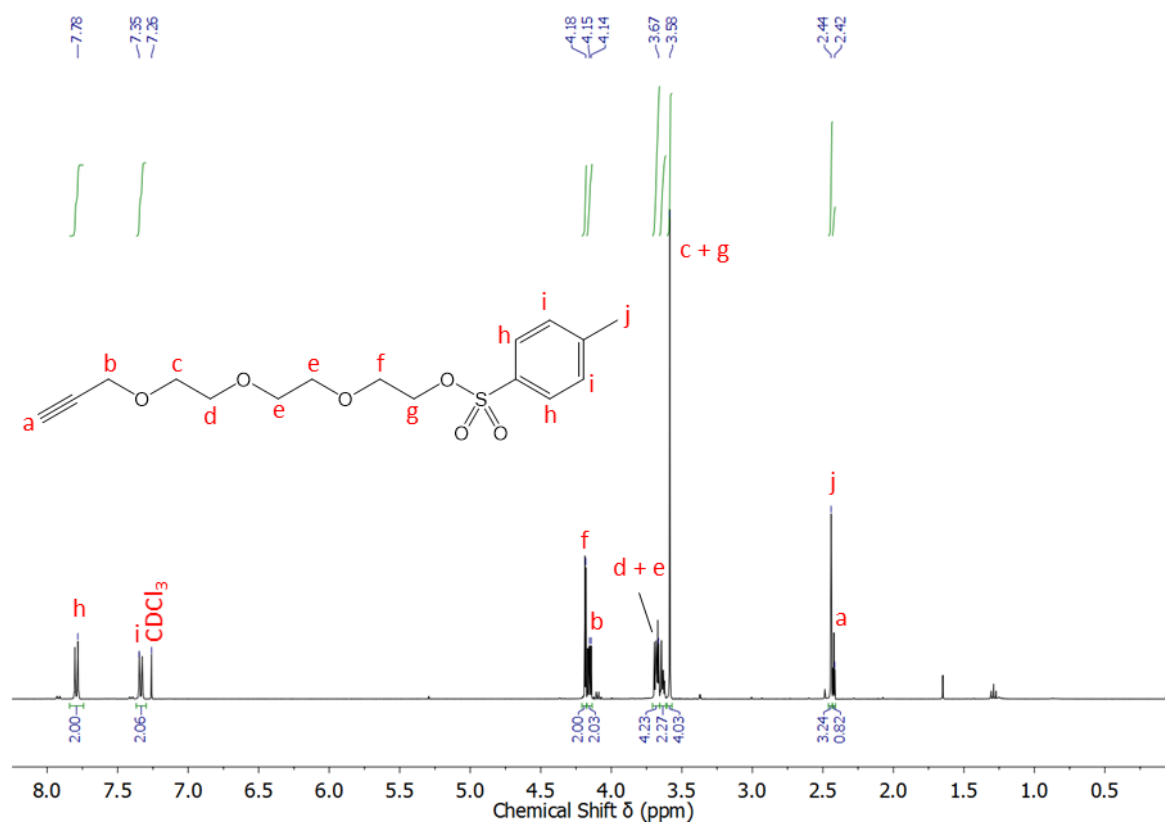
Figure 90: ^{1}H-NMR spectrum of 2-{2-[2-(prop-2-yn-1-yloxy)ethoxy]ethoxy}ethyl 4-methylbenzenesulfonate (CDCl$_3$).
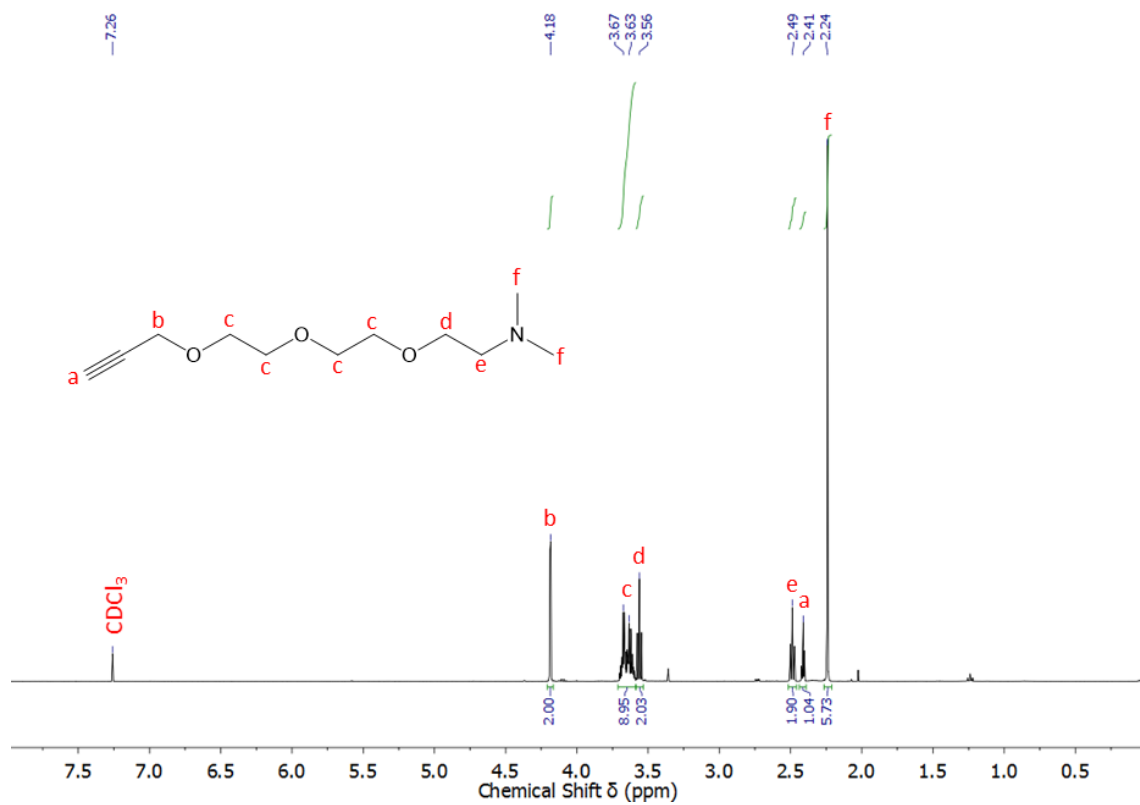
Figure 91: ^{1}H-NMR spectrum of *N,N*-dimethyl-2-{2-[2-(prop-2-yn-1-yloxy)ethoxy]ethoxy}ethan-1-amine (CDCl$_3$).
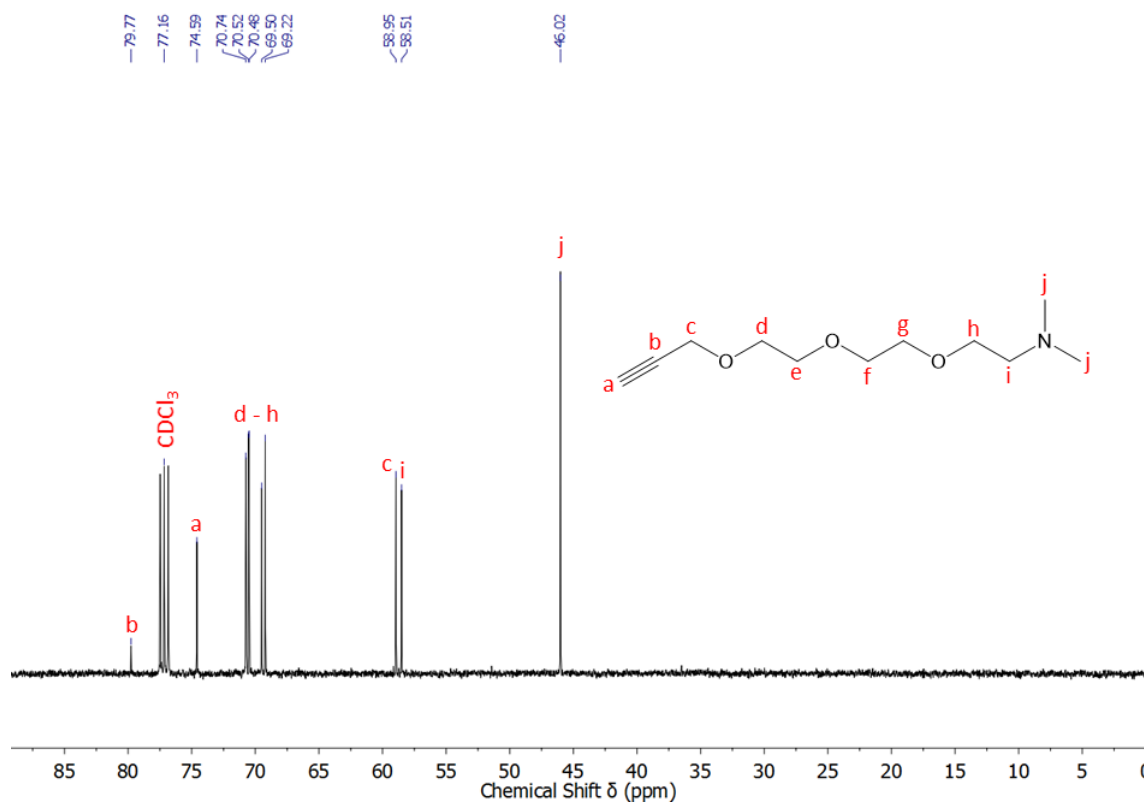
Figure 92: ^{13}C-NMR spectrum of *N,N*-dimethyl-2-{2-[2-(prop-2-yn-1-yloxy)ethoxy]ethoxy}ethan-1-amine (CDCl$_3$).
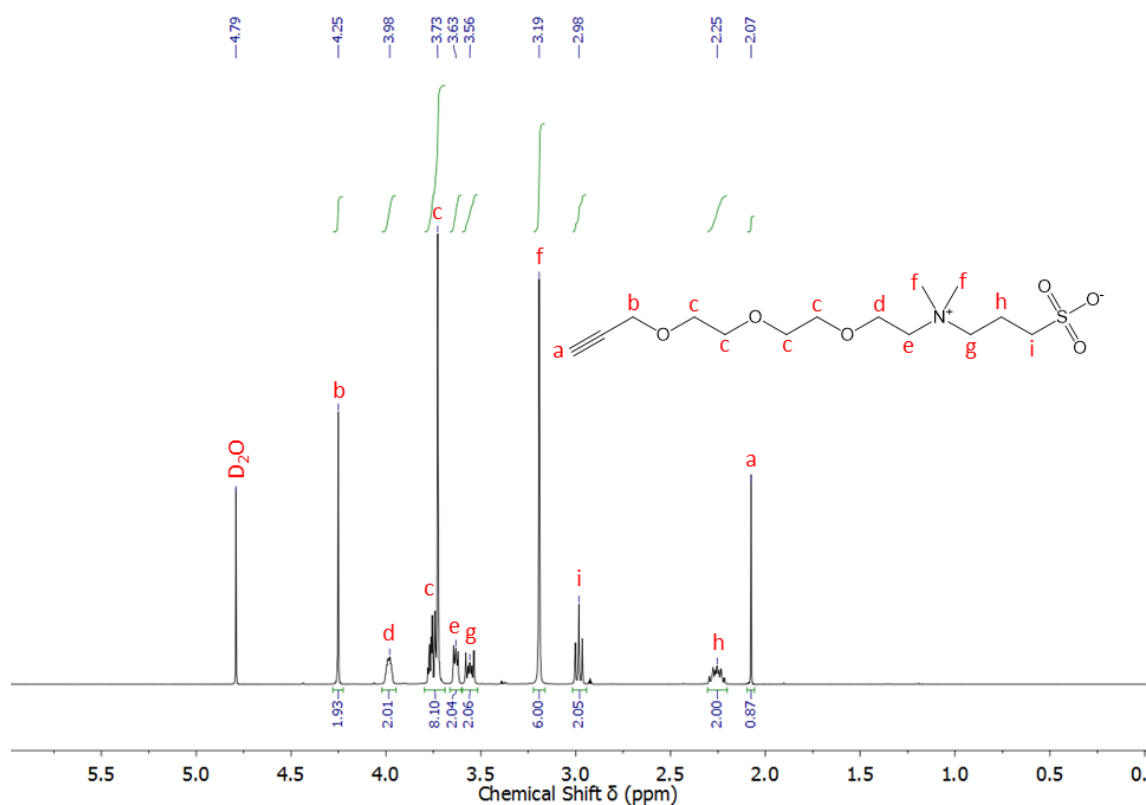
Figure 93: ¹H-NMR spectrum of 3-{dimethyl{2-[2-(prop-2-yn-1-yloxy)ethoxy]ethyl}ammonio}propane-1-sulfonate.
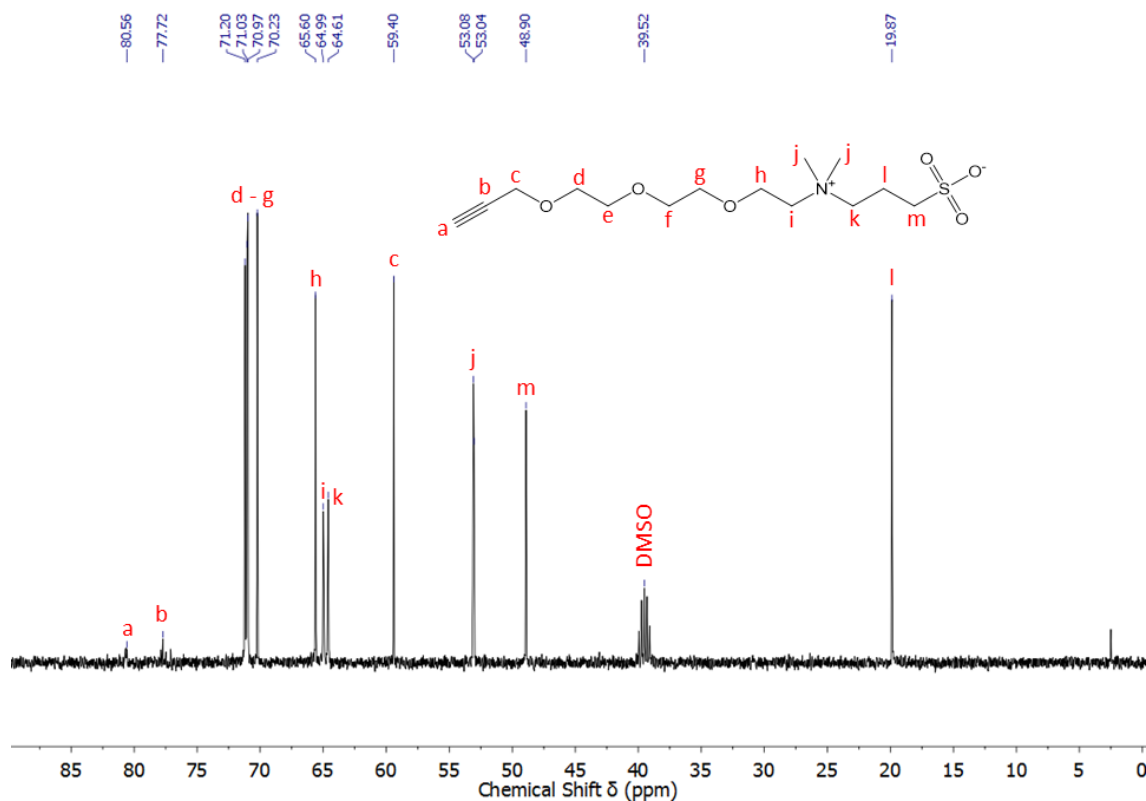
Figure 94: ¹³C-NMR spectrum of 3-{dimethyl{2-[2-(prop-2-yn-1-yloxy)ethoxy]ethyl}ammonio}propane-1-sulfonate.

7.2 Polymer Synthesis

7.2.1 Synthesis of Poly(2-Alkyl-2-Oxazoline)s
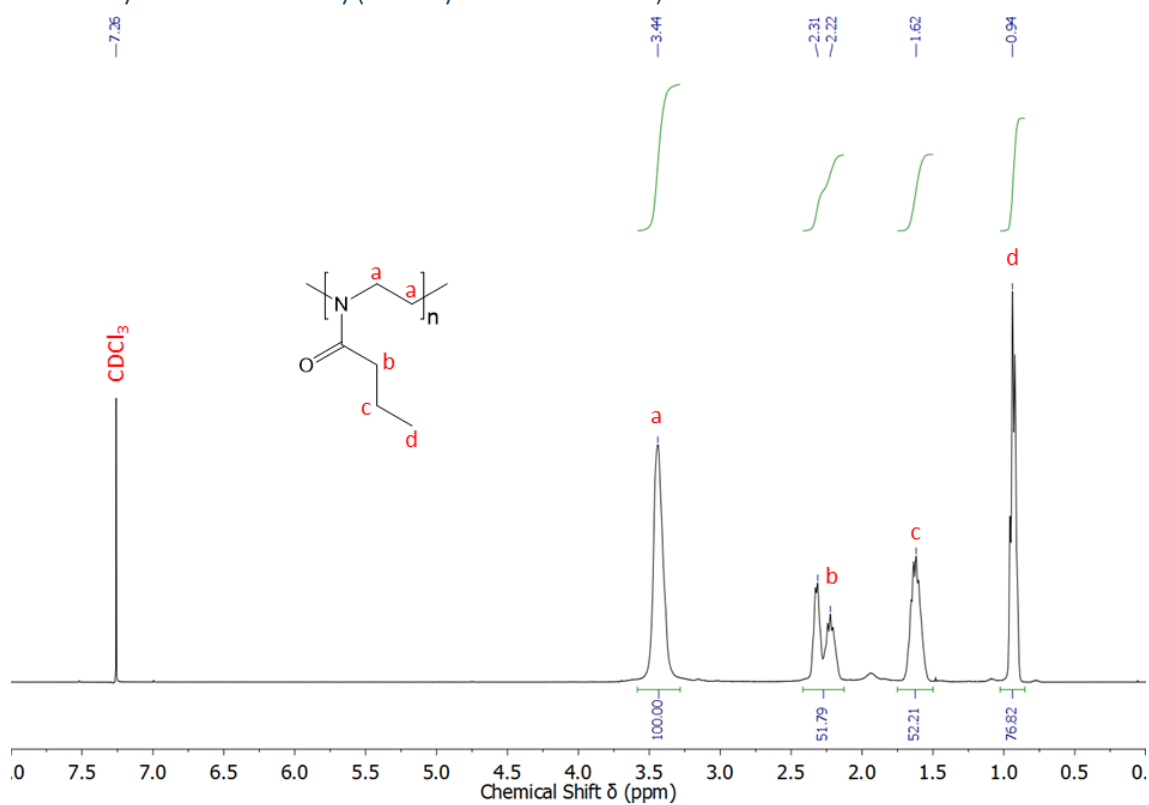
Figure 95: ^{1}H-NMR spectrum of poly(2-*n*-propyl-2-oxazoline) (CDCl$_3$).
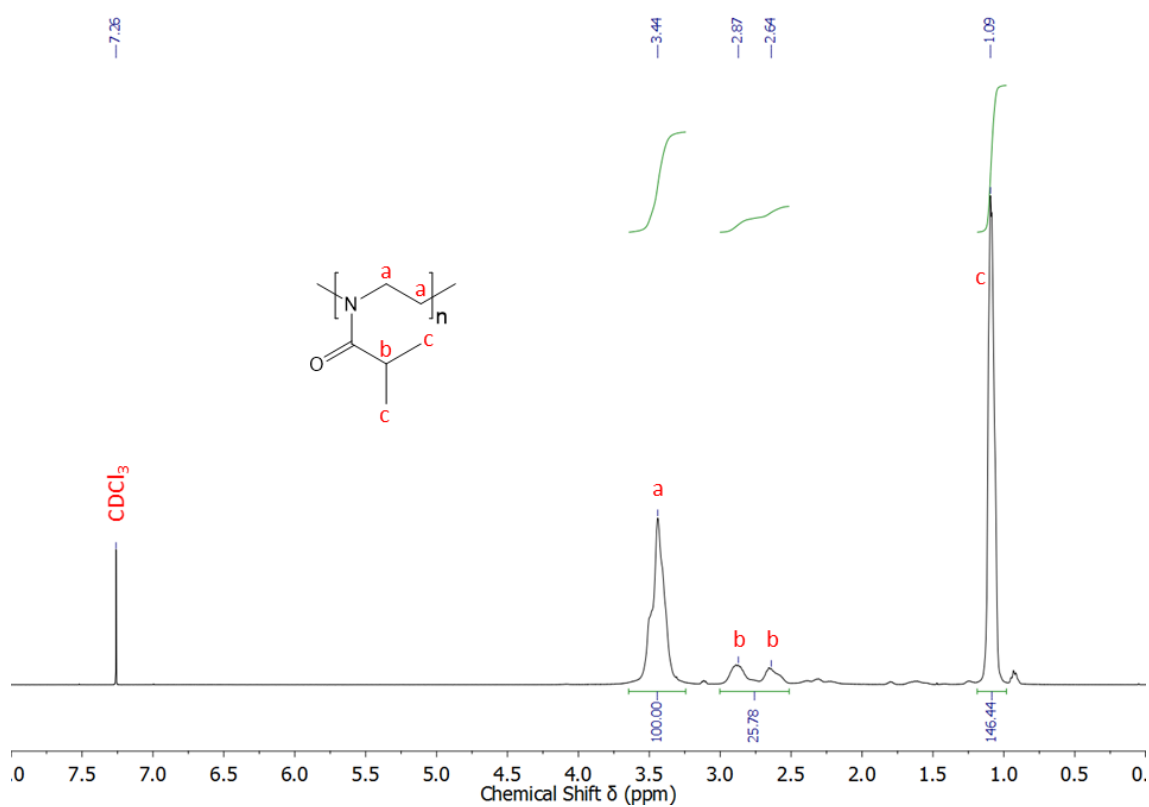
Figure 96: ^{1}H-NMR spectrum of poly(2-isopropyl-2-oxazoline) (CDCl$_3$).
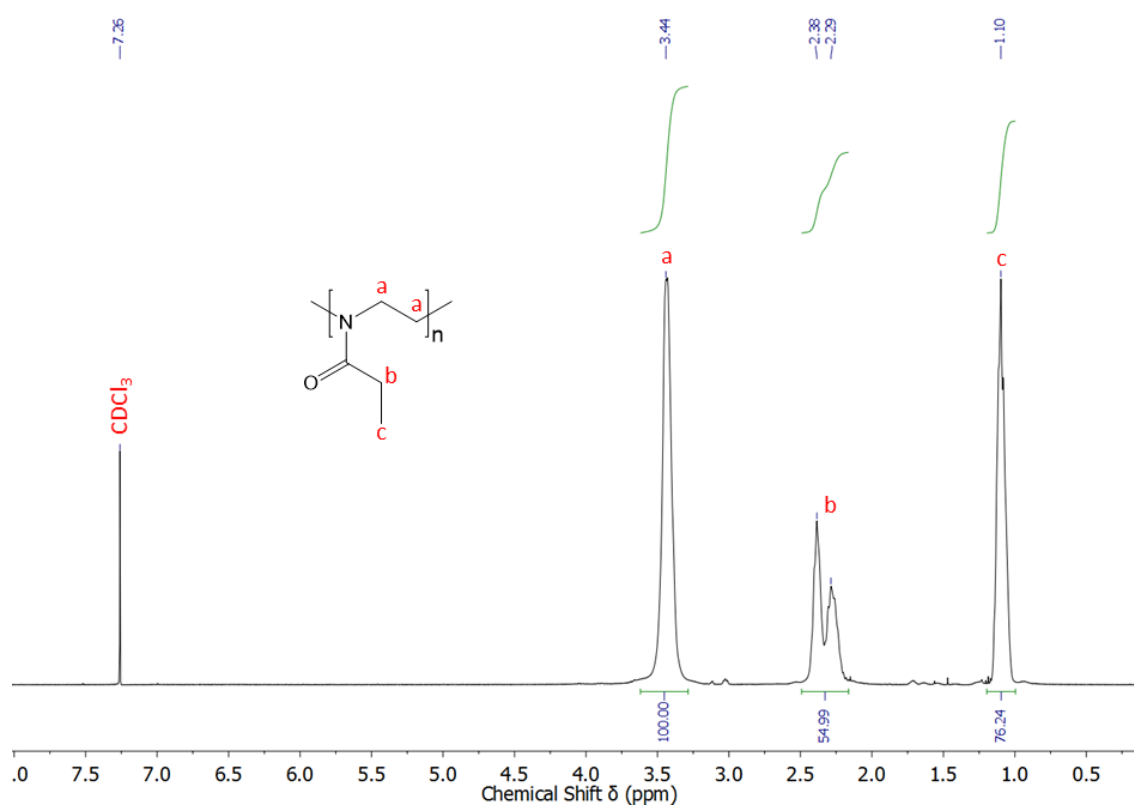
Figure 97: ^{1}H-NMR spectrum of poly(2-ethyl-2-oxazoline) (CDCl$_3$).

7.2.2 Synthesis of Poly(2-Alkyl-2-Oxazoline-*co*-2-Benzophenone-2-Oxazoline)
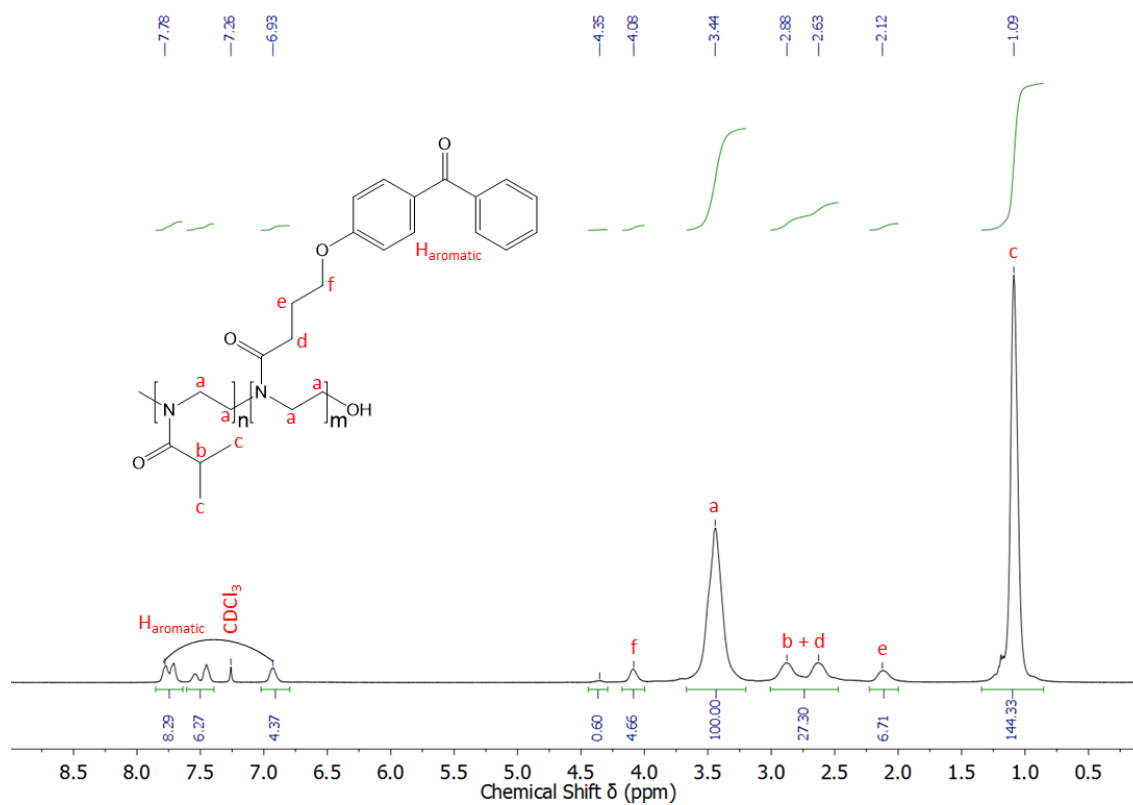
Figure 98: ^{1}H-NMR spectrum of poly(2-alkyl-2-oxazoline-*co*-2-benzophenone-2-oxazoline) (CDCl$_3$).

7.2.3 Synthesis of Poly(2-Alkyl-2-Oxazoline-co-2-(3-Azidopropyl)-2-Oxazoline)
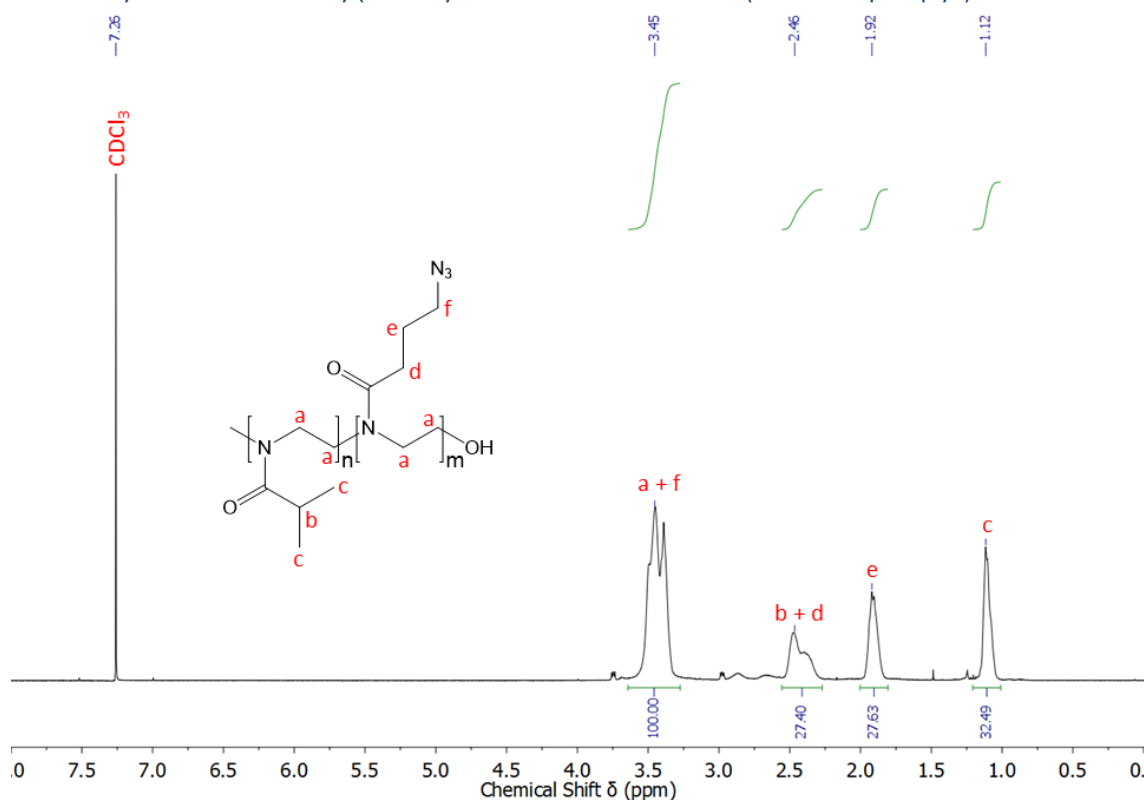
Figure 99: ^{1}H-NMR spectrum of poly(2-isopropyl-2-oxazoline-*co*-2-(3-azidopropyl)-2-oxazoline) (CDCl₃).
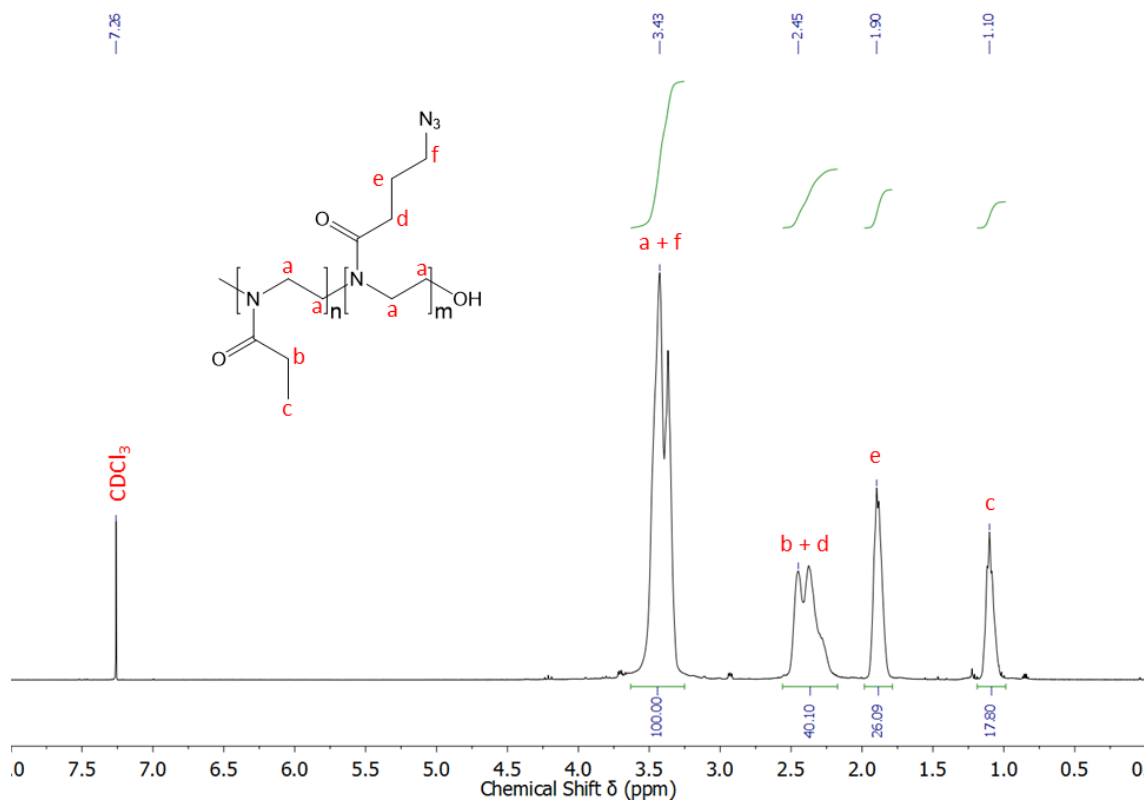
Figure 100: ^{1}H-NMR spectrum of poly(2-ethyl-2-oxazoline-*co*-2-(3-azidopropyl)-2-oxazoline) (CDCl₃).

7.2.4 Synthesis of Poly(2-isoPropyl-2-Oxazoline-*co*-2-(3-Azidopropyl)-2-Oxazoline-co-2-Benzophenone-2-Oxazoline)
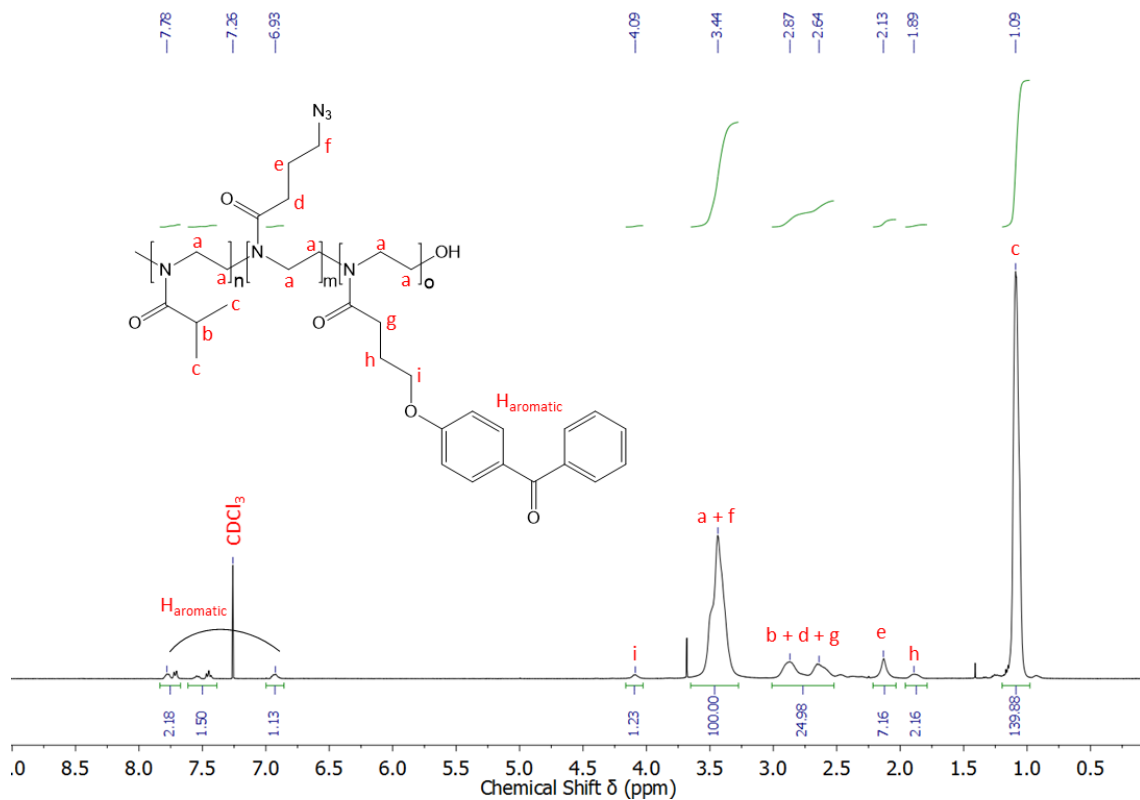
Figure 101: ¹H-NMR spectrum of poly(2-isopropyl-2-oxazoline-*co*-2-(3-azidopropyl)-2-oxazoline-*co*-2-benzophenone-2-oxazoline) (CDCl₃).

7.3 Modification of Poly(2-isoPropyl-2-Oxazoline-*co*-2-(3-Azidopropyl)-2-Oxazoline-*co*-2-Benzophenone-2-Oxazoline) by Copper Catalyzed Huisgen 1,3-dipolar Cycloaddition
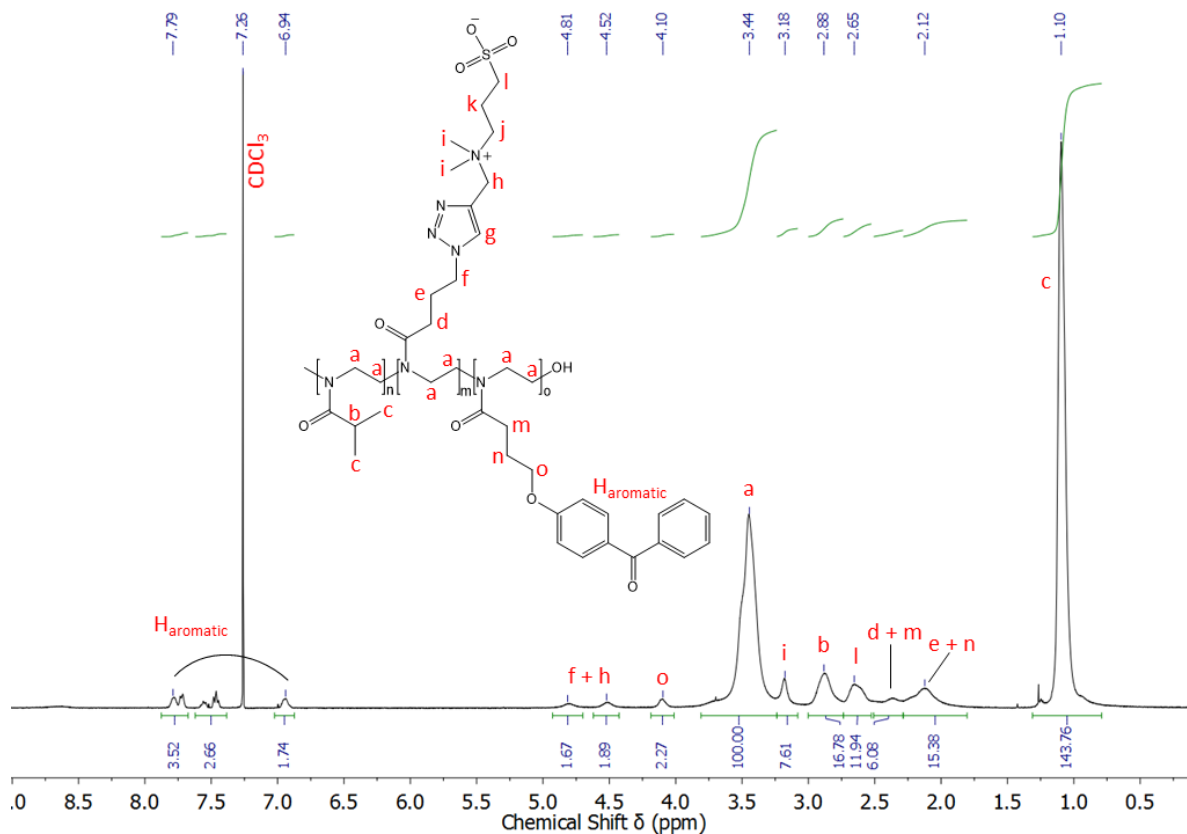
Figure 102: ^{1}H-NMR spectrum of poly(2-isopropyl-2-oxazoline-*co*-sulfobetaine-*co*-2-benzophenone-2-oxazoline) (CDCl$_3$).
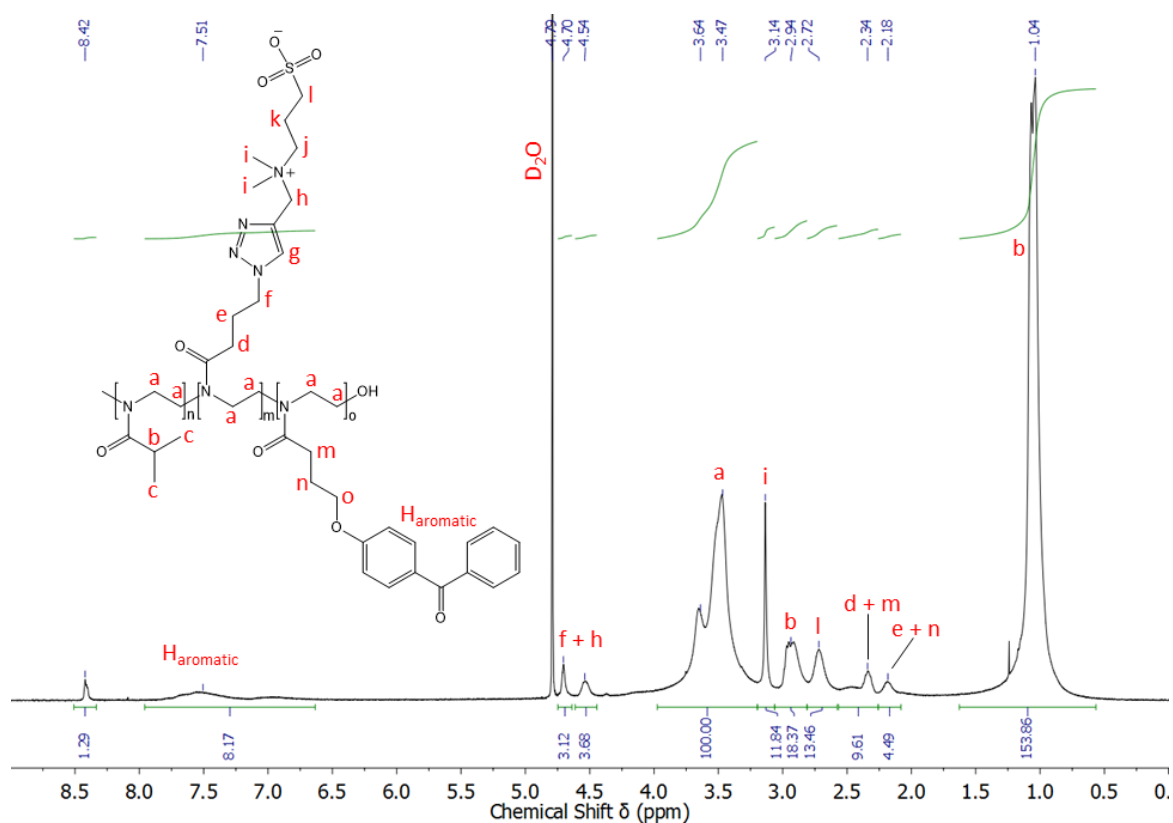
Figure 103: ^{1}H-NMR spectrum of ^{1}H-NMR spectrum of poly(2-isopropyl-2-oxazoline-*co*-sulfobetaine-*co*-2-benzophenone-2-oxazoline) (D$_2$O).
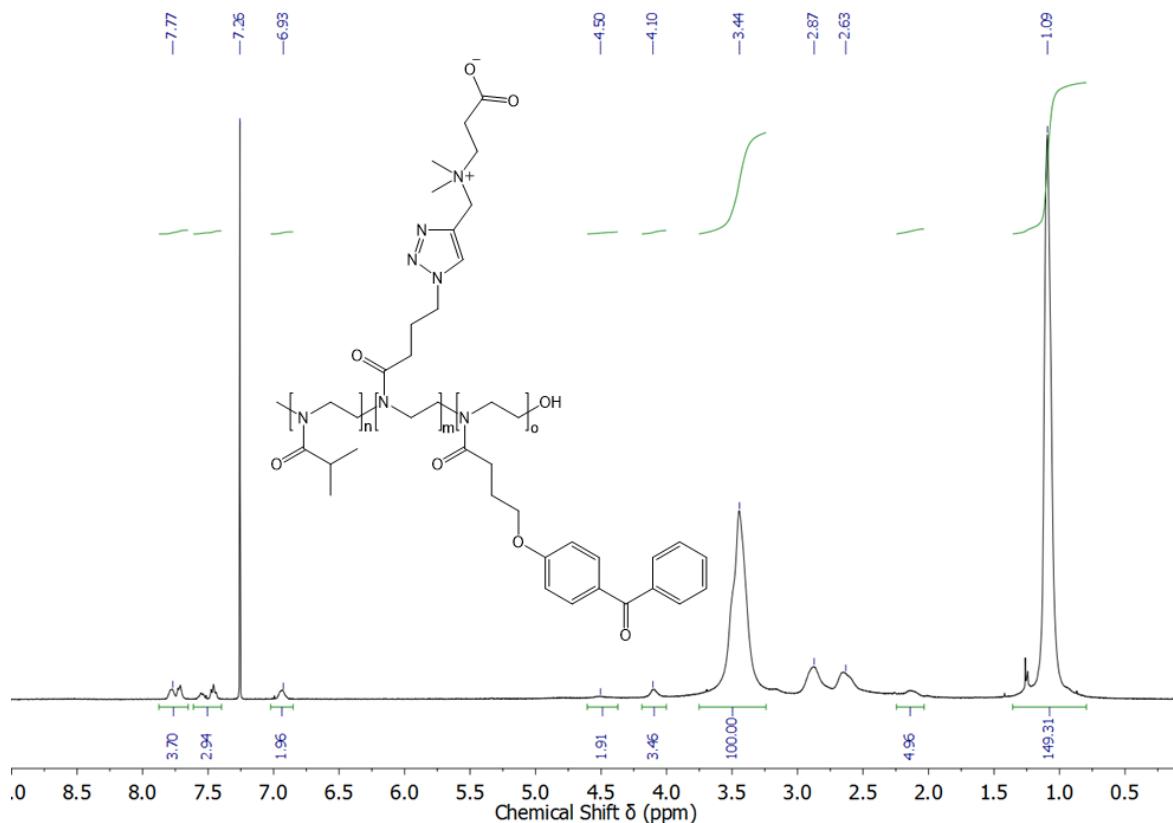
Figure 104: ^{1}H-NMR spectrum of poly(2-isopropyl-2-oxazoline-*co*-carboxybetaine-*co*-2-benzophenone-2-oxazoline) (CDCl$_3$).
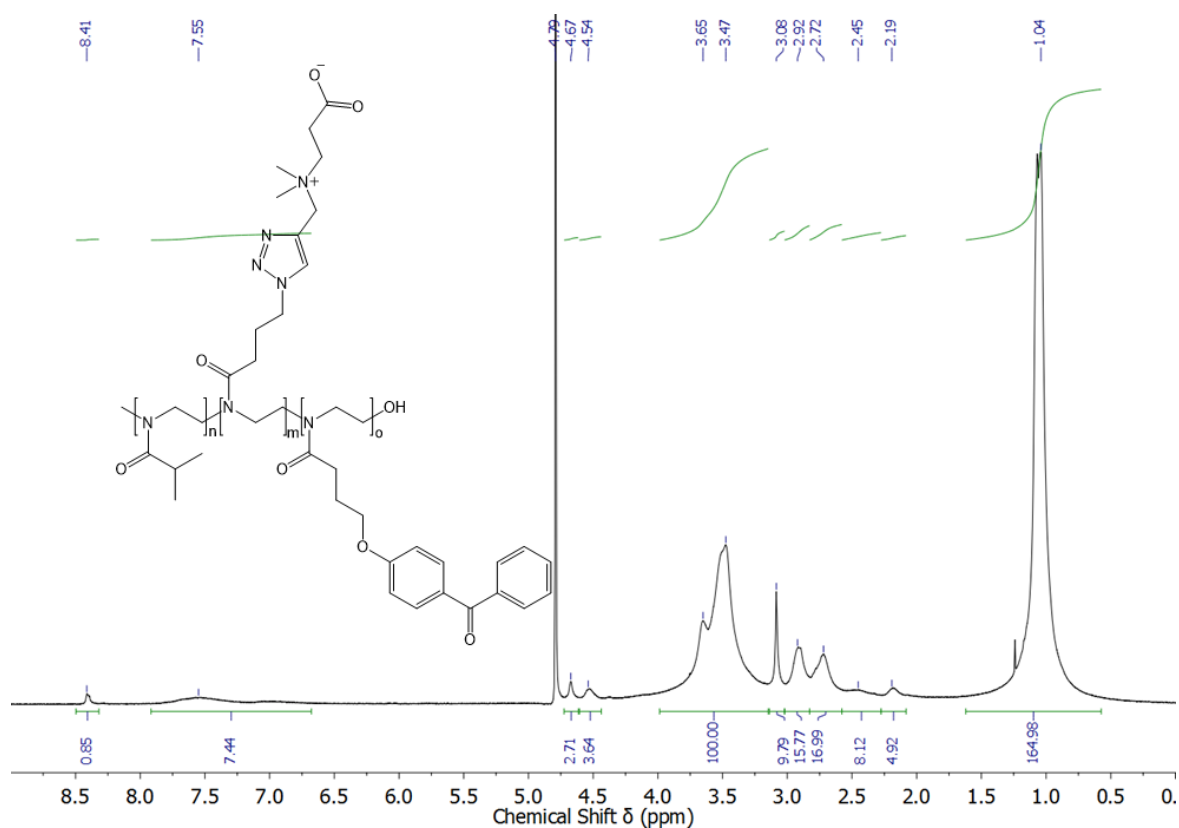
Figure 105: ^{1}H-NMR spectrum of poly(2-isopropyl-2-oxazoline-co-carboxybetaine-co-2-benzophenone-2-oxazoline) (D$_2$O).
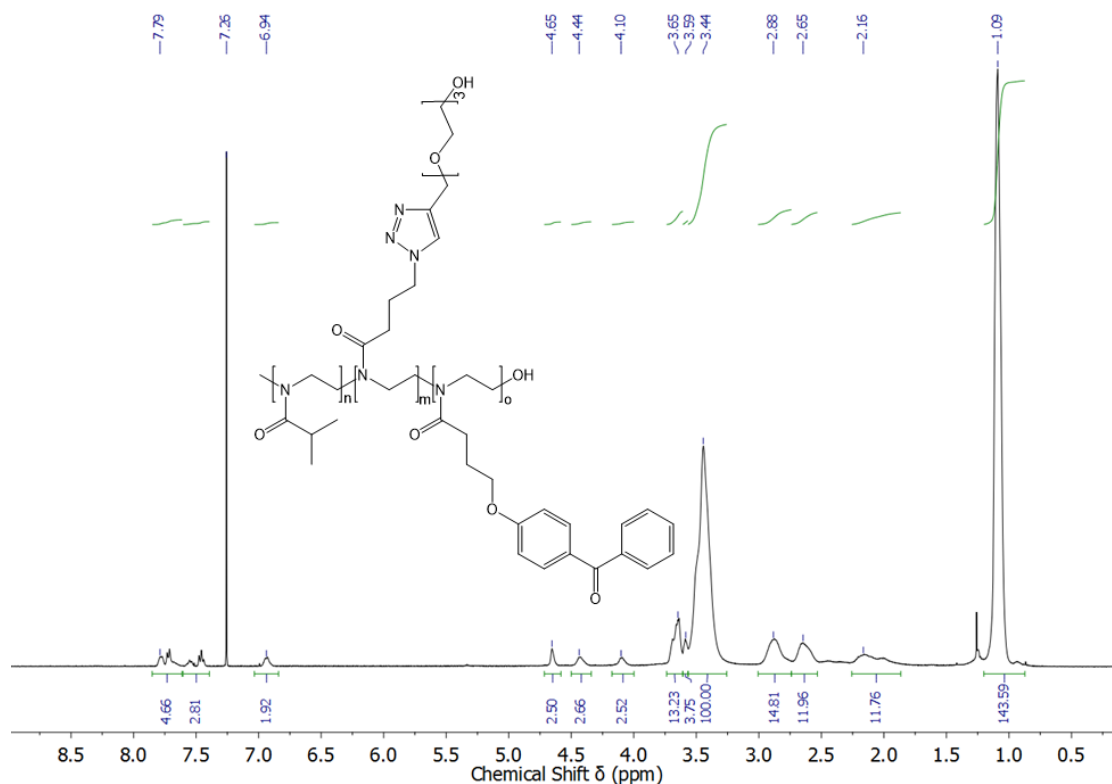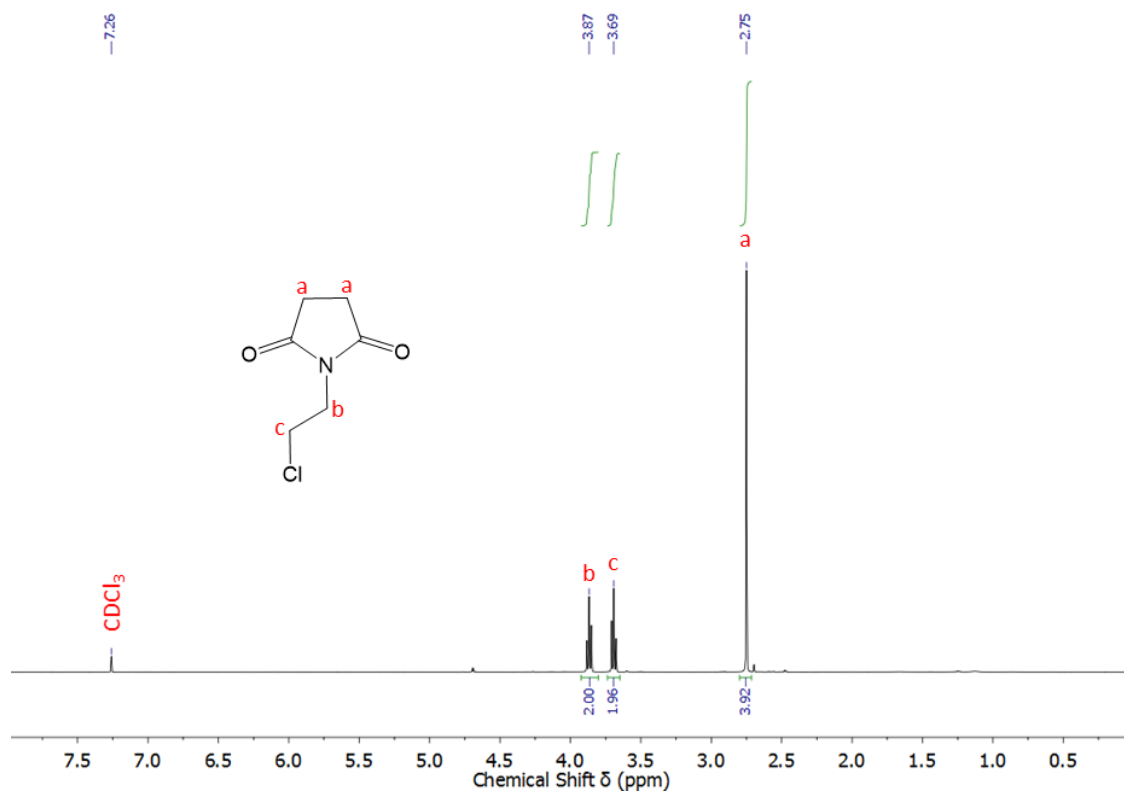

Figure 106: ^{1}H-NMR spectrum of poly(2-isopropyl-2-oxazoline-*co*-oligoethylene glycol-*co*-2-benzophenone-2-oxazoline) (CDCl$_3$).
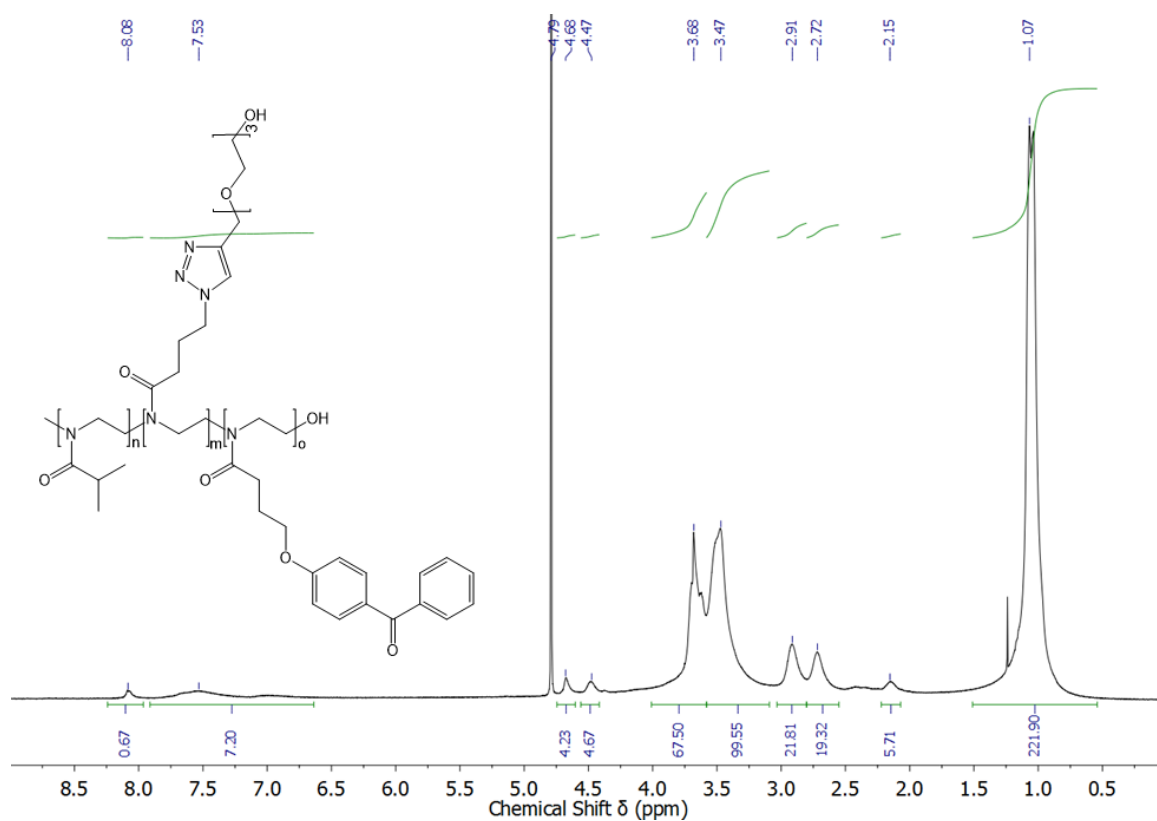
Figure 107: ^{1}H-NMR spectrum of poly(2-isopropyl-2-oxazoline-*co*-oligoethylene glycol-*co*-2-benzophenone-2-oxazoline) (D$_2$O).
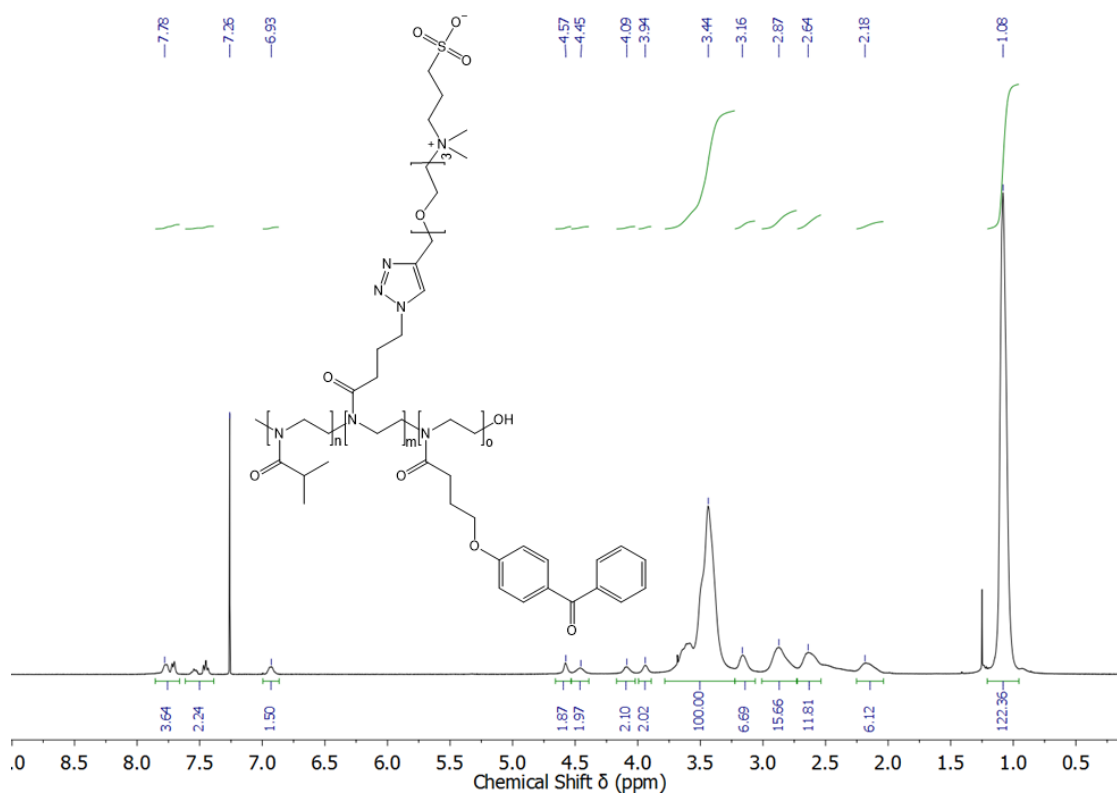
Figure 108: ^{1}H-NMR spectrum of poly(2-isopropyl-2-oxazoline-*co*-oligoethylene glycol-sulfobetaine-*co*-2-benzophenone-2-oxazoline) (CDCl$_3$).
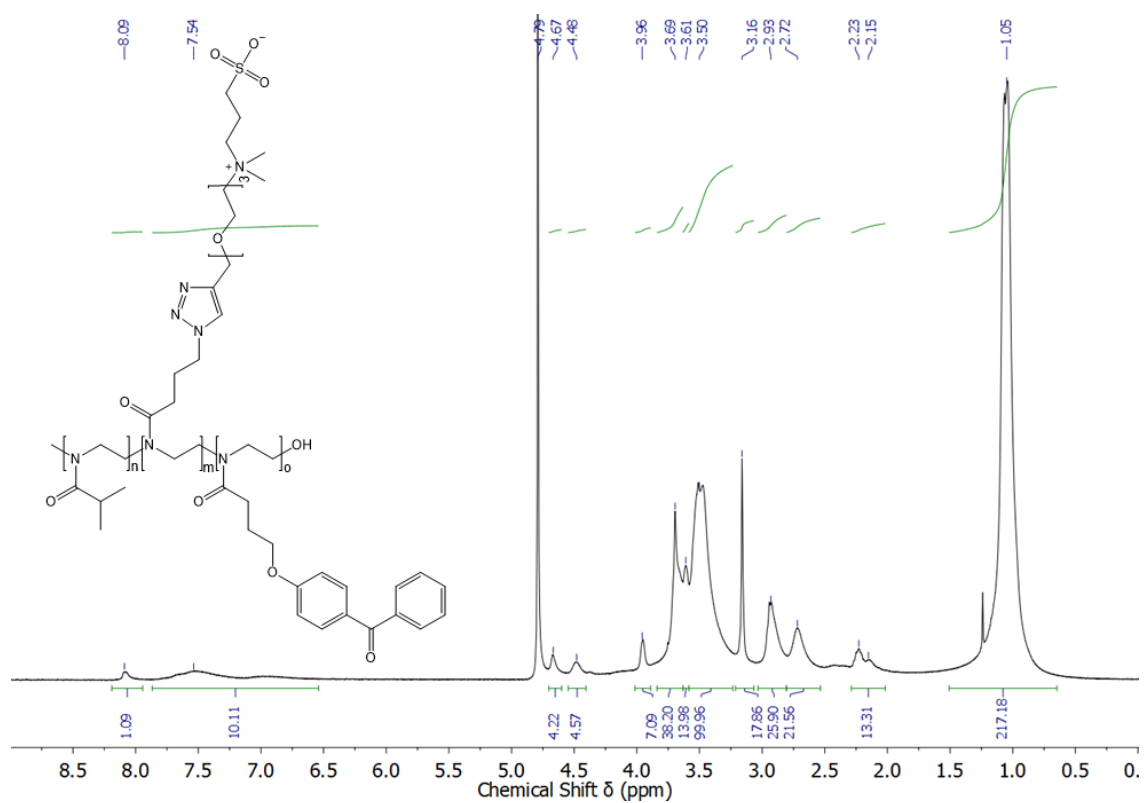
Figure 109: ^{1}H-NMR spectrum of poly(2-isopropyl-2-oxazoline-co-oligoethylene glycol-sulfobetaine-co-2-benzophenone-2-oxazoline) (D$_2$O).
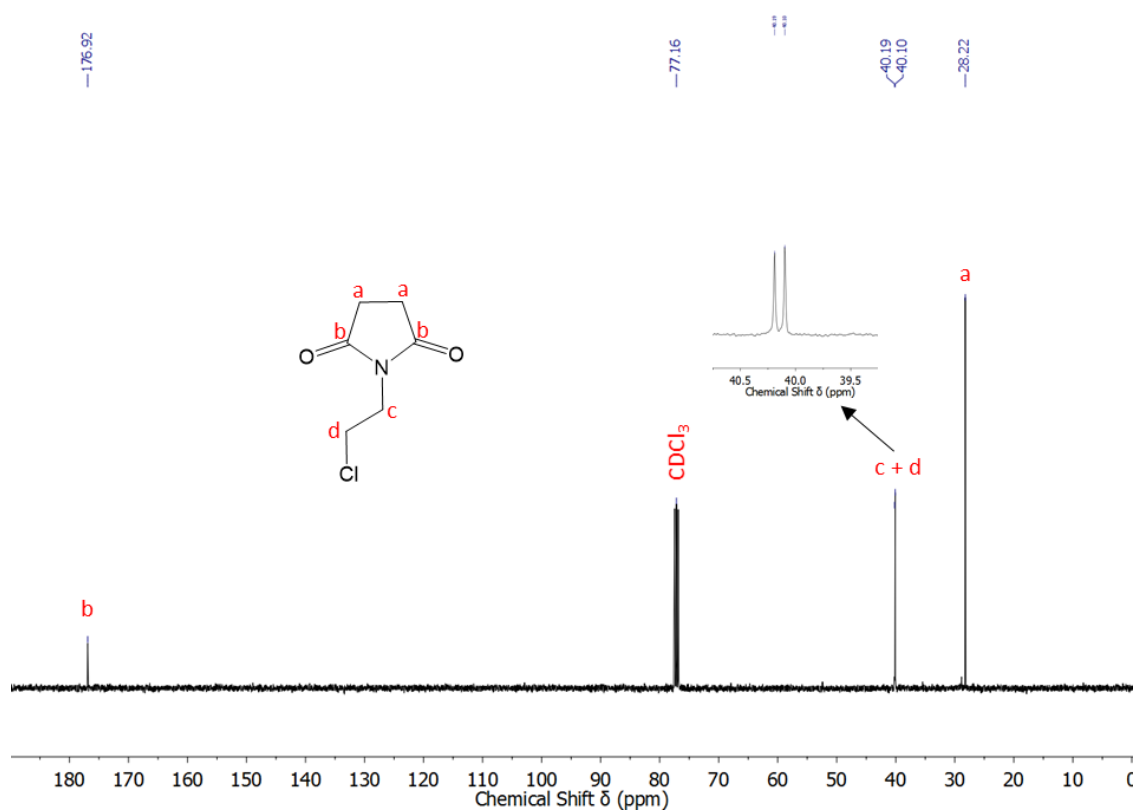
## 7.4 Synthesis 2-(prop-2-ynyloxy)propyl)-2-oxazoline

Figure 110: ¹H-NMR spectrum of prop-2-yn-1-yl 4-[(2-chloroethyl)amino]-4-oxobutanoate (CDCl₃).

Figure 111: ¹³C-NMR spectrum of prop-2-yn-1-yl 4-[(2-chloroethyl)amino]-4-oxobutanoate (CDCl₃).
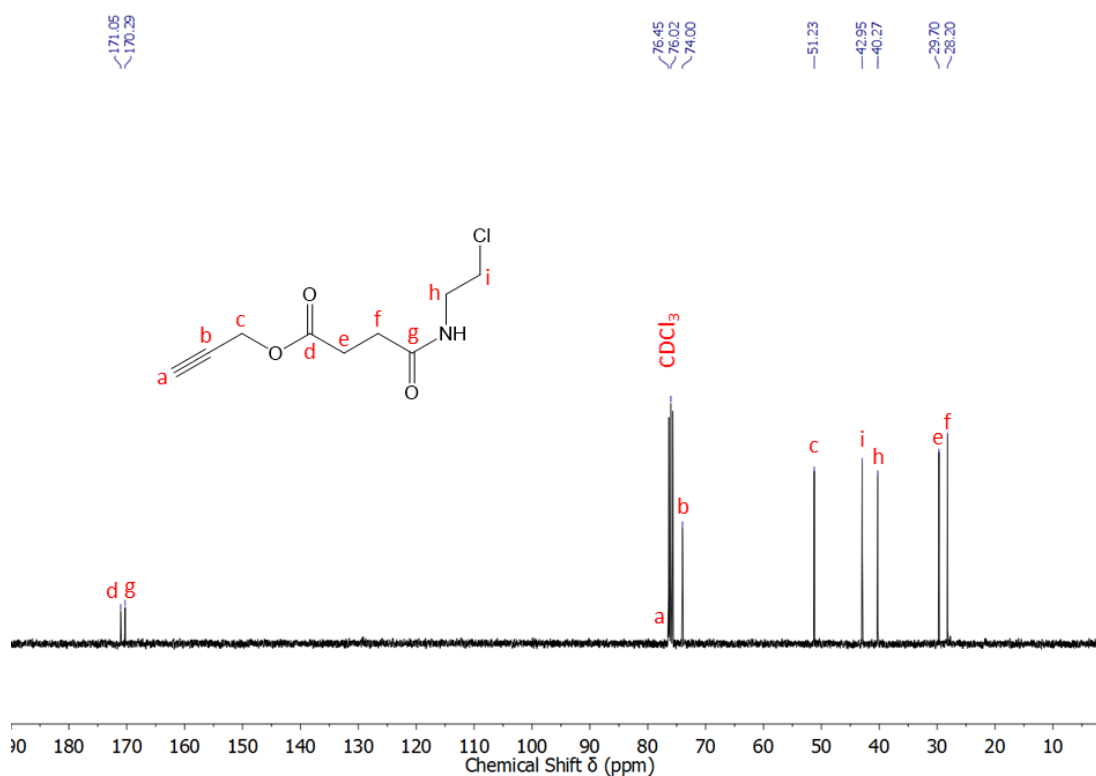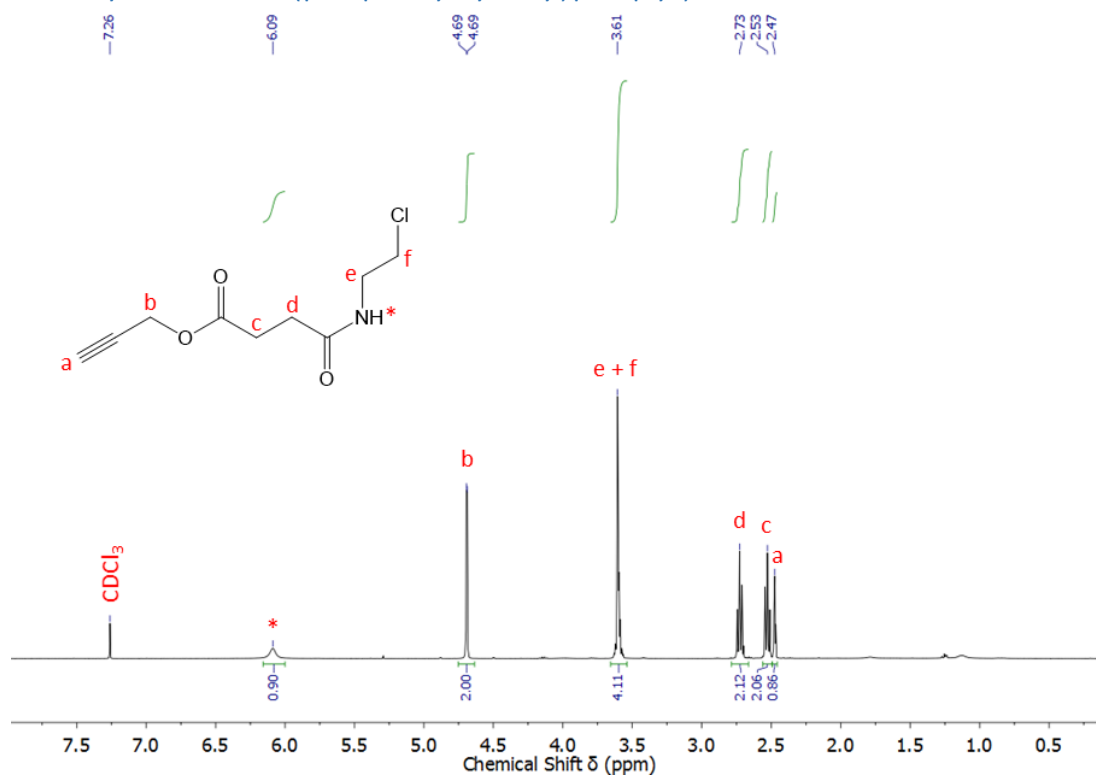
Figure 112: ^{1}H-NMR spectrum of 1-(2-chloroethyl)pyrrolidine-2,5-dione (CDCl$_3$).

Figure 113: ^{13}C-NMR spectrum of 1-(2-chloroethyl)pyrrolidine-2,5-dione (CDCl$_3$).

7.5 Additional UV/VIS Cloud Point Measurements

Transmittance curves (heating only) performed for the cloud point dependence on polymer volume fraction for poly(EtOxa$_{98}$-BPOxa$_2$), poly(isoPrOxa$_{79}$-EtOxa$_{19}$-BPOxa$_2$) and poly(isoPrOxa$_{98}$-BPOxa$_2$) as determined by turbidity measurements in aqueous solution with a heating rate of 1 K min^{-1}.
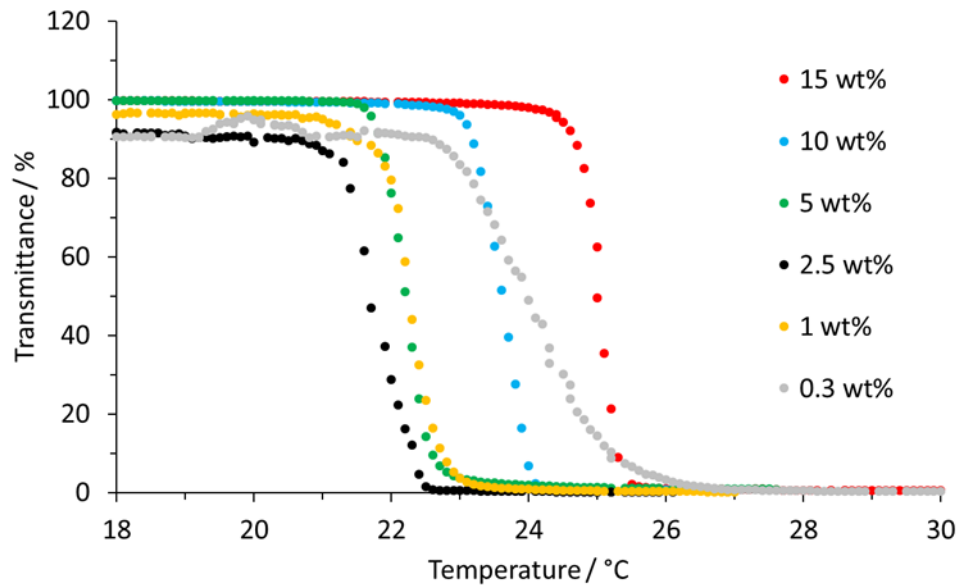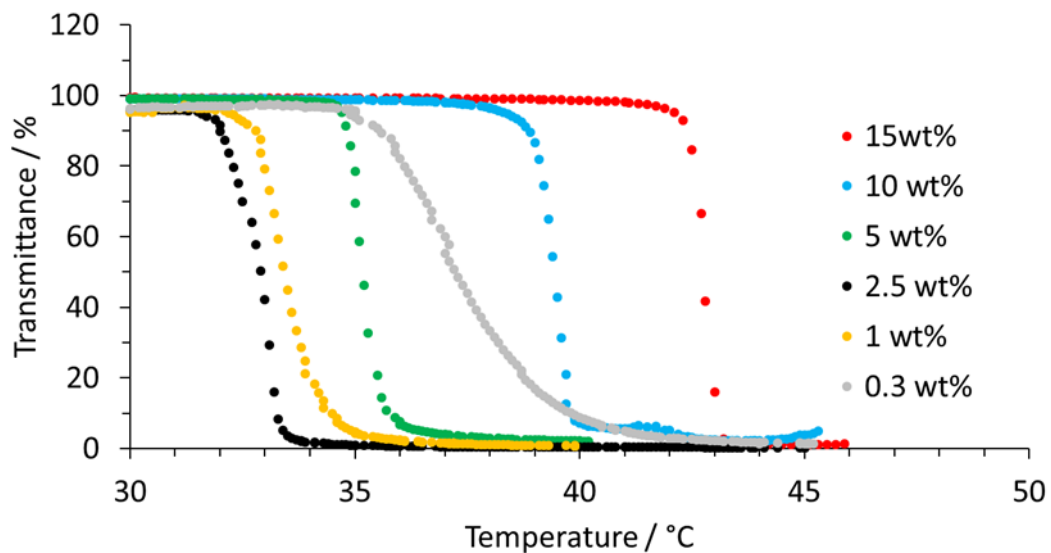

Figure 114: Transmittance curves at 550 nm for different concentrations of poly(isoPrOxa$_{98}$-BPOxa$_2$). Heating-rate = 1 K min^{-1}.
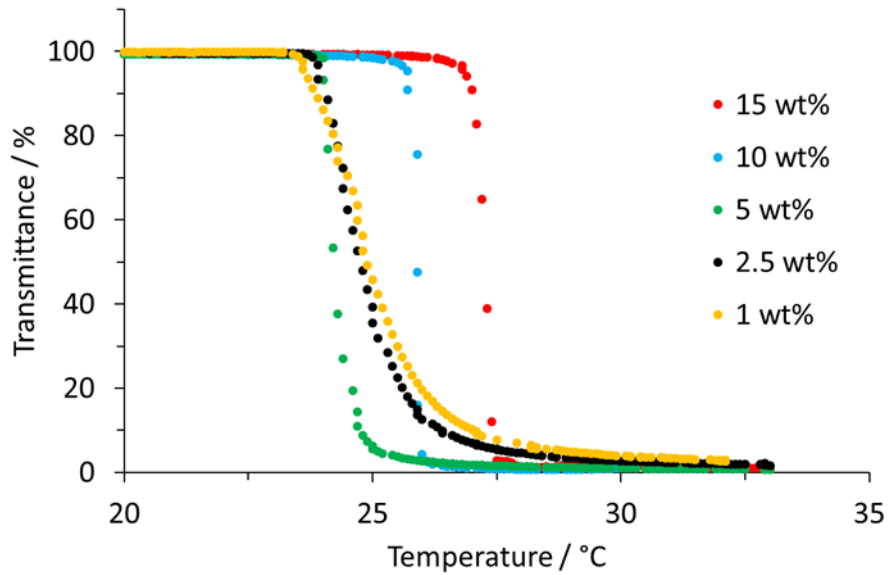
Figure 115: Transmittance curves at 550 nm for different concentrations of poly(isoPrOxa$_{79}$-EtOxa$_{19}$-BPOxa$_2$). Heating -rate = 1 K min^{-1}.

Figure 116: Transmittance curves at 550 nm for different concentrations of poly(EtOxa$_{98}$-BPOxa$_2$). Heating-rate = 1 K min^{-1}.
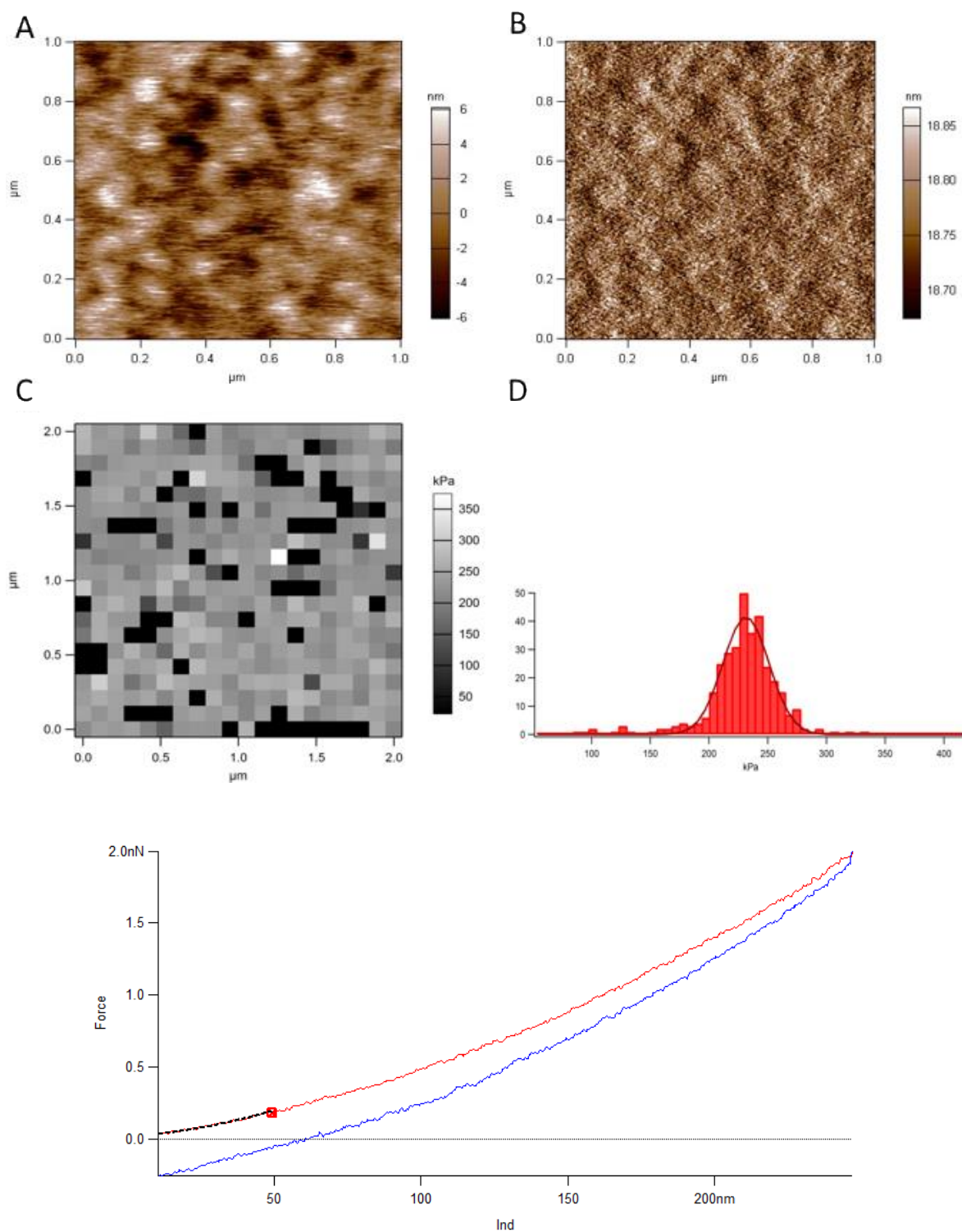
7.6 Additional AFM Data

Tapping mode images in water at 25°C and 38°C for poly(isoPrOxa$_{98}$-BPOxa$_2$) crosslinked at 365 nm with 4 and 8 J cm^{-2}. Height images, amplitude images, histograms, force maps (fitted with Gaussian function) and force curves for Young's modulus analysis (using parabolic Hertz model) for poly(isoPrOxa$_{98}$-BPOxa$_2$). All measurements as well as the data analysis were kindly performed by Cleiton Kunzler (Macromolecular Chemistry, University of Siegen). The access to the AFM was kindly provided by Prof. Dr. Holger Schönherr.
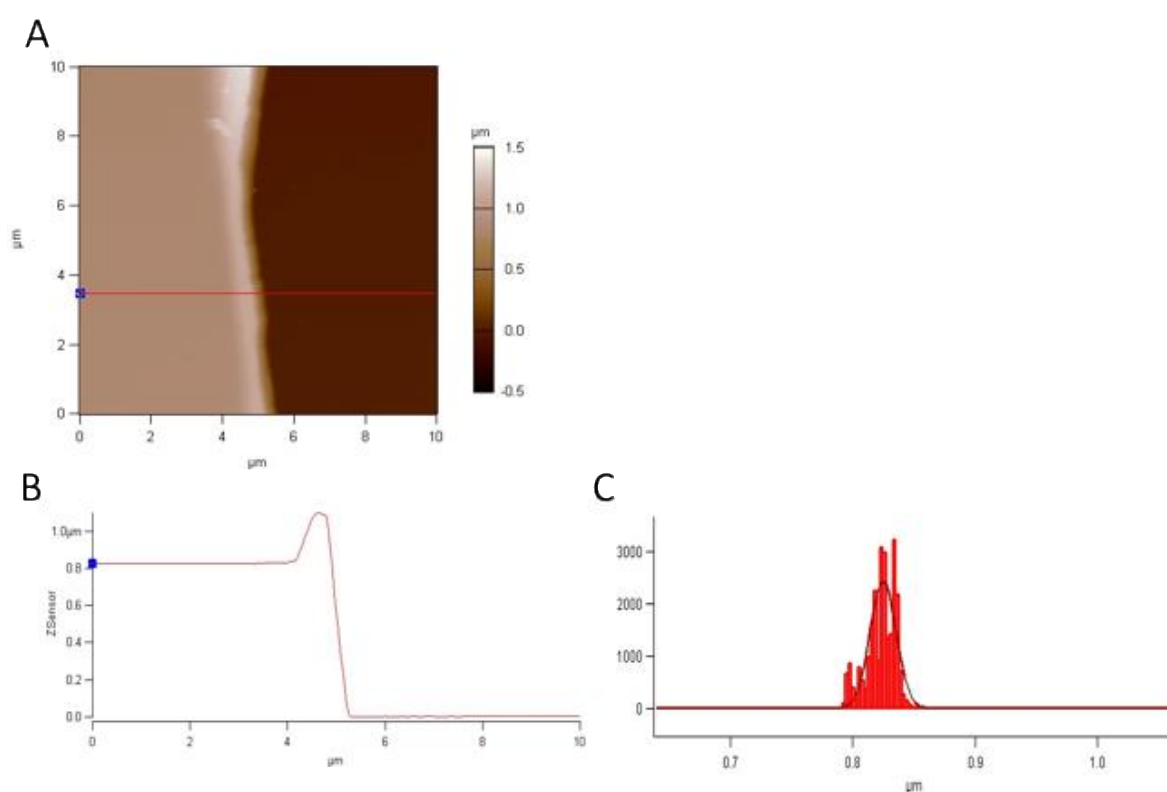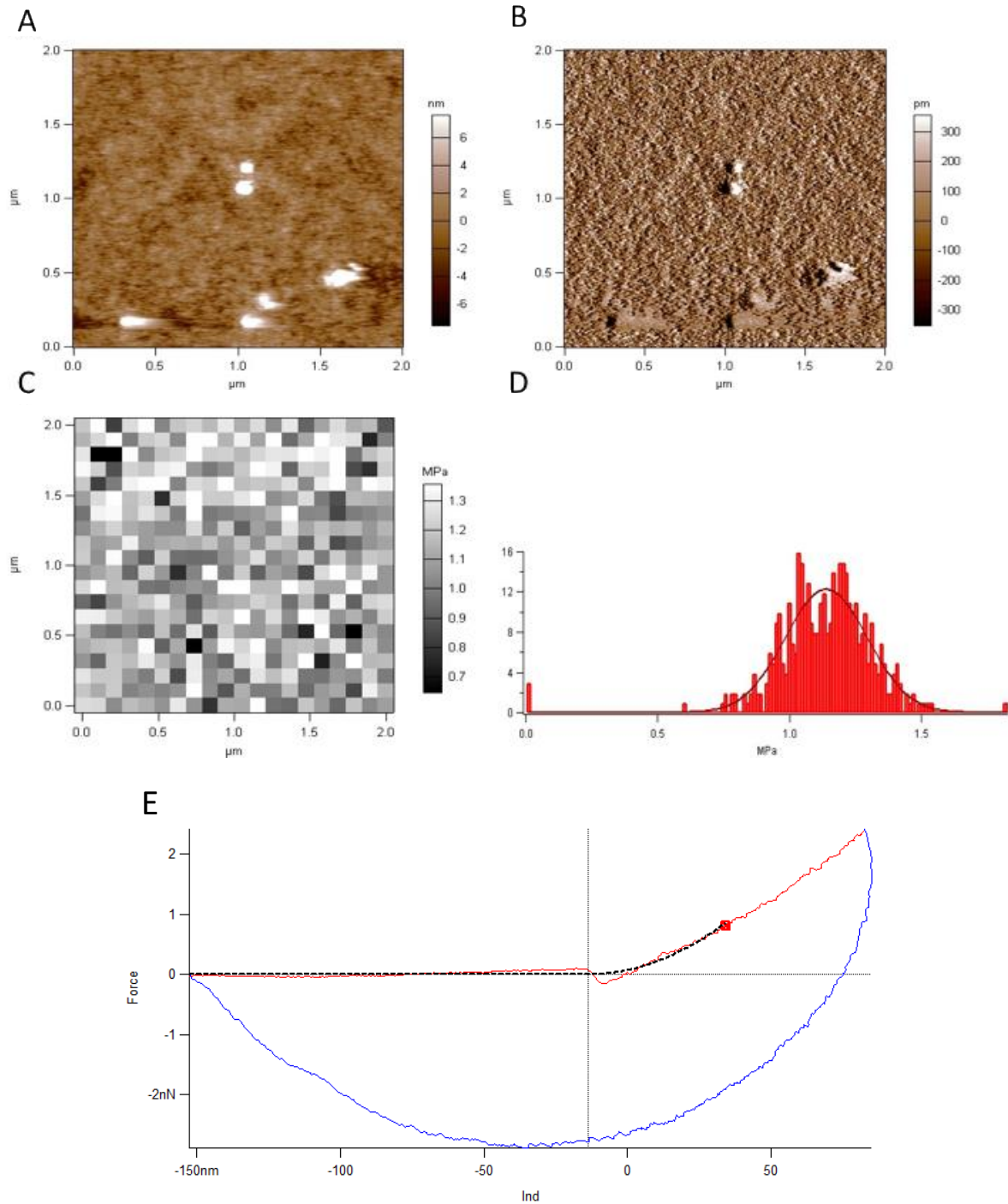

Figure 117: Height image (**A**), cross section (**B**) and histogram analysis (**C**) of dry state poly(isoPrOxa$_{98}$-BPOxa$_2$) crosslinked at 365 nm with 4 J cm^{-2}.

Figure 118: Tapping mode image in water at 25°C for poly(isoPrOxa$_{98}$-BPOxa$_2$) crosslinked at 365 nm with 4 J cm^{-2}. Height image (**A**) and amplitude image (**B**). Force map (**C**) and histogram (**D**) fitted with Gaussian function for Young's modulus analysis. (**E**) Force curve.

Figure 119: Tapping mode image in water at 38°C for poly(isoPrOxa$_{98}$-BPOxa$_2$) crosslinked at 365 nm with 4 J cm^{-2}. Height image (**A**) and amplitude image (**B**). Force map (**C**) and histogram (**D**) fitted with Gaussian function for Young's modulus analysis. (**E**) Force curve.
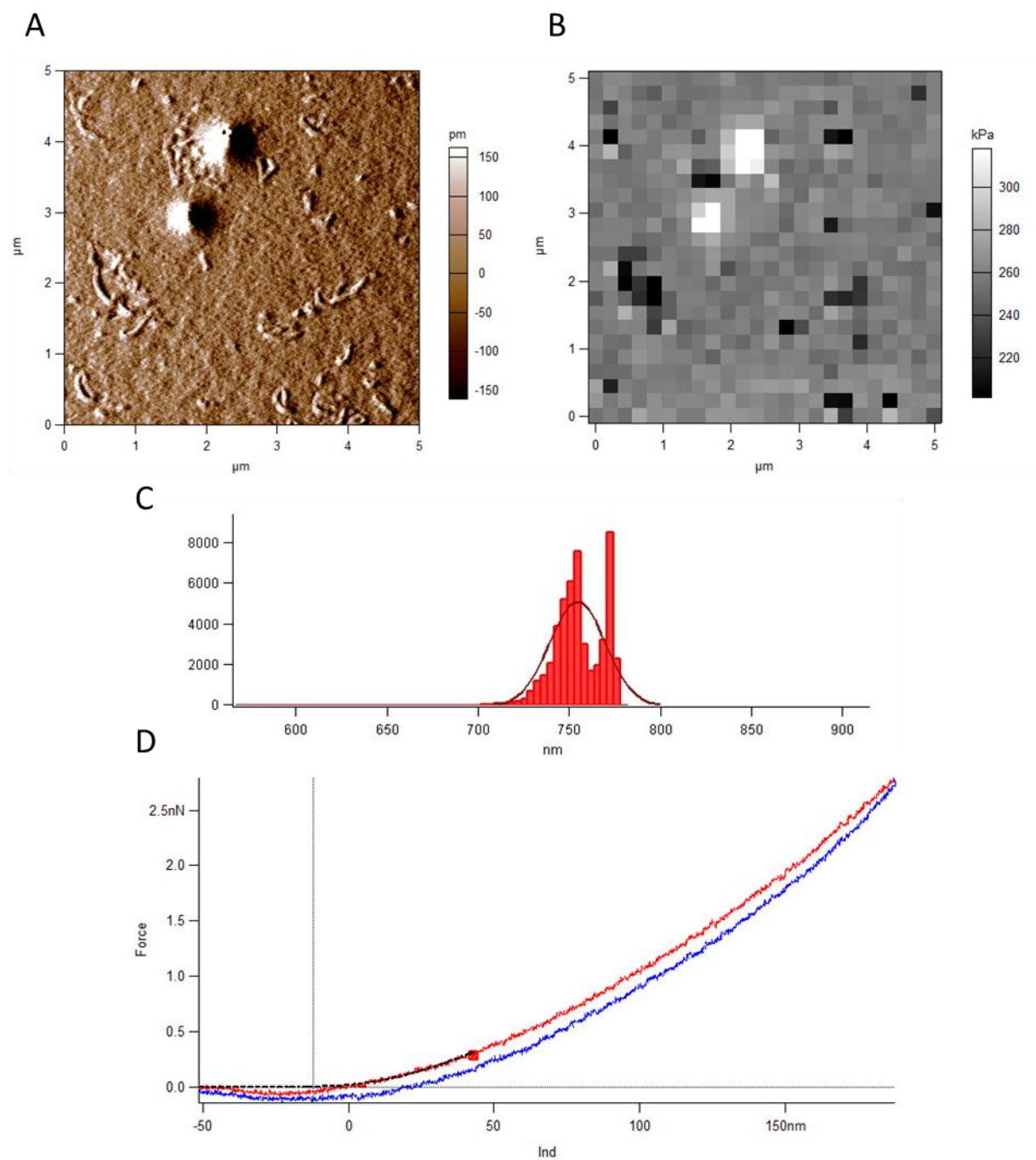
Figure 120: Tapping mode image in water at 25°C for poly(isoPrOxa$_{98}$-BPOxa$_2$) crosslinked at 365 nm with 8 J cm^{-2}. Amplitude image (**A**), force map (**B**) and histogram analysis (**C**) of swollen state poly(isoPrOxa$_{98}$-BPOxa$_2$) crosslinked at 365 nm. (**D**) Force curve.
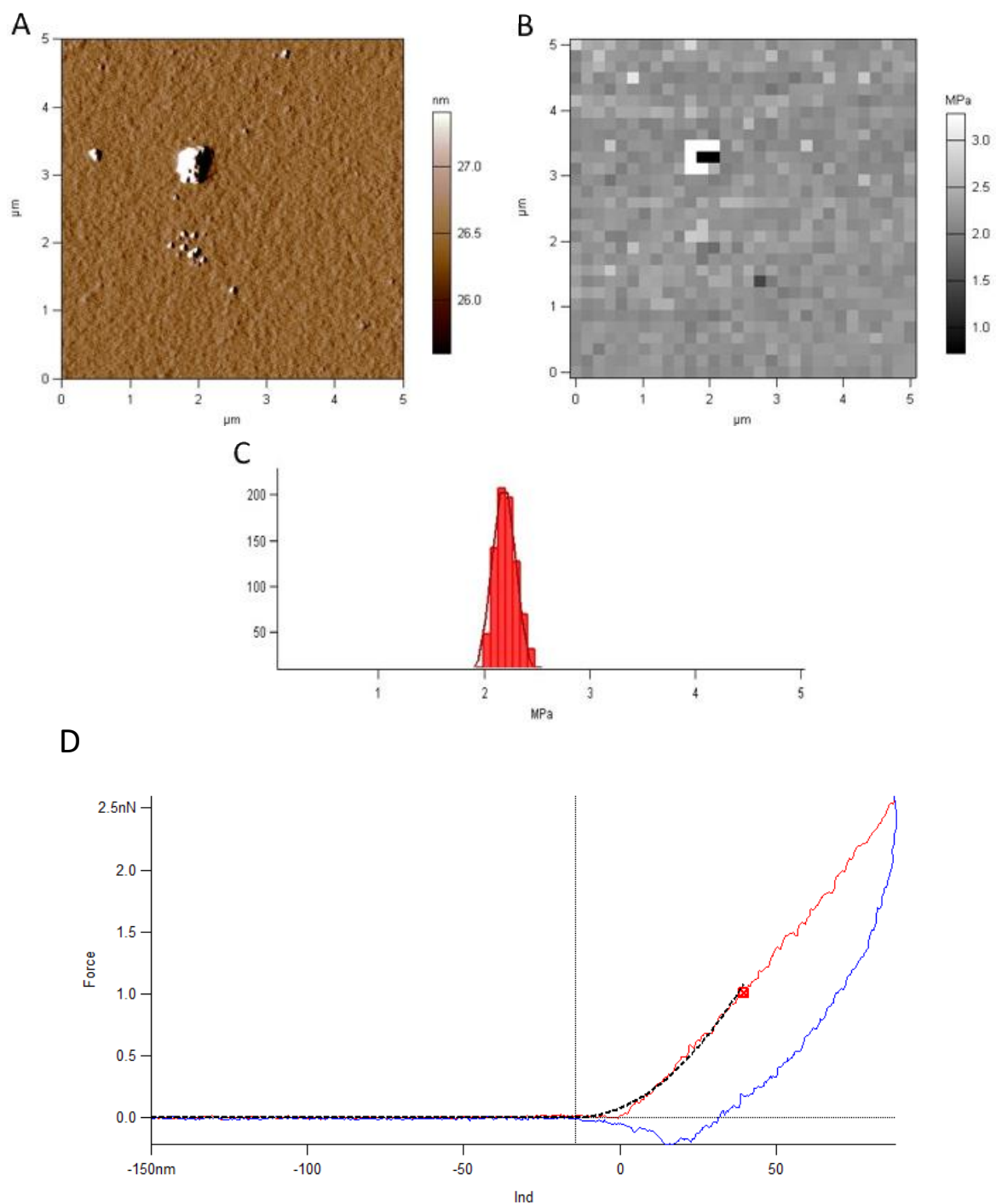
Figure 121: Tapping mode image in water at 38°C for poly(isoPrOxa$_{98}$-BPOxa$_2$) crosslinked at 365 nm with 8 J cm^{-2}. Amplitude image (**A**), force map (**B**) and histogram analysis (**C**) of swollen state poly(isoPrOxa$_{98}$-BPOxa$_2$) crosslinked at 365 nm. (**D**) Force curve.
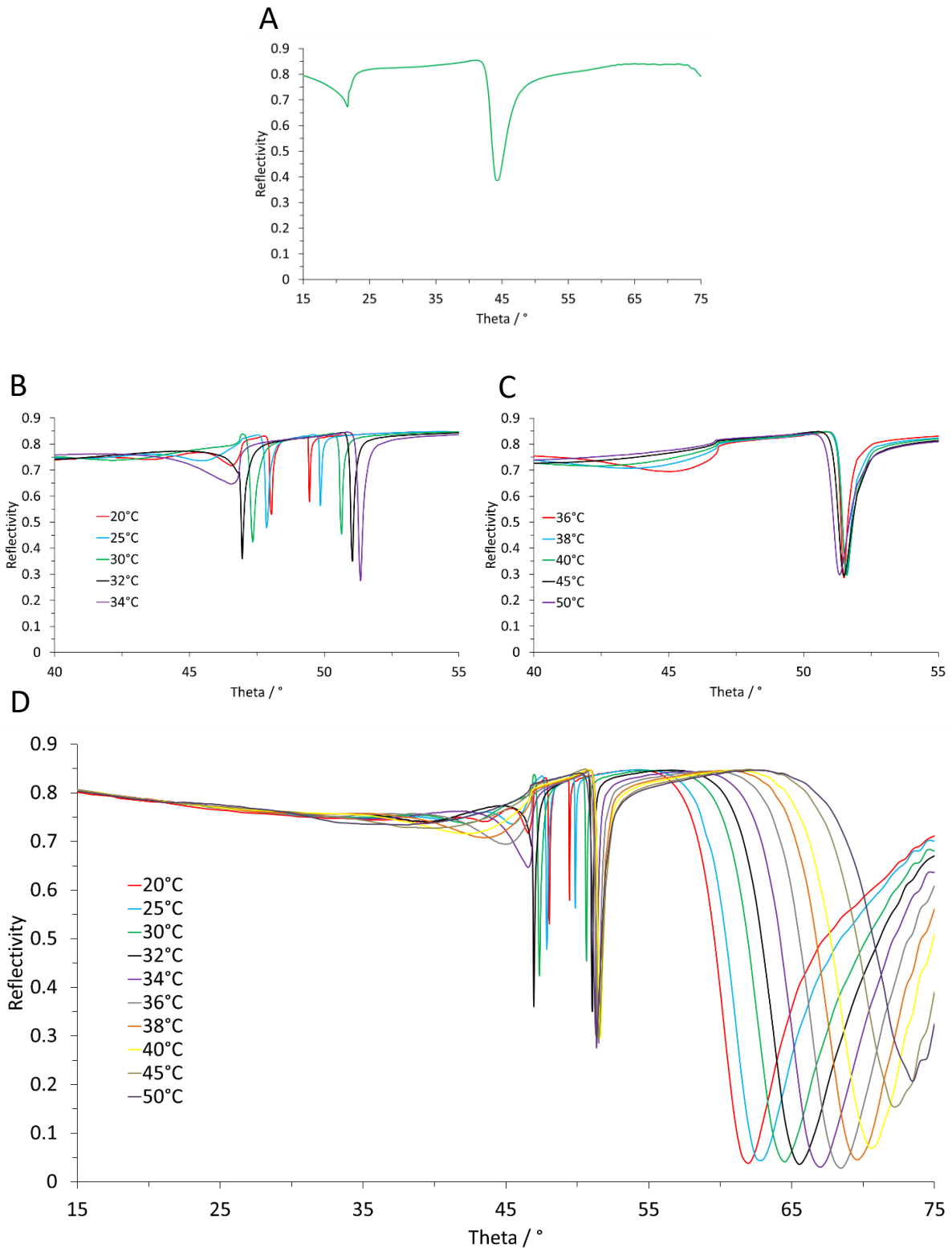
7.7 SPR/OWS Spectra

Exemplarily depicted data of the angular reflectivity spectra of a dry and swollen surface attached poly(2-isoPrOxa$_{98}$-BPOxa$_2$) hydrogel layer. Swollen state measurements were performed at different temperatures. The corresponding data obtained from SPR/OWS measurements using Fresnel simulation are summarized in **Table 24**.

Table 24: Analytical data of the SPR/OWS measurements of poly(2-isoPrOxa$_{98}$-BPOxa$_2$).

Layer	T / °C	d / nm	n	k
LASF9	20	0	1.845	0
Titanium	20	1.39	0.7088	1.8984
Gold	20	47.4	0.2604	3.5879
BDdiS	20	0.5	1.55	0
Poly(isoPrOxa$_{98}$BPOxa$_2$)	20	2250	1.365	0
Poly(isoPrOxa$_{98}$BPOxa$_2$)	25	1950	1.371	0
Poly(isoPrOxa$_{98}$BPOxa$_2$)	30	1422	1.387	0
Poly(isoPrOxa$_{98}$BPOxa$_2$)	32	1212	1.398	0
Poly(isoPrOxa$_{98}$BPOxa$_2$)	34	1102	1.407	0
Poly(isoPrOxa$_{98}$BPOxa$_2$)	36	952	1.417	0
Poly(isoPrOxa$_{98}$BPOxa$_2$)	38	882	1.423	0
Poly(isoPrOxa$_{98}$BPOxa$_2$)	40	812	1.431	0
Poly(isoPrOxa$_{98}$BPOxa$_2$)	45	732	1.440	0
Poly(isoPrOxa$_{98}$BPOxa$_2$)	50	702	1.443	0
Poly(isoPrOxa$_{98}$BPOxa$_2$)	45	722	1.443	0
Poly(isoPrOxa$_{98}$BPOxa$_2$)	40	732	1.441	0
Poly(isoPrOxa$_{98}$BPOxa$_2$)	35	922	1.419	0
Poly(isoPrOxa$_{98}$BPOxa$_2$)	30	1241	1.394	0
Poly(isoPrOxa$_{98}$BPOxa$_2$)	25	1780	1.374	0
Poly(isoPrOxa$_{98}$BPOxa$_2$)	20	2060	1.368	0

Polymer layer prepared form a 8 wt% ethanolic solution. Irradiation dose of 8 J cm^{-2}.

Figure 122: Measured data of the angular reflectivity spectra of a dry and swollen surface attached poly(2-isoPrOxa$_{98}$-BPOxa$_2$) hydrogel layer. Data points interconnected by spline lines. (**A**) Dry state polymer layer. (**B**) Optical waveguide modes for temperature dependent swelling experiments below the phase transition temperature and (**C**) above the phase transition temperature. (**D**) SPR/OWS spectra for temperature dependent swelling experiments.

Publications, Book Sections and Poster Contributions

Articles

[1] N. Sharma, C. Petri, U. Jonas, M. Bach, G. Tovar, K. Mrkvova, M. Vala, J. Homola, W. Knoll, J. Dostalek. Molecularly Imprinted Polymer Waveguides for Direct Optical Detection of Low-Molecular-Weight Analytes. Macromol. Chem. Phys. 2014, 215, 2295-2304. DOI: 10.1002/macp.201400260.

[2] N. Sharma, H. Keshmiri, X. Zhou, T. I. Wong, C. Petri, U. Jonas, B. Liedberg, J. Dostalek. Tunable Plasmonic Nanohole Arrays Actuated by a Thermoresponsive Hydrogel Cushion. J. Phys. Chem. C 2016, 120, 561–568. DOI: 10.1021/acs.jpcc.5b10336.

[3] N. Sharma, C. Petri, U. Jonas, J. Dostalek. Reversibly tunable plasmonic bandgap by responsive hydrogel grating. Optics Express 2016, 24, 2457-2465. DOI: 10.1364/OE.24.002457.

[4] F. Frascella, C. Petri, S. Ricciardi, L. Napione, P. Munzert, U. Jonas, J. Dostalek, F.Bussolino, C. F. Pirri and E. Descrovi. Hydrogel-Terminated Photonic Crystal for Label-Free Detection of Angiopoietin-1. Journal of Lightwave Technology. 2016, 34, 3641-3645. DOI: 10.1109/JLT.2016.2530876.

[5] F. Pirani, N. Sharma, A. Cencerrado, C. Petri, U. Jonas, E. Descrovi, J. L. Toca-Herrera and J. Dostalek. Optical Waveguide-Enhanced Diffraction for Observation of Responsive Hydrogel Nanostructures. Macromol. Chem. Phys. 2017, 218, 201600400. DOI: 10.1002/macp.201600400.

[6] K. Sergelen, C. Petri, U. Jonas, J. Dostalek. Free-standing hydrogel-particle composite membrane with dynamically controlled permeability for lab-on-chip applications. Biointerphases. 2017, 12, 051002-1-051002-9. DOI: 10.1116/1.4996952.

[7] C.Petri, S. Hageneder, C. Kunzler, S. Klees, P. Frank, J. Dostalek, W. Knoll, U. Jonas. Thermoresponsive and Photocrosslinkable Poly(2-alkyl-2-oxazoline) Hydrogel Coatings Derived from a Novel Benzophenone-2-oxazoline Comonomer. Macromol. Chem. Phys. (in preparation).

Book Sections

[1] U. Jonas, C. Petri, C. Kunzler, and H.W. Spiess. Polymeric Discotic Liquid Crystals. Reference Module in Materials Science and Materials Engineering 2017. doi:10.1016/B978-0-12-803581-8.02646-1.

Poster

[1] C. Petri, P. Frank, U. Jonas. Poly(2-alkyl-2-oxazoline) based Photocrosslinkable Hydrogel Systems. International Conference Soft Control 2014, Darmstadt.

[2] U. Ritz, I. Höfer, S. Gebhard, S. Klees, A. Mateescu, C. Petri, A. Hofmann, P. M. Rommens, U. Jonas. Photocrosslinkable Polysaccharide Hydrogel Films for Osteoblast and Endothelial Cell Growth.

[3] N. Sharma, C. Petri, U. Jonas, M. Bach, G. Tovar, K. Mrkvova, M. Vala, J. Homola, W. Knoll, J. Dostalek. Molecularly Imprinted Polymer Waveguides for Direct Optical Detection of Low-Molecular-Weight Analytes. Biosensor Conference 2014, Melbourne.

[4] D. Koltarek, K. Sergelen, C. Petri, U. Jonas, W. Knoll, J. Dostalek. Reversible plasmonic biosensor supported by responsive hydrogel for continuous monitoring of thrombin. Europt(r)ode Conference 2016, Graz.

[5] C. Petri, U. Jonas, J. Dostalek. Photocrosslinkable Poly(2-oxazoline)-Based Hydrogel Systems with improved Anti-fouling Properties for Biosensor Application. Jülich Soft Matter Days 2015, Bad Honnef.

[6] S. Hageneder, M. Bauch, C. Petri, U. Jonas, W. Knoll, J. Dostalek. Responsive hydrogel binding matrix for optical biosensor with microarray format. Europtrode 2016, Graz.

[7] D. Koltarek, N. Quilis, N. Sharma, K. Sergelen, C. Petri, U. Jonas, W. Knoll, J. Dostalek. Reversible plasmonic biosensor supported by responsive hydrogel for continuous monitoring of thrombin. Europtrode 2016, Graz.

[8] K. Sergelen, C. Petri, U. Jonas, B. Liedberg, W. Knoll, J. Dostalek. Continuous monitoring of small molecules: Surface plasmon resonance aptasensor. Europtrode 2016, Graz

[9] N. Quilis, N. Sharma, C. Petri, U. Jonas, W. Knoll, J. Dostalek. Nanostructured Thermoresponsive Hydrogels for Optical Biosensor Applications. Europtrode 2016, Graz.